

~~CONFIDENTIAL~~

~~CONFIDENTIAL~~

~~UNCLASSIFIED~~

LA-3091

Copy No. 51

# AEC RESEARCH AND DEVELOPMENT REPORT

## LOS ALAMOS SCIENTIFIC LABORATORY OF THE UNIVERSITY OF CALIFORNIA • LOS ALAMOS NEW MEXICO

---

~~UNCLASSIFIED~~

GROUP 1  
Excluded from Automatic  
Downgrading and Declassification

### A METAL DUMBO ROCKET REACTOR

#### NOTICE

PORTIONS OF THIS REPORT ARE ILLEGIBLE. It has been reproduced from the best available copy to permit the broadest possible availability.

DISTRIBUTION OF THIS DOCUMENT IS UNLIMITED

~~CONFIDENTIAL~~

~~UNCLASSIFIED~~

~~CONFIDENTIAL~~

~~CONFIDENTIAL~~

~~RESTRICTED DATA~~

~~SECRET~~

~~CONFIDENTIAL~~

NOTICE  
This report was prepared as an account of work sponsored by the United States Government neither the United States nor the United States Energy Research and Development Administration, nor any of their employees, nor any of their contractors, subcontractors, or their employees, makes any legal warranty, express or implied, or assumes any legal liability or responsibility for the accuracy, completeness or usefulness of any information, apparatus, product or process disclosed, or represents that its use would not infringe privately owned rights.

Classification cancelled  
by authority of TID-4200-52  
by EB DTIC, date 4-15-76

LA-2091  
NUCLEAR ROCKET ENGINES  
(Distributed according to  
M-3679, 18th ed.)

This document consists of 385 pages  
No. 51 of 75 copies, Series A

**LOS ALAMOS SCIENTIFIC LABORATORY  
OF THE UNIVERSITY OF CALIFORNIA LOS ALAMOS NEW MEXICO**

REPORT WRITTEN: January 1957  
REPORT DISTRIBUTED: February 21, 1957

**LEGAL NOTICE**  
This report was prepared as an account of work sponsored by the United States Government neither the United States nor the United States Energy Research and Development Administration, nor any of their employees, nor any of their contractors, subcontractors, or their employees, makes any legal warranty, express or implied, or assumes any legal liability or responsibility for the accuracy, completeness or usefulness of any information, apparatus, product or process disclosed, or represents that its use would not infringe privately owned rights.

~~CONFIDENTIAL~~

**A METAL DUMBO ROCKET REACTOR**

by  
B. W. Knight, Jr.  
B. B. McInteer  
R. M. Potter  
E. S. Robinson

Facsimile Price \$ 50.80  
Reproduction Price 5.10  
of Access Permittes  
Available from the  
Division of Technical Information Extension  
P. O. Box 1001  
Oak Ridge, Tennessee

Dale E. Armstrong  
Illustrations and Mathematical Typography

Classification cancelled on 10/1/64  
by authority of Isk. 2-25-64  
by J. J. Ridenour TISOR, date 4-15-64

Contract W-7405-ENG. 36 with the U. S. Atomic Energy Commission

**AEC RESEARCH AND DEVELOPMENT REPORT**

~~RESTRICTED DATA~~

This document contains restricted data as defined in the Atomic Energy Act of 1954. Its transmission or the disclosure of its contents in any manner to an unauthorized person is prohibited.

This document contains Confidential-Restricted Data relating to civilian applications of atomic energy.

~~SECRET~~  
DISTRIBUTION OF THIS DOCUMENT IS UNLIMITED  
~~CONFIDENTIAL~~

EB

~~CONFIDENTIAL~~

~~CONFIDENTIAL~~

SECRET

NUCLEAR ROCKET ENGINES

(M-3679, 18th ed.)

LA-2091

Los Alamos Report Library	1-31
Aerojet-General Corporation (Thomas Beehan)	32
Albuquerque Operations Office (Russell Ball)	33
Armed Forces Special Weapons Project, Sandia	34
Armed Forces Special Weapons Project, Washington	35
Assistant AF Plant Representative, Downey	36
Atomic Energy Commission, Washington	37-40
Bureau of Ordnance	41
Redstone Arsenal	42
San Francisco Operations Office	43
USAF Project RAND	44-45
University of California Radiation Laboratory, Livermore	46-47
Western Development Division	48
Wright Air Development Center (WCOSI-3)	49-50
Technical Information Service Extension	51-75

UNCLASSIFIED

~~CONFIDENTIAL~~

SECRET

~~CONFIDENTIAL~~

#### ACKNOWLEDGEMENTS

The authors are indebted to a large number of members of the Los Alamos Scientific Laboratory for advice and encouragement during the preparation of this report. Particular thanks are given to C. L. Longmire, J. L. Tuck, and H. T. Gittings. Important advice and assistance on nuclear design problems was given by G. I. Bell, J. J. Devaney, and G. E. Hansen. Assistance on metallurgical problems from R. B. Gibney, W. J. McCreary, R. J. Bard, J. A. Kircher, J. M. Taub, L. S. Levinson, and J. T. Waber is gratefully acknowledged. Fabrication problems have been handled by J. R. Lilienthal, D. K. Gestson, F. J. Miller, and A. C. Briesmeister. Problems of radiation damage have been considered by R. A. Penneman with tests by A. H. Zeltmann. Some preliminary tests relating to metallized plastics have been performed by R. C. Vandervoort and J. S. Church. Helpful discussions on high temperature gas kinetics problems have been held with W. M. Jones, L. H. Jones, and Dudley Herschbach.

For enlightening discussions and assistance on some mathematical problems, we thank J. T. Lehner, G. M. Wing, Garrett Birkhoff, Max Goldstein, Clarice L. Wruck, John von Neumann, and S. Chandrasekhar.

Particular gratitude is due N. H. Baker, Jr., W. A. Blanpied, F. A. Guevara, G. A. Peterson, and W. E. Wageman for their assistance in preparing and proofreading this report. We especially wish to thank Charlotte Mottaz for the patience and care in her stenographic assistance in the preparation of this report.

Thanks are due numerous other friends in the laboratory for advice and encouragement on many problems.

Finally, we wish to thank E. R. Jette and R. D. Fowler, without whose unswerving support and encouragement this program would have been impossible.

~~CONFIDENTIAL~~

UNCLASSIFIED

CONTENTS

	Page
CHAPTER 1	
INTRODUCTION	9
*1-1. Introduction	9
*1-2. General Description	10
*1-3. Dumbo Tube Design	13
*1-4. Flow in the Heat Exchanger	19
*1-5. Choice of Propellant	22
*1-6. Neutronics	23
*1-7. The Report	24
CHAPTER 2	
FLOW AND HEAT TRANSFER	29
2-1. Introduction	29
2-2. Basic Relations	30
2-3. Physical Approximation of the Equations	32
2-4. The Circular Channel	36
2-5. The Thin Channel Approximation	38
2-6. Higher Approximations	47
2-7. The Variational Method	51
CHAPTER 3	
TEMPERATURE-FLOW STABILITY	75
*3-1. Statement of the Problem	75
3-2. Viscous Flow Through a Uniform Channel with Uniform Power Density	78
3-3. Viscous Flow Through a Constricted Channel with Uniform Power Density	79
CHAPTER 4	
WALL TEMPERATURE DISTRIBUTION	85
*4-1. Introduction	85
4-2. Overall Temperature, and the Dynamic Insulation Effect	87

---

\*Sections marked with an asterisk are recommended for those making a first reading of this report.

~~SECRET~~

Contents, contd.

	Page
4-3. Temperature Distribution in the Periodic Wall for Normal Operation	90
4-4. Wall Temperature Distribution Under a Flow Aberration	98
4-5. The Single Channel Aberration	101
4-6. Effects of Channel Fabrication Errors	109
4-7. Other Heat Transfer Mechanisms	130
CHAPTER 5	
LOSS OF REACTOR MATERIAL BY EVAPORATION	135
*5-1. Statement of the Problem	135
5-2. Calculation of the Evaporation Loss	136
*5-3. Numerical Results	142
5-4. A Rapid Approximation Method	144
CHAPTER 6	
NUCLEAR REACTOR CONSIDERATIONS	149
*6-1. The Problem	149
6-2. Slowing-Down Leakage Through a Moderating Reflector	150
6-3. Effect of Slowing-Down Capture and Self- Shielding: The Conditions for Flat Flux	161
6-4. Calculation of Critical Conditions	170
6-5. Effects of Lumping and Doppler Broadening	175
6-6. Numerical Procedure	186
*6-7. Some Sample Results	194
6-8. Reflector Design Variations	201
6-9. Effects of the Approximations	208
CHAPTER 7	
HYDRODYNAMIC DESIGN CONSIDERATIONS	215
*7-1. Introduction	215
7-2. Turbulent Heat Exchangers	216
*7-3. Flow Uniformity Through the Composite Dumbo Wall	221

---

\*Sections marked with an asterisk are recommended for those making a first reading of this report.

6

~~SECRET~~

~~SECRET~~

Contents, contd.

	Page
7-4. Turbulent Flow in the Main Ducts	224
7-5. The Expected Hydrodynamics in Dumbo	233
7-6. Energy Relations for Compressible Flow in Dumbo	235
7-7. Solution of the Flow Equations	237
7-8. The Balancing of Pressures	245
7-9. Effects of Other Flow Laws	250
 CHAPTER 8  	
FABRICATION METHODS AND MATERIALS	255
*8-1. Introduction	255
*8-2. Metallurgical Considerations	255
*8-3. Methods for Addition of Uranium to the Refractory Metals	257
*8-4. Radiation Damage to the Metal Structure	259
*8-5. Radiation Damage to the Moderator	259
*8-6. Fabrication of Dumbo Rings	260
*8-7. Metallurgical Fabrication Problems	265
*8-8. The Moderator Material	268
 CHAPTER 9  	
NUMERICAL DESIGN OF SOME SELECTED MOTORS	271
*9-1. Introduction	271
*9-2. Description of Models A - D	271
*9-3. Model A Design Features	273
*9-4. Model B Design Features	289
*9-5. Model C Design Features	292
*9-6. Model D Design Features	298
*9-7. Comparison of the Four Models	298
*9-8. Variants on the Designs	301
 CHAPTER 10  	
CONCLUDING TOPICS	305
*10-1. Introduction	305
*10-2. Variants of Dumbo	305

---

\*Sections marked with an asterisk are recommended for those making a first reading of this report.

~~SECRET~~

Contents, contd.

	Page
*10-3. Other Uses of Dumbo-Type Reactors	307
*10-4. A Research and Development Program for Dumbo	310

APPENDICES

A. NUCLEAR CONSTANTS	313
B. PHYSICAL PROPERTIES OF REFRACTORY METALS	325
B-1. Introduction	325
B-2. Thermal Conductivity	325
B-3. Coefficient of Thermal Expansion	327
B-4. Tensile Strength	328
C. LAMINAR INCOMPRESSIBLE FLOW IN CHANNELS WITH POROUS WALLS	331
C-1. Introduction	331
C-2. Formulation of the Problem	333
C-3. Some Qualitative Features	339
C-4. Methods of Solution	340
C-5. Three Limiting Results	355
C-6. Some Unanswered Problems	358
C-7. Other Channel Shapes	359
C-8. Summary	364
C-9. Note on Previous Work	365
C-10. Acknowledgments	366
D. THE SUPER-DUMBO	367
D-1. Introduction	367
D-2. H <sub>2</sub> Dissociation-Recombination Applications	369
D-3. Ammonia Systems	373
D-4. Dumbo Design Modifications	375
E. HEAT EXCHANGE INSTABILITY	379
E-1. Introduction	379
E-2. Equilibrium Conditions	380
E-3. Effect of Perturbations	382
E-4. The Stability Criterion	384

---

\*Sections marked with an asterisk are recommended for those making a first reading of this report.

~~SECRET~~



~~SECRET~~

## CHAPTER 1

### INTRODUCTION

But there was one Elephant -- an Elephant's Child --  
who was full of 'satiabie curtiosity, and that means  
he asked ever so many questions.

R. Kipling, The Elephant's Child

#### 1-1: Introduction

It has been obvious for many years that, because of the great energy release in nuclear reactions as compared with chemical reactions, nuclear power has potential advantages in rocket propulsion. Many proposals for nuclear powered rockets have been made.<sup>1-8</sup> A complete bibliography and historical background has been prepared by R. W. Bussard<sup>9</sup> of LASL.

In this report, a type of nuclear reactor for rocket propulsion is described and the theoretical principles necessary for its design are developed. This reactor has a hydrogen moderated metallic core and utilizes laminar flow in the heat exchanger. An unusual feature of its design is the utilization of the heat-exchanger wall as a thermal barrier which protects the cold moderator regions of the reactor from the extremely high temperature of the effluent propellant gas.

The reactor has been described in its embryonic stage in LAMS-1887 ("Dumbo -- A Pachydermal Rocket Motor"). The very encouraging conclusions of that study led to the further and more detailed investigation of this

report, which describes a low mass rocket reactor of high performance and reliability using metals whose physical, chemical, and nuclear properties are desirable and whose technology is largely understood.

The development of this reactor has proceeded along several lines:

- (a) Theoretical development of energy transfer relations and gas flow behavior in laminar flow heat exchangers. These studies lead to the design of the Dumbo heat exchanger.
- (b) Study of the effects of fabrication errors, and the methods by which those effects may be reduced.
- (c) Assessment of nuclear design requirements for fissionable material and moderator. Uniform power generation throughout the reactor is achieved, utilizing uniform standardized fuel elements.
- (d) Investigation of the hydrodynamics of the propellant in the main Dumbo flow channels, leading to conditions for the uniform delivery of propellant to the whole heat exchanger.
- (e) An experimental program to explore the feasibility of producing fuel elements to the specifications required by the theoretical results.
- (f) Coordination of the studies a to e to obtain specific reactor designs.

These studies form the body of this report.

## 1-2: General Description

A nuclear rocket requires a reactor capable of heating a propellant gas to a high temperature. Dumbo is such a reactor, and consists of an

~~SECRET~~

array of metal tubes whose walls are made permeable to gas flow by myriads of tiny, regular channels. These walls contain the fissionable material which is the source of the heat for the propellant gas. The flow of gas through the tube walls effectively insulates the central region of each tube. This permits hydrogenous moderator in the form of plastic to be placed there. The tubes serve one other function: to provide the main flow path for the cold gas. This entire assembly is surrounded by a neutron reflector of beryllium.

Figure 1-1 shows a typical Dumbo reactor. The flow paths are as follows: The liquid hydrogen propellant flows first through the beryllium reflector, preventing it from being overheated by inelastic processes involving gamma rays and neutrons. The liquid hydrogen (27°K) is converted in this process to a low temperature gas (100°K). The path of the gas is then through a nuclear preheater (not shown, but described later in Secs. 7-2 and 9-3) at the cold gas entrance of a tube. This adjusts the gas temperature to the proper moderator inlet value (220°K). The gas then flows through the polystyrene moderator and is heated to 300°K in this process. On leaving the moderator, the gas passes through the Dumbo metal wall, where the fissionable material is confined, and is heated to the final exit temperature (2500°K). The flow path is then down the outside of the tube, through the gas exit ports in the bottom of the beryllium reflector, thence to the nozzle.

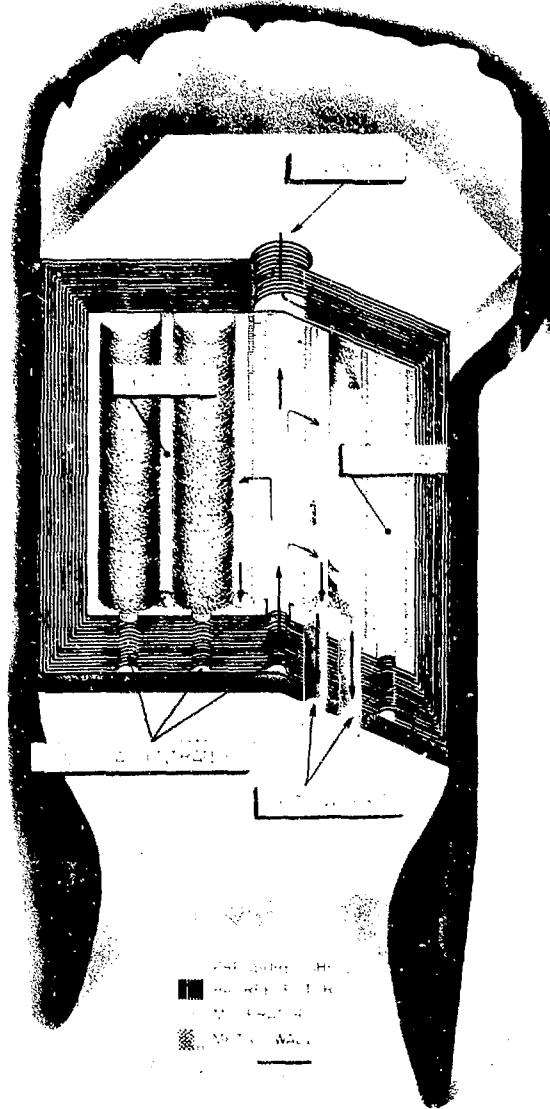


Fig. 1-1: Typical Dumbo Reactor. This diagram is essentially to scale with the exception of the nozzle, which has been distorted for clarity.

1-3: Dumbo Tube Design

In order to make clear the construction of the heating surface, the following step-by-step development is used. This development closely parallels the actual conception of the heat-exchanger design.

A thin metal strip is corrugated in a regular fashion (Fig. 1-2).

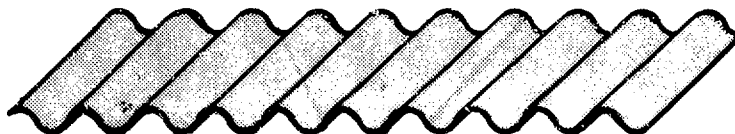


Fig. 1-2

To form channels, the foils are placed together in the following manner (Fig. 1-3).

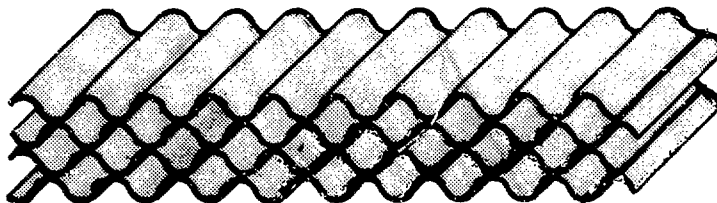


Fig. 1-3

To eliminate the problem of nesting, a flat strip is placed between the corrugated strips, thereby doubling the number of gas passages (Fig. 1-4).

~~SECRET~~

Chapter 1

Introduction

---

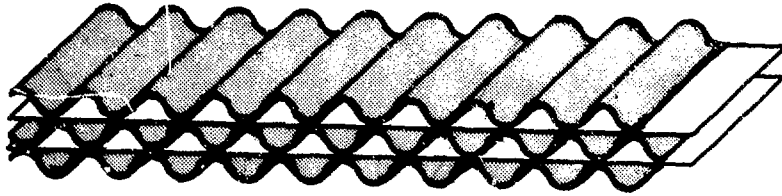


Fig. 1-4

To provide some flow impedance in the entering part of each gas passage, a deformation is needed in the cold leading edge of the flat strip. Since the flat strip must provide impedance for two channels, as shown in Fig. 1-5,

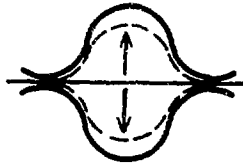


Fig. 1-5

the strip is made of two pieces, each of half thickness. These pieces are shown in Fig. 1-6.

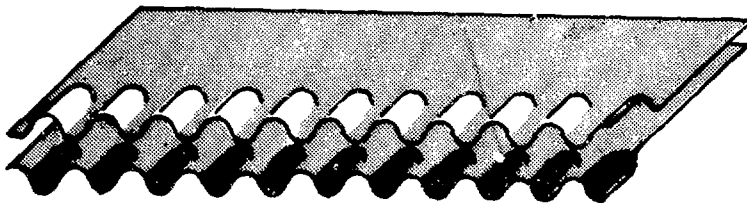
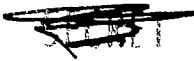


Fig. 1-6

The assembly of fully corrugated and flat, partially corrugated, strips

~~SECRET~~



are shown in Fig. 1-7.

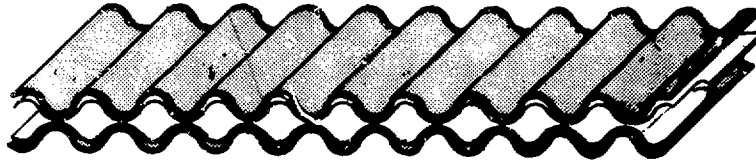


Fig. 1-7

In order to make the heat source as uniform as possible, alternate rows are shifted half a wave length (Fig. 1-8).

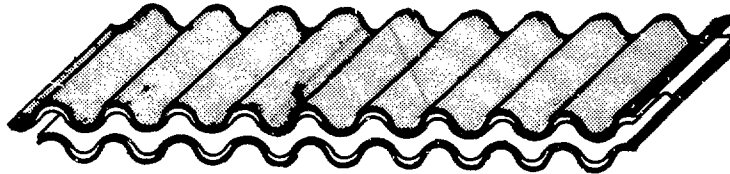


Fig. 1-8

The corrugated and flat sections are stamped from refractory metals, such as tungsten or molybdenum, which are impregnated with  $UO_2$  (uranium dioxide). Shown in Fig. 1-9 are linearized components of a molybdenum wall sample. In Fig. 1-10 are shown photomicrographs of the assembled components, viewed from both the entrance and exit sides. The light areas are the gas passages. These components were made for fabrication studies.

The Dumbo reactor requires circular rings or washers, convoluted similarly to the corrugated foils described above. An assembly of convoluted washers is shown schematically in Fig. 1-11. The Dumbo metal



~~SECRET~~

Chapter 1

Introduction

---

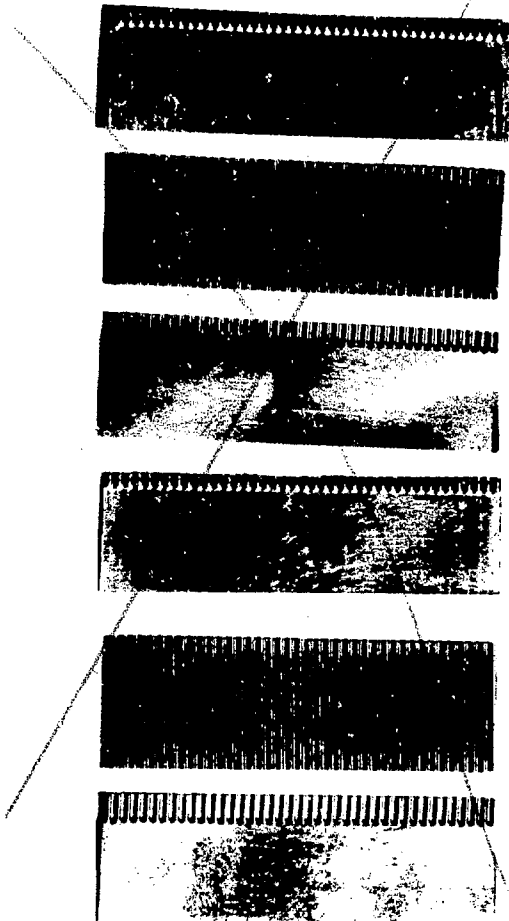


Fig. 1-9: Linearized Components of a Molybdenum Wall Sample

~~SECRET~~



~~SECRET~~

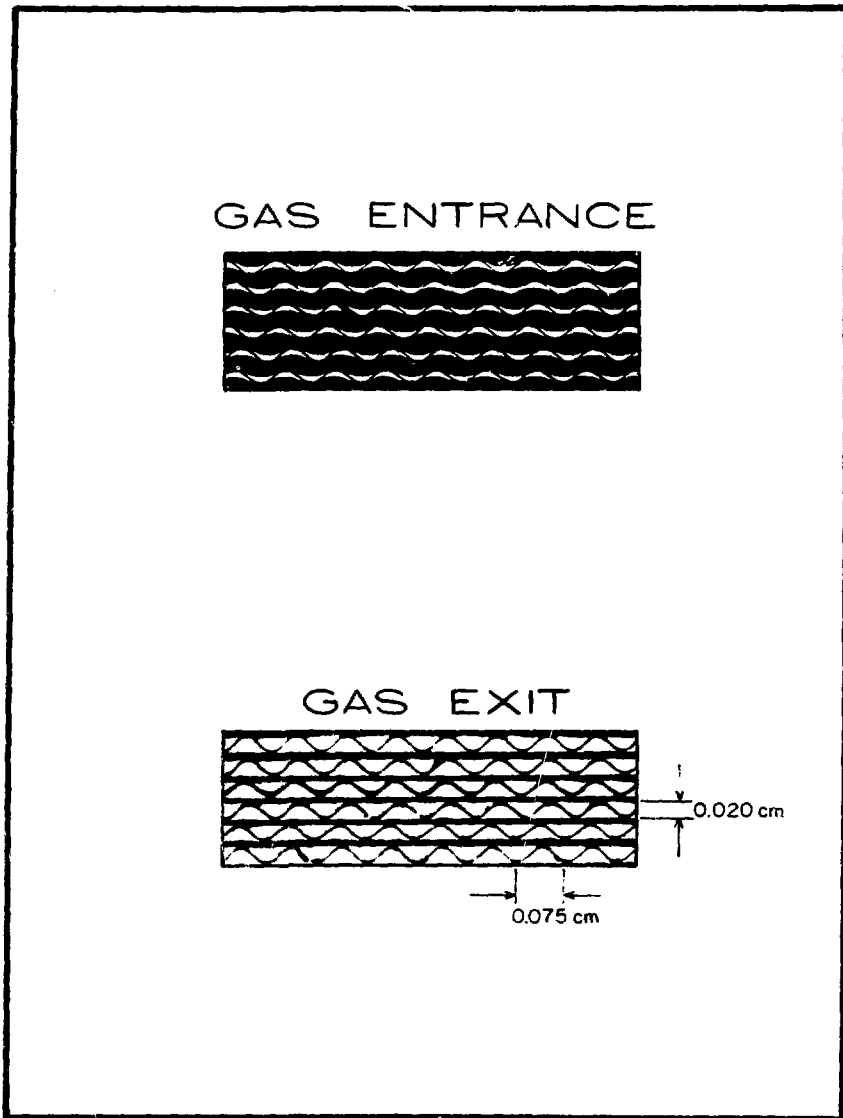


Fig. 1-10: A Photomicrograph of Assembled Wall Components. Microscopic study shows the irregular edges in the photomicrograph to be foreign matter, deposited by previous handling, and not constructional irregularities.

~~SECRET~~

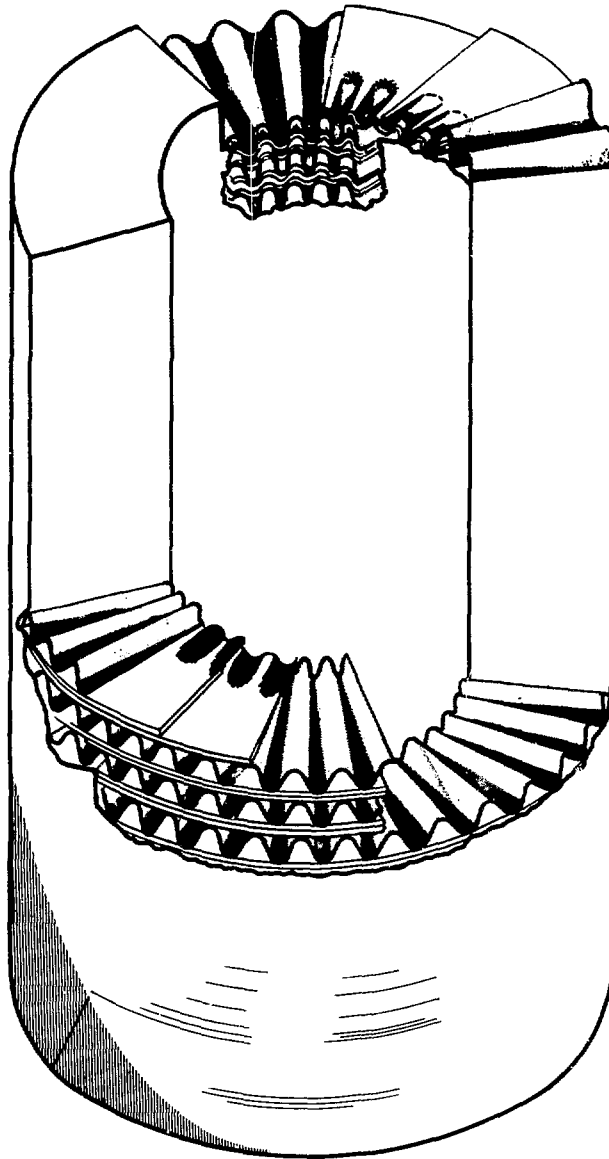


Fig. 1-11: A Dumbo Metal Tube. A schematic drawing distorted for clarity

tubes consist of such assemblies.

The moderator serves two purposes. Primarily, it moderates the reactor. Secondly, it prevents hot spotting of the metal wall. Details of this scheme are discussed in Chaps. 4 and 9. Moderator geometry is shown in Fig. 1-12. The moderator consists of polystyrene washers (flat rings) which are alternately stacked with Dural separator washers. The Dural washers, in conjunction with vertical ridges molded into the plastic, form a small box or "mosaic cell" which serves as a manifold to 40 channels of the Dumbo wall. Radial ducts are molded into the plastic washers as shown. In order to improve the thermal conductivity of the moderator, magnesium is distributed through the plastic.

#### 1-4: Flow in the Heat Exchanger

The heat transfer process in Dumbo is novel, in that the gas flow in the heat exchanger is laminar. This is the first serious attempt to transfer large amounts of energy to a gas moving in a non-turbulent or smooth manner. The laminar type of flow and the short length of flow path in the heat exchanger, 1 cm, results in a small pressure drop, typically 0.3 bar,\* across the heat exchanger. This type of heat exchanger has the following desirable features:

- (1) It is made of thin metal foil, which has the advantages that:

---

\*1 bar =  $10^6$  dynes/cm<sup>2</sup> = 0.98692 atmospheres.

~~SECRET~~

Chapter 1

Introduction

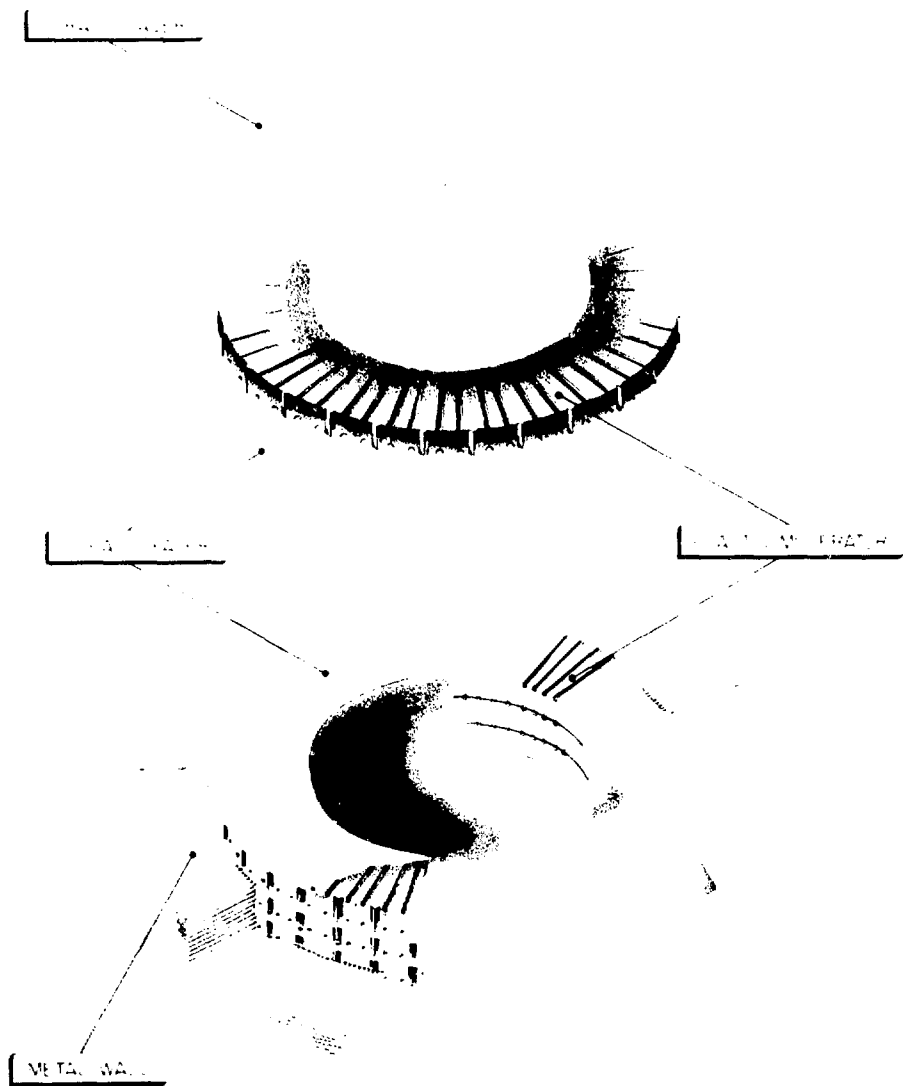


Fig. 1-12: A Dumbo Tube Assembly (not to scale)

~~SECRET~~

- 
- (a) The surface temperature of the foil differs from the maximum interior temperature by less than one degree.
  - (b) The heat capacity is so small that the response time of the exchanger is about one microsecond.
  - (c) The heat-exchanger walls are chemically inert to hydrogen or ammonia propellants.
  - (d) The heat transfer surface is 5,900,000 cm<sup>2</sup> and the exchanger is 75% gas passage.
- (2) It has a small pressure drop, which has the advantages that:
- (a) The tensile strength requirements are modest, permitting operation close to the melting point of the usable metals (2923 - 3623°K).
  - (b) The choice of operating pressure is flexible throughout the range, 10 - 100 bar.
  - (c) Other flow impedances may serve to assure proper flow uniformity throughout the reactor. The flow through the heat exchanger is regulated by the larger impedance of the moderator region where the pressure drop is 1.9 bar.
- (3) Its performance is calculable from basic hydrodynamic principles, which has the advantage that:
- (a) The heat exchanger is designed without experimental heat-transfer tests.

~~SECRET~~

Chapter 1

Introduction

---

- (b) The stability of the flows is examined theoretically, and the conditions assuring this stability are obtained without empirical tests.
- (4) It is an efficient heat exchanger, which has the advantages that:
  - (a) The gas is heated to temperatures within 200 degrees of the maximum working temperatures of the refractory metals.
  - (b) Design of the reactor is not limited by optimization of the heat exchanger.
- (5) It has a folded gas flow path, which has the advantages that:
  - (a) There are cool regions throughout the reactor into which plastic moderator is placed.
  - (b) Space is efficiently used, resulting in a compact, lightweight reactor of high power density.
  - (c) No local adjustment of flows is necessary.
  - (d) The flow area of the heat exchanger is great, and the channels of the metal wall are small. Consequently, a small sample of this wall of only 0.03 cm<sup>3</sup> volume is representative in performance tests. Tests of the heat exchanger require only 1200 watts power.

1-5: Choice of Propellant

Two attractive nuclear rocket propellants, compatible with metal reactors, are hydrogen and ammonia. In this report, hydrogen is used

for the following reasons:

(a) The chemical and physical properties of hydrogen are well understood over the range of temperature employed.<sup>10</sup> Ammonia is thermally decomposed in the heat exchanger, and data are not available to predict the kinetics of this reaction. The methods used to compute the transport properties for hydrogen<sup>10,11</sup> could be used to predict the viscosity, the thermal conductivity, and diffusion coefficients of three-component mixture H<sub>2</sub>, N<sub>2</sub>, and NH<sub>3</sub>.

(b) In the last few years the technology for handling large quantities of liquid hydrogen has been highly advanced and large-scale use of liquid hydrogen is no longer a formidable problem.

Both hydrogen and ammonia should work in Dumbo systems since neither of these materials presents a chemical corrosion problem with the refractory metals.

#### 1-6: Neutronics

The Dumbo reactor has uniform power generation (+7%) as well as uniform neutron flux, using uniform loading and construction. This is achieved by adjusting the reflector thickness, amount of UO<sub>2</sub>, and amount of polystyrene moderator. The amount of hydrogenous propellant in the reactor does not change the reactivity appreciably, since the system is already highly moderated. The Doppler broadening of the neutron resonances of the refractory metals acts as a built-in negative temperature

~~SECRET~~

Chapter 1

Introduction

---

coefficient and helps control the reactivity.

The damage to the refractory metals, as well as to the polystyrene, by neutrons and gamma rays is considered.

1-7: The Report

The analysis of Dumbo is given in sufficient detail to show the degree to which such a system may be designed, starting from well-known physical principles. The calculations are complete aside from intermediate steps of a routine nature. Much of the mathematical material of the report, while oriented toward the development of Dumbo, is equally applicable to a wide variety of rocket reactor designs. For the most part, this material is new and is presented in a general manner.

In Chap. 2 the subject of laminar-flow heat exchange for a steady state is developed. The basic physical equations are presented and from them are developed practical expressions for the flow of propellant and transfer of heat. The relations between channel geometry, pressure drop, and heat transfer are investigated, and methods of high precision are given for calculations involving particular geometries.

In Chap. 3 the stability of flow in the heat exchanger is considered. The requirements for stability are given, means of insuring stability are presented, and a design is given which is intrinsically stable.

In Chap. 4 the temperature distribution in the heat exchanger is considered. The temperature distribution is worked out for (a) a Dumbo

~~SECRET~~



wall which is perfectly constructed, (b) a Dumbo wall with one blocked channel, (c) a Dumbo wall with random construction errors, and (d) a Dumbo wall segmented into mosaic cells.

In Chap. 5 it is shown that effects due to the evaporation of hot metal into the flowing stream of propellant are negligible.

In Chap. 6 the device is considered as a nuclear reactor. The conditions are worked out for a uniform power generation in all fuel elements, which are of a single standard construction with uniform uranium loading. Calculations of criticality are presented for such reactors, involving reactor cores containing large quantities of refractory metals.

In Chap. 7 the hydrodynamic and heat-exchange problems not covered in Chap. 2 are considered. Conditions are found which give a highly uniform flow of propellant through the whole exchanger.

In Chap. 8 the properties of the materials from which Dumbo is built are considered, under the conditions of operation. The methods involved in fabricating the Dumbo wall are also discussed.

In Chap. 9 complete numerical designs of four models that satisfy the requirements of heat transfer, neutronics, and hydrodynamics are presented.

Chapter 10 is of a concluding nature. It lists several variants on the Dumbo design and some other possible used of reactors of this type. A potential developmental program for Dumbo is described.

There are five appendices of material supplementary to the main body of the report.

## REFERENCES

1. A. E. Ruark, et al., Nuclear Powered Flight, The Applied Physics Laboratory of The John Hopkins University, APL/JHU-TG-20, Jan. 14, 1947.
2. H. S. Seifert and M. M. Mills, Problems in the Application of Nuclear Energy to Rocket Propulsion, Jet Propulsion Laboratory, California Institute of Technology, JPL-Memo-3-4, Jan. 23, 1947.
3. Feasibility of Nuclear Powered Rockets and Ramjets, North American, NA 47-15, Feb. 11, 1947.
4. R. W. Bussard, Nuclear Energy for Rocket Propulsion, Union Carbide Nuclear Co., Reactor Science and Technology, TID-2011, Dec. 1953.
5. W. C. Cooley, Conceptual Design of a Nuclear-Powered Ballistic Missile, General Electric Aircraft Nuclear Propulsion Project, GE-ANP, XDC-55-2-20, Feb. 1955.
6. The Feasibility of Nuclear-Powered Long Range Ballistic Missiles, Los Alamos Scientific Laboratory Report LAMS-1870, March 1955.
7. E. S. Robinson, B. B. McInteer, R. M. Potter, The Epidermal Rocket Motor, Los Alamos Memorandum CMR-4-615, April 15, 1955 (internal memorandum).
8. B. B. McInteer, R. M. Potter, E. S. Robinson, Dumbo -- A Pachydermal Rocket Motor, Los Alamos Scientific Laboratory Report LAMS-1887, May 18, 1955.
9. R. W. Bussard, Nuclear Powered Rockets: A Historical Survey and Literature Summary, Appendix to Los Alamos Scientific Laboratory Report LAMS-2036, August 17, 1955, R. E. Schreiber.
10. W. A. Blanpied, Some Transport and Equilibrium Properties of Hydrogen at High Temperatures and Pressures, Los Alamos Scientific Laboratory Report LA-1937, July 1955.

~~SECRET~~

The Report

---

Section 1-7

11. J. O. Hirschfelder, Charles F. Curtiss, R. Byron Bird, Molecular Theory of Gases and Liquids, John Wiley and Sons, Inc., New York, 1954.

~~SECRET~~



CHAPTER 2

FLOW AND HEAT TRANSFER

He asked his tall uncle, the Giraffe, what made his skin spotty, and his tall uncle, the Giraffe, spanked him with his hard, hard hoof.

R. Kipling, The Elephant's Child

2-1: Introduction

In determining the performance and design requirements of a laminar-flow heat-exchanging system, three quantities are of particular interest:

- (1) The total flow Q, or the average flow density  $\bar{J} = Q/A$

$$Q = \int J dA$$

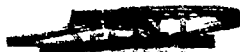
$$\bar{J} = \frac{1}{A} \int J dA \tag{2-1}$$

where A is the cross-sectional area of the channel and J is the flux.

- (2) The average temperature  $\bar{T}$  over a cross section

$$\bar{T} = \frac{1}{A} \int T dA \tag{2-2}$$

- (3) The weighted gas temperature  $T_g$  whose value satisfies the relation  $Q \cdot c T_g(z)$  equals the transport of internal energy, where z measures distance from the cold end of a duct of length w and c is the specific heat of the gas at constant pressure. Thus  $T_g(w)$  will be the final



~~SECRET~~

temperature of gas delivered from the exchanger. Summing the energy flow density over the cross-sectional area, we have

$$Q c T_g = \int J c T dA \quad (2-3)$$

Hence

$$T_g = \frac{1}{Q} \int J T dA \quad (2-4)$$

These integrated quantities evidently may be determined if we know the flow and temperature functions,  $J$  and  $T$ , which in turn must be determined from the basic relations which they satisfy.

In this chapter we derive methods of evaluating these quantities. Section 2-2 presents the necessary equations in a form which is exact but intractable for calculation except by numerical methods. In Sec. 2-3 the familiar linearized equations of fluid flow and heat transfer are derived. The subsequent sections present analytic methods of evaluation: an exact solution, a more general solution for limiting cases, an iterative technique, and a set of variational methods.

### 2-2: Basic Relations

Laws governing the flow and energy transport of a fluid have been formulated by Hirschfelder et al.<sup>1</sup> The equation of continuity is

$$\frac{\partial \rho}{\partial t} = - \partial_{\mu} \rho V_{\mu} \quad (2-5)$$

~~SECRET~~

where  $\rho$  is the density,  $t$  is the time, and  $V_\mu$  is the  $\mu$ -component of the velocity,  $\vec{V}$ . The tensor convention of summation over repeated indices is assumed. The equation of motion of the fluid is

$$\frac{\partial V_\mu}{\partial t} + V_\nu \partial_\nu V_\mu = -\frac{1}{\rho} \partial_\nu P_{\mu\nu} \quad (2-6)$$

where the stress tensor  $P_{\mu\nu}$  is given by

$$P_{\mu\nu} = p \delta_{\mu\nu} - \eta \left( \partial_\mu V_\nu + \partial_\nu V_\mu \right) + \left( \frac{2}{3} \eta - k \right) \partial_\lambda V_\lambda \delta_{\mu\nu} \quad (2-7)$$

Here  $p$  is the hydrostatic pressure,  $\eta$  the coefficient of shear viscosity, and  $k$  the coefficient of bulk viscosity.

The equation of energy balance is

$$\frac{\partial u}{\partial t} + V_\mu \partial_\mu u = -\frac{1}{\rho} \partial_\mu (q_\mu + R_\mu) - \frac{1}{\rho} P_{\mu\nu} \partial_\mu V_\nu \quad (2-8)$$

where  $u$  is the internal energy per gram, and  $q_\mu$  and  $R_\mu$  are the components of  $\vec{q}$  and  $\vec{R}$ , the energy fluxes conducted and radiated, respectively.

Although it is not appropriate to reproduce the development of these relations here, it is worthwhile to realize their origin. Equation 2-7 comes from the linearity and symmetry relations that arise from the thermodynamics of irreversible processes, based upon Onsager's "reciprocal relations" theorem. One important restriction here is that the microscopic thermodynamic situation be not too far removed from equilibrium. Equation 2-6 is a restatement of the second law of

~~SECRET~~

classical mechanics for a hydrodynamic medium. Equations 2-5 and 2-8 are formalized statements of matter and energy conservation.

The equations may be simplified at once in three respects: in a steady-state situation all time derivatives vanish; and in a gas such as hydrogen, which is both non-polar and transparent, both  $k$  and  $\frac{\partial R}{\partial \mu}$  vanish also.

2-3: Physical Approximation of the Equations

The functions  $T$  and  $\vec{J} = \rho \vec{V}$  are determined in principle by these equations together with the equations for  $\rho$ ,  $\eta$ ,  $u$ , and  $\vec{q}$ . With a specified geometry and specified rates of power generation and fluid flow, the quantities of interest to us should be obtainable to any desired accuracy by solving these equations numerically. However, for purposes of a general investigation, numerical results are far less useful than explicit analytic relationships. For this reason we will make some approximations to bring these equations to a form which is analytically more tractable, without heavily sacrificing physical accuracy.

At the outset we confine our attention to channels of uniform cross section, and of length very large compared to the wall to wall distance. In such a case the flow is constrained to be substantially parallel to the axis of the channel, the  $z$  axis. Thus  $V_x = V_y = 0$ . Moreover, if the total change in  $V_z$  takes place slowly over a very long tube, then

~~SECRET~~

$\partial V_z / \partial z = 0$ , and Eq. 2-6 reduces to

$$\frac{\partial}{\partial x} P_{zx} + \frac{\partial}{\partial y} P_{zy} + \frac{\partial}{\partial z} P_{zz} = 0 \quad (2-9)$$

Under the same conditions the stress-tensor (Eq. 2-7) similarly simplifies to

$$P_{zy} = -\eta \frac{\partial V_z}{\partial y}$$

$$P_{zx} = -\eta \frac{\partial V_z}{\partial x}$$

$$P_{zz} = p \quad (2-10)$$

Combining Eqs. 2-9 and 2-10 yields

$$\frac{\partial}{\partial x} \eta \frac{\partial V_z}{\partial x} + \frac{\partial}{\partial y} \eta \frac{\partial V_z}{\partial y} = \frac{\partial p}{\partial z} \quad (2-11)$$

If we now limit ourselves to the more usual cases, the relative variations in  $\eta$  and  $p$  over distances of the order of a channel diameter are small. Equation 2-11 may be brought to the final form

$$\nabla^2 J = \frac{\rho}{\eta} \frac{\partial p}{\partial z} \quad (2-12)$$

where  $\nabla^2$  involves only the variables  $x$  and  $y$ .



~~SECRET~~

Chapter 2

Flow and Heat Transfer

From Eq. 2-7 we may form the quantity

$$P_{\mu\nu} \partial_{\mu} V_{\nu} = \rho \partial_{\mu} V_{\mu} - \Phi$$

where

$$\Phi = \eta (\partial_{\mu} V_{\nu} + \partial_{\nu} V_{\mu}) \partial_{\mu} V_{\nu} - \left(\frac{2}{3} \eta - k\right) (\partial_{\mu} V_{\mu})^2 \quad (2-13)$$

Here the positive quantity  $\Phi$ , the dissipation function, is the power-density due to viscous effects, its two terms corresponding, respectively, to work done against shearing forces and compressional viscous effects. By use of Eq. 2-13, Eq. 2-8 may be recast into vector notation,

$$(\vec{V} \cdot \nabla) u = -\frac{1}{\rho} \nabla \cdot \vec{q} - \frac{1}{\rho} \rho \nabla \cdot \vec{V} + \frac{1}{\rho} \Phi \quad (2-14)$$

A rearrangement of terms gives

$$\rho \vec{V} \cdot \nabla \left(u + \frac{p}{\rho}\right) = -\nabla \cdot \vec{q} + \vec{V} \cdot \nabla p + \Phi \quad (2-15)$$

The quantity  $u + \frac{p}{\rho}$  is the enthalpy per gram of the gas. For hydrogen this quantity is insensitive to pressure and may be regarded as a function of temperature only. Hence

$$u + \frac{p}{\rho} = \int_{T_0}^T c_p(T') dT' = \bar{c}_p(T - T_0) \quad (2-16)$$

where  $T_0$  is some reference temperature. The heat-flow vector is given by

$$\vec{q} = -\lambda \nabla T. \quad (2-17)$$

~~SECRET~~

~~SECRET~~

where  $\lambda$  is the thermal conductivity of the gas. Substituting these expressions back into Eq. 2-15 and specializing to our channel geometry as before gives

$$\rho V_z \frac{\partial}{\partial z} \bar{c}_p T = \nabla \cdot (\lambda \nabla T) + V_z \frac{\partial p}{\partial z} + \Phi \quad (2-18)$$

We limit our consideration to exchangers where the heat transfer per second is very large compared either to the dissipation function  $\Phi$  or to the rate of work due to moving material across a pressure gradient, so that  $V_z \frac{\partial p}{\partial z} + \Phi$  will be negligible. Let us also make the same assumptions for  $\bar{c}_p (=c)$  and  $\lambda$  as we have for  $\eta$  and  $\rho$  above. Then Eq. 2-18 becomes

$$\nabla^2 T = \left( \frac{c}{\lambda} \frac{\partial T}{\partial z} \right) J \quad (2-19)$$

The temperature may be written in terms of its boundary value,  $T_b$ .

$$T = T_b(z) + \Theta(x,y) \quad (2-20)$$

If  $\Theta$  is small compared to  $T$ , then the  $z$  dependence of  $T$  must lie primarily in  $T_b$ ; further, if the power distribution in the channel is uniform,  $T_b$  depends nearly linearly on  $z$ , and Eq. 2-19 becomes

$$\nabla^2 \Theta = \left( \frac{c}{\lambda} \frac{\partial T_b}{\partial z} \right) J \quad (2-21)$$

~~SECRET~~

where  $\nabla^2$  now only involves the variables  $x$  and  $y$  as was the case in Eq. 2-12.

To summarize, our problem has been reduced to solving the two-dimensional equations

$$\nabla^2 J = -\kappa$$

where

$$\kappa(z) = -\frac{\rho}{\eta} \frac{\partial p}{\partial z} \quad (2-22)$$

and

$$\nabla^2 \Theta = \beta J$$

where

$$\beta(z) = \frac{c}{\lambda} \frac{\partial T_b}{\partial z} \quad (2-23)$$

with the conditions that both  $J$  and  $\Theta$  vanish at the boundary of the channel. These are particular cases of Poisson's equation in two dimensions. Once a solution has been obtained we may check back on the validity of our approximations.

#### 2-4: The Circular Channel

Flow and heat transfer results can be obtained exactly for a circular channel (to within the approximations of Eqs. 2-22 and 2-23) and have often been presented previously.<sup>2,3</sup> They are developed here

~~SECRET~~

The Circular Channel

Section 2-4

as an illustrative preliminary example, and to present the results within the framework of our present notation.

In radial coordinates Eq. 2-22 becomes

$$\frac{1}{r} \frac{\partial}{\partial r} r \frac{\partial J}{\partial r} = -\kappa \quad (2-24)$$

whose solution for a channel of diameter  $\alpha$  will be

$$J = -\frac{\kappa}{4} \left( r^2 - \frac{\alpha^2}{4} \right) \quad (2-25)$$

which gives

$$Q = \frac{\pi \kappa \alpha^4}{128}$$
$$\bar{J} = \frac{\kappa \alpha^2}{32} \quad (2-26)$$

Similarly by Eq. 2-23, the temperature distribution is given by

$$\frac{1}{r} \frac{\partial}{\partial r} r \frac{\partial \Theta}{\partial r} = -\frac{\kappa \beta}{4} \left( r^2 - \frac{\alpha^2}{4} \right) \quad (2-27)$$

from which

$$\Theta = -\frac{\kappa \beta}{64} \left[ r^4 - \alpha^2 r^2 + \frac{3\alpha^4}{16} \right] \quad (2-28)$$

~~SECRET~~



whence

$$\bar{\Theta} = -\frac{\beta \kappa a^4}{760}$$

$$\Theta_g = -\frac{11\beta \kappa a^4}{6144}$$

$$\Theta_{\min} = -\frac{3\beta \kappa a^4}{1024}$$

(2-29)

These results are considered further in Sec. 2-5.

#### 2-5: The Thin Channel Approximation

A convenient approximation for the flow problem is the "thin channel" approximation, in which Eq. 2-22 written as

$$\frac{\partial^2 J}{\partial x^2} + \frac{\partial^2 J}{\partial y^2} = -\kappa \quad (2-30)$$

is simplified by neglecting the x derivative. The resulting relation

$$\frac{\partial^2 J}{\partial y^2} = -\kappa \quad (2-31)$$

is to be solved subject to the condition that J shall vanish at the boundaries,  $Y_1(x)$  and  $Y_2(x)$ . (See Fig. 2-1.) The solution of Eq. 2-31 is immediate.

$$J = -\frac{\kappa}{2} (y - Y_1)(y - Y_2) \quad (2-32)$$



~~SECRET~~

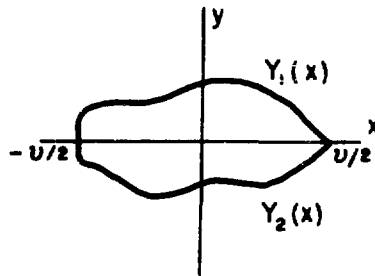


Fig. 2-1

Note that the local parabolic flow distribution is inherent in this treatment. This result is an exact solution of Eq. 2-22 for parallel plates. We may thus regard this approximation as a local fit to the parallel plate result.

The total flow defined by

$$Q = \int_{-u/2}^{u/2} \int_{Y_2}^{Y_1} J(x,y) dy dx \quad (2-33)$$

is given by

$$Q = \frac{\kappa}{12} \int_{-u/2}^{u/2} (Y_1 - Y_2)^3 dx \quad (2-34)$$

These results become simplified for thin channels bounded below by a

~~SECRET~~

~~SECRET~~

flat plate, so that  $Y_2 = 0$ . In this case

$$J = -\frac{\kappa}{2} y (y - Y_1) \quad (2-35)$$

$$Q = \frac{\kappa}{12} \int_{-u/2}^{u/2} Y_1^3 dx \quad (2-36)$$

Using the same approximation for the temperature distribution, Eq. 2-23 becomes

$$\frac{\partial^2 \Theta}{\partial y^2} = \beta J \quad (2-37)$$

which may be integrated at once if  $J$  is known. We substitute the value of  $J$  obtained from Eq. 2-35 to obtain

$$\frac{\partial^2 \Theta}{\partial y^2} = -\frac{\beta \kappa}{2} y (y - Y_1)$$

$$\Theta(x, 0) = \Theta(x, Y_1) = 0 \quad (2-38)$$

which integrates to

$$\Theta(x, y) = -(\beta \kappa / 24) y (y - Y_1) (y^2 - Y_1 y - Y_1^2) \quad (2-39)$$

Integration of  $\Theta$  yields for the average temperature

$$\bar{\Theta} = -(\beta \kappa / 120A) \int_{-u/2}^{u/2} Y_1^3 dx$$

~~SECRET~~

~~SECRET~~

where

$$A = \int_{-v/2}^{v/2} Y_1 dx \quad (2-40)$$

The value of  $\Theta_g$  may be obtained similarly

$$\Theta_g = - (17 \kappa^2 / 20,160 Q) \int_{-v/2}^{v/2} Y_1^7 dx \quad (2-41)$$

where  $Q$  is given by Eq. 2-36. Another temperature that is interesting for comparison purposes is  $\Theta_{\min}$ , the extreme temperature difference between fluid and wall on the given cross section.

We will consider as examples (Fig. 2-2) three channel shapes, all of height  $\alpha$  and width  $v$  to be treated in this manner. For comparison a circular channel of diameter  $\alpha$  has been solved exactly. Of course, the solutions of Example 1 are also exact.

For all the thin channels considered here this temperature is located at  $x = 0, y = \alpha/2$ . Inserting these coordinates into Eq. 2-39 gives the value

$$\Theta_{\min} = - \frac{5}{384} \beta \kappa a^4 = - 0.0130 \beta \kappa a^4 \quad (2-42)$$

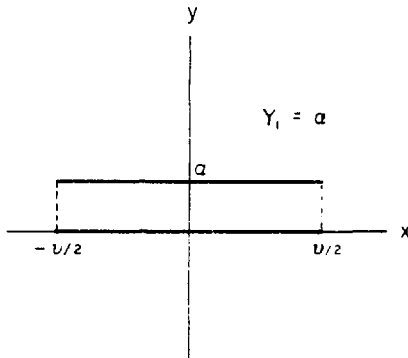
For the various geometries considered here we obtain the following results:

Table 2-1 indicates the values of  $A, Q,$  and  $\bar{J}$  for specified dimensions,  $\alpha$  and  $v,$  and the "pressure drop",  $\kappa.$  Thus for the same values of

~~SECRET~~

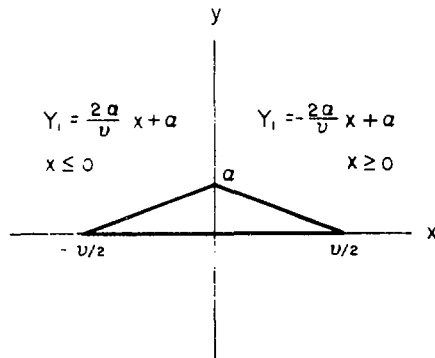


42



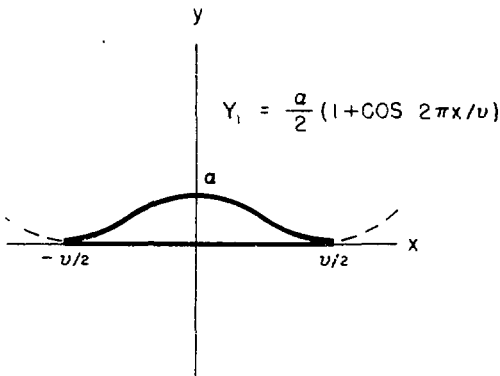
EXAMPLE 1

PARALLEL PLATES OR  
THIN RECTANGULAR CHANNEL



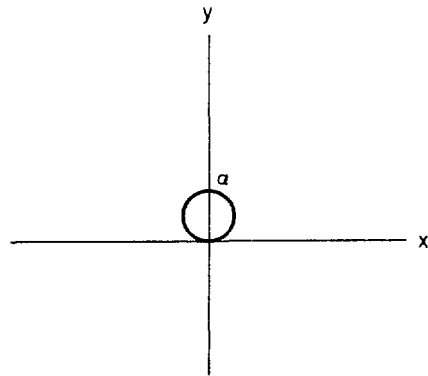
EXAMPLE 2

TRIANGULAR CHANNEL  
(THIN)



EXAMPLE 3

SINUSOIDAL CHANNEL  
(THIN)



EXAMPLE 4

CIRCULAR CHANNEL

Fig. 2-2: Examples of Channel Shapes

42

~~SECRET~~

these parameters the flow density  $\bar{J}$  is largest for the parallel plates (or thin rectangle).  $\bar{J}$  is smallest in the circular channel. For thin triangular and sinusoidal channels  $\bar{J}$  is intermediate.

Table 2-2 presents values of the temperatures  $\Theta_{\min}$ ,  $\bar{\Theta}$ , and  $\Theta_g$  for specified values of  $\kappa$ ,  $\beta$ , and  $\alpha$ . In terms of these parameters,  $\Theta_{\min}$  possesses the same value for the three thin channels, but  $\Theta_{\min}$  is much less for the circular channel.  $\bar{\Theta}$  and  $\Theta_g$  show this same pattern in comparing the thin channels with the circular one. The temperatures of the shaped thin channels are more uniform, however, than the temperatures of the thin rectangular one.

Table 2-3 presents the temperatures  $\Theta_{\min}$ ,  $\bar{\Theta}$ , and  $\Theta_g$  in terms of the  $\bar{J}$  results of Table 2-1, allowing the physical dimension  $\alpha$  to be eliminated. These quantities thus relate general heat exchange relations of pressure drops and temperature drops in terms of channel shapes but not of channel size. The quantities listed in this table are of order unity.

Table 2-4 presents the ratios  $\bar{\Theta}/\Theta_{\min}$ ,  $\Theta_g/\Theta_{\min}$ , and  $\Theta_g/\bar{\Theta}$ . The latter ratio is particularly surprising in that the values for shaped thin channels are not intermediate between the thin rectangle and the circular channel results. These results allow little hope that  $\Theta_g$  may be predicted accurately from the simpler quantity  $\bar{\Theta}$  for shaped channels.

Table 2-5 considers the case when the pressure drop,  $\kappa$ , is not of interest, but presents  $\bar{\Theta}$  and  $\Theta_g$  in terms of  $\beta$ ,  $\alpha$ , and  $\bar{J}$ . Thus, for

~~SECRET~~

TABLE 2-1  
**FLOWS AND AREAS IN TERMS OF  $\kappa, a, v$**

Ex	SHAPE	AREA, A	TOTAL FLOW, Q	AVG. FLOW DENSITY, $\bar{j}/\kappa a^2$
1	PARALLEL PLATES	$av$	$\kappa a^3 v/12$	1/12 (0.0833)
2	TRIANGULAR CHANNEL	$av/2$	$\kappa a^3 v/48$	1/24 (0.0416)
3	SINUSOIDAL CHANNEL	$av/2$	$5\kappa a^3 v/192$	5/96 (0.0521)
4	CIRCULAR CHANNEL	$\pi a^2/4$	$\pi \kappa a^4/128$	1/32 (0.0313)

TABLE 2-2  
**TEMPERATURES IN TERMS OF  $\kappa, \beta, a$**

Ex	SHAPE	$-\Theta_{\min}/\beta \kappa a^4$	$-\bar{\Theta}/\beta \kappa a^4$	$-\Theta_g/\beta \kappa a^4$
1	PARALLEL PLATES	5/384 (0.0130)	1/120 (0.00833)	17/1680 (0.0101)
2	TRIANGULAR CHANNEL	5/384 (0.0130)	1/360 (0.00278)	17/3360 (0.00506)
3	SINUSOIDAL CHANNEL	5/384 (0.0130)	21/5120 (0.00410)	2431/358,400 (0.00679)
4	CIRCULAR CHANNEL	3/1024 (0.00293)	1/760 (0.00131)	11/6144 (0.00179)

~~SECRET~~

TABLE 2-3  
TEMPERATURES IN TERMS OF  $\bar{J}$ ,  $\kappa$ ,  $\beta$

Ex	SHAPE	$-\frac{\kappa \bar{\Theta}}{\beta \bar{J}^2}$	$-\frac{\kappa \Theta_g}{\beta \bar{J}^2}$
1	PARALLEL PLATES	1.20	1.46
2	TRIANGULAR CHANNEL	1.60	2.91
3	SINUSOIDAL CHANNEL	1.51	2.50
4	CIRCULAR CHANNEL	1.35	1.83

TABLE 2-4  
 $\Theta_{\min}$ ,  $\bar{\Theta}$ ,  $\Theta_g$  IN TERMS OF EACH OTHER

Ex	SHAPE	$\frac{\bar{\Theta}}{\Theta_{\min}}$	$\frac{\Theta_g}{\Theta_{\min}}$	$\frac{\Theta_g}{\bar{\Theta}}$
1	PARALLEL PLATES	0.64	0.78	1.21
2	TRIANGULAR CHANNEL	0.21	0.39	1.82
3	SINUSOIDAL CHANNEL	0.32	0.52	1.65
4	CIRCULAR CHANNEL	0.45	0.61	1.37

~~SECRET~~

TABLE 2-5  
TEMPERATURES IN TERMS OF  $\bar{J}$ ,  $\beta$ ,  $\alpha$ 

Ex	SHAPE	$-\frac{\bar{\theta}}{\beta \alpha^2 \bar{J}}$	$-\frac{\theta_g}{\beta \alpha^2 \bar{J}}$
1	PARALLEL PLATES	0.100	0.121
2	TRIANGULAR CHANNEL	0.066	0.121
3	SINUSOIDAL CHANNEL	0.079	0.130
4	CIRCULAR CHANNEL	0.042	0.057

fixed values of these parameters,  $\Theta_g$  is sensibly equal for all three thin channels but is much less for the circular channel.

### 2-6: Higher Approximations

The thin channel results may be refined to obtain more precise results in the following way. Consider the differential recursion formula

$$\frac{\partial^2 J^{(n)}}{\partial y^2} = -\kappa - \frac{\partial^2 J^{(n-1)}}{\partial x^2}$$

$$J^{(n)}(Y_1) = J^{(n)}(Y_2) = 0 \quad (2-43)$$

by which  $J^{(n)}$  may be determined if  $J^{(n-1)}$  is already known. If, as  $n \rightarrow \infty$ , the sequence of  $J^{(n)}$  converges to a limiting function  $J$  with sufficient uniformity, then evidently  $J$  will be a solution of Eq. 2-22. For  $J^{(1)}$  the thin channel approximation may be used.

The technique is well demonstrated by the case of a semi-infinite duct for which  $Y_1 = cx$ ,  $Y_2 = -cx$ . Following the program outlined above

~~SECRET~~

$$J^{(0)} = 0$$

$$\frac{\partial^2 J^{(1)}}{\partial y^2} = -\kappa$$

$$J^{(1)} = \frac{1}{2} \kappa (c^2 x^2 - y^2)$$

$$\frac{\partial^2 J^{(2)}}{\partial y^2} = -\kappa (1 + c^2)$$

$$J^{(2)} = \frac{1}{2} \kappa (1 + c^2) (c^2 x^2 - y^2)$$

$$J^{(n)} = \frac{1}{2} \kappa \left[ \sum_{s=0}^{n-1} c^{2s} \right] (c^2 x^2 - y^2)$$

$$J^{(\infty)} = \frac{1}{2} \kappa \frac{1}{1-c^2} (c^2 x^2 - y^2) \tag{2-44}$$

The function  $J^{(\infty)}$  is indeed the solution of Eq. 2-22 with the imposed boundary conditions. Notice, however, that the sequence of  $J^{(n)}$  converges only if  $c < 1$ .

Returning to the more general case, and considering only problems with  $Y_2 = 0$ ,  $Y_1 = Y$ , one finds

~~SECRET~~

$$\begin{aligned} J^{(1)} &= -\frac{\kappa}{2} y(y-Y) \\ J^{(2)} &= -\frac{\kappa}{2} y(y-Y) - \frac{\kappa Y''}{12} y(y^2-Y^2) \\ J^{(3)} &= -\frac{\kappa}{2} y(y-Y) - \kappa \left[ \frac{Y''}{12} + \frac{Y'''' Y^2}{72} + \frac{Y''' Y' Y}{18} + \frac{(Y''')^2 Y}{36} \right. \\ &\quad \left. + \frac{Y''(Y')^2}{36} \right] y(y^2-Y^2) + \frac{\kappa}{240} Y'''' y(y^4-Y^4) \end{aligned} \quad (2-45)$$

where primes indicate differentiation with respect to  $x$ .  $Q^{(3)}$  is obtained as in Eq. 2-33.

$$Q^{(3)} = \int_{-Y/2}^{Y/2} \left\{ \frac{\kappa}{12} Y^3 + \frac{\kappa}{4} \left[ \frac{Y''}{12} + \frac{Y'''' Y^2}{120} + \frac{Y''' Y' Y}{18} + \frac{(Y''')^2 Y}{36} + \frac{Y''(Y')^2}{36} \right] Y^4 \right\} dx \quad (2-46)$$

A similar procedure may be applied to Eq. 2-23

$$\frac{\partial^2 \Theta^{(n)}}{\partial y^2} = \beta J(x, y) - \frac{\partial^2 \Theta^{(n-1)}}{\partial x^2} \quad (2-47)$$

This procedure requires some approximate function for  $J(x, y)$ . We have chosen  $J^{(2)}$  of Eq. 2-45. Neglecting the term  $\partial^2 \Theta / \partial x^2$  yields the result

$$\begin{aligned} \Theta^{(1)} &= -\frac{\beta \kappa}{24} y(y^3-Y^3) + \frac{\beta \kappa}{12} Y y(y^2-Y^2) - \frac{\beta \kappa}{240} Y'' y(y^4-Y^4) \\ &\quad + \frac{\beta \kappa}{72} Y'' Y^2 y(y^2-Y^2) \end{aligned} \quad (2-48)$$

~~SECRET~~



~~SECRET~~

For the next approximation we obtain

$$\begin{aligned} \Theta^{(2)} = & -\frac{\beta \kappa}{24} y(y^3 - Y^3) - \frac{\beta \kappa y(y^2 - Y^2)}{6} \left[ -\frac{Y}{2} - \frac{5Y''Y^2}{24} - \frac{Y'^2Y}{4} - \frac{7Y''''Y^4}{720} \right. \\ & - \frac{7Y''Y'Y^3}{90} - \frac{7Y''Y'^2Y^2}{60} - \left. \frac{7(Y'')^2Y^3}{180} \right] - \frac{\beta \kappa y(y^4 - Y^4)}{20} \left[ \frac{Y''}{6} + \frac{Y''''Y^2}{72} \right. \\ & \left. + \frac{Y''''Y'Y}{36} + \frac{Y''Y'^2}{36} + \frac{Y''''Y'^2}{36} + \frac{(Y'')^2Y'}{36} \right] - \frac{\beta \kappa y(y^6 - Y^6)}{10,080} Y'''' \end{aligned} \quad (2-49)$$

$\bar{\Theta}$  is obtained by averaging over the region.  $\Theta_g$  is obtained by averaging the product  $J \cdot \Theta$  as given by Eqs. 2-45 and 2-49.

For sinusoidal channels of the form

$$Y = \frac{a}{2} \left[ 1 + \cos \frac{2\pi x}{v} \right] \quad (2-50)$$

performing the indicated operations of Eq. 2-46 yields

$$\begin{aligned} Q^{(3)} = & \frac{5\kappa a^3 v}{192} \left[ 1 - \frac{7}{80} (2\pi)^2 \left(\frac{a}{v}\right)^2 + \frac{41}{3200} (2\pi)^4 \left(\frac{a}{v}\right)^4 \right] \\ = & 0.026042 \kappa a^3 v \left[ 1 - 3.4544 \left(\frac{a}{v}\right)^2 + 19.9690 \left(\frac{a}{v}\right)^4 \right] \end{aligned} \quad (2-51)$$

~~SECRET~~

~~SECRET~~

From Eqs. 2-45 and 2-49 for sinusoidal channels there results

$$\bar{\Theta} = -0.0041015 a^4 \beta \kappa \left[ 1 - 7.7553 \left( \frac{a}{v} \right)^2 + 48.786 \left( \frac{a}{v} \right)^4 \right] \quad (2-52)$$

$$\Theta_g = -0.0067829 a^4 \beta \kappa \left[ 1 - 9.7287 \left( \frac{a}{v} \right)^2 \right] \quad (2-53)$$

For the other examples considered in Sec. 2-5, the parallel plate result was exact and the corrections involving derivatives of  $Y(x)$  thus vanish. The triangular channel, however, is such that  $Y''$  and higher derivatives are zero except at the apex ( $x = 0$ ), at which point they become infinite. Hence Eqs. 2-45 and 2-49 are not usable directly and the method is inapplicable.

#### 2-7: The Variational Method

In a situation involving unusual boundaries, where Poisson type partial differential equations are difficult to solve exactly, integrated quantities may frequently be estimated accurately by means of some variational principle. The flow and temperature problems have been treated by such a variational approach to investigate the general usefulness of the variational techniques. It will be shown that these techniques allow evaluation of the desired integrated quantities  $Q$ ,  $\bar{T}$ , and  $T_g$ .

Total Flow: The problem is to find the total flow  $Q$  through the area  $A$  where the mass flow  $J(x,y)$  satisfies

$$\nabla^2 J = -\kappa \quad (2-22)$$

~~SECRET~~

with the boundary condition

$$J|_b = 0$$

The variational principle depends on guessing a flow function

$$j = J + \delta j \quad (2-54)$$

which is close to the actual (unknown) function  $J$ .

Proceed in the following way: By dropping small terms beyond the lowest order, one has

$$\int (\nabla j)^2 dA = \int [(\nabla J)^2 + 2\nabla J \cdot \nabla \delta j] dA \quad (2-55)$$

which is identical to

$$\int (\nabla j)^2 dA = \int \nabla \cdot [J \nabla J + 2\delta j \nabla J] dA - \int [J \nabla^2 J + 2\delta j \nabla^2 J] dA \quad (2-56)$$

The first integral on the right may be transformed to the boundary by using the divergence theorem, and the second may be simplified by using the differential equation 2-22 for  $J$ , to obtain

$$\int (\nabla j)^2 dA = \int [J \nabla J + 2\delta j \nabla J] \cdot d\vec{s} + \kappa \int [J + 2\delta j] dA \quad (2-57)$$

Here  $d\vec{s}$  is normal to the boundary. If we choose a  $j$  which vanishes at the boundary, then  $\delta j$  will also vanish at the boundary, and so will the

whole surface integral. This gives

$$\int (\nabla j)^2 dA = \kappa (Q + 2\delta q) \quad (2-58)$$

From this a variational expression may be constructed as follows

$$q(j) = \kappa \frac{[\int j dA]^2}{\int (\nabla j)^2 dA} \quad (2-59)$$

To the first order

$$\begin{aligned} q(J + \delta j) &= \kappa \frac{[\int J dA + \int \delta j dA]^2}{\kappa (Q + 2\delta q)} \\ &= \frac{Q^2 + 2Q\delta q}{Q + 2\delta q} = Q \end{aligned} \quad (2-60)$$

Thus,  $q(J + \delta j)$  departs from the true flow  $Q$  only by higher order terms, and a good estimate of  $J$  should lead to a proportionately much better estimate of  $Q$ . For the correct  $J$ , of course, the value of  $Q$  will be exact.\*

A feature of the variational principle should be noted. One may multiply  $j$  by an arbitrary constant without affecting the value of  $q(j)$ . Thus one need guess only the shape of the function  $j$ . The size is taken care of automatically.

---

\*This variational principle was suggested by J. Tiemann, who credits it to L. I. Schiff.

~~SECRET~~

In order to get a tight-fitting trial function, one may pick a  $j = j(\epsilon)$  depending on a parameter  $\epsilon$ . Then, due to the variational principle's stationary property,  $\delta q(j) \Big|_{j=J} = 0$ , the fit will be optimized when

$$\frac{d}{d\epsilon} q[j(\epsilon)] \Big|_{\epsilon=\epsilon_0} = 0 \tag{2-61}$$

This is an equation which may be solved for  $\epsilon_0$ .

Average Temperature: As shown in Eq. 2-20 the temperature is given by  $T(x,y,z) = T_b(z) + \Theta(x,y)$ . The average temperature drop between the wall and the gas is given, from analogy with Eq. 2-2, by

$$\bar{\Theta} = \frac{1}{A} \int \Theta \, dA$$

Let

$$\Lambda = -\frac{1}{\beta} \Theta \tag{2-62}$$

Then

$$-\bar{\Theta} = \frac{\beta}{A} \int \Lambda \, dA = \frac{\beta}{A} H$$

where

$$H = \int \Lambda \, dA \tag{2-63}$$

and the differential equation 2-23 becomes

$$\nabla^2 \Lambda = -J \quad (2-64)$$

If we take the Laplacian of this equation, we obtain from Eq. 2-22

$$\nabla^4 \Lambda = \kappa \quad (2-65)$$

with the boundary conditions,

$$\Lambda|_b = 0$$

and

$$\nabla^2 \Lambda|_b = 0$$

The integral to be estimated is  $H$  of Eq. 2-63. Closely following the procedure for the flow integral, with  $h = H + \delta h$  and  $\lambda = \Lambda + \delta \lambda$ , one may demonstrate that the proper variational expression is

$$h(\lambda) = \kappa \frac{[\int \lambda dA]^2}{\int (\nabla^2 \lambda)^2 dA} \quad (2-66)$$

The value of the denominator of this expression is, to first order terms

$$\int (\nabla^2 \lambda)^2 dA = \int (\nabla^2 \Lambda)^2 dA + 2 \int (\nabla^2 \Lambda) (\nabla^2 \delta \lambda) dA \quad (2-67)$$

This equation may be transformed to

~~SECRET~~

$$\int (\nabla^2 \lambda)^2 dA = \kappa H + 2 \int (\nabla^2 \Lambda) \nabla \delta \lambda \cdot d\vec{s} - 2 \int \delta \lambda \nabla (\nabla^2 \Lambda) \cdot d\vec{s} + 2 \kappa \delta h \quad (2-68)$$

The second term of Eq. 2-68 vanishes due to  $\nabla^2 \Lambda|_b = 0$ , while the third vanishes due to  $\delta \lambda|_b = 0$ . Thus while it is necessary that  $\lambda|_b = 0$  for the trial function,  $\nabla^2 \lambda$  need not vanish at the boundary. Expanding the numerator of Eq. 2-66 to first order terms yields

$$h(\lambda) = \kappa \frac{H^2 + 2H\delta h}{\kappa H + 2\kappa \delta h} = H \quad (2-69)$$

Weighted Gas Temperature: The weighted gas temperature  $T_g$  is given by

$$T_g = T_b(z) + \Theta_g$$

where

$$-\Theta_g = \frac{\beta}{Q} \int J \Lambda dA = \frac{\beta}{Q} \Psi \quad (2-70)$$

The integral to be estimated is

$$\Psi = \int J \Lambda dA \quad (2-71)$$

To obtain a variational principle for this quantity define a function  $F$  by

$$\nabla^2 F = -\Lambda ; \quad F|_b = 0 \quad (2-72)$$

~~SECRET~~

~~SECRET~~

so that

$$\begin{aligned}\nabla^4 F &= -\nabla^2 \Lambda = J \\ \nabla^6 F &= \nabla^2 J = -\kappa\end{aligned}\tag{2-73}$$

Applying the divergence theorem as before yields

$$\begin{aligned}\Psi &= \int (\nabla^2 F)(\nabla^4 F) dA \\ &= -\int F \nabla^6 F dA = \kappa \int F dA\end{aligned}\tag{2-74}$$

or

$$\int F dA = \Psi / \kappa\tag{2-75}$$

To obtain the variational expression for  $\Psi$  let

$$\psi = \Psi + \delta \Psi$$

and

$$f = F + \delta f$$

then

$$\psi(f) = \kappa^2 \frac{[\int f dA]^2}{\int [\nabla(\nabla^2 f)]^2 dA}\tag{2-76}$$

The value of the denominator to first order terms is given by

~~SECRET~~



~~SECRET~~

$$\int [\nabla(\nabla^2 f)]^2 dA = \int [\nabla(\nabla^2 F)]^2 dA + 2 \int (\nabla \nabla^2 \delta f) \cdot (\nabla \nabla^2 F) dA \quad (2-77)$$

This reduces to

$$\begin{aligned} \int [\nabla \nabla^2 f]^2 dA = & \Psi + 2 \int (\nabla^2 \delta f) \nabla \nabla^2 F \cdot d\vec{s} - 2 \int (\nabla^4 F) \nabla \delta f \cdot d\vec{s} \\ & + 2 \int \delta f \nabla \nabla^4 F \cdot d\vec{s} + 2 \delta \Psi \end{aligned} \quad (2-78)$$

Here the third term vanishes due to  $\nabla^4 F|_b = J|_b = 0$ ; the fourth due to  $\delta f|_b = 0$ . However, the first integral is equivalent to  $2 \int (\nabla^2 \delta f) \nabla \Lambda \cdot d\vec{s}$ , which will not vanish unless a trial function is chosen such that  $\nabla^2 f|_b = 0$ . While often this is not easy to do in practice, it is sometimes possible to satisfy this Laplacian condition approximately on some boundaries while doing so exactly on others. If, however, this term does vanish, then expanding the numerator of Eq. 2-76 to first order terms yields

$$\psi(f) = \kappa^2 \frac{\Psi/\kappa^2 + 2\Psi \delta\psi/\kappa^2}{\Psi + 2\delta\psi} = \Psi \quad (2-79)$$

Boundedness: It may be shown that the exact function gives a maximum value in any of these variational expressions. Thus, a variational estimate also establishes a lower bound for the true value. The proof will be shown in the case of the flow integral Q. The others are similar.

The proof depends on the relations  $q(cj) = q(j)$  and  $\nabla^2 J = -\kappa$ . Define the function

$$\xi = \frac{\delta j - sJ}{1 + s}$$

where

$$s = \frac{1}{Q} \int \delta j dA \tag{2-80}$$

This function possesses the properties that

$$\int \xi dA = 0$$

$$\xi|_b = 0 \tag{2-81}$$

Now

$$q(J + \delta j) = q[(1 + s)(J + \xi)] = q(J + \xi) \tag{2-82}$$

Retaining all terms in Eq. 2-59 and applying Eq. 2-81

~~SECRET~~

$$\begin{aligned} q(J + \xi) &= \kappa \frac{[\int J dA + \int \xi dA]^2}{\int (\nabla J)^2 dA + 2 \int \nabla J \cdot \nabla \xi dA + \int (\nabla \xi)^2 dA} \\ &= \kappa \frac{[\int J dA]^2}{\int (\nabla J)^2 dA + 2 \kappa \int \xi dA + \int (\nabla \xi)^2 dA} \\ &= \kappa \frac{[\int J dA]^2}{\int (\nabla J)^2 dA + \int (\nabla \xi)^2 dA} \leq \kappa \frac{[\int J dA]^2}{\int (\nabla J)^2 dA} \end{aligned} \quad (2-83)$$

Hence

$$q(J + \delta_j) \leq Q \quad (2-84)$$

Comparison with Exact Results: To estimate the accuracy of the variational treatments, these methods are applied to some problems which can be done exactly. The approach usually is to pick as a trial function a polynomial of the right general shape, which satisfies the boundary conditions of the problem.

Square channel -- An exact solution of  $\nabla^2 \phi(x,y) = \rho(x,y)$  or  $\nabla^4 \phi(x,y) = \rho(x,y)$  may be set up in terms of the proper Green's function. The Green's function may be expressed as an expansion in the eigenfunctions of the differential operator with the appropriate boundary conditions. For a square channel with an edge dimension a the

~~SECRET~~

eigenfunction problem may be solved, yielding sinusoidal solutions. The rest of the program amounts to standard integrations. The results are

$$Q = \kappa a^4 \frac{2^6}{\pi^6} \sum_{\text{odd } m,n} \frac{1}{m^2+n^2} \left( \frac{1}{mn} \right)^2 = 3.509 \times 10^{-2} \kappa a^4$$

$$H = \kappa a^6 \frac{2^6}{\pi^8} \sum_{\text{odd } m,n} \frac{1}{(m^2+n^2)^2} \left( \frac{1}{mn} \right)^2 = 1.703 \times 10^{-3} \kappa a^6 \quad (2-85)$$

In the variational principle for Q use the trial function

$$j = \left[ (a/2)^2 - x^2 \right] \cdot \left[ (a/2)^2 - y^2 \right] \quad (2-86)$$

since the flow profile may be expected to be roughly parabolic. The result is

$$Q(j) = (3.472 \times 10^{-2}) \kappa a^4 \quad (2-87)$$

This estimate differs from the exact result by about 1%.

If j is chosen to be

$$j = \cos(\pi/a)x \cos(\pi/a)y \quad (2-88)$$

which is a less parabola-like function, one obtains

$$Q(j) = (3.329 \times 10^{-2}) \kappa a^4 \quad (2-89)$$

which is still within 5% of the exact result.  $\lambda$  also may be chosen as

$$\lambda = \cos(\pi/a)x \cos(\pi/a)y \quad (2-90)$$

This satisfies  $\nabla^2 \lambda|_b = 0$  on all boundaries. Though  $\nabla^2 \lambda|_b = 0$  is not demanded by the variational principle for the temperature, fulfilling this condition will give a better fitting trial function. The operations are very simple to perform in this case, giving

$$H(\lambda) = (1.686 \times 10^{-3}) \kappa a^6 \quad (2-91)$$

which is only about 1% away from the exact result.

Parallel plates -- To illustrate the variational evaluation of  $\Theta_g$  consider flow between parallel plates which are long enough to make end effects negligible. The exact expression is given by Table 2-2 and is

$$\Theta_g = -(17/1680) \beta \kappa a^4 = -0.0101191 \beta \kappa a^4$$

Exact solutions in parallel plate geometry are polynomials. If the approximate trial function  $f = \sin \pi y/a$  is chosen the integrations of Eq. 2-76 become trivial, giving

$$\psi(f) = (8/\pi^8) \kappa^2 a^6 A \quad (2-92)$$

so that

$$\Theta_g = -(96/\pi^8) \beta \kappa a^4 = -0.0101175 \beta \kappa a^4 \quad (2-93)$$

which is correct to 1.5 parts in 10,000.

In the remainder of this section the variational techniques are applied to sinusoidal and triangular channels. Values of  $Q$ ,  $\bar{\Theta}$ , and  $\Theta_g$

are computed for these two shapes in Example 1 (Sinusoidal Channel Calculations) and Example 2 (Triangular Channel Calculations) which follow. These shapes appear typical of the forms encountered in the Dumbo metal wall.

Example 1: Sinusoidal Channel Calculations

The variational approach may be used for a channel with cross-sectional length  $v$  and height  $a$  bounded below by a flat surface and above by a sinusoidal one. Let the upper bounding surface satisfy the equation

$$Y(x) = \frac{a}{2} \left[ 1 + \cos \frac{2\pi x}{v} \right] = a \cos^2 \frac{\pi x}{v} \quad (2-94)$$

In the case of the flow integral, a one-parameter trial function is used. Suppose some linear combination of two trial functions,  $j_1$  and  $j_2$ , may be expected to be a good approximation of the actual flow. Let

$$I_1 = \int j_1 dA$$

$$I_2 = \int j_2 dA$$

$$I_{11} = \int (\nabla j_1)^2 dA$$

$$I_{12} = \int \nabla j_1 \cdot \nabla j_2 dA$$

$$I_{22} = \int (\nabla j_2)^2 dA$$

(2-95)

~~SECRET~~

and

$$I_{11} = \frac{I_{11}}{I_1^2}$$
$$I_{12} = \frac{I_{12}}{I_1 I_2}$$
$$I_{22} = \frac{I_{22}}{I_2^2} \tag{2-96}$$

Then if

$$j = (1 - \epsilon) \frac{j_1}{I_1} + \epsilon \frac{j_2}{I_2} \tag{2-97}$$

it follows from Eq. 2-59 that

$$q [j(\epsilon)] = \kappa / [(1 - \epsilon)^2 I_{11} + 2\epsilon(1 - \epsilon) I_{12} + \epsilon^2 I_{22}] \tag{2-98}$$

which is optimized as in Eq. 2-61 for

$$\epsilon_0 = \frac{I_{11} - I_{12}}{I_{11} - 2I_{12} + I_{22}} \tag{2-99}$$

The form of  $j(\epsilon)$  (Eq. 2-97) is chosen to make  $\epsilon_0$  the solution of a linear equation when Eq. 2-61 is used.

For the trial function  $j_1$  choose the thin channel approximation (Eq. 2-35).

~~SECRET~~

~~SECRET~~

$$j_1 = \frac{\kappa}{2} y [Y(x) - y] \quad (2-100)$$

The effect of the correction  $j_2$  should be to reduce  $\partial^2 j / \partial y^2$  where  $\partial^2 j / \partial x^2$  is largest. The proper admixture of  $j_2$  should do this if

$$j_2 = j_1 \cos^2 \frac{\pi x}{v} \quad (2-101)$$

The  $y$ -integrations can now be done at once, bringing all the final  $x$ -integrations to the form

$$\int_{-\pi/2}^{\pi/2} \cos^{2n} \theta d\theta = \pi \frac{1 \cdot 3 \cdot 5 \cdots (2n-1)}{2 \cdot 4 \cdot 6 \cdots 2n} \equiv \pi \frac{(2n-1)!!}{(2n)!!} \quad (2-102)$$

The results are

$$I_1 = -\frac{1}{12} \frac{5!!}{6!!} \kappa a^3 v$$

$$I_2 = -\frac{1}{12} \frac{7!!}{8!!} \kappa a^3 v$$

$$I_{11} = 48 \pi^2 \frac{7!! (6!!)^2}{10!! (5!!)} \frac{1}{a v^3} + 12 \frac{6!!}{5!!} \frac{1}{a^3 v}$$

$$I_{12} = 60 \pi^2 \frac{(9!!)(6!!)(8!!)}{(12!!)(5!!)(7!!)} \frac{1}{a v^3} + 12 \frac{6!!}{5!!} \frac{1}{a^3 v}$$

$$I_{22} = \frac{744}{5} \pi^2 \frac{(11!!)(8!!)}{(14!!)(7!!)} \frac{1}{a v^3} + 12 \frac{(9!!)(8!!)^2}{(10!!)(7!!)^2} \frac{1}{a^3 v} \quad (2-103)$$

~~SECRET~~



which upon substitution give

$$q [j(\epsilon)] = \kappa \alpha^3 v / \left\{ 38.40 + 1.0972 \epsilon^2 + \frac{\alpha^2}{v^2} \left[ 132.65(1-\epsilon)^2 + 284.24 \epsilon(1-\epsilon) + 316.47 \epsilon^2 \right] \right\} \quad (2-104)$$

$$\epsilon_0 = -1 / \left( 0.11579 \frac{v^2}{\alpha^2} + 17.401 \right) \quad (2-105)$$

Note that  $\epsilon_0 \rightarrow 0$  as  $\alpha/v \rightarrow 0$ . Thus,  $q$  reduces exactly to the thin channel value.

If  $\epsilon = 0$  in Eq. 2-104, then the thin channel flow function is the trial function. It is interesting to compare the results of the variational method with those of the successive approximation technique. The quantity  $(8/\kappa \alpha^3 v)Q$  is shown in Table 2-6 for the realistic value  $\alpha/v = 0.2$ .

THIN CHANNEL APPROXIMATION	0.2083
FIRST ORDER APPROXIMATION	0.1795
SECOND ORDER APPROXIMATION	0.1862
VARIATIONAL METHOD USING $\epsilon = 0$	0.18300
VARIATIONAL METHOD USING $\epsilon = \epsilon_0$	0.18312

Optimizing  $j$  introduces about a 5% admixture of  $j_2$ . However, the value of  $Q$  is altered by only 0.07%. Since the parabolic flow shape is



expected to be quite a good approximation, and since optimizing  $j$  must improve the estimate, the variational value of  $Q$  should be very accurate. Table 2-6 indicates that the crudest variational approximation is probably a bit better than the second order successive approximation.

Because of the success of the thin channel trial function in the case of the total flow, a similar approximation is considered sufficient for the case of the average temperature integral  $H$ . The trial function used is that of Eq. 2-39 and is

$$\lambda = y^4 + Y^3 y - 2y^3 Y \quad (2-106)$$

where  $\lambda$  is the approximation to  $\Lambda$  as defined by Eq. 2-62.

The denominator integrand in Eq. 2-66 involves

$$\begin{aligned} (\nabla^2 \lambda) = y \left[ -6 \pi^2 \frac{a^3}{v^2} \left( 5 \cos^4 \frac{\pi x}{v} - 6 \cos^6 \frac{\pi x}{v} \right) - 12 a \cos^2 \frac{\pi x}{v} \right] \\ + 12 y^2 + y^3 \left[ 4 \pi^2 \frac{a}{v^2} \left( 2 \cos^2 \frac{\pi x}{v} - 1 \right) \right] \end{aligned} \quad (2-107)$$

Upon squaring Eq. 2-107 and performing the  $y$ -integration only terms of the form  $\cos^{2n}(\frac{\pi x}{v})$  remain, though  $2n$  goes up to 18. Evaluation is straightforward but tedious, yielding the result

$$H = 0.0020508 a^5 v / \left[ 1 + 7.7578 \left( \frac{a}{v} \right)^2 + 57.214 \left( \frac{a}{v} \right)^4 \right] \quad (2-108)$$



~~SECRET~~

It is interesting to compare this result with that of the successive approximations method. Returning to Eq. 2-52

$$H = 0.0020508 a^5 \nu \left[ 1 - 7.7553 \left( \frac{a}{\nu} \right)^2 + 48.786 \left( \frac{a}{\nu} \right)^4 \right] \quad (2-109)$$

The first couple of terms are very close to the corresponding terms in the binomial expansion of Eq. 2-108. Thus, this is very close to the binomial expansion of H obtained by the variational technique.

The variational calculation for the weighted gas temperature  $T_g$  has not been performed, since the expressions become quite cumbersome. In analogy to what has been done, the procedure would be to pick as a trial function the solution of

$$\frac{\partial^6 f}{\partial y^6} = -\kappa \quad (2-110)$$

with boundary conditions  $f = 0$ ,  $\partial^2 f / \partial y^2 = 0$ ,  $\partial^4 f / \partial y^4 = 0$  at  $y = 0$  and  $y = Y(x)$ . Then the condition that  $\nabla^2 f|_b = 0$  will be satisfied exactly at the lower boundary, and approximately at the upper one, with the approximation becoming exact as  $(a/\nu) \rightarrow 0$ .

Example 2: Triangular Channel Calculations

These methods have been applied to the problem of the triangular channel bounded below by a surface  $Y_2 = 0$  and above by the surface

~~SECRET~~

~~SECRET~~

$$Y_1(x) = \begin{cases} a \left(1 - \frac{2x}{v}\right); & 0 \leq x \leq \frac{v}{2} \\ a \left(1 + \frac{2x}{v}\right); & -\frac{v}{2} \leq x \leq 0 \end{cases} \quad (2-111)$$

The thin-channel expressions for the approximate flow and temperature distribution functions  $j$  and  $\lambda$  which were used in Example 1, above, are used for the triangular channel calculations.

Total Flow, Q

The variational value,  $q$ , of the total flow

$$q = \kappa \frac{\left(\int j dA\right)^2}{\int (\nabla j)^2 dA} \quad (2-59)$$

For any thin channel with  $Y_2 = 0$ ,  $Y_1 = Y(x)$ , it has been shown

$$j = -\frac{\kappa}{2} (y - Y)y \quad (2-35)$$

Performing the indicated operations yields

$$q = \frac{\kappa}{12} \frac{\left[\int_{-v/2}^{v/2} Y^3 dx\right]^2}{\int_{-v/2}^{v/2} Y^3 (Y'^2 + 1) dx} \quad (2-112)$$

For the triangular channel described above, the flow is

~~SECRET~~

$$q = \frac{\kappa}{48} \frac{a^3 v}{1 + 4a^2/v^2} \quad (2-113)$$

Average Temperature,  $\bar{\Theta}$

To obtain  $\bar{\Theta}$ , the thin channel result for  $\Theta(x,y)$  is transformed to the function

$$\lambda = -\Theta/\beta$$

with  $\bar{\Theta}$  being given by

$$\bar{\Theta} = -\beta H/A \quad (2-63)$$

where H is estimated by

$$h = \kappa \frac{(\int \lambda dA)^2}{\int (\nabla^2 \lambda)^2 dA} \quad (2-66)$$

For any thin channel with  $Y_2 = 0$ ,  $Y_1 = Y$ , the result

$$\lambda = \frac{\kappa}{24} (y^4 + Y^3 y - 2Yy^3) \quad (2-114)$$

yields

$$\int \lambda dA = \frac{\kappa}{120} \int_{-v/2}^{v/2} Y^5 dx \quad (2-115)$$

and, if  $Y'' = 0$ ,

~~SECRET~~

$$\int (\nabla^2 \lambda)^2 dA = \frac{\kappa^2}{240} \int_{-v/2}^{v/2} (5Y'^4 - 5Y'^2 + 2) Y^5 dx \quad (2-116)$$

For the triangular channel

$$h = \frac{\kappa}{720} \frac{a^5 v}{1 - 10a^2/v^2 + 40a^4/v^4} \quad (2-117)$$

Hence

$$\bar{\Theta} = - \frac{\beta \kappa}{360} \frac{a^4}{1 - 10a^2/v^2 + 40a^4/v^4} \quad (2-118)$$

Weighted Average Temperature,  $\Theta_g$

As previously described,  $\Theta_g$  is obtained from an expression such that

$$\Theta_g = - \beta \Psi / Q \quad (2-70)$$

and a function F where

$$F|_b = 0$$

$$\nabla^2 F = - \Lambda \quad (2-72)$$

with the variational expression

$$\psi = \kappa^2 \frac{(\int f dA)^2}{\int [\nabla(\nabla^2 f)]^2 dA} \quad (2-76)$$

~~SECRET~~

~~SECRET~~

Using the thin channel result for  $\lambda$  (Eq. 2-114) let

$$\frac{\partial^2 f}{\partial y^2} = \frac{\kappa}{24} (y^4 + Y^3 y - 2Yy^3) \quad (2-119)$$

Thus

$$f = \frac{\kappa}{720} (y^6 - 3Yy^5 + 5Y^3y^3 - 3Y^5y) \quad (2-120)$$

Neglecting multiplying constants for  $Y'' = 0$  one has

$$\int f dA = - \frac{17}{840} \int_{-u/2}^{u/2} Y^7 dx \quad (2-121)$$

$$\int [\nabla(\nabla^2 f)]^2 dA = \frac{1}{35} (17 - 9Y'^2 + 129Y'^4 + 341Y'^6) \int_{-u/2}^{u/2} Y^7 dx \quad (2-122)$$

For the triangular channel

$$\psi = \frac{17}{161,280} \frac{\kappa^2 u a^7}{1 - \frac{36}{17} \frac{a^2}{u^2} + \frac{2064}{17} \frac{a^4}{u^4} + \frac{21,824}{17} \frac{a^6}{u^6}} \quad (2-123)$$

Hence

$$\Theta_g = - \frac{17}{3360} \frac{\beta \kappa a^4}{1 - \frac{36}{17} \frac{a^2}{u^2} + \frac{2064}{17} \frac{a^4}{u^4} + \frac{21,824}{17} \frac{a^6}{u^6}} \quad (2-124)$$

~~SECRET~~

~~SECRET~~

Variational Method

Section 2-7

REFERENCES

1. J. O. Hirschfelder, Charles F. Curtiss, R. Byron Bird, Molecular Theory of Gases and Liquids, p. 698ff., John Wiley and Sons, Inc., New York, 1954.
2. S. Goldstein, Modern Developments in Fluid Dynamics, Oxford, New York, 1938.
3. B. B. McInteer, R. M. Potter, and E. S. Robinson, Dumbo -- A Pachydermal Rocket Motor, Los Alamos Scientific Laboratory Report LAMS-1887, May 18, 1955.

73-74

~~SECRET~~



~~SECRET~~

CHAPTER 3

TEMPERATURE-FLOW STABILITY

One fine morning in the middle of the Precession of the Equinoxes, this 'satiabable Elephant's Child' asked a new fine question that he had never asked before.

R. Kipling, The Elephant's Child

3-1: Statement of the Problem

The uniform channels described in Chap. 2 have large differences in the absolute temperatures of their two ends. The pressure gradient  $dp/dz$  changes considerably with distance along the duct and is sensitive at every point to changes in the total mass flow because these modify the temperature distribution. This situation can lead to peculiar operating conditions in which any transient perturbation of the steady-state conditions does not die away with time but tends to build up to catastrophic proportions.

The flow law for any of these channels may be considered to be of the form

$$Q = -B \frac{\rho}{\eta} \frac{dp}{dz} \tag{3-1}$$

where B, the geometric conductance, is a cross-sectional geometry factor having the dimensions ( $cm^4$ ). This relation determines the pressure drop

~~SECRET~~

~~SECRET~~

$$\Delta p = Q \int_0^w \frac{\eta}{B\rho} dz$$

where

$$\Delta p = p(0) - p(w) \tag{3-2}$$

The quantity  $\eta/\rho$  is related to its value at the channel entrance by

$$\eta/\rho = (\eta_0/\rho_0)(T/T_0)^{1+n} \tag{3-3}$$

where the subscript 0 refers to entrance values and where it is assumed that  $\eta \propto T^n$ . For  $H_2$ ,  $n = 0.678$ .  $T(z)$  in turn is given by

$$T(z) = T_0 + (1/cQ) \int_0^z \sigma dz \tag{3-4}$$

where  $\sigma$  is the power per unit length of channel. Thus the dependence of the pressure drop  $\Delta p$  on the flow rate  $Q$  is complicated. Nevertheless the following general statements are evident: The pressure drop will be large if the mass flow is very high or if very high gas temperatures are involved. The latter condition, due to the temperature dependence of viscosity and density, will occur when the flow rate  $Q$  is very low. As shown in Fig. 3-1, a given pressure drop and power density may result in a large flow rate, slightly heated, or else in a small flow rate, strongly heated.

~~SECRET~~

~~SECRET~~

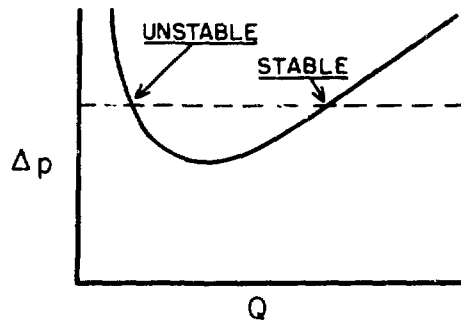


Fig. 3-1

Within the framework of the steady-state equations 3-2 and 3-3, either mode of flow is consistent with a given value of  $\Delta p$ .

C. L. Longmire of LASL has considered the case of viscous flow through a uniform tube of uniformly distributed power density. In this case he has shown that operation under conditions where

$$\frac{d\Delta p}{dQ} < 0 \tag{3-5}$$

corresponds to a state of unstable equilibrium. The quantity involved in Eq. 3-5 is called the resistance of the channel. Unless this quantity is non-negative, the flow will either shift to the stable point or tend to shut off entirely, resulting in excessively high temperatures. It should be noted that this instability problem exists only for fixed  $\Delta p$  but disappears for problems in which either  $Q$  or  $T(z)$  is held constant in time.

Longmire's argument is generalized in App. E. The same criterion for stability is established for any flow law (viscous, turbulent, or

~~SECRET~~

mixed as in porous media) for any shape of channel, and for any power distribution function, so long as the temperatures of the gas and of the exchanger are not too different.

It is shown in Sec. 3-2 that viscous flow through a uniformly heated channel of uniform cross section will be unstable when the ratio of the final temperature to the initial temperature is greater than 3.604. Such instability may be overcome by appropriately constricting a portion of the channel at the gas entrance end. The specifications for this constriction are developed in Sec. 3-3.

### 3-2: Viscous Flow Through a Uniform Channel with Uniform Power Density

In this case, Eq. 3-2 may be written

$$\Delta p = \frac{\eta_0 Q}{B \rho_0 T_0^{1-n}} \int_0^{w} T^{1-n} dz \quad (3-6)$$

For uniform power density  $\sigma = \Sigma/w$ , where  $\Sigma$  is the total power per channel, and Eq. 3-4 becomes

$$T(z) = T_0 + \frac{\Sigma}{cQw} z \quad (3-7)$$

Substituting  $T(z)$  into Eq. 3-6 and integrating yields

$$\Delta p = \frac{\eta_0 \Sigma w}{\rho_0 T_0 cB(2+n)} \frac{1}{x^2} [(x+1)^{2+n} - 1] \quad (3-8)$$

~~SECRET~~

where

$$x = \frac{\Sigma}{cQT_o} = \frac{T_w - T_o}{T_o} \quad (3-9)$$

The function of  $x$  in Eq. 3-8 is indeed double-valued, having a minimum for  $x = 2.604$  when  $n = 0.678$ , the value of  $n$  for hydrogen. For values of  $x$  larger than 2.604 the system is unstable while for smaller values it is stable.

3-3: Viscous Flow Through a Constricted Channel with Uniform Power Density

Stable operation of the uniform-bore heat exchanger discussed in Sec. 3-2 is limited to a temperature gain factor of 3.604, as seen above. However, a uniform-power exchanger which is stable at higher temperature gains is shown in Fig. 3-2. The enhanced stability of this device comes from the increased channel drag at the cold end, where the density and viscosity of the gas are less influenced by the mass-flow rate.

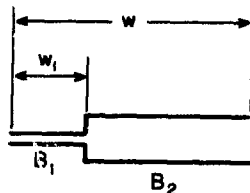


Fig. 3-2

~~SECRET~~

For this problem let the channel be composed of an initial region of length  $w_1$  (Fig. 3-2) and a "geometrical conductance"  $B_1$  while beyond this point the conductance is  $B_2$ . Equation 3-7 still applies, but Eq. 3-6 must be divided over two intervals  $0 \leq z \leq w_1$  and  $w_1 \leq z \leq w$ .

The total pressure drop is given by

$$\Delta p = \frac{\eta_0 \Sigma w}{\rho_0 T_0 c(2+n)} \frac{1}{x^2} \left[ \frac{1}{B_2} (x+1)^{2+n} + \left( \frac{1}{B_1} - \frac{1}{B_2} \right) \left( \frac{w_1}{w} x + 1 \right)^{2+n} - \frac{1}{B_1} \right] \quad (3-10)$$

where  $x$  is given by Eq. 3-9. The minimum of this function of  $x$  is given by

$$\frac{1}{B_2} \left[ (x+1)^{2+n} - \frac{(2+n)x}{2} (x+1)^{1+n} \right] + \left( \frac{1}{B_1} - \frac{1}{B_2} \right) \left[ \left( x \frac{w_1}{w} + 1 \right)^{2+n} - \frac{(2+n)w_1 x}{2w} \left( x \frac{w_1}{w} + 1 \right)^{1+n} \right] - \frac{1}{B_1} = 0 \quad (3-11)$$

Equation 3-11 may be rewritten as

$$\frac{B_2}{B_1} = \frac{F(w_1 x/w) - F(x)}{F(w_1 x/w) - 1}$$

where

~~SECRET~~

Constricted Channel

Section 3-3

$$F(\xi) = (\xi + 1)^{2+n} - \frac{2+n}{2} \xi (\xi + 1)^{1+n} \quad (3-12)$$

Some values of  $F(\xi)$  are shown in Table 3-1 for  $n = 0,678$ . An important characteristic of this function is the existence of the maximum at  $\xi \approx 1.5$ . It may be shown that this is given by  $\xi = 1/n = 1.47$ . If, for a desired  $x$ ,  $(w_1x)/w = 1/n$ , then  $B_2/B_1$  is at a minimum value for typical temperatures used for the Dumbo design. Figure 3-3 shows Eq. 3-12 in parametric form.

TABLE 3-1 THE FUNCTION  $F(\xi)$

$\xi$	$F(\xi)$	$\xi$	$F(\xi)$
0	1.00	3	-0.17
0.5	1.64	4	-5.3
1	2.12	5	-13.6
1.5	2.28	10	-130
2.0	2.08	20	-965
2.5	1.32		

In design application one would select a temperature ratio  $x$  in excess of desired operating temperatures, presumably corresponding to the melting point of the metals. The system would then be stable under fluctuations of temperature up to this disaster condition.

Considering the composite channel to have been stabilized according to the foregoing method, the overall pressure drop of Eq. 3-10 may be expressed in terms of the desired flow  $Q$  and the expected temperature

~~SECRET~~

~~SECRET~~

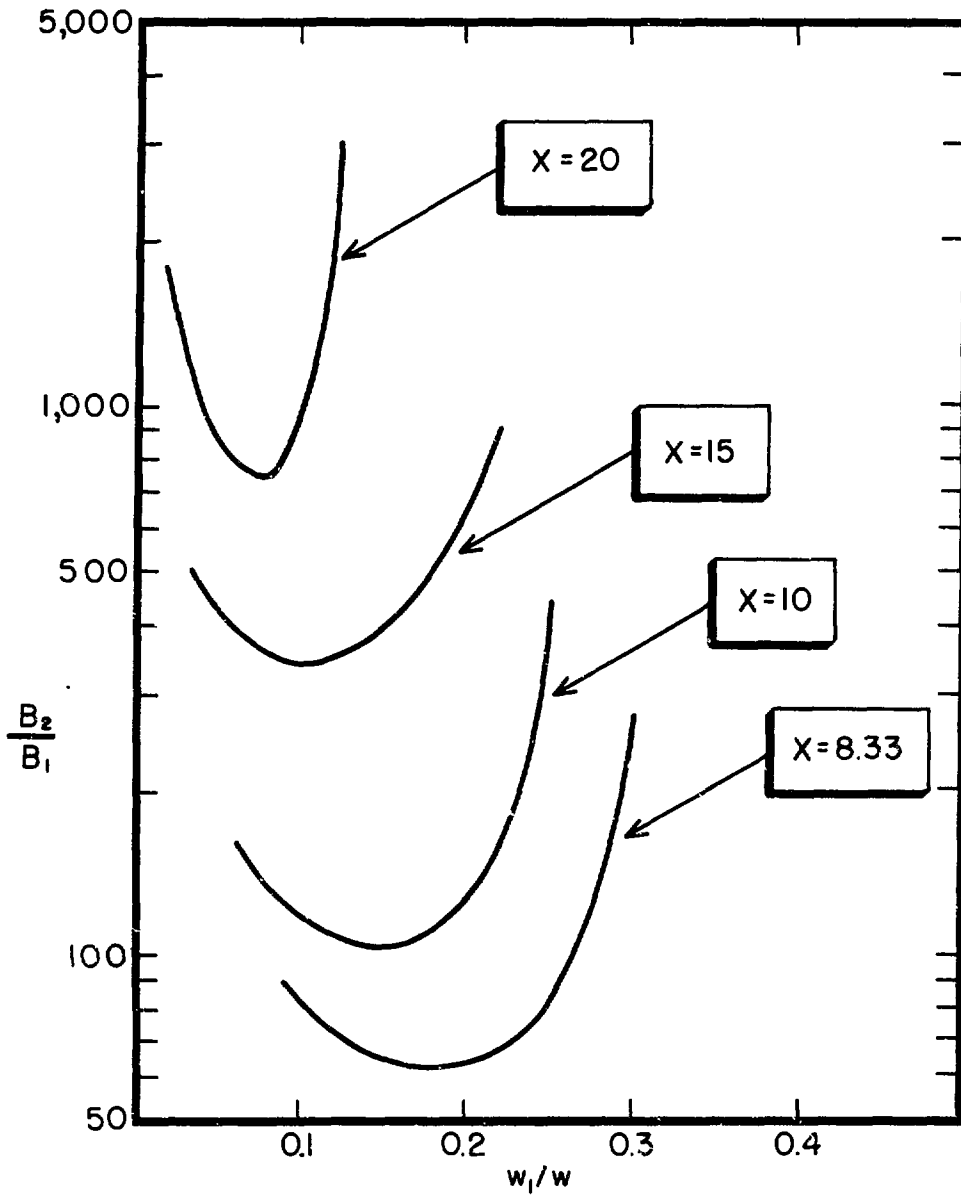


Fig. 3-3: Introductory Impedance Tube for Borderline Stability

~~SECRET~~



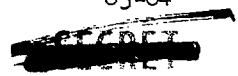


Constricted Channel

Section 3-3

ratio  $x$  as

$$\Delta p = \frac{\eta_0 w Q}{B_2 \rho_0 (2+n)} \frac{1}{x} \left[ (x+1)^{2+n} + \left( \frac{B_2}{B_1} - 1 \right) \left( \frac{w_1}{w} x + 1 \right)^{2+n} - \frac{B_2}{B_1} \right] \quad (3-13)$$



~~SECRET~~

## CHAPTER 4

### WALL TEMPERATURE DISTRIBUTION

Then he went away, a little warm, but not at all astonished.

R. Kipling, The Elephant's Child

#### 4-1: Introduction

To understand the temperature distribution throughout the metal wall structure requires the solution of several problems. Some of these problems concern the behavior of a perfectly constructed wall under normal operation. Others deal with abnormalities of operation due to fabrication errors, blocking of channels, etc. In this chapter the processes affecting the temperature distribution are studied, and the expected temperature variations are evaluated.

Section 4-2 deals with the gross temperature profile in the wall. The temperature is shown to rise linearly through the wall. The "dynamic insulation" property of the wall is demonstrated. The process of convection, the bodily transport of internal energy in the flowing gas, is shown to strongly predominate over heat conduction. Conduction parallel to the gas flow is ignored in the subsequent sections.

The sections which follow treat various perturbations and their effects on the overall temperature distribution. These perturbations are

~~SECRET~~

~~SECRET~~

so small that their interaction effects may be neglected, and the various temperature variations may be superimposed. Because the primary object of this investigation is to keep the wall material below the failure temperature, the calculations particularly concern the temperature distribution of the hottest part of the wall. Although various approximations are made in these sections, they are approximations justified by the Dumbo wall geometry; a more lengthy and detailed analysis would furnish only small corrections to the temperature deviations calculated here.

Section 4-3 investigates the temperature distribution over the walls of the individual flow channels. These temperatures are affected by the channel shape because of the manner in which power from a wall divides itself between neighboring channels. From this standpoint the temperature variations are found for normal operating conditions.

Section 4-4 discusses the effect of thermal conductivity normal to the gas flow direction, under conditions of aberrated flow. The basic equations are developed for analyzing such situations.

Section 4-5 deduces the result of upsetting the flow in a single channel.

Section 4-6 deals with the more general problem of distributed errors in the Dumbo wall, including the effects of channel interactions, temperature-flow interaction, and the effect of temperature on thermal conductivity. The effect of sectioning the Dumbo wall into individual

~~SECRET~~

~~SECRET~~

"mosaic cells," each with a fixed total flow, is included. Numerical results are presented on the basis of experimental wall error measurements on a sample section of Dumbo wall.

Section 4-7 deals briefly with other heat-transfer mechanisms which will tend further to equalize the temperature distribution.

4-2: Overall Temperature, and the Dynamic Insulation Effect

The one-dimensional problem of combined convection, thermal conduction, and power generation has been presented previously.<sup>1,2</sup> It will be shown that for the Dumbo device the heat conducted to the cooler inlet region is small compared to that added to the gas; this will justify neglect of heat conduction in the z direction in the following sections.

To do this one needs the temperature distribution of the gas assuming intimate temperature equilibrium with the walls. For a uniform power density with the gas issuing from a source at a temperature  $T^*$  the distribution is given by

$$T(z) = T^* + (T_w - T^*) \left[ \frac{1 - e^{-\phi(1-z/w)}}{\phi} + \frac{z}{w} \right] \quad (4-1)$$

where

$$\phi = c J_0 w / \lambda$$

and  $\lambda$  is an average linear thermal conductivity of the wall structure,  $J_0$  is the flow per unit total area,  $w$  is the wall thickness, and  $c$  is

~~SECRET~~

the specific heat of the gas. This relation applies only for  $0 \leq z \leq w$ . Beyond the heating region  $T = T_w$ . Thus the temperature  $T(0)$  at the entrance to the heating region is given by

$$T(0) = T^* + (T_w - T^*) \left[ \frac{1 - e^{-\phi}}{\phi} \right] \quad (4-2)$$

The value of  $\phi$  encountered in this relation is typically so large that the functional dependence of Eq. 4-2 is  $1/\phi$ , and the temperature distribution from Eq. 4-1 is linear. The conducted heat flow  $I_0$  at the gas entrance ( $z = 0$ ) is given by

$$I_0 = -\lambda \left( \frac{dT}{dz} \right)_{z=0} = \frac{-\lambda(T_w - T^*)}{w} (1 - e^{-\phi}) \xrightarrow{\phi \gg 0} \frac{-\lambda(T_w - T^*)}{w} \quad (4-3)$$

A quantity of interest is the ratio of heat conducted into the incoming region to the total heat to be added to the stream. When  $\phi$  is large this ratio is

$$\frac{-I_0}{c \rho (T_w - T^*)} = \frac{1}{\phi} \quad (4-4)$$

This relation indicates  $\phi$  to be a true indicator of the insulating ability of a permeable wall through which fluid is flowing. For typical values in the Dumbo designs proposed here  $\phi \approx 100$  so that the preheating predicted by Eq. 4-2 is circa  $25^\circ$  for a temperature increase of  $2500^\circ$ . This represents an approximately 1% conducted heat loss to the upstream region immediately preceding the metal grill-work structure. The energy

transport by convection strongly dominates over that by conduction.

It is worth noting that if a wall does not contain a power source but serves only to insulate from an upstream temperature  $T_w$  the functional form of Eq. 4-1 is modified to be

$$T(z) = T^* + (T_w - T^*) e^{-\phi(1-z/w)} \quad (4-5)$$

In this case the entering temperature  $T(0)$  is given by

$$T(0) = T^* + (T_w - T^*) e^{-\phi} \quad (4-6)$$

For a comparable insulation to the preceding example, such an arrangement would require  $e^{-\phi} \approx 10^{-2}$  or  $\phi \approx 4.6$ . Thus such a wall may have a far greater thermal conductivity and still insulate effectively.

In summary:

- (1) The temperature rise through the wall is effectively linear.
- (2) The presence of gas flow through the wall leads to the dynamic-insulation effect. Back conduction can raise the temperature of the cold side of the wall about 25° only.
- (3) Energy transport in the direction of flow is so predominantly by convection that thermal conduction parallel to the flow can be neglected in the analysis of the subsequent sections.
- (4) The flow of gas through a non-power-generating region, such as the space preceding the Dumbo wall, brings about an extreme improvement in the insulating effectiveness of that region in comparison with a

~~SECRET~~

Chapter 4                      Wall Temperature Distribution

similar but power-generating region.

4-3: Temperature Distribution in the Periodic Wall for Normal Operation

Previously there have been considered only problems in which the wall temperature profile for a fixed  $z$  is uniform. This corresponds to the assumption of infinite transverse thermal conductivity of the channel walls. However, with finite metallic thermal conductivity and with the channels proposed here, there must be some variation in this transverse temperature profile. In this section the locations of the "hot" and "cold" spots of this wall and the magnitude of these variations are estimated. To do this one may obtain the normal derivative of  $T$  into the gas from the wall, from which the heat flow in the wall and the wall temperature distribution follow.

For this purpose, the limiting form of the thin channel geometry is used in three different ways:

(1) The differential equations governing the gas flow and temperature within the channels as previously developed are applied (see Sec. 2-5).

$$\frac{\partial^2 J}{\partial y^2} = -\kappa$$

$$J(x, Y) = J(x, 0) = 0$$

(4-7)

$$\frac{\partial^2 T}{\partial y^2} = \beta J$$

(4-8)

~~SECRET~~

~~SECRET~~

Normal Operation

Section 4-3

(2) The heat flux  $I_n$  from any wall to the gas is given by

$$I_n = -\lambda_g \left. \frac{\partial T}{\partial n} \right|_b \quad (4-9)$$

where  $\vec{n}$  is the normal surface vector to the wall and  $\lambda_g$  is the local thermal conductivity of the gas. Because of the thin channel geometry, conduction along the x component of this gradient is neglected so that for the upper surface of the wall

$$I_{n\uparrow} = -\lambda_g \left. \frac{\partial T}{\partial y} \right|_{b\uparrow} \quad (4-10)$$

while for the lower surface

$$I_{n\downarrow} = \lambda_g \left. \frac{\partial T}{\partial y} \right|_{b\downarrow} \quad (4-11)$$

(3) Because of the thin channel geometry the channel boundaries may be assumed to be so nearly parallel that only their relative separation is of significance. This corresponds to assuming  $T_b$  to be a function of x only and hypothesizes the same wall temperature distribution  $T_b(x)$  for both flat and convoluted plates, as shown in Fig. 4-1.

~~SECRET~~



~~SECRET~~

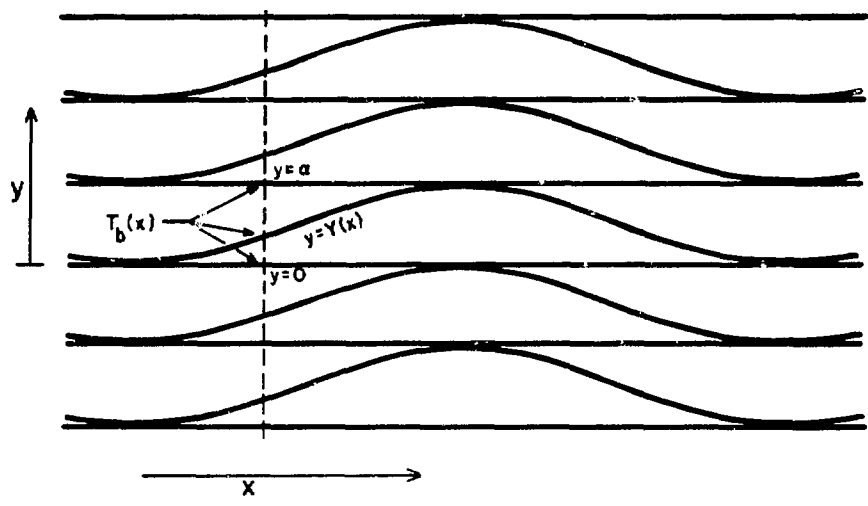


Fig. 4-1

The energy dissipation per unit wall area is given by

$$\sigma = -\tau \lambda_m \frac{d^2 T_b}{dx^2} + I_{nf} + I_{nl} \tag{4-12}$$

where  $\sigma$  is the power generated per unit area of the wall,  $\tau$  is the wall thickness, and  $\lambda_m$  is the local thermal conductivity of the metal.

First  $I_{nl}$  is evaluated at  $y = Y$ . From the symmetry implied in assumption (3) it is evident that

$$\left. \frac{\partial T}{\partial y} \right|_{ot} = - \left. \frac{\partial T}{\partial y} \right|_{Yl} \tag{4-13}$$

Equation 4-8 is integrated once, applying Eq. 4-13

~~SECRET~~

$$\left. \frac{\partial T}{\partial y} \right|_{y \uparrow} = + \frac{\beta}{2} \int_0^Y J dy = \frac{I_{nl}}{\lambda_g} \quad (4-14)$$

In Eq. 4-14 Y is the local channel height (bounded by y = 0 below).

To evaluate  $\left. \frac{\partial T}{\partial y} \right|_{y \uparrow} = - \left. \frac{\partial T}{\partial y} \right|_{\alpha \downarrow}$  a similar treatment of the region  $Y \leq y \leq \alpha$  may be performed, yielding

$$\left. \frac{\partial T}{\partial y} \right|_{y \uparrow} = - \frac{\beta}{2} \int_Y^\alpha J dy = - \frac{I_{nl}}{\lambda_g} \quad (4-15)$$

Combining Eqs. 4-14 and 4-15 with Eq. 4-12 then yields the differential equation for  $T_b(x)$

$$\tau \lambda_m \frac{d^2 T_b}{dx^2} = + \lambda_g \frac{\beta}{2} \int_0^\alpha J dy - \sigma \quad (4-16)$$

The last term of this expression may be transformed by the energy relation

$$\sigma = \frac{cQ}{v} \frac{dT}{dz} = \frac{\beta \lambda_g Q}{v} \quad (4-17)$$

to give

$$\frac{d^2 T_b}{dx^2} = - \frac{\lambda_g \beta}{\lambda_m \tau} \left[ \frac{Q}{v} - \frac{1}{2} \int_0^\alpha J dy \right] \quad (4-18)$$

~~SECRET~~

Chapter 4 Wall Temperature Distribution

To solve this equation, a function

$$J(x) = \int_0^a J dy \tag{4-19}$$

is defined. This function has the property that

$$Q = \frac{1}{2} \int_0^u J(x) dx = \frac{\bar{J}u}{2} \tag{4-20}$$

The differential equation 4-18 becomes

$$\frac{d^2 T_b}{dx^2} = -\frac{\lambda_g \beta}{2\lambda_m \tau} [\bar{J} - J(x)] \tag{4-21}$$

This relation is integrated twice, using the condition that from symmetry,

$$\left. \frac{dT_b}{dx} \right|_{x=0} = 0$$

yielding

$$T_b(x) - T_b(0) = -\frac{\lambda_g \beta}{2\lambda_m \tau} \int_0^x dx' \int_0^{x'} [\bar{J} - J(x'')] dx'' \tag{4-22}$$

Equation 4-7 is integrated as before to yield

$$J = -\frac{\kappa}{2} y(y - Y) \tag{4-23}$$

~~SECRET~~

~~SECRET~~

and Eq. 4-19 becomes

$$\begin{aligned} J &= -\frac{\kappa}{2} \int_0^Y y(y-Y) dy - \frac{\kappa}{2} \int_Y^a (y-a)(y-Y) dy \\ &= \frac{\kappa a}{12v} [3Y^2 - 3aY + a^2] \end{aligned} \tag{4-24}$$

from Eq. 4-2

$$\bar{J} = \frac{\kappa a}{12v} \int_0^v 3Y(Y-a) dx + \frac{\kappa a^3}{12} \tag{4-25}$$

Equation 4-24 is subtracted from Eq. 4-25 to yield

$$\bar{J} - J = \frac{\kappa a}{4} \left[ \frac{1}{v} \int_0^v Y(Y-a) dx - Y(Y-a) \right] \tag{4-26}$$

For any channel shape this expression may be used in Eq. 4-22 to obtain  $T_b(x)$ .

For a sinusoidal channel in which

$$Y = \frac{a}{2} \left[ 1 + \cos \frac{2\pi x}{v} \right] \tag{4-27}$$

Eq. 4-26 becomes

$$\bar{J} - J = \frac{\kappa a^3}{16} \left[ \frac{1}{2} - \cos^2 \frac{2\pi x}{v} \right] \tag{4-28}$$

~~SECRET~~

and from Eq. 4-22

$$T_b(x) - T_b(0) = \frac{-1}{1024\pi^2} \frac{\lambda_g \beta \kappa a^3 v^2}{\lambda_m \tau} \left( \cos \frac{4\pi x}{v} - 1 \right) \quad (4-29)$$

Equation 4-29 may be written in terms of  $\frac{\partial T}{\partial z}$  and  $\bar{J}$  where

$$\beta = \frac{c}{\lambda_g} \frac{\partial T}{\partial z}$$

$$\bar{J} = (5/96) \kappa a^2 \quad (4-30)$$

and Eq. 4-29 becomes

$$T_b(x) - T_b(0) = \frac{3}{160\pi^2} \frac{av^2}{\tau} \frac{c\bar{J}}{\lambda_m} \frac{\partial T}{\partial z} (1 - \cos \frac{4\pi x}{v}) \quad (4-31)$$

The location of the temperature extremes as predicted by this formula is shown in Fig. 4-2. The difference between these two extremes  $\Delta T_b$  is given by

$$\Delta T_b = \frac{3}{80\pi^2} \frac{c\bar{J}}{\lambda_m} \frac{av^2}{\tau} \frac{\partial T}{\partial z} \quad (4-32)$$

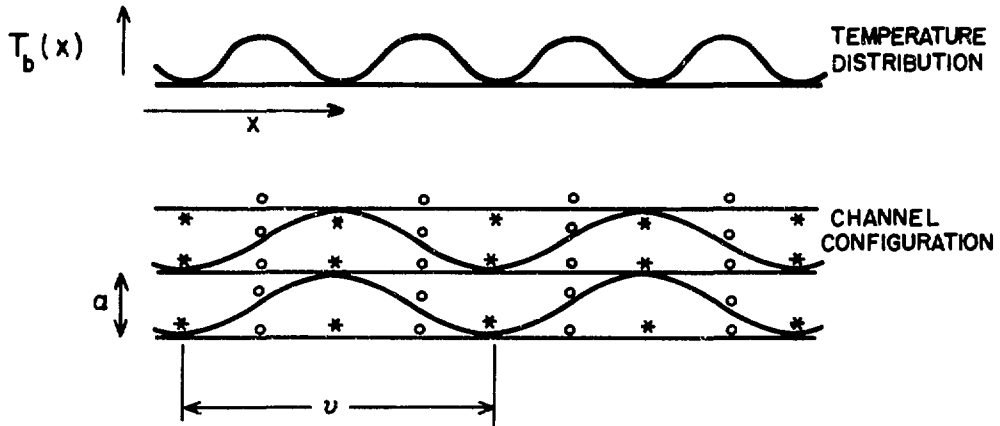
A numerical example may be computed using the following typical values

$$c = 3.5 \text{ cal / gm - deg} \quad a = 1.5 \times 10^{-2} \text{ cm}$$

$$\bar{J} = 1 \text{ gm / cm}^2 \text{ - sec} \quad v = 7.5 \times 10^{-2} \text{ cm}$$

$$\lambda_m = 0.1 \text{ cal / cm - sec - deg} \quad \tau = 2.5 \times 10^{-3} \text{ cm}$$

$$\frac{\partial T}{\partial z} = 2500 \text{ degrees / cm}$$



- o MAXIMUM TEMPERATURE POINTS
- \* MINIMUM TEMPERATURE POINTS

FIGURE 4-2  
TEMPERATURE DISTRIBUTION  
UNDER NORMAL FLOW IN SINUSOIDAL CHANNELS

with the result

$$\Delta T_b = 11.2 \text{ degrees}$$

#### 4-4: Wall Temperature Distribution Under a Flow Aberration

In this section the effect of some isolated irregularities on the temperature profile is investigated. The approach is to replace the complicated mesh of heat-flow paths at right angles to the stream by a continuous and homogeneous, though nonisotropic, medium with thermal conductivities  $\lambda_x$  and  $\lambda_y$  in its horizontal and vertical directions, respectively, normal to the flow. The validity of this approximation will be discussed with a specific example.

The energy flow through the system is given by

$$\vec{I} = cT \vec{J} - \lambda_x \frac{\partial T}{\partial x} \vec{e}_x - \lambda_y \frac{\partial T}{\partial y} \vec{e}_y \quad (4-33)$$

where  $\vec{e}_x$  and  $\vec{e}_y$  are unit vectors. If the power density is  $\sigma$ , the divergence of Eq. 4-33 becomes

$$\sigma = cJ \frac{\partial T}{\partial z} - \lambda_x \frac{\partial^2 T}{\partial x^2} - \lambda_y \frac{\partial^2 T}{\partial y^2} \quad (4-34)$$

An equation of this form will be satisfied by  $T$  whether the power density is that intended in the design or not. If the power density is perturbed in a small local region, then outside that region both the original temperature  $T^0$  and the new perturbed temperature  $T^0 + T'$  satisfy

Eq. 4-34, so that the perturbation in temperature satisfies

$$cJ \frac{\partial T'}{\partial z} - \lambda_x \frac{\partial^2 T'}{\partial x^2} - \lambda_y \frac{\partial^2 T'}{\partial y^2} = 0 \tag{4-35}$$

A perturbation of the flow distribution is clearly equivalent to the power perturbation formulated here.

In some cases there will be important variations in the conductivities in passing from the cold to the hot regions of the wall. However, the two conductivities are in a fixed proportion

$$\frac{\lambda_x}{\lambda_{x_0}} = \frac{\lambda_y}{\lambda_{y_0}} = \Lambda(z) \tag{4-36}$$

where the subscript zero denotes the value at the cold side of the wall.

It is convenient to introduce the dimensionless quantities

$$\begin{aligned} \xi &\equiv \sqrt{\frac{\sigma}{T_0 \lambda_{x_0}}} x \\ \eta &\equiv \sqrt{\frac{\sigma}{T_0 \lambda_{y_0}}} y \\ \bar{\rho} &= \xi \bar{\epsilon}_x + \eta \bar{\epsilon}_y \\ \nabla' &= \bar{\epsilon}_x \frac{\partial}{\partial \xi} + \bar{\epsilon}_y \frac{\partial}{\partial \eta} \end{aligned} \tag{4-37}$$

where  $T_0$  is the temperature at which gas enters the wall. In terms of



these expressions, Eq. 4-35 becomes

$$\Delta \nabla'^2 T' = \frac{cT_o J}{\sigma} \frac{\partial T'}{\partial z} \quad (4-38)$$

The conductivities  $\lambda_x$  and  $\lambda_y$  may be estimated in the following way: The heat conduction in the metal only is considered, neglecting for the moment gaseous conduction effects. In situations where the slope of the channel boundary is always small,  $\lambda_x$  is given by

$$\lambda_x = 2 \frac{\tau}{\alpha} \lambda_m \quad (4-39)$$

because  $2 \frac{\tau}{\alpha}$  is the proportion of the horizontal flow path which is metallic. The value of  $\lambda_y$  is obtained by the same general method: For Dumbo wall geometry two flat plates separated by a height  $\alpha$  enclose a single sinusoidal plate. For one sinusoidal channel of length  $v$  this provides two metallic conduction paths of length  $v/2$  and thickness  $\tau$  connecting upper and lower plates. In each path the temperature gradient is only  $\alpha/(v/2)$  times the vertical average gradient. Combining these factors gives

$$\lambda_y = \frac{4 \tau \alpha}{v^2} \lambda_m \quad (4-40)$$

The conductivity of the gas will tend to increase these values to some extent. It may be argued that

$$\lambda_x = 2 \frac{\tau}{a} \lambda_m + \lambda_g$$

$$\lambda_y = \frac{4\tau a}{u^2} \lambda_m + \lambda_g \quad (4-41)$$

will still underestimate the conductivities, as these are the values one would arrive at if the heat flows in the metal and gas were somehow magically isolated from one another. In actual cases of interest the metallic part of the conduction seems to predominate.

#### 4-5: The Single Channel Aberration

Consider in detail the case for constant conductivities,  $\Lambda = 1$ , which brings Eq. 4-38 to the form of a standard diffusion equation. In this case, a solution everywhere except at the point  $\vec{\rho} = \vec{\rho}'$ ,  $z = z'$  is

$$G' = \begin{cases} \frac{1}{4\pi} \frac{cT_0J}{\sigma} \frac{1}{z-z'} e^{-\frac{1}{4} \frac{cT_0J}{\sigma} \frac{1}{z-z'} |\vec{\rho}-\vec{\rho}'|^2} & \text{for } z > z' \\ 0 & \text{for } z < z' \end{cases} \quad (4-42)$$

where the coefficient has been chosen to make

$$\int G' d\xi d\eta = 1 \quad (z > z') \quad (4-43)$$

This is the usual Green's function for a point source at  $\vec{\rho}'$ ,  $z'$ . However, in this problem a unit point source will yield a solution  $G$  such that

$$\int G dx dy = 1,$$

or

$$\int G \, d\xi \, d\eta = \frac{\sigma}{T_0} \frac{1}{\sqrt{\lambda_{x_0} \lambda_{y_0}}}$$

so that

$$G = \frac{\sigma}{T_0} \frac{1}{\sqrt{\lambda_{x_0} \lambda_{y_0}}} G'$$

(4-44)

Hence

$$G(x, y, z, z') = \frac{\gamma}{z-z'} e^{-\frac{\Omega}{z-z'}}$$

where

$$\gamma = \frac{cJ}{4\pi\sqrt{\lambda_{x_0} \lambda_{y_0}}}$$

and

$$\Omega = \frac{1}{4} \frac{cT_0J}{\sigma} \rho^2 = \frac{cJ}{4} \left( \frac{x^2}{\lambda_{x_0}} + \frac{y^2}{\lambda_{y_0}} \right)$$

(4-45)

where the point source is specialized to the  $z$  axis ( $\vec{\rho}' = 0$ ).

The temperature distribution resulting from any source now may be expressed as a superposition of solutions for elementary sources. The remainder of Sec. 4-5 is devoted to consideration of the extreme situation where one channel is blocked. There will be an amount of power  $\frac{1}{2} c\omega v\sigma$  generated in this region which must be dissipated to neighboring

~~SECRET~~

channels and hence must be carried by the rest of the gas stream. This power will constitute a uniform line source, so that the total temperature perturbation will be of the form

$$T'(x, y, z) = B \int_0^w G(x, y, z, z') dz' \quad (4-46)$$

The constant B is determined from the total power delivered due to the perturbation, whence

$$\begin{aligned} \frac{1}{2} \alpha \sigma v w &= c J \int T'(x, y, w) dx dy \\ &= c J B \int_0^w dz' \int G(x, y, w, z') dx dy \\ &= c J B \int_0^w dz' = c J B w \end{aligned} \quad (4-47)$$

so that

$$B = \frac{1}{2} \frac{\alpha v \sigma}{c J} \quad (4-48)$$

There remains the job of performing the integral in Eq. 4-46

$$\int_0^w \frac{1}{w-z'} e^{-\frac{\Omega}{w-z'}} dz' = \int_{\Omega/w}^{\infty} \frac{1}{\xi} e^{-\xi} d\xi = E(\Omega/w) \quad (4-49)$$

where  $E(\Omega/w)$  is the exponential integral, which is a tabulated function.

Thus the temperature perturbation is given by

~~SECRET~~

$$\begin{aligned}
 T'(x, y, w) &= B \gamma E(\Omega/w) \\
 &= \sqrt{\frac{1}{\lambda_{x_0} \lambda_{y_0}}} \frac{\alpha \sigma v}{8\pi} E \left[ \frac{cJ}{4w} \left( \frac{x^2}{\lambda_{x_0}} + \frac{y^2}{\lambda_{y_0}} \right) \right] \quad (4-50)
 \end{aligned}$$

The same procedure may be used to obtain a formal solution in the case of variable  $\Lambda(z)$ . In Eq. 4-38 the substitution of variables is made

$$t = \int_0^z \Lambda(z') dz' \quad (4-51)$$

The equation becomes

$$\nabla'^2 T' = \frac{cT_0J}{\sigma} \frac{\partial T'}{\partial t} \quad (4-52)$$

which is the form dealt with earlier in this section. However, the power density will not be distributed uniformly in the new variable  $t$  so that the transformation is inclined to lead to unpleasant integrals at the stage equivalent to Eq. 4-49. The remainder of this section is confined to the case of constant conductivities.

The expression for  $T'(x, y, w)$  given by Eq. 4-50 defines two characteristic lengths

~~SECRET~~

$$x_0 = \sqrt{\frac{4 w \lambda x_0}{c J}}$$
$$y_0 = \sqrt{\frac{4 w \lambda y_0}{c J}} \tag{4-53}$$

which are the semi-major and semi-minor axes of an ellipse on which the exponential integral assumes the value  $E(1)$ . From symmetry considerations the temperature distribution would be of the same form as that of Eq. 4-50 if the perturbing power were generated not in a line source but in an ellipsoidal cylinder whose axes were in the ratio  $x_0/y_0$ .

The average conductivity approximation should be good provided the heat flow distributes itself over a large number of channels. This will be true if the dimensions  $v$  and  $\alpha$  of the channels are, respectively, much smaller than the dimensions  $x_0$  and  $y_0$  of the characteristic ellipse. The ratio of total energy transport to energy transport through the characteristic ellipse will be the ratio of the two integrals

$$\int_0^{\infty} r E(r) dr = \frac{1}{2}$$
$$\int_0^1 r E(r) dr = \frac{1}{2} [E(1) + 1 - 2e^{-1}]$$
$$= \frac{1}{2} (0.4736) \tag{4-54}$$

~~SECRET~~



so that slightly more than half the energy transport takes place outside the characteristic ellipse.

The results of a pilot calculation give an indication of the extent to which this method may be trusted. The following typical values are assumed:

$$\tau = 2.5 \times 10^{-3} \text{ cm}$$

$$a = 1.5 \times 10^{-2} \text{ cm}$$

$$v = 7.5 \times 10^{-2} \text{ cm}$$

$$\lambda_m = 0.1 \text{ cal / cm - sec - deg}$$

$$\lambda_g = 1 \times 10^{-3} \text{ cal / cm - sec - deg}$$

$$c = 3.5 \text{ cal / gm - deg}$$

$$J = 1 \text{ gm / cm}^2 \text{ - sec}$$

$$w = 1 \text{ cm}$$

$$\sigma v = 4.92 \text{ cal / cm}^2 \text{ - sec}$$

The thermal conductivity components from Eq. 4-41 are

$$\lambda_{x_0} = 3.3 \times 10^{-2} \text{ cal / cm - sec - deg}$$

$$\lambda_{y_0} = 3.60 \times 10^{-3} \text{ cal / cm - sec - deg}$$

which give characteristic lengths (Eq. 4-53) of



~~SECRET~~

Single Channel Aberration

Section 4-5

$$x_0 = 1.95 \times 10^{-1} \text{ cm}$$

$$y_0 = 6.48 \times 10^{-2} \text{ cm}$$

These values indicate that

$$\frac{x_0}{v/2} = 5.2$$

$$\frac{y_0}{a/2} = 8.6$$

The number of channels contained in the characteristic ellipse is

$$\frac{2\pi x_0 y_0}{av} = 70.2$$

This indicates that the approximation should be accurate enough for estimation purposes, though spectacular precision is not expected.

The temperature perturbation as given by Eq. 4-50 is

$$T'(x, y, w) = 35.6 E \left( \frac{\Omega}{w} \right) \text{ degrees}$$

where

$$\frac{\Omega}{w} = 26.5x^2 + 239y^2$$

(4-55)

Values of this temperature increase are mapped in Fig. 4-3.

~~SECRET~~



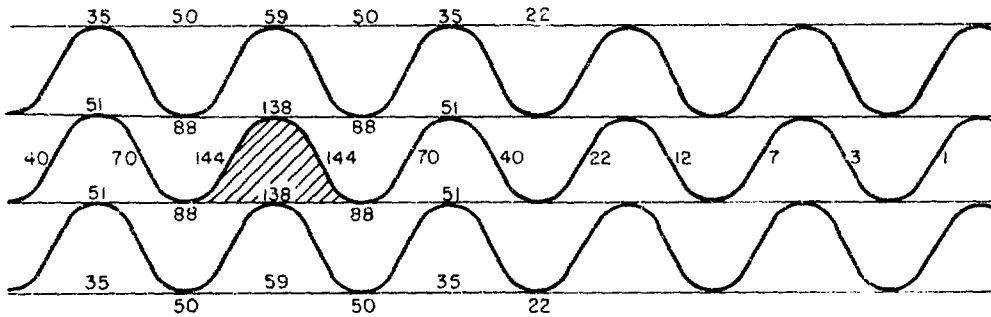


FIG. 4-3: WALL TEMPERATURE INCREASES ABOVE NORMAL FROM ONE BLOCKED CHANNEL.

While the average conductivity approach might seem to become rapidly worse as  $x, y \rightarrow 0$ , due to large temperature variations over distances comparable to channel dimensions, evidently the temperature in this region is largely determined by the extent of heat diffusion outward through the more distant regions, where the approximation is on firmer ground. It is easy to get a rough upper limit on the expected temperatures as follows: Only about half the power generated in the blocked channel remains within the characteristic ellipse. Suppose this much power were given up to the four channels only which share walls with the blocked channel. Since the power of one tube would raise the gas flow of one channel some 2500 degrees, half that power will raise these four gas flows  $1/8$  as much, or about 300 degrees. It is reasonable to suppose that the other 65 channels within the characteristic ellipse

~~SECRET~~

share at least 1/3 of that power, which would bring the hottest temperature down to about 200 degrees.

Isolated partial channel blockages and actual fluctuations in power generations may be treated in the same manner as for the case of a totally blocked channel.

One assumption is implicit throughout this analysis: The flow through the open channels is fixed and remains unchanged by the temperature perturbation. Actually, the flow will be influenced to some extent by the temperature change, through changes in the density and viscosity of the flowing gas. From Fig. 4-3 it may be noted that the average temperature deviation within a channel adjacent to the blocked channel will be less than 100 degrees, or 4%. This corresponds to a change of 4% in density and 3% in viscosity at the hot end of the channel, with smaller percentage deviations elsewhere. The uniform flow assumption seems consistent to within the accuracy of other approximations in this treatment. Further justification of this approximation is given in Sec. 4-6, which investigates a situation where the interaction between temperature and gas flow can become very important.

4-6: Effects of Channel Fabrication Errors

The most important fabrication errors in the Dumbo wall design are likely to be in the introductory channel constrictions, since that is where the structure is most fine-grained. The Dumbo wall is divided

~~SECRET~~



---

into a mosaic array of rectangular cells, each consisting of a cluster of single channels. Through each cell of this structure gas flows from a relatively high impedance source so that the flow through a cell is insensitive to conditions within the metal wall. Since the flow is fixed, the average temperature within the cell is unaffected by channel fabrication errors. However, distributed channel errors will lead to nonuniformities of flow and consequent temperature variations within a cell. It is such variations that are investigated in the present section. The problem differs from that of Sec. 4-5 in that a clustering of errors may conspire to nullify the effect of thermal conductivity to such an extent that temperature-induced changes in viscosity and density become very important. It is shown that the size of the mosaic cell serves to limit the extent of temperature deviations therein. A sufficiently small cell results in a smoothed temperature distribution due to increased thermal conduction within the cell. The approach is to solve the problem for particular patterns of errors, which subsequently can be superimposed in order to obtain the temperature distribution from an arbitrary error pattern.

The heat flow is described by Eq. 4-34. This equation may be transformed to dimensionless variables, given by



~~SECRET~~

Fabrication Errors

Section 4-6

$$\zeta = z / w$$

$$\theta = T / T_0$$

$$q = \frac{c T_0}{\sigma w} (JA) \tag{4-56}$$

which using the definitions in Eq. 4-36 and 4-37 brings Eq. 4-34 to the form

$$q \frac{\partial \theta}{\partial \zeta} - \Lambda \nabla^2 \theta = 1 \tag{4-57}$$

where  $\theta$  is a function of  $\xi$ ,  $\eta$ , and  $\zeta$  and where  $\nabla^2$  refers to  $\xi$  and  $\eta$  only (i.e., the  $\nabla'^2$  notation of Sec. 4-5 has been replaced by  $\nabla^2$ ). According to Eq. 3-1 the gas flow for a single channel is determined by an equation of the form

$$\frac{dp}{dz} = - \frac{1}{B} \frac{\eta}{\rho} (JA) \tag{4-58}$$

where  $A$  is the total area allotted to one channel. The geometric conductance function  $B(z)$  is given, as shown in Fig. 3-2, by

$$B(z) = \begin{cases} B_1 & \text{for } 0 < z < w_1 \\ B_2 & \text{for } w_1 < z < w \end{cases} \tag{4-59}$$

and the viscosity-density ratio is given by

$$\frac{\eta}{\rho} = \frac{\eta_0}{\rho_0} (T / T_0)^{n+1} \tag{4-60}$$

~~SECRET~~



In terms of the dimensionless quantities

$$\beta(\zeta) = \frac{B_2}{B(w\zeta)}$$

$$\omega = w_1/w$$

$$\pi = B_2 \frac{\rho_0}{\eta_0} \frac{c T_0}{A \sigma w^2} p \quad (4-61)$$

Eq. 4-58 becomes

$$\frac{d\pi}{d\zeta} = -\beta \theta^{n+1} q \quad (4-62)$$

A two-dimensional array of such channels is governed by a general flow law of the form

$$\frac{\partial \pi}{\partial \zeta} = -g(q, \theta, \zeta, \bar{p}) \quad (4-63)$$

which is more convenient to use in the following analysis. The following conventions are used:

$$g_q \equiv \frac{\partial g}{\partial q}$$

$$g_\theta \equiv \frac{\partial g}{\partial \theta}$$

(4-64)

In any realistic flow situation  $g$ ,  $g_q$ , and  $g_\theta$  are positive.



~~SECRET~~

Within a cell the pressure across the wall must be constant

$$\Delta \pi = - \int_0^l g d \zeta = \text{const} \quad (4-65)$$

That is, it must not depend on  $\bar{\rho}$ , in spite of variations in  $q$  and  $\theta$ .

Equation 4-65, together with Eq. 4-57, determines the problem.

The variables are expressed as a sum of an unperturbed part and a small perturbation

$$\begin{aligned} g &= g_0(q, \theta, \zeta) + g_1(q, \theta, \zeta, \bar{\rho}) \\ \theta &= \theta_0(\zeta) + \theta_1(\zeta, \bar{\rho}) \\ q &= q_0 + q_1(\bar{\rho}) \end{aligned} \quad (4-66)$$

The channel errors appear in the drag perturbation  $g_1$ . If there is no perturbation, then  $\nabla^2 \theta = 0$  and Eq. 4-57 may be solved to obtain

$$\theta_0 = 1 + \frac{1}{q_0} \zeta \quad (4-67)$$

which is the solution of the unperturbed problem and also gives a convenient evaluation of  $q_0$  in terms of the final temperature ratio. The expressions of Eq. 4-66 are substituted into Eqs. 4-57 and 4-65. For small perturbations the following perturbation equations are obtained.

$$q_0 \frac{\partial \theta_1}{\partial \zeta} - \Lambda \nabla^2 \theta_1 = - \frac{1}{q_0} q_1 \quad (4-68)$$

~~SECRET~~

$$\int_0^1 \left\{ g_{0q}(q_0, \theta_0, \zeta) \cdot q_1(\vec{\rho}) \right. \\ \left. + g_{0\theta}(q_0, \theta_0, \zeta) \cdot \theta_1(\zeta, \vec{\rho}) \right. \\ \left. + g_1(q_0, \theta_0, \zeta, \vec{\rho}) \right\} d\zeta = 0 \quad (4-69)$$

The arguments of  $g_{0q}$ ,  $g_{0\theta}$ , and  $g_1$  are  $\theta_0(\zeta)$  and  $q_0$ , so that these are known functions. Although the perturbation affects  $\Lambda$ , it enters into Eq. 4-68 in the form  $\Lambda \nabla^2 \theta_0$  only, which vanishes.

As Eqs. 4-68 and 4-69 constitute only two relations among the three perturbation variables, the  $\vec{\rho}$  dependence of  $g_1$  may be specified as desired and the equations solved for  $q_1$  and  $\theta_1$ . Because the relations are linear in  $q_1$ ,  $\theta_1$ , and  $g_1$ , a linear combination of solutions is also a solution. An arbitrary problem may be solved entirely in terms of a complete set of choices of  $g_1$ , each of which may be chosen for analytical convenience. Now any drag function  $\beta(\zeta, \vec{\rho})$  may be expressed as a Fourier series in complex exponentials of the variable  $\vec{\rho}$ , and this dependence is reflected in  $g$ . This leads to perturbations of the form

$$g_1(q, \theta, \zeta, \vec{\rho}) = g_1(q, \theta, \zeta) e^{i\vec{k} \cdot \vec{\rho}} \\ \theta_1(\zeta, \vec{\rho}) = \theta_1(\zeta) e^{i\vec{k} \cdot \vec{\rho}} \\ q_1(\vec{\rho}) = q_1 e^{i\vec{k} \cdot \vec{\rho}} \quad (4-70)$$

~~SECRET~~

Fabrication Errors

Section 4-6

which on substitution into Eqs. 4-68 and 4-69 yield

$$q_0 \frac{d\theta_1}{d\xi} + \Lambda k^2 \theta_1 = -\frac{1}{q_0} q_1 \quad (4-71)$$

$$\int_0^1 \{ g_{0q} q_1 + g_{0\theta} \theta_1 + g_1 \} d\xi = 0 \quad (4-72)$$

Equation 4-71 may be solved for  $\theta_1$  in terms of the yet undetermined constant  $q_1$

$$\theta_1 = -\frac{1}{q_0^2} I(\xi) q_1 \quad (4-73)$$

where

$$I(\xi) = e^{-\frac{k^2}{q_0} \int_0^\xi \Delta(\xi') d\xi'} \int_0^\xi e^{\frac{k^2}{q_0} \int_0^{\xi'} \Delta(\xi'') d\xi''} d\xi' \quad (4-74)$$

This has the proper initial value,  $\theta_1(0) = 0$ , showing the inlet gas temperature to be unaffected by the perturbation. This result now may be substituted into Eq. 4-72 to give

$$\int_0^1 \left\{ g_{0q} q_1 - \frac{1}{q_0^2} I(\xi) g_{0\theta} q_1 + g_1 \right\} d\xi = 0 \quad (4-75)$$

or

~~SECRET~~



$$q_1 = \frac{-\int_0^1 q_1 d\zeta}{\int_0^1 \left\{ q_0 q - \frac{1}{q_0^2} I(\zeta) q_{0\theta} \right\} d\zeta} \quad (4-76)$$

The integrations of Eq. 4-76 all involve known functions, so that  $q_1$  is determined. Substitution into Eq. 4-73 gives the temperature perturbation.

To recapitulate: According to Eqs. 4-62 and 4-63 the functional form of  $g$  is given by

$$g = \beta \theta^{n+1} q \quad (4-77)$$

where the function  $\beta$  according to Eqs. 4-59 and 4-61 is given by

$$\beta(\zeta) = \begin{cases} \beta_1 & \text{for } 0 < \zeta < \omega \\ 1 & \text{for } \omega < \zeta < 1 \end{cases} \quad (4-78)$$

In the formulas above, the expressions for  $q$  and  $\theta(\zeta)$  to be used in the various partial derivatives of  $g$  are  $q_0$  and  $\theta_0(\zeta)$  as given by Eq. 4-67. Of course, the differentiations are to be done before the substitutions. The drag perturbation  $g_1$  is the result of a perturbation  $\delta\beta_1$  in the inlet impedance, and hence is given by

$$g_1 = \frac{\partial g}{\partial \beta_1} \delta \beta_1 = g_{\beta_1} \delta \beta_1 \quad (4-79)$$

which vanishes for  $\zeta > \omega$ . Substituting into Eqs. 4-76 and 4-73 gives finally

~~SECRET~~

$$\theta_i(l) = \left\{ \frac{\frac{1}{q_0^2} I(l)}{\int_0^l g_{0q} d\zeta - \frac{1}{q_0^2} \int_0^l I(\zeta) g_{00} d\zeta} \int_0^l g_{p1} d\zeta \right\} \delta \beta_1 = f(k^2) \delta \beta_1 \quad (4-80)$$

The integrals are elementary except the one involving I. The only dependence on  $k^2$  is through I.

The specific form of  $I(\zeta)$  is determined by the conductivity function  $\Lambda(\zeta)$ . Two cases are of particular interest:

For tungsten

$$\Lambda_w(\zeta) = 1 \quad (4-81)$$

For molybdenum

$$\Lambda_{Mo}(\zeta) = 1 - \frac{1}{\zeta^n} \zeta \quad (4-82)$$

The corresponding expressions for  $I(\zeta)$  are

$$I_w(\zeta) = \frac{q_0}{k^2} \left( 1 - e^{-\frac{k^2}{q_0} \zeta} \right) \quad (4-83)$$

$$I_{Mo}(\zeta) = \frac{\sqrt{\pi}}{2a} e^{a^2(\zeta^* - \zeta)^2} \left\{ \operatorname{erf}(a \zeta^*) - \operatorname{erf}(a [\zeta^* - \zeta]) \right\} \quad (4-84)$$

where  $\zeta^*$  is defined by Eq. 4-82,

~~SECRET~~

$$a = \sqrt{\frac{k^2}{2q_0 \zeta^*}}$$

(4-85)

and

$$\operatorname{erf}(x) = \frac{2}{\sqrt{\pi}} \int_0^x e^{-u^2} du$$

(4-86)

Equation 4-86 defines the error function, which is tabulated. With the values of these functions the remaining integrals of Eq. 4-80 may be evaluated numerically. In fact, for the tungsten case the integral involving  $I(\zeta)$  may be expressed in terms of incomplete gamma functions, which are tabulated. In Figs. 4-4 and 4-5 the function  $f^2(k^2)$  is plotted against  $k^2$ , in connection with specific cases investigated below.

The procedure for finding the temperature distribution produced by a given impedance distribution is straightforward. If the impedance perturbation is expressed as the Fourier expansion

$$\delta \beta_1(\bar{\rho}) = \sum_{\bar{k}} e^{i\bar{k} \cdot \bar{\rho}} \delta \beta_1(\bar{k})$$

(4-87)

then the temperature perturbation is given by

$$\theta_1(\bar{\rho}) = \sum_{\bar{k}} e^{i\bar{k} \cdot \bar{\rho}} f(k^2) \delta \beta_1(\bar{k})$$

(4-88)

According to the usual theory of Fourier series, the values assumed by

~~SECRET~~

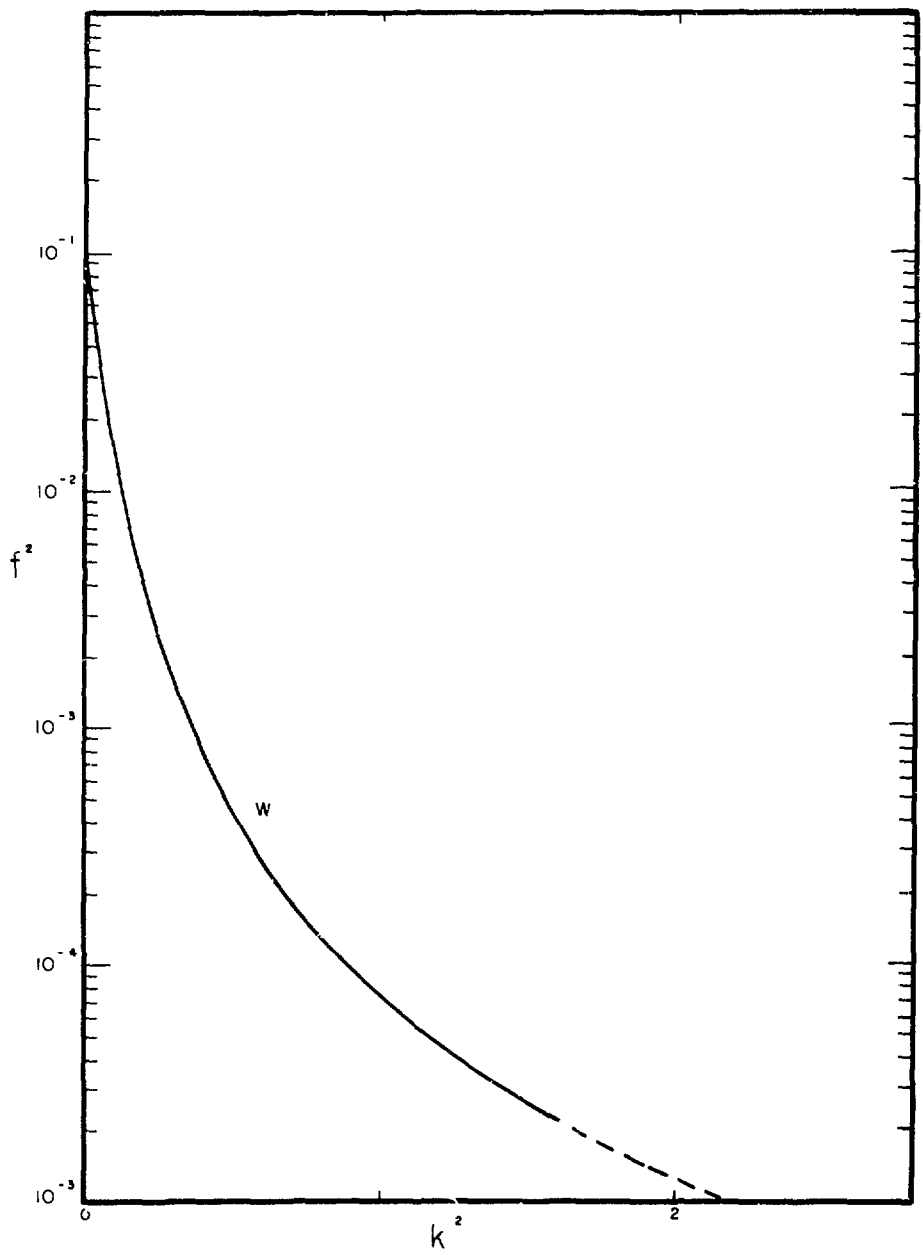


Fig. 4-4: The Function  $f^2(k^2)$  for Tungsten

~~SECRET~~

~~SECRET~~

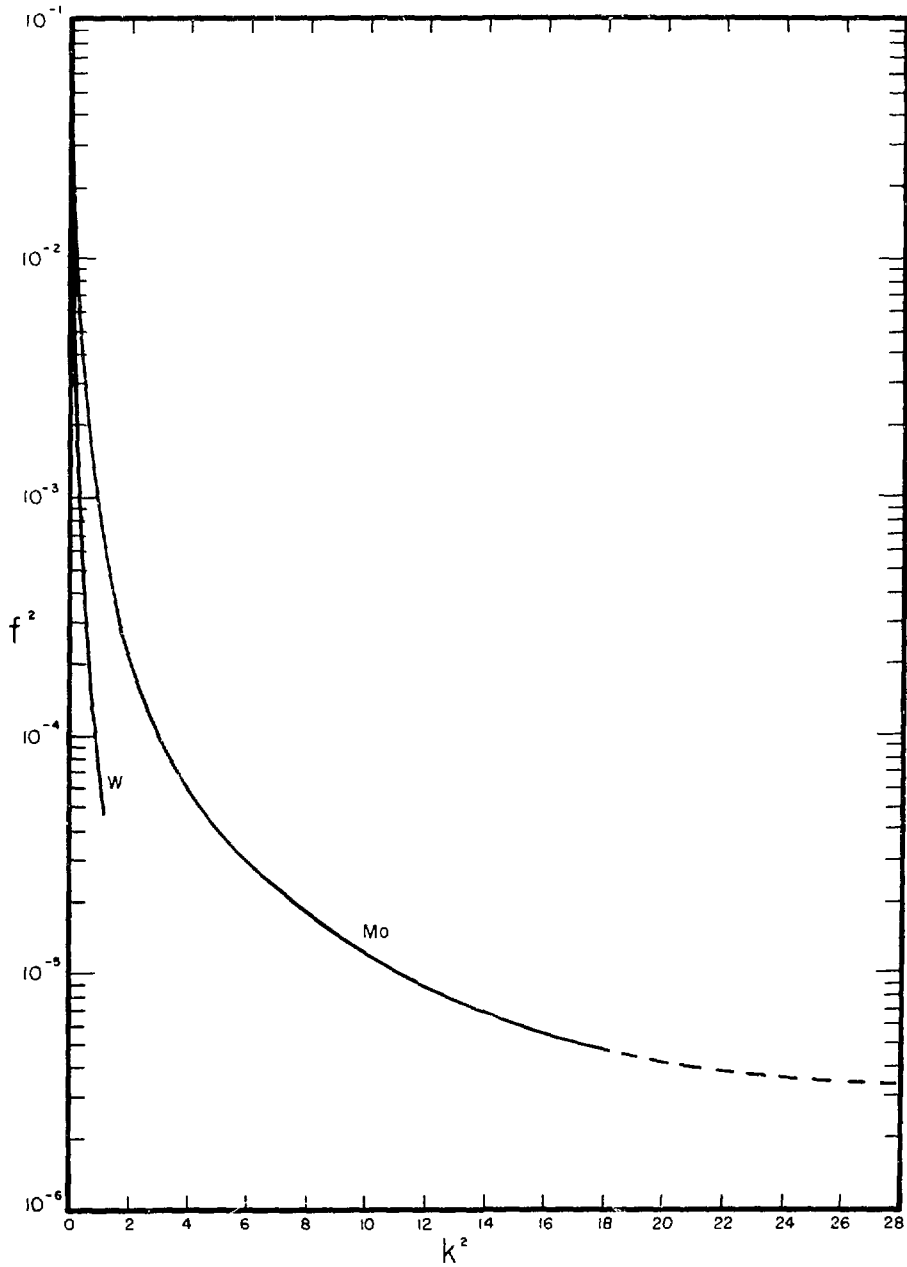


Fig. 4-5: The Function  $f^2(k^2)$  for Tungsten and Molybdenum

~~SECRET~~

$$\vec{k} = k_x \vec{\epsilon}_x + k_y \vec{\epsilon}_y \quad (4-89)$$

are determined by the condition that the exponentials must be periodic on the boundary of the cell. If  $x_0$  and  $y_0$  are the two dimensions of the mosaic cell, this determines two fundamental expansion modes.

For the x mode

$$2\pi = k_{x0} \xi_0 = \sqrt{\frac{\sigma}{T_0 \lambda_{x0}}} x_0 k_{x0}$$

or

$$k_{x0}^2 = 4\pi^2 \frac{T_0 \lambda_{x0}}{\sigma} \frac{1}{x_0^2} \quad (4-90)$$

For the y mode

$$2\pi = k_{y0} \eta_0 = \sqrt{\frac{\sigma}{T_0 \lambda_{y0}}} y_0 k_{y0}$$

or

$$k_{y0}^2 = 4\pi^2 \frac{T_0 \lambda_{y0}}{\sigma} \frac{1}{y_0^2} \quad (4-91)$$

All values of  $\vec{k}$  are given by

$$\vec{k} = n_x k_{x0} \vec{\epsilon}_x + n_y k_{y0} \vec{\epsilon}_y \quad (4-92)$$

where  $n_x$  and  $n_y$  may assume all positive and negative values. The lowest modes will be "fundamental" only to within complex conjugates. The mode

corresponding to  $n_x = n_y = 0$  will be absent because the total flow through the cell is fixed. As may be seen from Eq. 4-92,  $k^2$  is given by

$$k^2 = n_x^2 k_{x0}^2 + n_y^2 k_{y0}^2 \quad (4-93)$$

There are four values of  $\vec{k}$  leading to the same  $k^2$  unless one component of  $\vec{k}$  vanishes. In the actual Dumbo designs the relative dimensions of a cell are very close to those of a characteristic ellipse, as given in Eq. 4-53, so that fortuitously

$$k_{x0}^2 = k_{y0}^2 \equiv k_0^2 \quad (4-94)$$

In this case the number of modes belonging to a value of  $k^2$  is doubled unless  $n_x^2 = n_y^2$ .

In Eqs. 4-76 and 4-80 there is no mathematical reason to expect a given sign for the denominator. However, a negative denominator is indicative of unstable flow, according to the general theory of flow stability developed in App. E. For  $k^2 = 0$  the vanishing of the denominator is equivalent to the condition of borderline stability without thermal conductivity. Since  $I(\zeta)$  is a decreasing function of  $k^2$ , the effect of thermal conductivity is to enhance the stability of the higher modes of flow.

If the continuous wall approximation is to be used down to wavelengths which are not large compared to channel diameters, it is important to get an idea of what sort of errors the approximation

~~SECRET~~

introduces. The shortest meaningful wavelength is that for which alternate adjacent channels possess flow deviations which are equal and opposite. Equation 4-80 always predicts finite temperature deviations. However, from physical considerations there can be no wall temperature deviations, because high and low flows are on opposite sides of each wall common to adjacent channels, and the walls of each channel are confronted with the same situations. Thus at the shortest wavelengths the continuous wall approximation will over-estimate temperature deviations.

For design evaluation purposes Eq. 4-88 is not as convenient as a relation between expected temperature variations and overall fabrication tolerances. Such a relation will now be developed. The mean-square value of a real-valued function

$$h(\vec{\rho}) = \sum_{\vec{k}} e^{i\vec{k} \cdot \vec{\rho}} h(\vec{k}) \quad (4-95)$$

is given by

$$\bar{h}^2 \equiv \frac{1}{\xi_0 \eta_0} \int h^2(\vec{\rho}) d\xi d\eta = \sum_{\vec{k}} |h(\vec{k})|^2 \quad (4-96)$$

This may be seen at once by integrating the product  $h(\vec{\rho}) h^*(\vec{\rho})$  as given by Eq. 4-95. Using Eq. 4-96 on Eq. 4-88 gives

$$\bar{\theta}_1^2 = \sum_{\vec{k}} f^2(k^2) |\delta \beta_1(\vec{k})|^2 \quad (4-97)$$

~~SECRET~~



If all the channel errors within a mosaic cell are independent of one another (i.e., random), and all arise from the same probability distribution, then  $\delta\beta_1(\vec{k})$  will have a probability distribution independent of  $\vec{k}$  until the wavelength corresponding to  $\vec{k}$  gets close to the diameter of a single channel. The reason for this is that by Eq. 4-87

$$\delta\beta_1(\vec{k}) = \frac{1}{\xi_0\eta_0} \int e^{-i\vec{k}\cdot\vec{\rho}} \delta\beta_1(\vec{\rho}) d\xi d\eta \quad (4-98)$$

is, until  $\vec{k}$  gets large, a sum of complex numbers, one from each channel, whose magnitudes all derive from a fixed probability distribution, and which are systematically arranged not to point in any preferred direction on the complex plane. For wavelengths shorter than channel dimensions, Eq. 4-98 gives cancellation within each channel, and so automatically imposes a cut-off where the continuous wall approximation becomes meaningless. This cut-off may be approximated by treating all modes alike up to a number  $N$ , but assuming that the coefficients of all higher modes are negligible. The number  $N$  should be close to the number of channels through the mosaic cell.

This same approximation appears in the Debye theory of crystalline specific heats, where its justification is evident: the number of degrees of freedom of the system is independent of choices of coordinates. More rigorous justification is given below.

~~SECRET~~

Applying Eq. 4-96 to Eq. 4-87, indicates that on the average

$$\overline{(\delta \beta_i)^2} = N [\delta \beta_i(\vec{k})]^2 \quad (4-99)$$

where  $\vec{k}$  is any one of the low modes. Substitution into Eq. 4-97 gives

$$\overline{\theta_i^2} = \frac{1}{N} \left( \sum_{\vec{k}} f^2(k^2) \right) \overline{(\delta \beta_i)^2} \quad (4-100)$$

This may be restated as a ratio between percentage root-mean-square deviations in temperature and in introductory channel height  $a_1$ . The geometrical conductance factor B for the thin channels described in Chap. 2 is proportional to  $\alpha^3$ . Hence

$$\frac{\delta \beta_i}{\beta_i} = 3 \frac{\delta a_1}{a_1} \quad (4-101)$$

which with Eq. 4-100 defines a multiplication factor R relating rms deviations of temperature and fabrication errors, where

$$R = \frac{\sqrt{\overline{\theta_i^2}}}{\theta_o} \left( \frac{\sqrt{(\delta a_1)^2}}{a_1} \right)^{-1} = \frac{3}{\sqrt{N}} \frac{\beta_i}{\theta_i} \left( \sum_{\vec{k}} f^2(k^2) \right)^{1/2} \quad (4-102)$$

This is a convenient form for evaluation. The maximum temperature deviation is larger than the rms value. The ratio of values is 1.41 for a sinusoidal deviation. To exceed this value by an appreciable amount requires a function involving sharp variations, or "spikes." However, such spiked functions are discriminated against by the effect of thermal

~~SECRET~~



---

conductivity. They have large Fourier components of short wavelength, and these are suppressed by the small value of  $f(k^2)$  for large  $k$ .

A great deal of what has been developed here does not depend on the continuous wall approximation. To better justify some features of the formulation already given (e.g., treatment of the shorter wavelengths and cut-off point), a more rigorous and elegant approach which assumes an array of discrete channels at the outset is outlined briefly. The set of functions defined at the  $N$  channel positions may be regarded as a vector space of  $N$  dimensions. The transformation from an impedance deviation pattern to the corresponding temperature deviation pattern is linear for small deviations, and may be regarded as a linear operator upon the vector space, which may be called the "temperature operator." "Translation operators," which shift the position of a deviation pattern, may also be defined. Since temperature and impedance deviations are related in a manner that does not depend on the location of the impedance pattern, the temperature operator and translation operators commute. Hence they have the same set of eigenvectors. But translations are unitary operators, so that their eigenvectors (a) span the vector space, and (b) are orthogonal. From (a) there must be just  $N$  eigenvectors. This justifies the previous heuristic procedure of keeping only  $N$  modes. The eigenvectors of translations are complex-exponential functions of the position points, which justifies the functional form that was chosen ad hoc in Eq. 4-70. Moreover, the translation eigenvectors must be both



periodic on the boundary, and, due to (b), orthogonal over the mosaic array. Either of these conditions restricts  $\vec{k}$  to the values given by Eq. 4-93. Thus the eigenfunctions of the expansion given in Eq. 4-95 are exact. The continuous wall approximation is an approximate method of evaluating the eigenvalues of the temperature operator, substituting a differential equation for a more exact and more difficult system involving difference equations. The approximation should be asymptotically correct for the highest eigenvalues (long wavelengths) and, as has been mentioned, gives too high a value for the smallest eigenvalues which should, in fact, drop to zero.

The fourfold eigenvalue degeneracy mentioned with Eq. 4-93 is a consequence of the property that the temperature operator also commutes with the unitary operators of reflection about horizontal and vertical central axes -- which is a fairly ornate way of saying something quite plain. The exceptional cases arise when a reflection operator maps an eigenvector back into itself. The further degeneracy arising from the fortuitous choice of the mosaic cell's boundary shape depends on the continuous wall approximation. It would be expected to arise from a further symmetry of the temperature operator under 90° rotations. Since the sinusoidal geometry of the detailed wall structure does not have this symmetry one may expect a "fine structure splitting" of these degenerate eigenvalues. This splitting should be slight down to quite short wavelengths, since the degeneracy would be exact if the sinusoidal

geometry were replaced by either a very nearly similar array of diamond-shaped channels of the appropriate relative dimensions, or any one of several other properly symmetric geometric forms. Although it is interesting to note what general features of the temperature operator can be predicted in advance, the more exact calculation of the actual eigenvalues would involve some rather heavy mathematical work.

The rms deviation ratio given by Eq. 4-102 is evaluated numerically for three different cases. Data given in Table 4-1 are typical for Dumbo designs described in Chap. 9. Problems 1 and 2 are concerned with metal walls assuming constant thermal conductivities of 0.1 and 0.2 cal/cm-sec-deg, respectively. Both of these values of thermal conductivity are less than that of tungsten given in Table B-1 (0.24 cal/cm-sec-deg). The presence of  $UO_2$  or of possible alloying metals may decrease the thermal conductivity to that chosen in problems 1 or 2. In problem 3 the empirical values of the thermal conductivity of molybdenum as a function of temperature are used. These data are given in App. B.

~~SECRET~~

TABLE 4-1  
THREE TYPICAL PROBLEMS

$\omega = 0.134$	$x_o = 0.300 \text{ cm}$
$\beta_1 = 134$	$y_o = 0.100 \text{ cm}$
$q_o = 0.120$	$c = c_p = 3.85 \text{ cal/gm-deg}$
$\alpha = 0.015 \text{ cm}$	$w = 1.00 \text{ cm}$
$v = 0.075 \text{ cm}$	$J = 1.00 \text{ gm/cm}^2\text{-deg}$

PROBLEM	1	2	3
$\lambda_o$	0.100	0.200	0.389 cal/cm-sec-deg
$\zeta^*$	—	—	1.121
$k_o$	0.4468	0.8936	1.738
R (Eq 4-100)	0.130	0.346	0.288
$\delta T$ for $\frac{\delta a_1}{a_1} = 1\%$	9.7	3.6	8.1 degrees

The function  $f^2(k^2)$  is shown in Figs. 4-4 and 4-5 for the two metals. The values of  $k^2$  are determined by Eqs. 4-91, 4-93, and 4-94.

From Eq. 4-91

$$k_o^2 = 4 \pi^2 \frac{T_o \lambda_{x_o}}{\sigma} \frac{1}{x^2} = 4 \pi^2 \frac{\lambda_{x_o} w q_o}{c J} \frac{1}{x_o^2} \quad (4-103)$$

The value of  $\lambda_{x_o}$  is obtained from Eq. 4-41.

Actual measurements of fabrication errors have been made on a sample section of Dumbo wall. This section is shown in Fig. 1-10. Although it

~~SECRET~~

was made without excessive heed for uniformity and was measured after considerable handling, the measured rms deviation in  $\alpha_1$  was only 12%.\*

Use of the results of problem 3 together with the assumption that

$\delta T_{\max} = 1.5 \delta T_{\text{rms}}$  indicates that  $\delta T_{\max} = 145$  degrees. This extreme tem-

perature increment within a mosaic cell is tolerable, and might be

decreased by improved fabrication and handling techniques. In the numer-

ical designs of Chap. 9 two extreme assumptions are made regarding this

uniformity. As the pessimistic extreme, a 12% rms error is assumed,

while the assumed optimistic extreme is a 1% rms error.

#### 4-7: Other Heat Transfer Mechanisms

Thus far the transfer of heat only by thermal conduction of the metal and of the molecular hydrogen has been considered. Two other heat transfer mechanisms are now considered: namely, the effects of thermal radiation and the influence of molecular dissociation.

Thermal radiation manifests itself in two ways:

(1) Radiative transfer along the x or y direction (see Fig. 4-6) serves primarily to smooth out the temperature distributions developed in Secs. 4-3 and 4-4.

(2) Radiative transfer along the z direction distorts the linear temperature distribution along this axis as developed in Sec. 4-2.

It is shown that both effects are small.

---

\*A large portion of the rms value was due to a few channels, not shown in Fig. 1-10, damaged by excessive handling.

~~SECRET~~

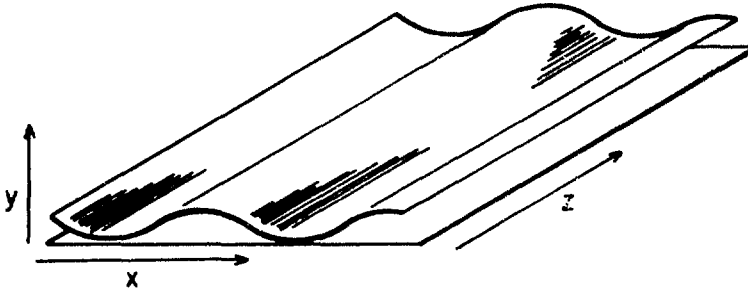


Fig. 4-

For effects of thermal radiation in the x-y plane the hot end of a channel may be considered to be filled with black-body radiation at the average temperature  $\bar{T}$  of this region. A wall at a temperature  $T_b$  flows energy into this region with a flux  $I_R$  given by

$$I_R = \epsilon \sigma (T_b^4 - \bar{T}^4) \quad (4-104)$$

where  $\epsilon$  is the emissivity of the surface and  $\sigma$  is the Stefan-Boltzman constant\* having the value  $1.355 \times 10^{-12}$  cal/cm<sup>2</sup>-sec-deg<sup>4</sup>. To a first approximation, Eq. 4-104 may be written

$$I_R = 4 \epsilon \sigma \bar{T}^3 (T_b - \bar{T}) \quad (4-105)$$

If radiation effects are not present the distribution  $T_b(x)$  for a sinusoidal channel is given by Eq. 4-31 as

---

\*Not to be confused with wall power density also denoted by  $\sigma$ .

~~SECRET~~





$$T_b - T = - \frac{3}{160\pi^2} \frac{\alpha v^2}{\tau} \frac{\bar{J}c}{\lambda_m} \frac{\partial T}{\partial z} \cos \frac{4\pi x}{v} \quad (4-106)$$

The term of Eq. 4-102 corresponding to the influence of the metallic thermal conductivity  $\lambda_m$  on this distribution is given by

$$-\lambda_m \tau \frac{d^2 T_b}{dx^2} = - \frac{3}{5} \alpha \bar{J}c \frac{\partial T}{\partial z} \cos \frac{4\pi x}{v} \quad (4-107)$$

Because the x variation of these two quantities is the same, one may form their ratio and regard the radiation effect as introducing an apparent additional metallic thermal conductivity. Because both faces of the wall are involved, the ratio of interest is

$$2 I_R / \left[ \lambda_m \tau \frac{d^2 T_b}{dx^2} \right] = \frac{1}{4\pi^2} \frac{\epsilon \sigma T^3 v^2}{\lambda_m \tau} \quad (4-108)$$

The following typical values are used

$$\bar{T} = 2800^\circ\text{K}$$

$$v = 7.5 \times 10^{-2} \text{ cm}$$

$$\lambda_m = 0.1 \text{ cal/cm-sec-deg}$$

$$\tau = 2.5 \times 10^{-3} \text{ cm}$$

The ratio given in Eq. 4-108 is  $0.017\epsilon$  where  $\epsilon < 1$ . Thus radiative transfer in the x-y plane contributed less than 2% to the total thermal conduction.

The problem of radiative heat transfer along the z axis may be handled similarly. Since each channel is very long compared to its



height ( $\frac{w}{\alpha} \approx 65$ ), it may be assumed that in every region the temperature of black-body radiations is affected by the local wall temperature distribution only. If two parallel walls are separated by a distance  $\alpha$  with a constant temperature gradient, it may be shown that the radiation received at a point  $z$  from another point  $z'$  is maximized when  $z' - z = \alpha$ , i.e., along a  $45^\circ$  angle. The temperature difference between these two points is given by  $\frac{\Delta T}{w} \alpha$  so that the temperature of the local radiation may be regarded as approximately  $T(z) + \frac{\Delta T}{w} \alpha$ , thus causing a radiative transfer to the wall given by Eq. 4-105 as

$$I_R = 4\epsilon\sigma T(z)^3 \cdot \frac{\Delta T}{w} \alpha \quad \text{cal/cm}^2\text{-sec} \quad (4-109)$$

Hence for a length  $\alpha$  of the wall with cross sectional perimeter  $2\alpha$  the radiative heat received is

$$8\epsilon\sigma T^3 \frac{\Delta T}{w} \alpha^2, \quad \text{cal/sec}$$

This may be compared to the total heat, added by nuclear heating to the gas causing a temperature rise of  $\frac{\Delta T}{w} \alpha$ , given by

$$cJ\alpha v \cdot \frac{\Delta T}{w} \alpha \quad \text{cal/sec}$$

The ratio of the radiative heating to the total heat is

$$\frac{8\epsilon\sigma T^3}{cJ} \quad (4-110)$$

~~SECRET~~

Chapter 4

Wall Temperature Distribution

For  $T = 2500^{\circ}\text{K}$ ,  $c = 3.5 \text{ cal/gm-deg}$ , and  $J = 1 \text{ gm/cm}^2\text{-sec}$ , this ratio is  $0.04\epsilon$ , which indicates a power modification at the hottest end of the channel of less than 4%. Because of the  $T^3$  dependence of the above quantity this value decreases strongly at any cooler location.

From simple solid angle considerations it may be argued that negligible thermal radiation reaches the moderator.

Another heat-transfer mechanism is due to the partial dissociation of hydrogen at high temperatures to atomic hydrogen in the hottest regions and the subsequent recombination of the diffusing atoms in cooler regions. This phenomenon has been studied by I. Langmuir<sup>3</sup> and still earlier by W. Nernst. Potentially this effect may be dominant over normal thermal conduction processes in  $\text{H}_2$  gas at high temperatures because of the large heat of dissociation which is involved. However, because realistic theoretical studies and experimental information are lacking, its influence has been neglected in this report. It can serve only to decrease the value  $\theta_g$ . However, the dissociation and recombination of hydrogen may greatly enhance rocket performance, as is shown in App. D.

REFERENCES

1. B. B. McInteer, R. M. Potter, and E. S. Robinson, Dumbo -- A Pachydermal Rocket Motor, Los Alamos Scientific Laboratory Report LAMS-1887, May 18, 1955.
2. L. Green, Jr., J. App. Mech. 19, 173 (1952).
3. I. Langmuir, Phys. Rev. 34, 401 (1912).

~~SECRET~~

~~SECRET~~

## CHAPTER 5

### LOSS OF REACTOR MATERIAL BY EVAPORATION

The Elephant's Child sat there for three days waiting for his nose to shrink. But it never grew any shorter.

R. Kipling, The Elephant's Child

#### 5-1: Statement of the Problem

The role of the process of evaporation of the refractory metals from the hot regions of a metal rocket motor requires investigation, particularly when the channel walls are constructed of thin foil as in the Dumbo design. Since molybdenum is the most volatile of the various refractory metals considered in this design, it will be used as an example in the discussion that follows.

At first glance it might appear that, because of the low vapor pressure of the metal (less than 10 microns) and the large amounts of hydrogen flowing through the Dumbo wall, metal vapor would be exhausted by the propellant stream at a rate limited by the molecular evaporation process. However, it may easily be shown that this molecular evaporation process is sufficient to maintain a partial pressure at the metal surfaces which is effectively that of thermodynamic equilibrium. Therefore the rate of loss requires solution of a problem of diffusion of the metal atoms into the moving stream. It is with this diffusion problem

~~SECRET~~



Chapter 5      Loss of Reactor Material by Evaporation

---

that this chapter is concerned.

Numerical results for typical design values are presented which show that the material losses are negligible.

5-2: Calculation of the Evaporation Loss

In this problem  $\vec{J}$  denotes the molar flow density of the gas,  $\vec{J}_1$  that of the molybdenum vapor, and  $c$  the molybdenum concentration. The flows satisfy the familiar continuity equations

$$\nabla \cdot \vec{J} = 0 \quad (5-1)$$

$$\nabla \cdot \vec{J}_1 = 0 \quad (5-2)$$

and are also related by a diffusion equation of the form

$$\vec{J}_1 = c \vec{J} - n D \nabla c \quad (5-3)$$

where  $n$  is the total molar density,  $D$  is the diffusion coefficient of molybdenum in hydrogen gas, and  $c$  is the mole fraction of molybdenum.

If the flow is along the  $z$  axis of a heat-exchange passage (Fig. 5-1), then  $\vec{J}$  has a  $z$  component only. Combining Eqs. 5-1, 5-2, and 5-3 gives

$$J_z \frac{\partial c}{\partial z} - n D \nabla^2 c = 0 \quad (5-4)$$

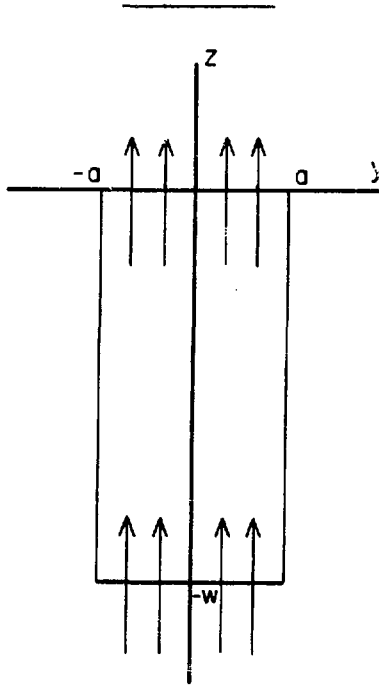


Fig. 5-1

If the problem is further specialized to the case of flow between parallel plates this equation becomes

$$J_2 \frac{\partial c}{\partial z} - nD \left( \frac{\partial^2 c}{\partial y^2} + \frac{\partial^2 c}{\partial z^2} \right) = 0 \quad (5-5)$$

The boundary condition on the y boundaries of the differential equation 5-5 is that the vapor at the metal surface must be saturated. The vapor pressure of molybdenum is given by a relation of the form

$$P = P_1 e^{-E/RT} \quad (5-6)$$

Chapter 5            Loss of Reactor Material by Evaporation

---

However, the evaporation is important only where the temperature is close to its maximum. In this region one may make the linear approximation

$$\frac{1}{T} \cong \frac{1}{T_m} \left( 1 - \frac{T - T_m}{T_m} \right) \quad (5-7)$$

which brings Eq. 5-6 to the form

$$P = P_m e^{-\frac{E}{R} \frac{T_m - T}{T_m^2}} \quad (5-8)$$

where the subscripts m stand for maximum values. In the *Dumbo* wall the temperature increase is linear with distance z, so that if the z origin is chosen at the hot end of the flow passage (for purposes of this problem), it follows that

$$T_m - T = \frac{T_m - T_0}{W} (-z) \quad (5-9)$$

which brings Eq. 5-8 to the form

$$P = P_m e^{\beta z} \quad (5-10)$$

where

$$\beta = \frac{E}{R} \frac{T_m - T_0}{W T_m^2} \quad (5-11)$$

Thus, the y boundary condition on c in Eq. 5-5 is

$$c(a, z) = c(-a, z) = c_m e^{\beta z} \quad (5-12)$$

The approximation used in Eq. 5-7 is good in the case of actual interest, since the exponential term of Eq. 5-12 drops rapidly as  $z \rightarrow -w$ , where  $w$  is the length of the flow passage.

The boundary condition given by Eq. 5-12 leads to a fortuitous simplification in the solution of Eq. 5-5. This solution is of the form

$$c(y, z) = c_m e^{\beta z} F(y) \quad (5-13)$$

which reduces Eq. 5-5 to the ordinary differential equation in  $F(y)$

$$J_z(y) \beta F - nD \left( \frac{d^2 F}{dy^2} + \beta^2 F \right) = 0 \quad (5-14)$$

The boundary condition imposed on  $F$  by Eqs. 5-12 and 5-13 is

$$F(a) = F(-a) = 1 \quad (5-15)$$

The rate at which molybdenum vapor flows through the heat exchanger is given by the area integral normal to the flow

$$\int \vec{J}_1 \cdot d\vec{A} = \int J_{1z} \, dx dy \quad (5-16)$$

so that the loss rate per centimeter of plate edge will be

$$\Phi = \int J_{1z} dy = \int \left( c J_z - nD \frac{\partial c}{\partial z} \right) dy \quad (5-17)$$

where the last form follows from Eq. 5-3 and the integration extends



~~SECRET~~

Chapter 5                      Loss of Reactor Material by Evaporation

across the channel. By Eqs. 5-13 and 5-14 it follows that at the hot side of the Dumbo wall, where  $z = 0$ ,

$$cJ_z - nD \frac{\partial c}{\partial z} = \frac{c_m}{\beta} nD \frac{d^2F}{dy^2} \quad (5-18)$$

so that Eq. 5-17 becomes

$$\Phi = \frac{c_m}{\beta} nD \int \frac{d^2F}{dy^2} dy = 2 \frac{c_m}{\beta} nD \left. \frac{dF}{dy} \right|_B \quad (5-19)$$

where  $dF/dy|_B$  is evaluated at the boundary. The problem is reduced to performing this evaluation, which involves solving Eq. 5-14.

The flow distribution through the channel is given by

$$J_z(y) = -\frac{3}{2} \frac{\bar{J}}{a^2} (y^2 - a^2) \quad (5-20)$$

where  $\bar{J}$  is the mean flow rate. Substituting into Eq. 5-14 gives

$$\frac{d^2F}{dy^2} - \left\{ \left( \frac{3}{2} \frac{\beta \bar{J}}{nD} - \beta^2 \right) - \frac{3}{2} \frac{\beta \bar{J}}{nD a^2} y^2 \right\} F = 0 \quad (5-21)$$

This differential equation may be reduced by use of dimensionless quantities defined by

~~SECRET~~

$$\frac{1}{\lambda^4} = \frac{3}{2} \frac{\bar{J}\beta}{nD a^2}$$

$$\epsilon^2 = \frac{a^2}{\lambda^2} - \lambda^2 \beta^2$$

$$x = y/\lambda$$

$$F(\lambda x) = f(x) \tag{5-22}$$

Eq. 5-21 then becomes

$$f'' - (\epsilon^2 - x^2) f = 0 \tag{5-23}$$

with the boundary conditions

$$f\left(\pm \frac{a}{\lambda}\right) = 1 \tag{5-24}$$

The required value is

$$\left. \frac{dF}{dy} \right|_B = \frac{1}{\lambda} f' \left( \frac{a}{\lambda} \right) \tag{5-25}$$

It may be shown that there are two power series which satisfy Eq. 5-23, consisting respectively of odd and even powers of  $x$ . Because the boundary conditions given by Eq. 5-24 and the symmetry of the problem require an even function of  $x$ , the desired solution is that consisting of even powers

$$f(x) = b \left( 1 + \sum_{k=1}^{\infty} a_{2k} x^{2k} \right) \tag{5-26}$$

The successive terms of the summation are given by the recursion relation

$$a_2 x^2 = \frac{\epsilon^2}{2} x^2$$

$$a_n x^n = \frac{1}{n(n-1)} \left\{ (a_{n-2} x^{n-2}) \epsilon^2 x^2 - (a_{n-4} x^{n-4}) x^4 \right\} \quad (5-27)$$

which may be summed for  $x = a/\lambda$  to obtain the value of  $b$  from Eqs. 5-24 and 5-26. The value of  $f'(a/\lambda)$  may be obtained from

$$f'(x) = \frac{b}{x} \sum_{k=1}^{\infty} (2k) a_{2k} x^{2k} \quad (5-28)$$

which may be evaluated from the terms used in the summation indicated by Eq. 5-26.

### 5-3: Numerical Results

For the Dumbo problem reasonable values of the necessary parameters are

$\bar{J} = 1 \text{ mole/cm}^2\text{-sec}$	$E = 14 \times 10^3 \text{ cal/mol}$
$n = 4 \times 10^{-4} \text{ moles/cm}^3$	$T_m = 2800^\circ \text{K}$
$\alpha = 0.625 \times 10^{-2} \text{ cm}$	$T_0 = 300^\circ \text{K}$
$w = 1 \text{ cm}$	$D = 0.27 \text{ cm}^2/\text{sec}$

The value of  $E$  is derived from Dushman<sup>1</sup> and the value of  $D$  was estimated from the semi-empirical Lennard-Jones intermolecular potential between

~~SECRET~~

Numerical Results

Section 5-3

hydrogen and mercury according to the method described by Hirschfelder.<sup>2</sup>

The resulting values of the intermediate parameters of interest are

$$\begin{aligned}
c_m &= 1.3 \times 10^{-7} & \epsilon &= 1.857 \\
\beta &= 22.3 \text{ cm}^{-1} & b &= 0.09718 \\
\lambda &= 3.365 \times 10^{-3} \text{ cm} & f\left(\frac{a}{\lambda}\right) &= 1.057
\end{aligned}$$

Here  $c_m$  was again obtained from Dushman,<sup>1</sup> using a partial pressure of 10 microns in 100 bar.

Of the two terms constituting  $\epsilon^2$ , according to Eq. 5-22, the second,  $\lambda^2\beta^2$ , is responsible for only 0.1% of the total value. That this term is negligible is not surprising, since it arises from the upstream diffusion term  $nD\partial c/\partial z$  of Eq. 5-3. From Eqs. 5-19 and 5-25 the value of  $\Phi$  is

$$\Phi = \frac{2c_m D f(a/\lambda)}{\beta \lambda} = 8.06 \times 10^{-10} \text{ moles / cm-sec} \tag{5-29}$$

For gas saturated with molybdenum vapor the loss rate  $\Phi_s$  per centimeter of plate edge is

$$\Phi_s = 2a c_m \bar{J} = 3.25 \times 10^{-9} \text{ moles / cm-sec} \tag{5-30}$$

Thus the ratio is

$$\Phi / \Phi_s = 0.284 \tag{5-31}$$

In the Dumbo design 1 cm of hot heat-exchanger edge forms one bounding edge of 1 cm<sup>2</sup> of 0.0025 cm thick molybdenum foil, or

~~SECRET~~

$2.657 \times 10^{-4}$  moles. According to Eq. 5-29 this sustains a loss of  $8.07 \times 10^{-10}$  moles in one second, or  $16.14 \times 10^{-6}$  moles in 200 seconds. This corresponds to a total loss of 0.027%, which is not serious. Equation 5-30 indicates a loss of 0.11% for complete saturation.

5-4: A Rapid Approximation Method

A rapid method may be used for estimating  $dF/dy|_B$ , avoiding the summations of equations 5-26 and 5-28, which constitute the major job in the procedure just given. According to Eq. 5-20, the value of the flow derivative at the boundary is

$$\frac{d}{dy} J_z(y) \Big|_a = 3 \frac{J}{a} \tag{5-32}$$

If the  $y$  origin is moved to the boundary and the condition  $y \ll a$  is assumed, then

$$J_z(y) = 3 \frac{J}{a} y \tag{5-33}$$

is a reasonable approximation. Thus for large  $a$  (or small  $D$ , which would confine the molybdenum vapor to a layer close to the boundary) the problem is that for a channel of semi-infinite width, which may be solved with the actual width appearing only in the expression given by Eq. 5-33 for  $J_z(y)$ . The resulting value of  $dF/dy|_B$  is an overestimate for two reasons: The mass flow rate  $J_z$  at a particular value of  $y$  is overstated by Eq. 5-33, and the inhibiting influence of diffusion from the opposite

~~SECRET~~

wall is neglected.

Neglecting the upstream diffusion term  $\beta^2 F$ , Eq. 5-14 becomes

$$\frac{d^2 F}{dy^2} - 3 \frac{\beta \bar{J}}{n Da} y F = 0 \quad (5-34)$$

This equation may be reduced by the use of dimensionless quantities defined by

$$\begin{aligned} \frac{3\beta \bar{J}}{n Da} &= \frac{1}{\lambda^3} \\ x &= y/\lambda \\ F(\lambda x) &= f(x) \end{aligned} \quad (5-35)$$

which reduces Eq. 5-34 to

$$\frac{1}{x} f'' - f = 0 \quad (5-36)$$

with the boundary condition

$$f(0) = 1 \quad (5-37)$$

from Eq. 5-15. The other boundary condition is

$$f \rightarrow 0 \quad \text{as } x \rightarrow \infty \quad (5-38)$$

Because Eq. 5-38 makes solution by power series awkward, it is more convenient to seek a solution of the form

$$f(x) = \int K(x,t) g(t) dt \quad (5-39)$$

~~SECRET~~

Chapter 5      Loss of Reactor Material by Evaporation

Substitution of this form into Eq. 5-36 gives

$$\int \left( \frac{1}{x} K_{xx} - K \right) g dt = 0 \tag{5-40}$$

It is identically true that

$$\left( x^{2-n} \frac{\partial^2}{\partial x^2} - n \frac{\partial}{\partial t} \right) t^{\frac{1-n}{n}} e^{-\frac{1}{n} \frac{x^n}{t}} = 0 \tag{5-41}$$

and in particular for  $n = 3$ , if

$$K(x,t) = t^{-\frac{2}{3}} e^{-\frac{1}{3} \frac{x^3}{t}} \tag{5-42}$$

then

$$\frac{1}{x} K_{xx} = 3K_t \tag{5-43}$$

which brings Eq. 5-40 to the form

$$\int (3K_t - K) g dt = 0 \tag{5-44}$$

Choice of 0 and  $\infty$  as the limits of the  $t$  integration allows Eq. 5-44 to be integrated by parts, yielding

$$\int_0^{\infty} K(3g_t + g) dt = 0 \tag{5-45}$$

where the integrated terms at the limits vanish by Eq. 5-42 unless  $g(t)$  behaves unreasonably at these limits. Equation 5-45 is evidently solved by

~~SECRET~~

$$g = b e^{-\frac{1}{3}t} \tag{5-46}$$

which together with Eq. 5-42 brings Eq. 5-39 to the form

$$f(x) = b \int_0^{\infty} t^{-\frac{2}{3}} e^{-\frac{1}{3}(t + \frac{x^3}{t})} dt \tag{5-47}$$

Equation 5-47 requires b to be given by

$$\int_0^{\infty} t^{-\frac{2}{3}} e^{-\frac{1}{3}t} dt = 3^{\frac{1}{3}} \Gamma(1/3) \tag{5-48}$$

In Eq. 5-47, introduction of the transformation  $t = x^3\tau$ , differentiation, and specialization to  $x = 0$  gives

$$f'(0) = b \int_0^{\infty} \tau^{-\frac{5}{3}} e^{-\frac{1}{3}\tau} d\tau = \frac{3^{\frac{2}{3}} \Gamma(2/3)}{3^{\frac{1}{3}} \Gamma(1/3)} = 0.72905 \tag{5-49}$$

Thus, in Eq. 5-49,  $f'$  has been evaluated definitively as a number independent of design parameters. For the numerical example, this method shows that

$$f'/\lambda = 3.356 \times 10^2 \text{ cm}^{-1} \tag{5-50}$$

This result is to be compared to the better value  $f'/\lambda = 3.141 \times 10^2 \text{ cm}^{-1}$  obtained by the long method. The difference of only 7% in the two results suggests that the short method is sufficiently accurate whenever it indicates loss that is much less than that from saturated vapor.

~~SECRET~~



~~SECRET~~

Chapter 5            Loss of Reactor Material by Evaporation

---

REFERENCES

1. Saul Dushman, Scientific Foundation of Vacuum Technique, John Wiley and Sons, Inc., New York, 1949.
2. Joseph O. Hirschfelder, Charles F. Curtiss, and R. Byron Bird, Molecular Theory of Gases and Liquids, John Wiley and Sons, Inc., New York, 1954.

~~SECRET~~



## CHAPTER 6

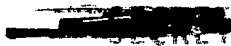
### NUCLEAR REACTOR CONSIDERATIONS

Then the Elephant's Child felt his legs slipping,  
and he said through his nose, which was now nearly  
five feet long, "This is too butch for be."

R. Kipling, The Elephant's Child

#### 6-1: The Problem

In a nuclear rocket motor design there are two reactor considerations of great importance: the quantity of fissionable material required and the distribution of power density in the heat exchanger. The second point is naturally of particular interest in these devices because some of the materials operate under conditions not far removed from thermal failure. In this chapter these two questions are investigated theoretically. Because the theory becomes rather involved, some approximations must be made. The uncertainties due to these approximations are discussed in Sec. 6-9. For the purpose of this report there is less interest in several-place accuracy than in a reasonably tractable pencil-and-paper method for obtaining estimates accurate enough to determine whether a device is practical or not. Also, for a preliminary investigation an approximate and largely analytic approach has evident conceptual advantages over more accurate numerical machine methods.



6-2: Slowing-down Leakage Through a Moderating Reflector

The life history of a reactor neutron born at fission energy involves three important sorts of events: degradation, leakage, and capture. The slowing-down process in systems in which capture is unimportant at energies above thermal is investigated initially.

The system contemplated here is a hydrogen moderated reactor core with a beryllium reflector. The hydrogen moderated core region is denoted by the subscript H and the reflector region by the subscript R.  $D_H$  and  $D_R$  are the transport mean free paths in the two regions, and  $\Sigma_H$  and  $\Sigma_R$  are the slowing-down macroscopic cross sections for these regions.

The slowing-down equation for the neutron flux in the reflector is

$$D_R \nabla^2 \phi = \xi \frac{\partial}{\partial u} \Sigma_R \phi \quad (6-1)$$

according to the usual Fermi age approach<sup>1</sup> where

$$u = \log (E_0/E) \quad (6-2)$$

is the logarithmic energy decrement or "lethargy",  $E_0$  is the fission energy of a neutron,  $\phi$  is the neutron flux, and  $\xi$  is the average change in  $u$  per collision. In beryllium  $\xi$  is 0.209.

The slowing-down equation for the hydrogenous core states that at a given lethargy the rate of loss by degradation and by diffusion balances the appearance rate of neutrons degraded from higher energies. This equation is

$$\left[ \sum_H(u) \phi(u) - D_H(u) \nabla^2 \phi(u) \right] = \int_0^u du' e^{u'-u} \sum_H(u') \phi(u') \quad (6-3)$$

This is the basic equation of Bell's "Simple Method of Calculating Critical Masses of Proton Moderated Assemblies."<sup>2</sup> A function

$$q(u) = \sum_H(u) \phi(u) \quad (6-4)$$

which is dimensionally neutrons/cm<sup>3</sup>-sec, is defined. Equation 6-3 becomes

$$\left( 1 - \frac{D_H}{\sum_H} \nabla^2 \right) q(u) = \int_0^u du' e^{u'-u} q(u') \quad (6-5)$$

The neutron source intensity at fission energy must be equal to the loss rate of Eq. 6-3 at that energy. Therefore, the fast neutron source intensity is

$$\left( \sum_H(0) - D_H(0) \nabla^2 \right) \phi(0) = \left( 1 - \frac{D_H(0)}{\sum_H(0)} \nabla^2 \right) q(0) \quad (6-6)$$

On the other hand the source intensity at thermal energy is derived from contributions at all energies. From Eq. 6-3 the thermal energy source intensity is

$$\int_0^{u_{th}} du' e^{u'-u_{th}} \sum_H(u') \phi(u') = \left( 1 - \frac{D_H(u_{th})}{\sum_H(u_{th})} \nabla^2 \right) q(u_{th}) \quad (6-7)$$

where the subscript th denotes thermal energy. Differentiating Eq. 6-5

~~SECRET~~

with respect to  $u$  gives

$$\begin{aligned} \frac{\partial}{\partial u} \left( 1 - \frac{D_H}{\Sigma_H} \nabla^2 \right) q &= q - \int_0^u du' e^{u'-u} q(u') \\ &= \frac{D_H}{\Sigma_H} \nabla^2 q \end{aligned} \tag{6-8}$$

where Eq. 6-5 is used a second time in the final step. Now  $D_H$  and  $1/\Sigma_H$  are transport distances characteristic of the moderator composition. The result of the  $\nabla^2$  operation on  $q$  is similar to twice dividing  $q$  by a length comparable to the geometric dimensions of the moderating region, provided  $q$  has no sharp space fluctuations within the core. Further,  $D_H$  and  $1/\Sigma_H$ , which are transport distances characteristic of the moderator composition, are small compared to the dimensions of the core. Therefore, the effect of the dimensionless operator  $\frac{D_H}{\Sigma_H} \nabla^2$  upon  $q$  is to multiply it by a quantity much smaller than 1, and this term may be dropped from Eqs. 6-6, 6-7, and 6-8. This is equivalent to the Bell approximation:<sup>2</sup> this approximation has been used to predict critical masses to within the 5% accuracy of experimental data.

This approximation is applied to Eqs. 6-6, 6-7, and 6-8 with the result that the fast source intensity is given by  $q(0)$ , the slow source intensity is given by  $q(u_{tH})$ , and the slowing-down equation is given by

$$\nabla^2 q = \frac{\Sigma_H}{D_H} \frac{\partial q}{\partial u} \tag{6-9}$$

~~SECRET~~

~~SECRET~~

Slowing-down Leakage

Section 6-2

To this approximation  $q$  is a bona fide slowing-down density in the core region. The ratio  $q(u_{th})/q(0)$  is the slowing-down nonleakage probability.

The preceding development parallels Bell's treatment of hydrogen moderated assemblies. The following approximation may be used to extend the theory to a system with a moderating reflector: In the reflector  $\Sigma$  and  $D$  are in a fixed proportion to their values in the core, i.e.,  $\Sigma_R/\Sigma_H$  and  $D_R/D_H$  are independent of  $u$ . This is a good approximation over most of the range of  $u$  (see Ref. 3) and errs in the direction of conservatism (see concluding paragraph of Sec. 6-2). Equation 6-4 is substituted into Eq. 6-1 and this approximation is applied, yielding

$$\nabla^2 q = \xi \frac{\Sigma_R}{D_R} \frac{\partial q}{\partial u} \quad (6-10)$$

in the reflector. On the interface between core and reflector there is continuity of current, which gives

$$D_R \nabla q \cdot \vec{N} \Big|_R = D_H \nabla q \cdot \vec{N} \Big|_H \quad (6-11)$$

where  $\vec{N}$  is normal to the interface. It is necessary that  $q$  vanish on the extrapolated boundary of the reflector. Specification of  $q(0)$  is enough to determine the solution of the problem.

A change of variables, from the lethargy  $u$  to the Fermi age  $\tau$  in the moderator, is introduced, where

~~SECRET~~

$$\tau = \int_0^u \frac{D_H(u')}{\Sigma_H(u')} du' \quad (6-12)$$

Equations 6-9 and 6-10 become

$$\nabla^2 q = \frac{\partial q}{\partial \tau} \quad (6-13)$$

$$\nabla^2 q = \xi \frac{\Sigma_R}{\Sigma_H} \frac{D_H}{D_R} \frac{\partial q}{\partial \tau} \quad (6-14)$$

for the moderator and reflector regions, respectively. Two functions,  $S(\vec{x})$  and  $\omega(\vec{x})$ , are defined by

$$S(\vec{x}) = \begin{cases} 1 & \text{for } \vec{x} \text{ in H} \\ \frac{D_R}{D_H} = S_1 & \text{for } \vec{x} \text{ in R} \end{cases}$$

$$\omega(\vec{x}) = \begin{cases} 1 & \text{for } \vec{x} \text{ in H} \\ \xi \frac{\Sigma_R}{\Sigma_H} = \omega_1 & \text{for } \vec{x} \text{ in R} \end{cases} \quad (6-15)$$

Using these definitions Eqs. 6-13 and 6-14 are combined to give

$$\nabla \cdot S \nabla q = \omega \frac{\partial q}{\partial \tau} \quad (6-16)$$

Here the form  $S \nabla q$  has been used because it is continuous across the moderator-reflector interface as shown by Eq. 6-11.

~~SECRET~~

The slowing-down equation 6-16 is now in a tractable form. Solutions of Eq. 6-16 are assumed to be of the form

$$q_n(\bar{x}, \tau) = q_n(\bar{x}) e^{-B_n^2 \tau} \quad (6-17)$$

Substitution into Eq. 6-16 yields

$$\nabla \cdot S \nabla q_n = -B_n^2 \omega q_n \quad (6-18)$$

This is an eigenvalue problem leading to eigenvalues  $B_n^2$  and to corresponding eigenfunctions  $q_n(\bar{x})$  which represent neutron flux buckling modes for the system. The slowing-down nonleakage probability for the  $n$ th mode is  $e^{-B_n^2 \tau}$ .

Equation 6-18 leads to an orthogonality property. It is seen that

$$B_m^2 \int_V q_n q_m \omega dV = - \int_V q_n \nabla \cdot S \nabla q_m dV = \int_V S \nabla q_m \cdot \nabla q_n dV \quad (6-19)$$

where the divergence theorem is used in the usual way in the last step.

A similar result follows if  $B_m^2$  is replaced by  $B_n^2$ . If  $B_m^2 \neq B_n^2$ , it follows that

$$\int_V q_m(\bar{x}) q_n(\bar{x}) \omega(\bar{x}) dV = 0 \quad (6-20)$$

Thus the functions  $q_n(\bar{x})$  are orthogonal with respect to the weighting function  $\omega(\bar{x})$ . If the completeness of the set of  $q_n$  functions is



assumed, they may be used as a basis for the expansion of arbitrary functions

$$f(\vec{x}) = \sum_n a_n q_n(\vec{x})$$

where

$$a_n = \int_V q_n(\vec{x}) f(\vec{x}) \omega(\vec{x}) dV \quad (6-21)$$

and where the functions  $q_n(\vec{x})$  are normalized

$$\int_V q_n^2(\vec{x}) \omega(\vec{x}) dV = 1 \quad (6-22)$$

The proper initial condition is applied by expanding the fast neutron source in terms of the buckling modes of the system by using Eq. 6-21. The quantity  $1/B_n$  is a measure of the nodal separation distance for the  $n$ th eigenfunction. Hence  $B_n^2$  is rapidly increasing with  $n$ , and consequently  $e^{-B_n^2 \tau_{th}}$  is rapidly decreasing. Leakage becomes very severe in the higher modes, and it is a reasonable approximation that leakage is soon complete in all modes except the lowest. The profile of the thermal flux in the core region is close to that of the thermal source. The fast source in turn has the same profile within the core, but vanishes in the reflector, where no fissions take place. Thus the shape of the distribution in which new fission neutrons appear is not that of a normal mode but is of the form

$$q_H(\vec{x}) = \begin{cases} q_0(\vec{x}) & \text{for } \vec{x} \text{ in H} \\ 0 & \text{for } \vec{x} \text{ in R} \end{cases} \quad (6-23)$$

Substituting  $f(\vec{x}) = q_H(\vec{x})$  in Eq. 6-21 gives

$$a_0 = \frac{\int_H q_0^2 \omega dV}{\int_V q_0^2 \omega dV} \quad (6-24)$$

where the denominator is included to make the expression hold whether  $q$  is normalized or not.  $a_0$  is the probability that a neutron does not leak out of the reactor in spite of the contribution of higher modes to the fast source. The total slowing-down nonleakage probability for the actual distribution is  $a_0 e^{-B_0^2 \tau_{th}}$ .

It is interesting to note that, from Eqs. 6-15 and 6-24,  $a_0 \rightarrow 1$  as  $\xi \rightarrow 0$ . This implies that no high-mode leakage correction is necessary for a nonmoderating reflector in a steady state situation. Physically, this is plausible in that such a reflector cannot act as a neutron sink at any energy. Mathematically, it is plausible in that the modes in this case are orthogonal within the moderating region alone, because in this case Eq. 6-11 is a self-adjoint boundary condition, and the interface is regarded as the boundary of the problem.

The same treatment may be used to find slowing-down leakage at any energy, so long as the corresponding Fermi age is large enough to allow complete leakage from the higher modes.

Determination of slowing-down leakage is reduced to determining the proper Fermi age at thermal energies and solving an eigenvalue problem. There is a simple prescription for calculation of Fermi ages.<sup>2</sup> Solution of the eigenvalue problem depends on the geometry of the reactor. If a cylindrical geometry is used, the solution is in terms of Bessel functions. The solution of the present eigenvalue problem is not completed in detail, because the preceding development is modified by slowing-down capture. However, straightforward mathematics leads quickly to the following results: For a reactor, which is shielded on the top and sides but not on the bottom, the interface condition from Eq. 6-11 yields two equations for the top and side interfaces. If the eigenvalue is

$$B = \sqrt{a^2 + \beta^2} \quad (6-25)$$

then the side equation is

$$\beta \frac{J_1(\beta R_0)}{J_0(\beta R_0)} = S_1 \left| \frac{\omega_1}{S_1} \beta^2 + \left( \frac{\omega_1}{S_1} - 1 \right) a^2 \right|^{1/2} \cot \coth \left\{ (R_1 - R_0) \left| \frac{\omega_1}{S_1} \beta^2 + \left( \frac{\omega_1}{S_1} - 1 \right) a^2 \right|^{1/2} \right\} \quad (6-26)$$

and the top equation is

$$a \cot a L_0 = S_1 \left| \frac{\omega_1}{S_1} a^2 + \left( \frac{\omega_1}{S_1} - 1 \right) \beta^2 \right|^{1/2} \cot \coth \left\{ (L_1 - L_0) \left| \frac{\omega_1}{S_1} a^2 + \left( \frac{\omega_1}{S_1} - 1 \right) \beta^2 \right|^{1/2} \right\} \quad (6-27)$$

where  $L_0$  is the core height,  $R_0$  the core radius,  $L_1$  the external height,

~~SECRET~~

Slowing-down Leakage

Section 6-2

and  $R_1$  the external radius. In Eqs. 6-26 and 6-27 the trigonometric cotangent should be chosen if the absolute bars contain a positive quantity, and the hyperbolic cotangent otherwise. In these equations the approximation is made that the side reflector is so thin, compared to the core diameter, that the radial solution in the side reflector may be expressed as a sinusoidal function. Equations 6-25 and 6-26 must be solved simultaneously for  $\alpha$  and  $\beta$  to determine the eigenvalue  $B$ . The following substitutions are made

$$f(\xi) = \xi \frac{J_1(\xi)}{J_0(\xi)}$$
$$g(\xi) = \xi \frac{\cot}{\coth} \left\{ \xi \right\}$$

(6-28)

$$\alpha = \frac{\xi}{L_0}$$
$$\beta = \frac{\eta}{R_0}$$

(6-29)

$$\frac{L_1 - L_0}{L_0} = \lambda$$
$$\frac{R_1 - R_0}{R_0} = \rho$$
$$\frac{L_0}{R_0} = h$$

(6-30)

~~SECRET~~

*Aut*

$$\frac{\omega_1}{S_1} = \epsilon \tag{6-31}$$

whereupon Eqs. 6-26 and 6-27 become

$$f(\eta) = \frac{S_1}{\rho} g\left(\rho \left| \epsilon \eta^2 + \frac{1}{h^2}(1-\epsilon)\zeta^2 \right|^{1/2}\right) \tag{6-32}$$

$$g(\zeta) = \frac{S_1}{\lambda} g\left(\lambda \left| \epsilon \zeta^2 + h^2(1-\epsilon)\eta^2 \right|^{1/2}\right) \tag{6-33}$$

Equations 6-32 and 6-33 are to be solved for  $\eta$  and  $\zeta$ . In the thin reflector limit, as  $\rho \rightarrow 0$  and  $\lambda \rightarrow 0$ , these equations become

$$f(\eta) = \frac{S_1}{\rho} \tag{6-34}$$

$$g(\zeta) = \frac{S_1}{\lambda} \tag{6-35}$$

which are just the equations one would obtain by fitting the flux in the core to the outside boundary by a naive linear extrapolation. The eigenvalue is obtained by first solving for approximate values of  $\eta$  and  $\zeta$  from Eqs. 6-34 and 6-35. These values are substituted into the right-hand sides of Eqs. 6-32 and 6-33 to obtain better values. The process may then be repeated until a stable result is obtained. The routine is quick and convergence is rapid.

The approximation of proportional nuclear parameters implicitly assumes that the diffusion rate in the reflector increases with

~~SECRET~~

increasing neutron energy as rapidly as it does in the hydrogenous core. Thus leakage through the reflector is overestimated at high energies, and the approximation is conservative.

6-3: Effect of Slowing-down Capture and Self-shielding; The Conditions for Flat Flux

A term is introduced into Eq. 6-3 to include capture, yielding

$$\left[ \Sigma_H(u) + \Sigma_C(u) - D_H(u) \nabla^2 \right] \phi(u) = \int_0^u du' e^{u'-u} \Sigma_H(u') \phi(u') \quad (6-36)$$

Application of the same steps as before gives, instead of Eq. 6-8,

$$\frac{\partial}{\partial u} \left( 1 + \frac{\Sigma_C}{\Sigma_H} - \frac{D_H}{\Sigma_H} \nabla^2 \right) q = \left( \frac{D_H}{\Sigma_H} \nabla^2 - \frac{\Sigma_C}{\Sigma_H} \right) q \quad (6-37)$$

Transforming to the Fermi age variable gives

$$\frac{\partial}{\partial \tau} \left( 1 + \frac{\Sigma_C}{\Sigma_H} - \frac{D_H}{\Sigma_H} \nabla^2 \right) q = \left( \nabla^2 - \frac{\Sigma_C}{D_H} \right) q \quad (6-38)$$

For a well moderated reactor without strong capture resonances

$\Sigma_C/\Sigma_H \ll 1$ , so that this term as well as the Laplacian term on the left hand side of Eq. 6-38 may be dropped, yielding

$$\nabla^2 q - \frac{\Sigma_C}{D_H} q = \frac{\partial q}{\partial \tau} \quad (6-39)$$

~~SECRET~~

~~SECRET~~

For an unreflected reactor Eq. 6-39 is reduced to the form of Eq. 6-13 by the substitution

$$q = q' e^{-\int_0^{\tau} \frac{\Sigma_c}{D_H} d\tau'} \quad (6-40)$$

where  $q'$  is a solution of Eq. 6-13, and hence  $q$  is a solution of Eq. 6-39. The correct solution to Eq. 6-39 at thermal energies is obtained by solution of the equation

$$\nabla^2 q - \left( \frac{1}{\tau_{th}} \int_0^{\tau_{th}} \frac{\Sigma_c}{D_H} d\tau \right) q = \frac{\partial q}{\partial \tau} \quad (6-41)$$

which has the simplicity of an equation with constant coefficients.

Since Eq. 6-39 does not treat resonance capture properly the constant coefficient is modified in such a way that an expression is obtained which takes account of resonance absorption as in the more exact equation 6-38. As given by Eq. 6-40, the slowing-down noncapture probability is

$$e^{-\int_0^{\tau_{th}} \frac{\Sigma_c}{D_H} d\tau} = e^{-\int_0^{u_{th}} \frac{\Sigma_c}{\Sigma_H} du} \quad (6-42)$$

which should be substantially correct for good moderation and no resonances. In an infinite hydrogenous moderator the slowing-down noncapture probability may be calculated exactly. It is

$$e^{-\int_0^{u_{th}} \frac{\Sigma_c}{\Sigma_H + \Sigma_c} du} \quad (6-43)$$

The exact equation 6-38 is replaced by the simpler approximate equation

$$\nabla^2 q - C_0^2 q = \frac{\partial q}{\partial \tau} \quad (6-44)$$

where

$$C_0^2 = \frac{1}{\tau_{th}} \int_0^{u_{th}} \frac{\Sigma_c}{\Sigma_H + \Sigma_c} du \quad (6-45)$$

and which is obtained from Eqs. 6-41, 6-42, and 6-43. The effect of the approximation is discussed in Sec. 6-9. Since Eq. 6-44 gives an exact result at thermal energies for an infinite core where there are no neutron currents, it is approximate in its treatment only of the effect of capture on neutron transport.

As in Eq. 6-15, a function

$$C^2(\vec{x}) = \begin{cases} C_0^2 & \text{for } \vec{x} \text{ in H} \\ 0 & \text{for } \vec{x} \text{ in R} \end{cases} \quad (6-46)$$

is defined. Combining Eqs. 6-44 and 6-15 gives

$$(\nabla \cdot S \nabla - S C^2) q = \omega \frac{\partial q}{\partial \tau} \quad (6-47)$$

in close correspondence to Eq. 6-16. The substitution



$$q_n(\vec{x}, \tau) = q_n(\vec{x}) e^{-B_n^2 \tau}$$

yields

$$(\nabla \cdot S \nabla - S C^2) q_n = -B_n^2 \omega q_n \quad (6-48)$$

This eigenvalue equation clearly has a close mathematical kinship with Eq. 6-18. In particular it has the weighted orthogonality property. The slowing-down nonleakage probability is still given by  $a_0 e^{-B_0^2 \tau}$ , which now includes effects of reflector moderation, slowing-down capture, and slowing-down self-shielding. The eigenvalue equation becomes

$$\nabla^2 q = (C_0^2 - B^2) q \quad (6-49)$$

$$\nabla^2 q = -\frac{\omega_1}{S_1} B^2 q \quad (6-50)$$

for the moderator and reflector regions, respectively. The solution to Eq. 6-49 depends on two considerations: the boundary conditions on the surface of the core, and eigenvalue  $B^2$ . Both of these depend on the external boundary of the reactor. If a reflector is chosen giving  $B_0^2 = C_0^2$  and a constant value of  $q_0$  over the core surface, then the slowing-down density satisfying Eq. 6-49 is constant throughout the core, and the condition of uniform power generation is achieved. The physical requirement for the flat flux condition is that capture loss in the core and leakage loss in the reflector proceed at the same rate, so that the flux

~~SECRET~~

level sinks uniformly across the whole reactor as energy degradation goes on, without requiring neutron currents in the core.

For a cylindrical geometry the solution of Eq. 6-49 is in terms of Bessel functions. If there is little reflection and low slowing-down capture, then  $C_0^2 - B_0^2$  is large and negative, and the solution is the familiar humped  $J_0$  flux distribution as shown in Fig. 6-1-a, indicative, of neutrons leaking out.

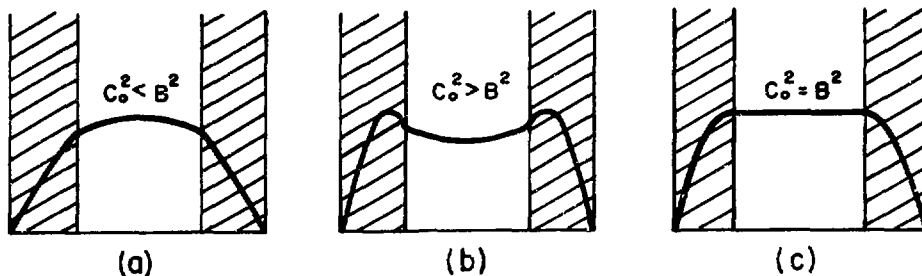


Fig. 6-1

If, on the other hand, poisoning is large and moderation is accomplished in the reflector primarily,  $C_0^2 - B_0^2$  is large and positive and the flux profile is a Bessel function of imaginary argument, of maximum size at the surface of the core, as shown in Fig. 6-1-b. The neutron current is directed inward in this case. For some reflector thickness intermediate between the two extreme situations is a transition between the two types of flux profile corresponding to the flat flux situation, as shown in Fig. 6-1-c. Achievement of all the conditions necessary for flat flux requires both moderation in the reflector and slowing-down absorption in

~~SECRET~~

*[Handwritten signature]*

the core.

The expressions given in Eqs. 6-44 and 6-45 represent an approximation in the treatment of neutron current effects. However, in the flat flux situation neutron currents are reduced to a low value, making the approximation most valid under these conditions.

The solution of Eq. 6-48 for the case of a cylindrical reactor reflected on the top and sides is quite straightforward when the flat flux condition is imposed. The  $z$  coordinate is measured downward from the top of the core. Since the flux profile is flat radially within the core, it follows that in this region

$$q_0(r, z) = \cos \gamma z \tag{6-51}$$

where  $\gamma$  is determined by the bottom boundary condition. Because some reflection takes place at the bottom boundary, a probability-of-return or "albedo" boundary condition<sup>4</sup> is used, i.e.,

$$\frac{1}{q} \left. \frac{\partial q}{\partial z} \right|_{z=L_0} = \frac{1}{2D_{\text{eff}}} \frac{1-\beta}{1+\beta} \tag{6-52}$$

where  $\beta$  is the probability of return,  $D_{\text{eff}}$  is the effective diffusion coefficient of the core, and  $L_0$  is the location of the lower boundary. The numerical critical masses are insensitive to  $\beta$  and  $D_{\text{eff}}$ . Substitution of Eq. 6-51 into Eq. 6-52 gives

~~SECRET~~

Flat Flux Conditions

Section 6-3

$$x \tan x = \frac{1}{2} \frac{L_0}{D_{\text{eff}}} \frac{1-\beta}{1+\beta}$$

where

$$x = \gamma L_0 \tag{6-53}$$

which determines  $\gamma$ . Substitution of Eq. 6-51 into Eq. 6-49 gives

$$B_0^2 = C_0^2 + \gamma^2 \tag{6-54}$$

In the top reflector Eq. 6-50 becomes

$$\frac{\partial^2 q_0}{\partial z^2} = - \frac{\omega_1}{S_1} B_0^2 q_0 \tag{6-55}$$

giving

$$q_0 = \cos \sqrt{\frac{\omega_1}{S_1}} B_0 z \tag{6-56}$$

If the thickness of the top reflector is  $L_1$  (notational change from Sec. 6-2), then the vanishing of Eq. 6-56 gives

$$L_1 = \frac{\pi}{2} \sqrt{\frac{S_1}{\omega_1}} \frac{1}{B_0} \tag{6-57}$$

The treatment of the side boundaries is similar. Equation 6-50 is written in cylindrical coordinates as

$$\left( \frac{\partial^2}{\partial r^2} + \frac{1}{r} \frac{\partial}{\partial r} \right) q = - \left( \frac{\omega_1}{S_1} B_0^2 - \gamma^2 \right) q \tag{6-58}$$

~~SECRET~~

The solution fitting that of the core at the core boundary is

$$q_0(r, z) = \cos \gamma z \frac{J_0(Er) - \alpha Y_0(Er)}{J_0(ER_0) - \alpha Y_0(ER_0)} \quad (6-59)$$

where

$$E^2 = \frac{\omega_1}{S_1} B_0^2 - \gamma^2 \quad (6-60)$$

The constant  $\alpha$  is determined such that

$$\left. \frac{\partial q}{\partial r} \right|_{R_0, z} = 0 \quad (6-61)$$

and

$$q(R_1, z) = 0 \quad (6-62)$$

where  $R_0$  is known and  $R_1$  is to be found. Substitution of Eq. 6-59 into Eq. 6-61 gives

$$\frac{J_1(ER_0)}{Y_1(ER_0)} = \alpha \quad (6-63)$$

which evaluates  $\alpha$ . The substitution

$$ER_1 = y \quad (6-64)$$

reduces Eq. 6-62 to

$$\frac{J_0(y)}{Y_0(y)} = \alpha \quad (6-65)$$

~~SECRET~~

Flat Flux Conditions

Section 6-3

which now may be solved for  $y$  to determine  $R_1$ . For a reactor with a typical reflector, the value of  $R_1 - R_0$  obtained in this way is quite close to  $L_1$ , but is a bit larger.

The high mode nonleakage probability is evaluated by substitution of Eqs. 6-51, 6-56, and 6-59 into Eq. 6-24, yielding

$$a_0 = \frac{1}{1 + \omega_1(H+K)} \quad (6-66)$$

where

$$K \equiv \frac{L_1}{L_0 + \frac{1}{\gamma} \sin 2\gamma L_0}$$

$$H \equiv \frac{R_1^2 Z_1^2}{R_0^2 Z_0^2} - 1$$

$$Z_0 \equiv J_0(ER_0) - aY_0(ER_0)$$

$$Z_1 \equiv J_1(ER_1) - aY_1(ER_1) \quad (6-67)$$

A more compact approximate expression for  $a_0$  may be obtained by considering the asymptotic behavior of Bessel functions. This is

$$a_0 \approx \frac{1}{1 + \frac{\omega_1}{2} \frac{V_R}{V_H}} \quad (6-68)$$

where  $V_H$  is the volume of the core and  $V_R$  that of the reflector. Equation 6-68 is of value chiefly for intuitive understanding of reactor design considerations, and is not used for the numerical results of this

~~SECRET~~

report. As a rapid method of estimating reflector thickness and higher mode nonleakage, the approximation that  $B_0 \approx C_0$  may be made in Eq. 6-57 to obtain the reflector thickness, and  $a_0$  may be obtained from Eq. 6-68.

6-4: Calculation of Critical Conditions

The methods developed thus far are used in this section to examine the whole neutron economy of a reactor. The procedure is to divide the neutrons into energy groups, and to determine how many neutrons each energy range adds to, or subtracts from, the total neutron balance.

At the outset of the slowing-down process, higher-mode leakage is severe. It is assumed to be complete immediately, so that the probability that a neutron ever gets well embarked on the slowing-down process is  $a_0$ .

If the reactor is reflected in such a manner that the flux is flat in all directions, then, after the initial higher-mode leakage, slowing down proceeds just as in an infinite reactor. For an infinite reactor, if in the process of slowing down to a given lethargy there are  $F$  fissions per initial fission neutron, and  $N$  neutrons per initial neutron survive, then

$$-\frac{dF}{dN} = \frac{\Sigma_F}{\Sigma_C} \tag{6-69}$$

where  $\Sigma_F$  is that part of the capture cross section which results in fission. From Eq. 6-43

$$N(u) = e^{-\int_0^u \frac{\Sigma_c}{\Sigma_H + \Sigma_c} du'} \quad (6-70)$$

Differentiating Eq. 6-70 and combining with Eq. 6-69 yields

$$\frac{dF}{du} = \frac{\Sigma_F}{\Sigma_H + \Sigma_C} e^{-\int_0^u \frac{\Sigma_c}{\Sigma_H + \Sigma_c} du'} \quad (6-71)$$

Thus the number of fissions occurring in the lethargy interval between  $u_i$  and  $u_{i+1}$  is

$$\Delta F_i = e^{-\int_0^{u_i} \frac{\Sigma_c}{\Sigma_H + \Sigma_c} du} \int_{u_i}^{u_{i+1}} \frac{\Sigma_F}{\Sigma_H + \Sigma_C} e^{-\int_{u_i}^u \frac{\Sigma_c}{\Sigma_H + \Sigma_c} du'} du \quad (6-72)$$

Now

$$\int_{u_i}^{u_{i+1}} du \frac{\Sigma_c}{\Sigma_H + \Sigma_C} e^{-\int_{u_i}^u \frac{\Sigma_c}{\Sigma_H + \Sigma_c} du'} = 1 - e^{-\int_{u_i}^{u_{i+1}} \frac{\Sigma_c}{\Sigma_H + \Sigma_c} du}$$

since the integrand is an exact differential, so that Eq. 6-72 may be written as



$$\Delta F_i = e^{-\int_0^{u_i} \frac{\Sigma_c}{\Sigma_H + \Sigma_c} du} \frac{\int_{u_i}^{u_{i+1}} du \frac{\Sigma_F}{\Sigma_H + \Sigma_c} e^{-\int_{u_i}^u \frac{\Sigma_c}{\Sigma_H + \Sigma_c} du'}}{\int_{u_i}^{u_{i+1}} du \frac{\Sigma_c}{\Sigma_H + \Sigma_c} e^{-\int_{u_i}^u \frac{\Sigma_c}{\Sigma_H + \Sigma_c} du'}} (1 - e^{-\int_{u_i}^{u_{i+1}} \frac{\Sigma_c}{\Sigma_H + \Sigma_c} du}) \quad (6-73)$$

This expression is exact. However, if the lethargy interval is not too large, the exponential weighting factor in the integrands is always close to unity. Furthermore, this factor has a similar effect on both the numerator and denominator integrals in Eq. 6-73 so that the approximation

$$\Delta F_i = e^{-\int_0^{u_i} du \frac{\Sigma_c}{\Sigma_H + \Sigma_c}} \frac{\int_{u_i}^{u_{i+1}} du \frac{\Sigma_F}{\Sigma_H + \Sigma_c}}{\int_{u_i}^{u_{i+1}} du \frac{\Sigma_c}{\Sigma_H + \Sigma_c}} (1 - e^{-\int_{u_i}^{u_{i+1}} du \frac{\Sigma_c}{\Sigma_H + \Sigma_c}}) \quad (6-74)$$

may be made. This expression is exact if  $\Sigma_F$  and  $\Sigma_C$  are in constant proportion throughout the lethargy interval. The interpretation of Eq. 6-73 or Eq. 6-74 is as follows: The first term is the probability that a neutron survives to lethargy  $u_i$ , the last term is the subsequent probability that the neutron is captured before reaching lethargy  $u_{i+1}$ , and the middle term is the probability that capture results in fission. The virtue of Eq. 6-74 is that it is readily evaluated from tabulated nuclear data.

~~SECRET~~

The total number of second-generation neutrons per initial neutron is

$$k_{\infty} = \nu \left( \sum_i \Delta F_i + F_{th} \right) \tag{6-75}$$

where  $\nu$  is the number of neutrons released per fission, and

$$F_{th} = e^{-\int_0^{u_{th}} \frac{\Sigma_c}{\Sigma_H + \Sigma_c} du} \cdot \frac{\Sigma_F(u_{th})}{\Sigma_C(u_{th})} \tag{6-76}$$

is the contribution of fissions which are caused by thermal neutrons. Since in a finite reactor the proportion  $a_0$  of the initial fission neutrons are not transferred to the reflector at the outset of the slowing-down process, the actual criticality is given by

$$k = a_0 k_{\infty} \tag{6-77}$$

where  $k = 1$  is the condition for a critical reactor.

In a reactor which is not thoroughly reflected on the bottom, the thermalization probability is given by

$$e^{-B_0^2 \tau_{th}} = e^{-(C_0^2 + \gamma^2) \tau_{th}} \tag{6-78}$$

instead of  $e^{-C_0^2 \tau_{th}}$  which is given by Eq. 6-43. The factor  $e^{-\gamma^2 \tau_{th}}$  arises from neutron leakage from the bottom. The effect of bottom leakage is effectively to increase the rate of neutron capture by a factor

~~SECRET~~

~~SECRET~~

$$A = \frac{B_o^2}{C_o^2} = 1 + \left( \frac{\gamma}{C_o} \right)^2 \quad (6-79)$$

The term  $(\gamma/C_o)^2$  typically is quite small. The only effect on the previous analysis is to replace the exponential terms in Eq. 6-74 and 6-76 by exponentials of the form

$$e^{-A \int \frac{\Sigma_c}{\Sigma_H + \Sigma_C} du} \quad (6-80)$$

The overall calculation procedure is to assume a core composition, calculate reflector dimensions, and obtain a value of  $k$  from Eq. 6-77. The composition is then modified and a new  $k$  calculated. This process is repeated until a composition is found which gives  $k = 1$ .

To recapitulate, the steps of the calculation are:

- (1) Core composition and dimensions are specified.
- (2) An albedo value  $\beta$  is assumed. An effective diffusion coefficient  $D_{\text{eff}}$  is obtained by the Bell prescription.<sup>2</sup>  $\gamma$  is determined by Eq. 6-53.
- (3) The Fermi age  $\tau_{\text{th}}$  is found by the Bell prescription.<sup>2</sup>
- (4) The integrals appearing in Eqs. 6-76 and 6-80 are evaluated from tabulated nuclear data.
- (5)  $C_o$  is evaluated from (4) and (3), using Eq. 6-45.  $B_o$  is evaluated from Eq. 6-54, using (3).  $E$  is evaluated from Eq. 6-60.
- (6) The reflector dimensions, top and side, are determined from

Eq. 6-57 and from Eqs. 6-63, 6-64, and 6-65.

(7) The value of  $a_0$  is obtained from Eq. 6-66.

(8) The various other terms of the form of Eq. 6-80 are evaluated from the integrals already calculated in (4), and the value of  $k$  is determined.

It is convenient, when searching for the condition  $k = 1$ , to vary the amount of moderator and leave other core compositions fixed. This approach leaves much of the preliminary arithmetic for the integrations unchanged.

#### 6-5: Effects of Lumping and Doppler Broadening

When a neutron passes a capture resonance in the process of slowing down to thermal energy, two effects modify the capture probability from that predicted from the raw nuclear data. These are the effects of self-shielding in the interior finite lumps of core materials and of resonance broadening caused by the thermal motion of capturing nuclei. A precise treatment of these effects is difficult, particularly for a lump of capturing material in which there is a strong temperature gradient. Approximations are made which yield to simple analysis and which are realistic enough to give reasonable estimates.

For a homogeneous reactor the capture integral for a resonance is given by

~~SECRET~~

$$G_o = \int_{-\infty}^{\infty} \frac{\Sigma_c}{\Sigma_H + \Sigma_c} du \tag{6-81}$$

where

$$\Sigma_c = \rho_c \sigma_c = \rho_c \sigma_m \frac{1}{1 + (u/\delta)^2} \tag{6-82}$$

at 0°K. Here  $\rho_c$  is the capture atom density,  $\sigma_m$  the microscopic cross section peak value,  $\delta$  the half-width in lethargy units. The moderating cross section  $\Sigma_H$  is assumed constant. The integral is extended to  $\infty$  for analytical convenience, and the lethargy origin is moved to the center of the peak.

The capture cross section within a metallic lump is

$$\Sigma_M = \frac{V_H}{V_M} \Sigma_c \tag{6-83}$$

where  $V_M$  is the volume of metallic lumps and  $V_H$  the volume of the core. The capture rate is proportional to the product of flux and capture cross section  $\phi \Sigma_M$  at any point. At the center of a lump, where the flux is reduced, the capture process is less effective by a factor  $\phi/\phi_o$ , where  $\phi_o$  is the flux outside the lump. The effective capture cross section is

$$\Sigma_c^* = \Sigma_c \frac{1}{V_M} \int_M (\phi/\phi_o) dV \tag{6-84}$$

~~SECRET~~

~~SECRET~~

Lumping and Doppler Broadening

Section 6-5

The lumps are chosen to be slabs of thickness  $2w$ . Scattering in the lumps is assumed negligible, and all neutrons are assumed to enter normal to the face of the slab. Both assumptions should underestimate the effect of lumping. Equation 6-84 becomes

$$\begin{aligned}\Sigma_C^* &= \Sigma_C \frac{1}{2w} \int_{-w}^w \frac{\cosh \Sigma_M z}{\cosh \Sigma_M w} dz \\ &= \frac{\Sigma_C}{\Sigma_M} \frac{1}{w} \tanh \Sigma_M w \\ &= \frac{V_M}{V_H} \frac{1}{w} \tanh \Sigma_M w\end{aligned}\tag{6-85}$$

The capture integral with the effect of lumping is

$$\begin{aligned}G &= \int_{-\infty}^{\infty} \frac{\Sigma_C^*}{\Sigma_C^* + \Sigma_H} du \\ &= \int_{-\infty}^{\infty} \frac{\left(\frac{V_M}{V_H} \frac{1}{w}\right) \tanh w \Sigma_M}{\left(\frac{V_M}{V_H} \frac{1}{w} \tanh w \Sigma_M\right) + \Sigma_H} du \\ &= \frac{V_M}{V_H} \frac{1}{w \Sigma_H} \int_{-\infty}^{\infty} \frac{1}{\frac{V_M}{V_H} \frac{1}{w \Sigma_H} + \coth w \Sigma_M} du\end{aligned}\tag{6-86}$$

~~SECRET~~

~~SECRET~~

Chapter 6

Nuclear Reactor Considerations

The substitutions

$$a = \frac{V_M}{V_H} \frac{1}{w \Sigma_H} \quad (6-87)$$

$$\epsilon = \left( w \frac{V_H}{V_M} \rho_c \sigma_m \right)^{-1/2} \quad (6-88)$$

$$x = (\epsilon / \delta) u \quad (6-89)$$

are made. Using Eqs. 6-82 and 6-83 the capture integral Eq. 6-86 becomes

$$G = \frac{\delta}{\epsilon} a I(a) \quad (6-90)$$

where

$$I(a) = \int_{-\infty}^{\infty} \frac{1}{a + \coth \frac{1}{\epsilon^2 + x^2}} dx \quad (6-91)$$

For small  $\epsilon$  the approximation

$$\tanh \frac{1}{\epsilon^2 + x^2} \cong \tanh \frac{1}{x^2} \quad (6-92)$$

may be made, which is valid for all  $x$  and for  $\epsilon$  up to about  $1/3$ . With this simplification Eq. 6-91 becomes

~~SECRET~~

~~SECRET~~

$$\begin{aligned} I(a) &= \int_{-\infty}^{\infty} \frac{1}{a + \coth \frac{1}{x^2}} dx \\ &= \int_{-\infty}^{\infty} \frac{1}{a + \coth y^2} \frac{1}{y^2} dy \\ &= \int_{-\infty}^{\infty} \frac{\sinh y^2}{a \sinh y^2 + \cosh y^2} \frac{1}{y^2} dy \end{aligned} \tag{6-93}$$

Equation 6-93 may be simplified by

$$a \sinh y^2 + \cosh y^2 = \sqrt{1-a^2} \cosh(y^2 + \beta) \tag{6-94}$$

and

$$\sinh y^2 = \sqrt{\frac{a}{1-a^2}} \cosh(y^2 + \beta) + \sqrt{\frac{1}{1-a^2}} \sinh(y^2 + \beta) \tag{6-95}$$

where

$$\beta = \frac{1}{2} \log \frac{1+a}{1-a} \tag{6-96}$$

so that

$$I(a) = \frac{1}{1-a^2} \int_{-\infty}^{\infty} \left\{ a + \tanh(y^2 + \beta) \right\} \frac{1}{y^2} dy \tag{6-97}$$

~~SECRET~~



~~SECRET~~

It is clear from Eq. 6-93 that the integrand has no singularity at the y origin, hence the path of integration may be deformed to run above the origin on the complex y plane, as shown in Fig. 6-2. However,  $1/y^2$

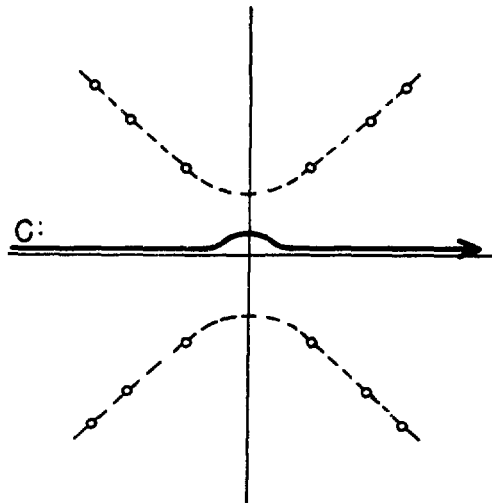


Fig. 6-2

integrates to zero over such a path, so that

$$I(a) = \frac{1}{1-a^2} \int_C \frac{1}{y^2} \tanh(y^2 + \beta) dy \quad (6-98)$$

The integral may be evaluated by lifting the contour to  $i \infty$  and evaluating the residues. The poles are taken in pairs by making use of the relation

$$\tanh \xi = 2 \sum_{n=0}^{\infty} \frac{\xi}{\xi^2 + (\pi/2)^2 (2n+1)^2} \quad (6-99)$$

~~SECRET~~

giving

$$I(a) = \frac{2}{1-a^2} \sum_{n=0}^{\infty} \int_c^{\infty} \frac{1}{y^2} \frac{y^2 + \beta}{(y^2 + \beta)^2 + c_n^2} dy \quad (6-100)$$

where

$$c_n = \frac{\pi}{2} (2n+1) \quad (6-101)$$

Evaluating the integral gives

$$I(a) = \frac{1}{1-a^2} \frac{4}{\sqrt{\pi}} \sum_{n=0}^{\infty} \frac{1}{(2n+1)^{3/2}} g\left(\frac{\beta}{c_n}\right) \quad (6-102)$$

where

$$g(x) = \frac{(\sqrt{1+x^2} - x)^{1/2} - x(\sqrt{1+x^2} + x)^{1/2}}{(1+x^2)^{3/2}} \quad (6-103)$$

For small  $x$  Eq. 6-103 becomes

$$g(x) \cong 1 - \frac{3}{2} x \quad (6-104)$$

which is valid for  $x$  smaller than 0.2. The convergence of Eq. 6-102 is slow. However, Eq. 6-102 may be written as

$$I(a) = \frac{1}{1-a^2} \left\{ I(0) + \frac{4}{\sqrt{\pi}} \sum_{n=0}^{\infty} \frac{1}{(2n+1)^{3/2}} \left[ g\left(\frac{\beta}{c_n}\right) - 1 \right] \right\} \quad (6-105)$$

A portion of the summation is evaluated in terms of the Riemann Zeta-function which is

~~SECRET~~

$$\zeta(z) = \sum_{n=1}^{\infty} \frac{1}{n^z}$$

from which

$$\sum_{n=0}^{\infty} \frac{1}{(2n+1)^z} = \left(1 - \frac{1}{2^z}\right) \zeta(z) \tag{6-106}$$

Equation 6-105 may be written as

$$\begin{aligned} I(a) = & \frac{1}{1-a^2} \left\{ \frac{4}{\pi^{1/2}} \left(1 - \frac{1}{2^{3/2}}\right) \zeta\left(\frac{3}{2}\right) - \frac{12}{\pi^{3/2}} \left(1 - \frac{1}{2^{3/2}}\right) \zeta\left(\frac{5}{2}\right) \beta \right. \\ & \left. + \frac{4}{\sqrt{\pi}} \sum_{n=0}^{\infty} \frac{1}{(2n+1)^{3/2}} \left[ g\left(\frac{2\beta}{(2n+1)\pi}\right) - 1 + \frac{3}{2} \frac{2\beta}{(2n+1)\pi} \right] \right\} \tag{6-107} \end{aligned}$$

where the first of the three terms is a closed expression for  $I(0)$ . The Zeta-function is a tabulated function and the remaining summation initially converges very rapidly, due to Eq. 6-104. For  $I(a)$  see Fig. 6-3.

The development following Eq. 6-90 evaluates the resonance capture integral between infinite limits. However, in actual numerical work the integral is performed analytically over only a finite region  $\Delta u$  about the peak, and is continued numerically outside this region. Hence the correction

$$G' = 2 \int_{-\infty}^{\frac{\Delta u}{2}} \frac{\Sigma_c^*}{\Sigma_H + \Sigma_c^*} du \tag{6-108}$$

~~SECRET~~

~~SECRET~~

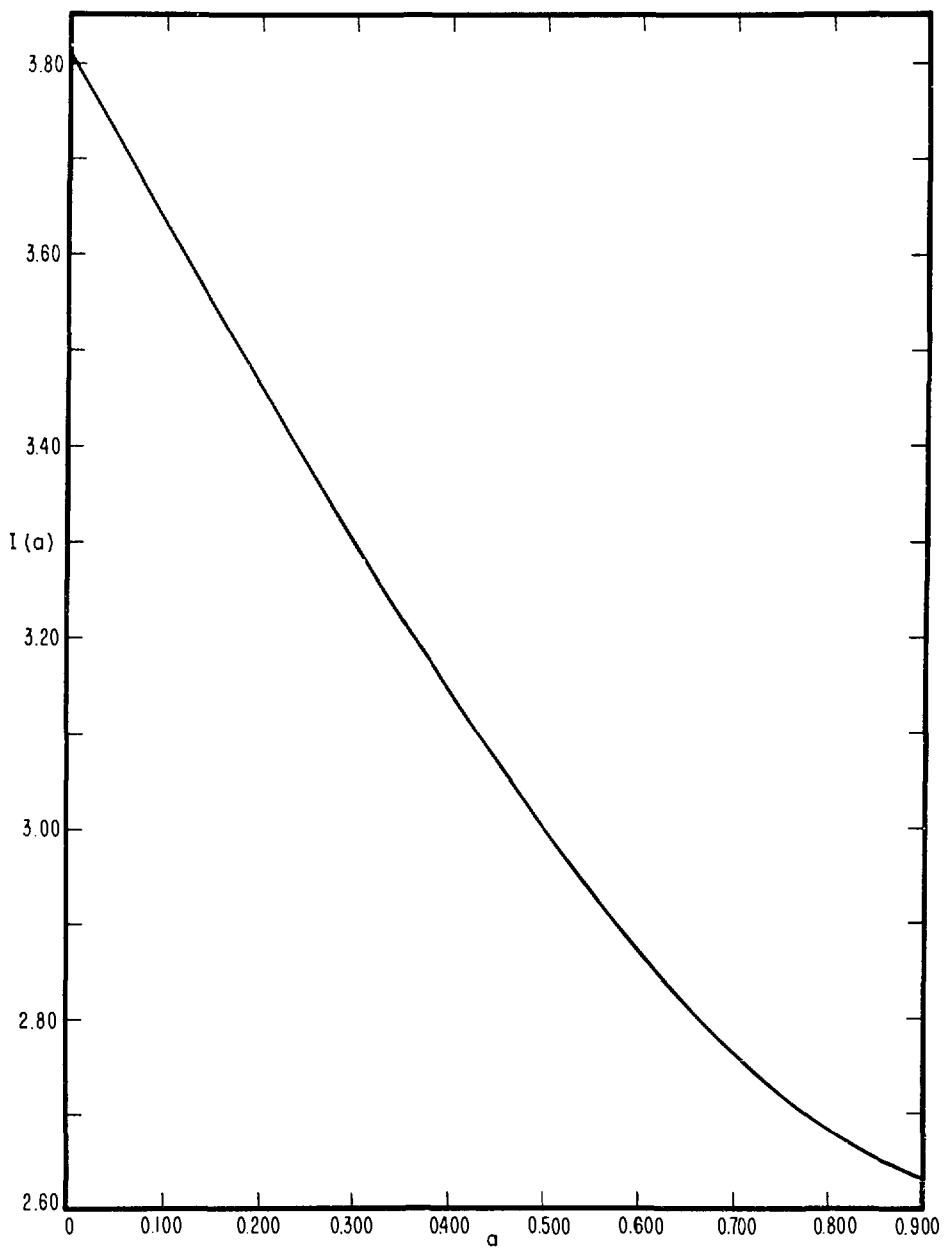


Fig. 6-3: The Function I(a)

~~SECRET~~

needs to be subtracted from  $G$ . In all cases  $\Delta u$  is chosen so large that

$$\Sigma_c^* \cong \Sigma_c \cong \rho_c \sigma_m (\delta/u)^2 \quad (6-109)$$

and that  $\Sigma_c^*$  has a negligible effect on the denominator of Eq. 6-108.

The integral of Eq. 6-108 is

$$G' = 4 \frac{\rho_c \sigma_m}{\Sigma_H} \delta^2 \frac{1}{\Delta u} \quad (6-110)$$

which gives a proper expression for the resonance capture

$$G(\Delta u) = a \left\{ I(a) \frac{\delta}{\epsilon} - \frac{4}{\Delta u} \left( \frac{\delta}{\epsilon} \right)^2 \right\} \quad (6-111)$$

This differs typically from the value of Eq. 6-90 by several percent.

In an unlumped core at uniform temperature the effect of Doppler broadening may be treated without difficulty. A resonance peak which is a delta function at 0°K is broadened at a finite temperature to a shape given by a normalized Gaussian distribution  $\Delta(u)$ . A resonance peak  $\sigma_0(u)$  of finite width at 0°K has, when raised to the same temperature, a cross section given by the convolution

$$\sigma(u) = \int_{-\infty}^{\infty} \sigma_0(u_1 + u) \Delta(u_1) du_1 \quad (6-112)$$

The function  $\sigma_0(u)$  is given by the Breit-Wigner formula as in Eq. 6-82, and the integration of Eq. 6-112 may be performed to obtain a result

~~SECRET~~

expressible in terms of the error function. An approximation is made, however, in order to obtain an analytic form for subsequent operations. A normalized distribution which is short-tailed compared to the Breit-Wigner function is substituted for the Gaussian function. It is fitted to the Gaussian function over most of the range of integration. This distribution function is given by

$$\Delta(u) = \frac{2}{\pi b} \frac{1}{[1+(u/b)^2]^2} \tag{6-113}$$

where b is chosen to fit the proper Gaussian function at half-height. Equations 6-113 and 6-82 are substituted into Eq. 6-112, yielding

$$\sigma(u) = \frac{2\delta^2}{\pi b} \sigma_m \int_{-\infty}^{\infty} \frac{1}{\delta^2+(u_1+u)^2} \frac{1}{(b^2+u_1^2)^2} du_1 \tag{6-114}$$

With the substitutions

$$x = u/b$$

$$w = \delta/b$$

$$\tag{6-115}$$

Eq. 6-114 becomes

$$\begin{aligned} \sigma(u) &= \frac{2}{\pi b^4} \sigma_m w^2 \int_{-\infty}^{\infty} \frac{1}{w^2+(x_1+x)^2} \frac{1}{(1+x_1^2)^2} dx_1 \\ &= \sigma_m w \frac{(w+1)^3+(w+1)^2+w(u/b)^2}{[(w+1)^2+(u/b)^2]^2} \end{aligned} \tag{6-116}$$

~~SECRET~~

~~SECRET~~

Chapter 6                      Nuclear Reactor Considerations

---

The Doppler-broadened cross section equation 6-116 is substituted into Eq. 6-81, and the integration is performed, yielding

$$G = \pi \frac{\left(\frac{w^2}{c} + \frac{a}{\epsilon}\right)}{\sqrt{2(\eta + \gamma)}}$$

where

$$c = \frac{\sigma_H \rho_H}{\sigma_m \rho_c}$$

$$\eta^2 = (1 + w)^4 + a$$

$$a = \frac{w}{c} [(w+1)^3 + (w+1)^2]$$

$$\gamma = (1 + w)^2 + \frac{w^2}{2c} \tag{6-117}$$

Correction of this equation for the finite range of integration is given by Eq. 6-110.

6-6: Numerical Procedure

The calculational steps described in Sec. 6-4 separate naturally into two parts: determination of nuclear parameters, and subsequent calculation of reflector dimensions and criticality.

Evaluation of the nuclear constants consists primarily of the evaluation of the integral

~~SECRET~~

$$P = \int_0^{u^{\text{th}}} \frac{\Sigma_c}{\Sigma_H + \Sigma_C} du \tag{6-118}$$

and the similar integrals over the individual energy groups. The integrand expressions are obtained from the nuclear data given in App. A. The trapezoidal rule is used for integration except at the resonances, for which the effects described in Sec. 6-5 are considered. Nine energy groups are used, ranging from  $10^6$  ev to 0.025 ev.

In integrating over the resonances one must remember that each resonance peak stands above a finite "plateau," i.e.,

$$\Sigma_C = \Sigma_R + \kappa \tag{6-119}$$

where  $\Sigma_R$  is the resonance capture cross section as given in Sec. 6-5 and  $\kappa$  is the plateau value of the cross section. The integration may be reduced to a form not involving a plateau by means of the identity

$$\int \frac{\Sigma_R + \kappa}{\Sigma_H + \Sigma_R + \kappa} du = \frac{\Sigma_H}{\Sigma_H + \kappa} \int \frac{\Sigma_R}{(\Sigma_H + \kappa) + \Sigma_R} du + \int \frac{\kappa}{\Sigma_H + \kappa} du \tag{6-120}$$

where  $\Sigma_H$  and  $\kappa$  are regarded as constants. The change introduced by the finite value of  $\kappa$  is small.

The Doppler-broadening correction makes only a slight difference in the critical conditions. Since the small detrimental effect of Doppler-broadening is masked by the conservative method of estimating the lumping correction, this correction is not applied to the bulk of the



~~SECRET~~

calculations. In molybdenum systems the lumping correction may be omitted.

Integration over a set of resonances involves a sum of terms of the form of Eq. 6-111

$$\sum_R G_R = a I(a) \sum_R \left[ \frac{\delta_R}{\epsilon_R} - \frac{4}{I(a)} \frac{1}{\Delta u_R} \left( \frac{\delta_R}{\epsilon_R} \right)^2 \right] \quad (6-121)$$

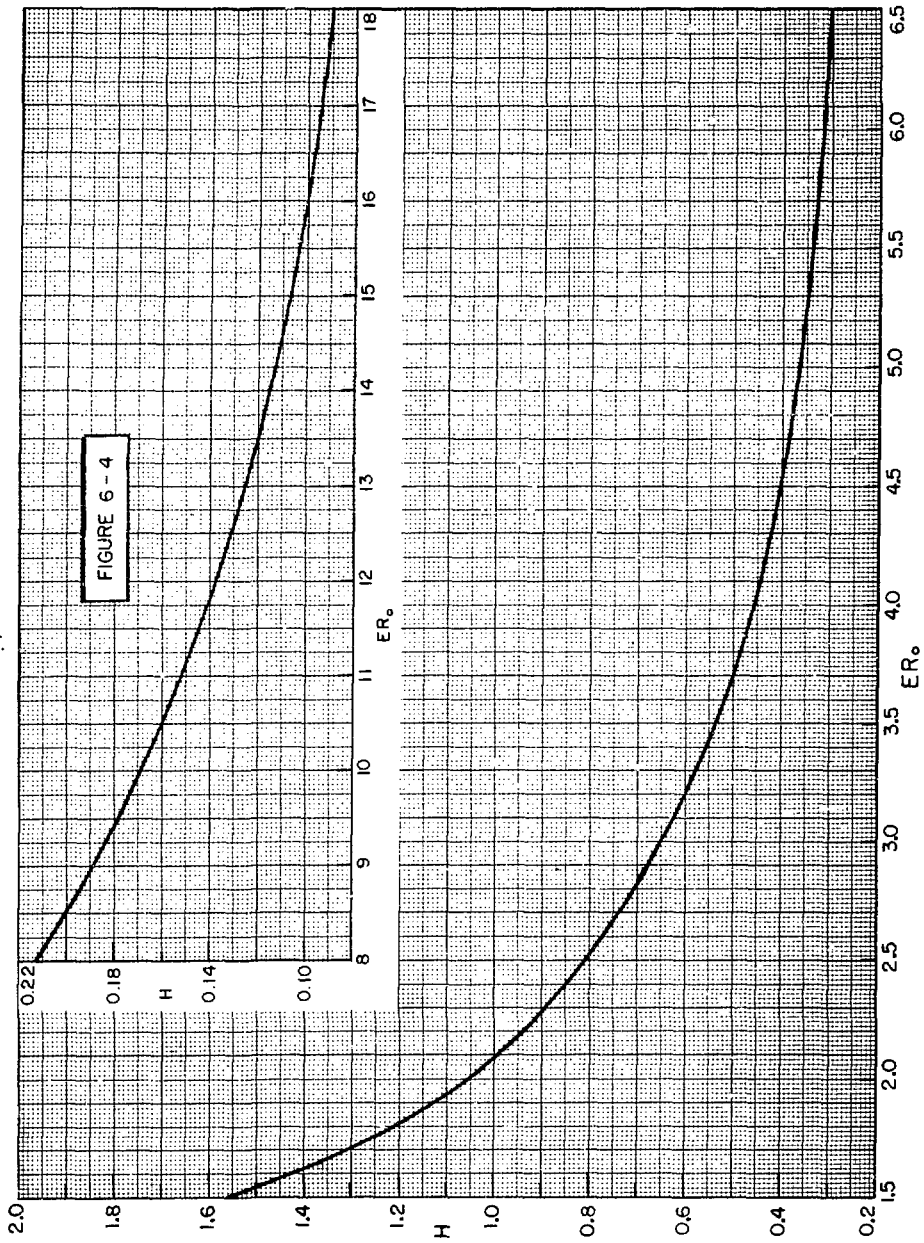
The only dependence of this expression on the hydrogen concentration is through a. Because the procedure is to obtain criticality by adjusting the hydrogen concentration, it is convenient to replace  $4/I(a)$  in the bracketed term by an average value. This step is justified both by the insensitivity of I to a, as shown in Fig. 6-3, and by the smallness of this term.

The second portion of the computation is complicated by the relations involving the Bessel functions of  $ER_0$  and  $ER_1$ . Inspection of the equations 6-63 to 6-66 indicates that  $ER_1$  is a function of  $ER_0$  only, and that  $H$ , occurring in  $a_0$ , is similarly determined by  $ER_0$ . These two functions are shown in Fig. 6-4 and 6-5.

The preceding developments are summarized as two separate procedures for reactor calculation: The first is used when the albedo condition is assumed at the bottom of the cylindrical reactor. The second procedure is used for a symmetric reactor with equal top and bottom reflection, and which has no axial flux variation.

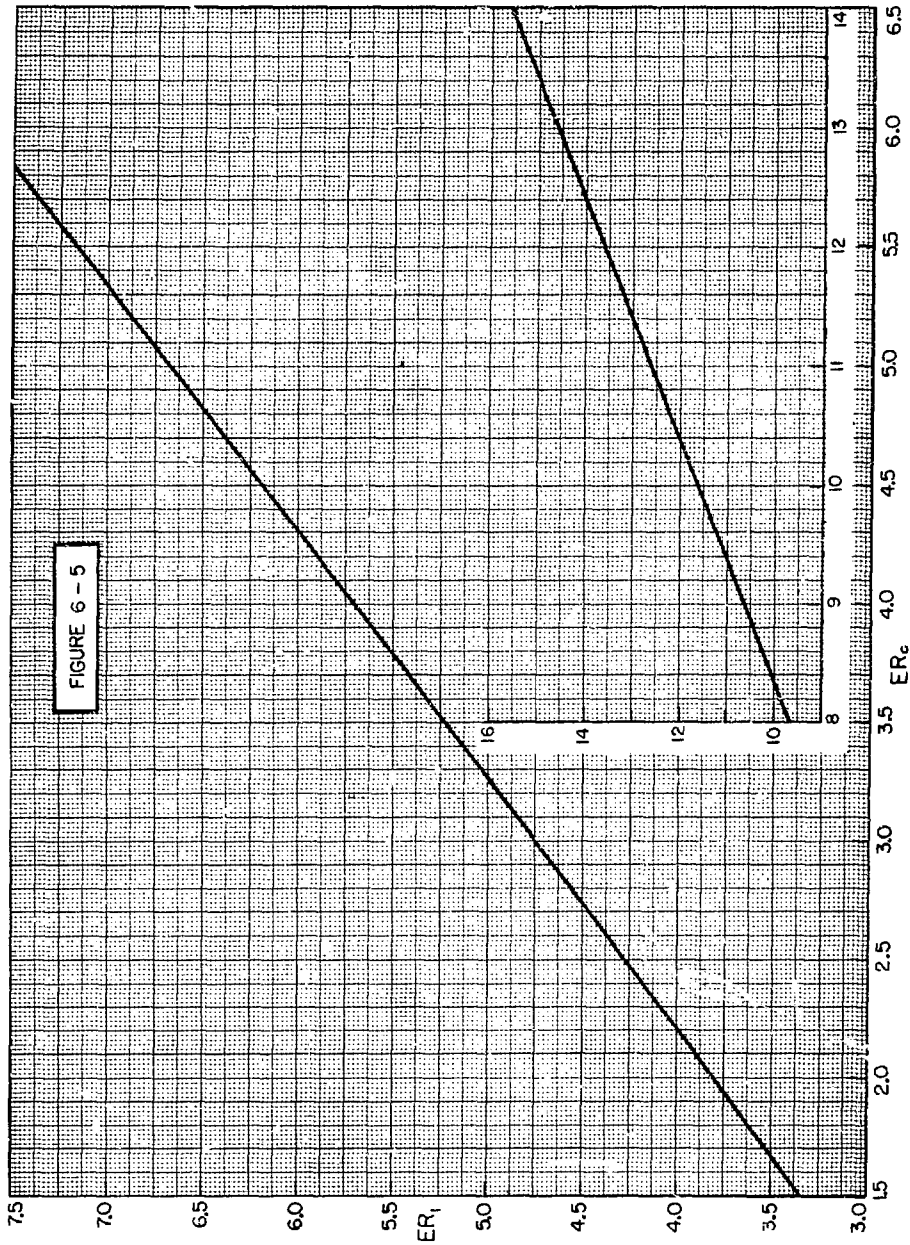
~~SECRET~~

~~SECRET~~



~~SECRET~~

~~SECRET~~



~~SECRET~~

~~SECRET~~

Procedure I. Albedo Assumption

(1) Assume trial reactor core dimensions  $R_0$  and  $L_0$ , densities  $N_i$  (moles/liter), and an albedo  $\beta$ .

(2) Compute  $\Sigma_{tr}$ .

(3) Compute  $S_1$ , given by

$$S_1 = D_{B_0}/D = D_{B_0} \Sigma_{tr} = 1.340 \Sigma_{tr}$$

(4) Compute  $\Sigma_H$  using the full ~20 barn cross section for hydrogen.

Then evaluate  $\omega_1$ , given by

$$\omega_1 = \xi \Sigma_{B_0} / \Sigma_H = 0.1560 / \Sigma_H$$

(5) Compute  $D_{eff}$  by Bell's criterion, given by

$$D_{eff} = 1010 / \sum_i \rho_i^* N_i$$

(6) Compute  $\tau_{th}$  by Bell's criterion, given by

$$\tau_{th} = \frac{0.51 \times 10^6}{(\sum_i \eta_i N_i)(\sum_i \rho_i^* N_i)}$$

(7) Solve the transcendental equation

$$x \tan x = \frac{L_0}{2D_{eff}} \frac{1-\beta}{1+\beta}$$

and compute

$$\gamma = x/L_0$$

~~SECRET~~

~~SECRET~~

Chapter 6

Nuclear Reactor Considerations

- (8) Compute  $P$ , from Eq. 6-118, and  $C_0^2$  from

$$C_0^2 = P/\tau_{th}$$

- (9) Compute  $B^2$ ,  $L_1$ ,  $E$ ,  $A$ , and  $ER_0$  from the relations

$$B^2 = C_0^2 + \gamma^2$$

$$L_1 = \frac{\pi}{2} \sqrt{\frac{S_1}{w_1} \frac{1}{B^2}}$$

$$E = \sqrt{\frac{w_1}{S_1} B^2 - \gamma^2}$$

$$A = B^2/C_0^2$$

- (10) From Figs. 6-4 and 6-5 and the value of  $ER_0$  determine  $H(ER_0)$  and  $ER_1(ER_0)$ . Compute  $R_1$ .

- (11) Compute  $K$  and  $a_0$  from the relations

$$K = \frac{L_1}{L_0 + \frac{1}{2\gamma} \sin 2x}$$

$$a_0 = \frac{1}{1 + \omega_1 (H + K)}$$

- (12) Compute  $k_\infty$  as described previously and the criticality  $k$  from

$$k = k_\infty a_0$$

Procedure II. Bottom Reflector

- (1) Assume trial reactor core dimensions  $R_0$  and  $L_0$ , and densities  $N_i$  (moles/liter).

- (2) Compute  $\Sigma_{tr}$ .

~~SECRET~~

~~SECRET~~

Numerical Procedure

Section 6-6

- (3) Compute  $S_1$ , given by

$$S_1 = D_{B_0} / D = D_{B_0} \Sigma_{tr} = 1.340 \Sigma_{tr}$$

- (4) Compute  $\Sigma_H$  using the full ~20 barn cross section for hydrogen and evaluate  $\omega_1$ , given by

$$\omega_1 = \xi \Sigma_{B_0} / \Sigma_H = 0.1560 / \Sigma_H$$

- (5) Compute  $\tau_{th}$  by Bell's criterion, given by

$$\tau_{th} = \frac{0.51 \times 10^6}{(\sum_i \eta_i N_i)(\sum_i \rho^* N_i)}$$

- (6) Compute  $P$  from Eq. 6-118, and  $B^2$ , given by

$$B^2 = P / \tau_{th}$$

- (7) Compute  $E$ ,  $L_1$ , and  $K$ , given by

$$E = \sqrt{\frac{W_1}{S_1} B^2}$$

$$L_1 = \pi / 2E$$

$$K = L_1 / L_0$$

- (8) From Figs. 6-4 and 6-5 and the value of  $ER_0$  determine  $H(ER_0)$  and  $ER_1(ER_0)$ . Compute  $R_1$ .

- (9) Compute  $a_0$ , given by

~~SECRET~~

~~SECRET~~

$$a_0 = \frac{1}{1 + \omega_1(H+K)}$$

(10) Compute  $k_\infty$  as described previously and the criticality  $k$ , given by

$$k = k_\infty a_0$$

6-7: Some Sample Results

The foregoing numerical procedures are applied to a family of preliminary and exploratory problems in which the geometry and composition of the reactor core are specified arbitrarily, in contrast to the motor design problems of Chap. 9 which require consistency of nuclear design with hydrodynamic considerations, etc.

The values of  $k_\infty$  for two typical metallurgical compositions and various degrees of moderation are shown in Figs. 6-6a and 6-6b. On the molybdenum curve the condition of optimum moderation is eventually passed. Thermal neutron capture by hydrogen becomes an important effect for  $H/U > 100$ .

The major group of preliminary reactor studies is shown in Table 6-1 and Fig. 6-7. These reactors have a core of radius 30 cm and length 60 cm. A concentration of  $UO_2$  in the refractory metal is specified, where the volume of this impregnated metal is chosen to be  $7720 \text{ cm}^3$ . The amount of CH is varied to obtain a criticality of 1, and the beryllium reflector dimensions appropriate to the flat flux condition. Each

~~SECRET~~

~~SECRET~~

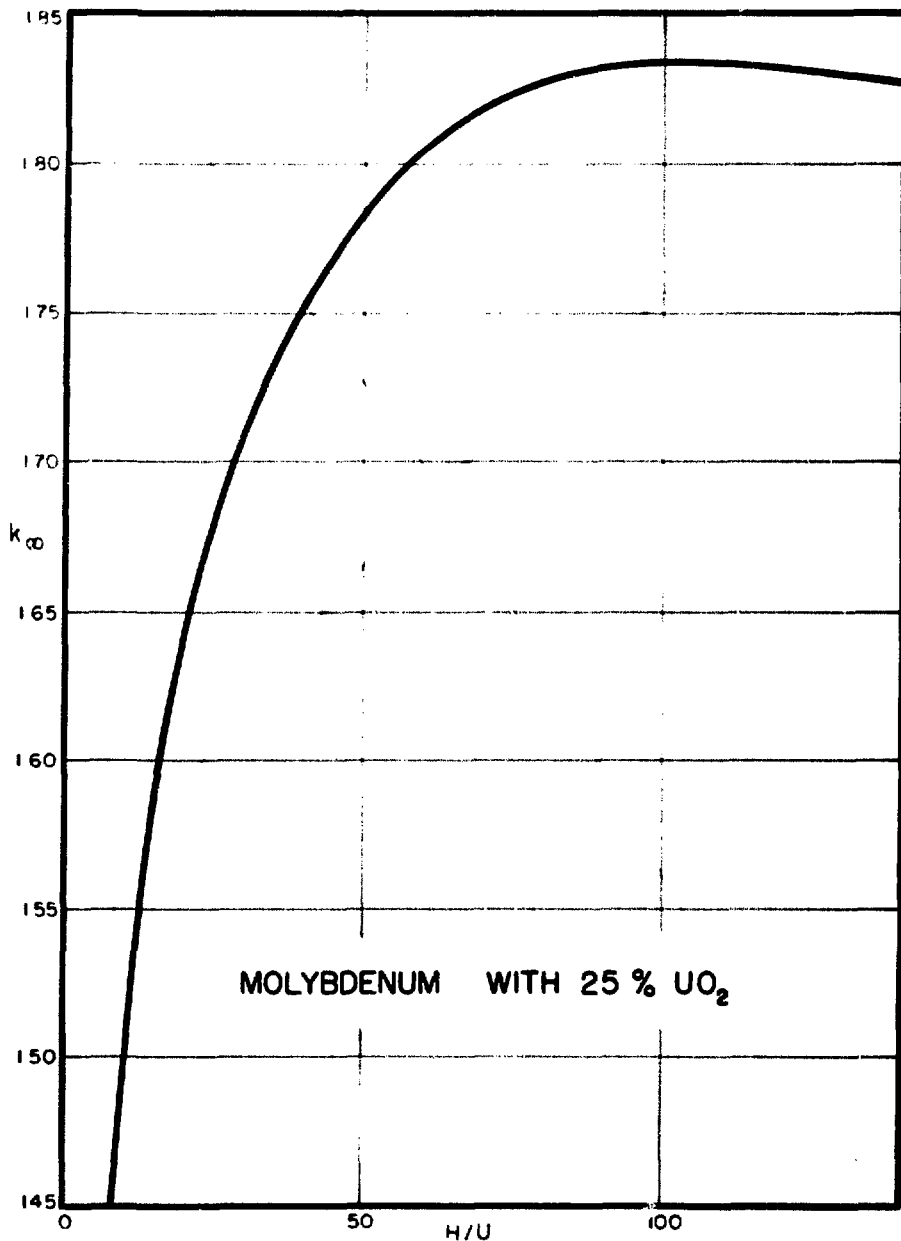


Fig. 6-6a: Values of k<sub>∞</sub> for Sample Molybdenum Reactors

~~SECRET~~



~~SECRET~~

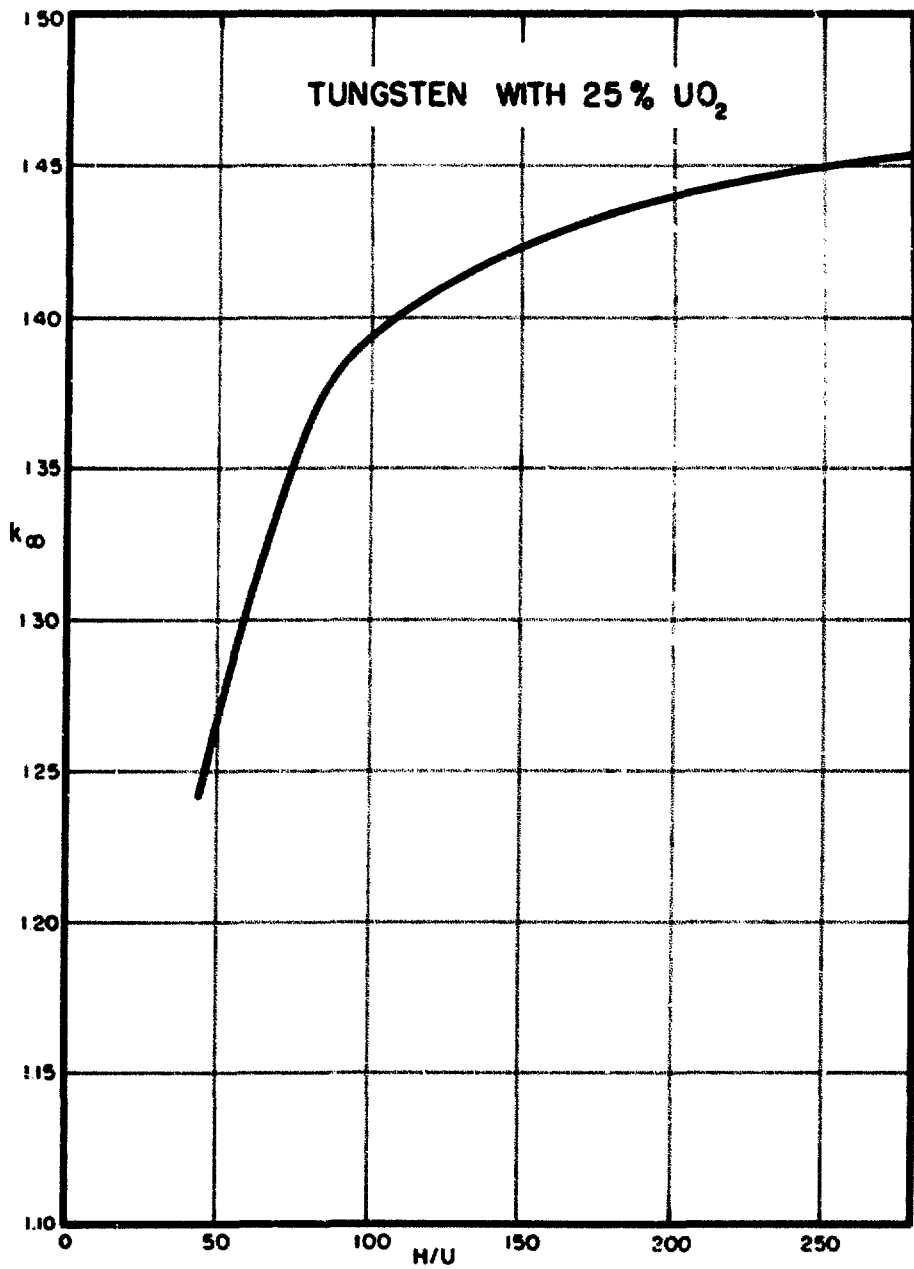


Fig. 6-6b: Values of k<sub>∞</sub> for Sample Tungsten Reactors

TABLE 6-1

## TYPICAL FLAT FLUX REACTOR CALCULATIONS

TOTAL VOLUME OF REFRACTORY METAL &  $UO_2$ , 7720  $cm^3$ 

ASSUMED ALUMINUM CONTENT, 14.2 kg

 $R_o = 30cm$  $L_o = 60cm$ 

WALL MAT'L	VOL. % $UO_2$ IN METAL	kg U	kg CH <sup>*</sup>	TOP * REFLECTOR THICKNESS, cm	SIDE * REFLECTOR THICKNESS, cm	kg CH <sup>†</sup>	END † REFLECTOR THICKNESS, cm	SIDE † REFLECTOR THICKNESS, cm
M <sub>o</sub>	10	7.44	74.9	28.00	33.40	110.2	33.65	41.65
	16	12.0	36.1	16.05	17.70	45.2	18.10	20.45
	25	18.6	24.2	11.10	11.75	30.2	12.50	14.05
	30.7	22.8	18.0	8.55	8.85	20.3	9.15	11.85
M <sub>o</sub> W	20	14.9	71.4	18.90	21.25	83.0	20.40	23.30
	25	18.6	56.0	14.55	17.25	61.6	15.25	18.25
	30.7	22.8	42.0	12.70	13.25	50.8	14.15	17.85
W	20	14.9	130.1	24.35	28.75	149.8	26.25	31.35
	25	18.6	82.7	18.35	20.55	95.8	19.65	22.30
	30.7	22.8	63.7	15.20	16.80	72.8	16.30	18.45

\* USING ALBEDO ASSUMPTION FOR BOTTOM LEAKAGE WITH  $\beta = 0.6$ 

† USING SYMMETRICAL END REFLECTORS

Some Sample Results

Section 6-7

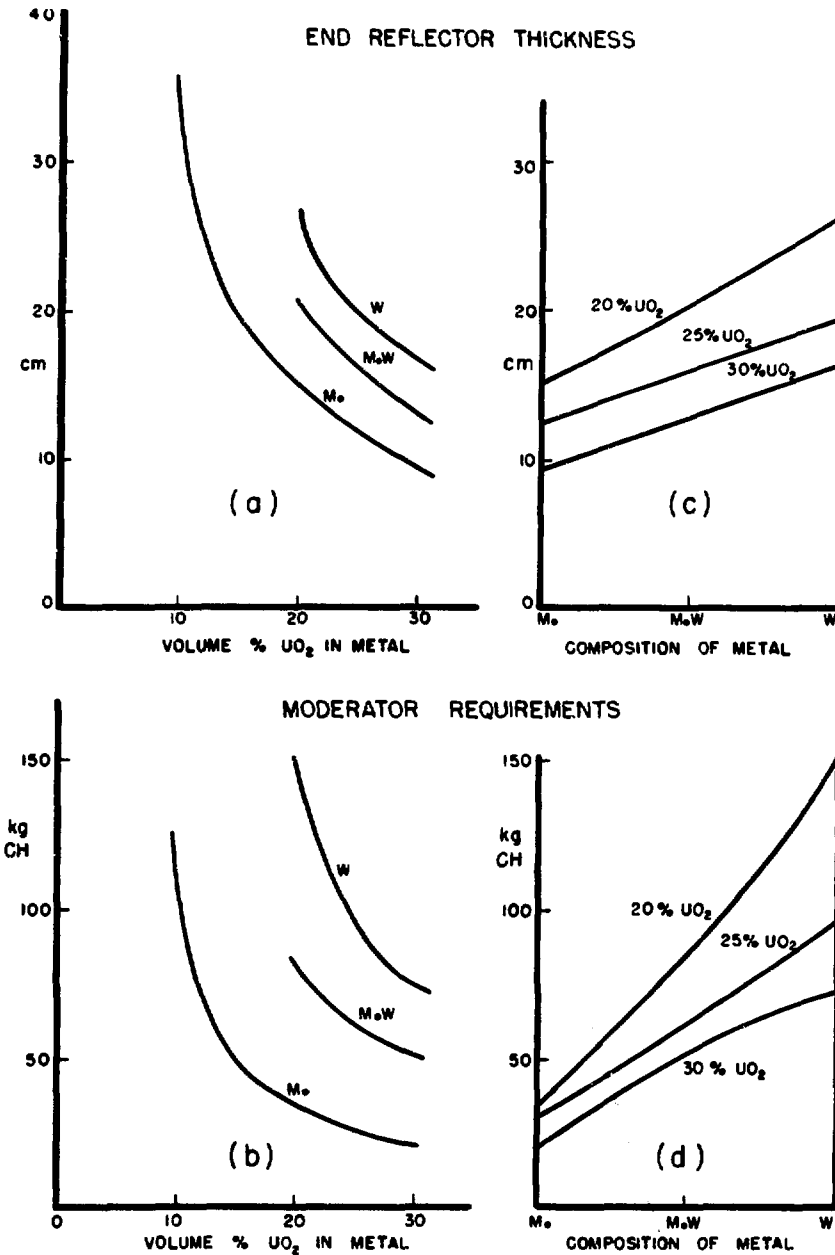


Fig. 6-7: Some Results for Sample Reactors

~~SECRET~~

Some Sample Results

Section 6-7

reactor is assumed to include 14.2 kg of aluminum. Refractory metals were taken to be (a) pure Mo, (b) 50:50 Mo and W (denoted by MoW), and (c) pure W.

Details of the neutron economy are shown in Fig. 6-8 for typical tungsten and molybdenum reactors. The severity of fast leakage and the importance of epithermal neutron capture are indicated by this figure.

The results given in Table 6-1 and Figs. 6-6, 6-7, and 6-8 are indicative of those encountered in a rocket motor. Several conclusions are evident: From the standpoint of uranium conservation the preferable motor is a highly moderated molybdenum heat exchanger. However, resulting reflector thickness is large, and in a realistic motor design the core volume needs to be increased in order to accommodate the large amount of moderator; this in turn increases the reflector mass even more. As a result the motor which shows the most economy in fissionable material is large and heavy. In addition, the refractory metals exhibit a certain perversity between their nuclear and their thermal properties, so that the motor designed to operate at the highest temperature is the most demanding of active material. From these considerations it seems likely that economy of active material should not be the primary consideration in the selection of a motor design. To the contrary, it seems that one should be as lavish with uranium as is consistent with good metallurgical properties of the metal-UO<sub>2</sub> system.

~~SECRET~~

~~SECRET~~

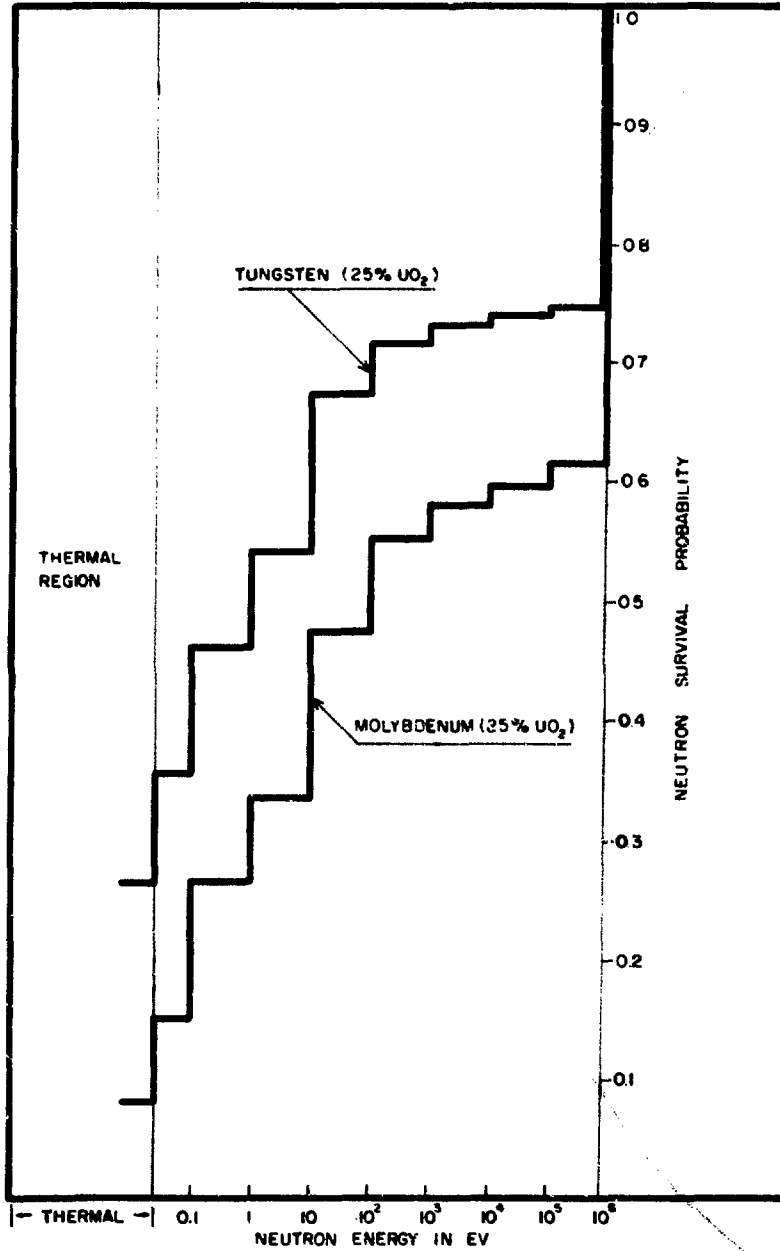


Fig. 6-8: Neutron Survival Probabilities for Sample Reactors

~~SECRET~~

~~SECRET~~

Reflector Design Variations

Section 6-8

Two conclusions are evident from the results shown in Fig. 6-7a and b.

(a) For a given metal the addition of excess  $UO_2$  gives great savings in CH requirements and in reflector thickness.

(b) Similar savings are available when it is sufficient to use molybdenum instead of tungsten, with a given amount of  $UO_2$ .

The data of Table 6-1 are plotted parametrically in Fig. 6-7c and d to show the effects of various Mo-W alloy compositions. It is remarkable that this variation produces no more structure than this figure depicts.

Figure 6-9 shows the moderator requirements corresponding to various core shapes. These curves suggest that there is considerable flexibility in the core geometry, and that fairly large departures from the best core shape necessitate a modest increase in moderation.

6-8: Reflector Design Variations

The flat flux condition is determined by the requirement that in the slowing-down process there is no net neutron current across the interface between reflector and core. For a reflector of given composition the determination of the reflector thickness is independent of the criticality. The dimensions specified in this way may be undesirable on the basis of other design considerations. A reflector yielding a flat flux may make a practical core design highly super-critical. The reflector may also be excessively massive. In this section it is shown that there

~~SECRET~~

~~SECRET~~

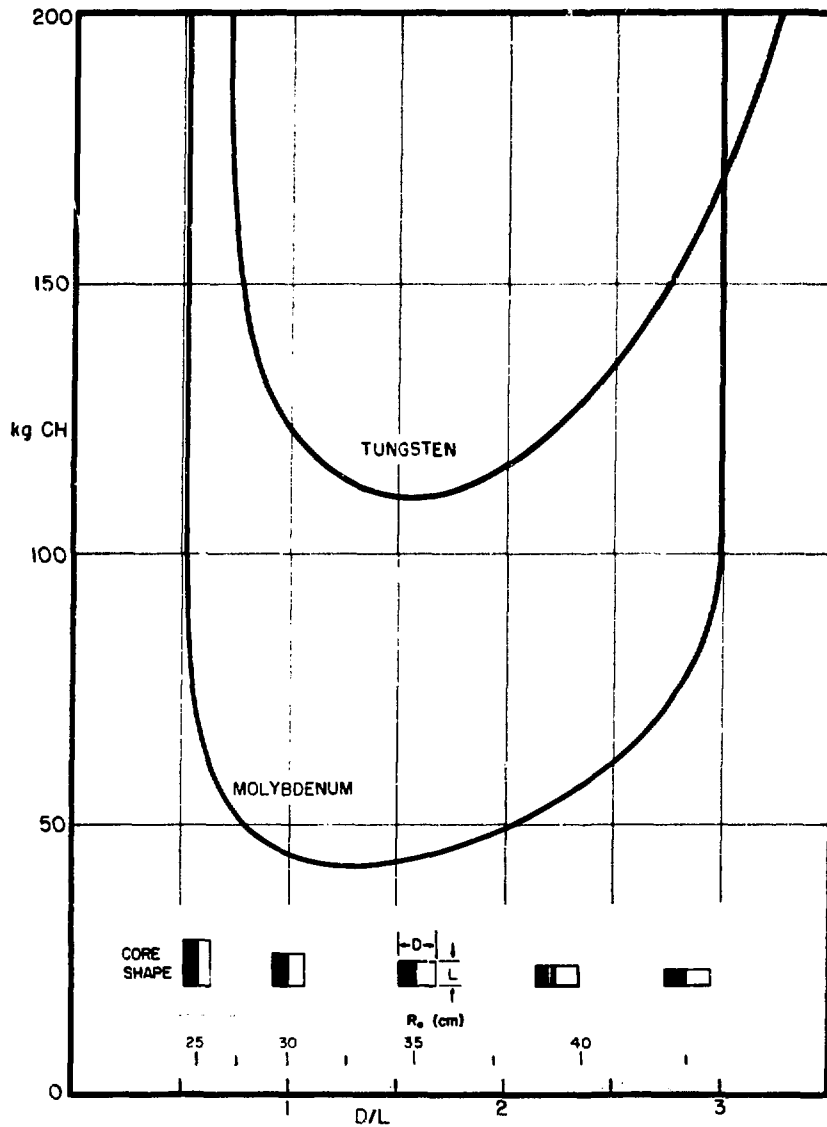


Fig. 6-9: Effect of Core Shape. The sudden rise of the molybdenum curve at  $D/L = 3$  is due to the breakdown of the approximation of total fast leakage from higher buckling modes for a reactor which is very well moderated and surrounded by a large reflector.

~~SECRET~~

can be considerable flexibility in choice of reflector, between effectiveness in neutron reflection and lightness in weight. This flexibility arises from the fact that reflector thickness is basically determined by the ability of the reflector to moderate neutrons, and that this ability may be regulated by incorporating a layer of hydrogenous material in the reflector.

The theory developed in Sec. 6-2 is applied to a reactor with a two-layer reflector. If the inner hydrogenous layer region is called A and the outer beryllium layer region B, Eq. 6-50 becomes

$$\begin{aligned}\nabla^2 q &= -\frac{\omega_A}{S_A} B^2 q \\ \nabla^2 q &= -\frac{\omega_B}{S_B} B^2 q\end{aligned}\tag{6-122}$$

for regions A and B, respectively. An additional boundary condition that  $q$  must be continuous across the new interface is

$$q \Big|_A = q \Big|_B\tag{6-123}$$

and the neutron current continuity condition is

$$S_A \frac{\partial q}{\partial n} \Big|_A = S_B \frac{\partial q}{\partial n} \Big|_B\tag{6-124}$$

In the top reflector the solution which has a zero derivative at the core boundary and vanishes at the extrapolated boundary is of the form



~~SECRET~~

Chapter 6

Nuclear Reactor Considerations

$$q = \cos \sqrt{\frac{\omega_A}{S_A}} B z$$

$$q = M \sin \sqrt{\frac{\omega_B}{S_B}} B (L_1 - z) \quad (6-125)$$

for regions A and B, respectively. The A - B interface is at  $z = L'$ .

Equation 6-125 is applied to Eqs. 6-123 and 6-124, which become

$$\cos \sqrt{\frac{\omega_A}{S_A}} B L' = M \sin \sqrt{\frac{\omega_B}{S_B}} B (L - L') \quad (6-126)$$

$$S_A \sqrt{\frac{\omega_A}{S_A}} B \sin \sqrt{\frac{\omega_A}{S_A}} B L' = S_B \sqrt{\frac{\omega_B}{S_B}} B M \cos \sqrt{\frac{\omega_B}{S_B}} B (L_1 - L') \quad (6-127)$$

which are simultaneous equations determining the total thickness  $L_1$  and the interface matching constant  $M$  in terms of the parameter  $L'$ . If the thickness of a pure beryllium reflector is assumed to be  $L_{10}$  (the value of  $L_1$  when  $L' = 0$ ), then the following dimensionless quantities may be defined:

$$r = \sqrt{\frac{\omega_A}{S_A}} / \sqrt{\frac{\omega_B}{S_B}} = \sqrt{\frac{\xi_A \Sigma_A}{\xi_B \Sigma_B}} \sqrt{\frac{D_B}{D_A}}$$

$$\lambda_1 = L_1 / L_{10}$$

$$\lambda' = L' / L_{10}$$

(6-128)

~~SECRET~~

~~SECRET~~

Reflector Design Variations

Section 6-8

Equations 6-126 and 6-127 are combined to give

$$\frac{1}{\frac{S_A}{S_B} r \tan \frac{\pi}{2} r \lambda'} = \tan \frac{\pi}{2} (\lambda_1 - \lambda') \quad (6-129)$$

$$M = \frac{\cos \frac{\pi}{2} r \lambda'}{\sin \frac{\pi}{2} (\lambda_1 - \lambda')} \quad (6-130)$$

Equation 6-129 is solved for  $\lambda_1$  which then determines the value of M in Eq. 6-130.

The value of  $a_0$ , as given by Eq. 6-24, depends on the overall reactor dimensions and also on the value  $\omega$  in the reflector: hence it is a function of  $\lambda'$ . However, its only dependence on  $\lambda'$  is from the part of the denominator integration which involves the reflector. For the generalization of Eq. 6-66, which is for the case  $\lambda' = 0$ , the denominator must be modified such that

$$\omega_1 (H + K) = \frac{\int_R q_0^2 \omega dV}{\int_H q_0^2 \omega dV} \quad (6-131)$$

In the general case of variable  $\lambda'$ , it is the numerator of this ratio that depends on  $\lambda'$ . In the side reflector the Bessel functions are like the trigonometric functions in the top reflector, so that approximately

~~SECRET~~

~~SECRET~~

$$\frac{\int_{R(\lambda')} q_0^2(\lambda') \omega(\lambda') dV}{\int_{R(\lambda=0)} q_0^2(\lambda=0) \omega(\lambda=0) dV} = \frac{\int_0^{L_1} q_0^2(\lambda') \omega(\lambda') dz}{\int_0^{L_{10}} q_0^2(0) \omega(0) dz}$$

$$= \frac{\omega_A}{\omega_B} \left( \lambda' + \frac{1}{\pi r} \sin \pi r \lambda' \right) + M^2(\lambda') \left[ \lambda_1 - \lambda' - \frac{1}{\pi} \sin \pi (\lambda_1 - \lambda') \right]$$

$$\equiv J(\lambda')$$

(6-132)

where the integrals are evaluated using Eq. 6-125. Combining Eq. 6-132 with Eq. 6-131 gives the generalization of Eq. 6-66,

$$q_0(\lambda') = \frac{1}{1 + \omega_B(H+K) J(\lambda')} \tag{6-133}$$

where H and K are determined as in Eq. 6-66. This approximation is more accurate than simple substitution of trigonometric functions for the corresponding Bessel functions because Eq. 6-133 becomes exact for  $\lambda' \rightarrow 0$ .

The variables  $\lambda_1$ ,  $\lambda_1 - \lambda'$ , and  $J(\lambda')$  are plotted as functions of  $\lambda'$  in Fig. 6-10. The function  $J_1(\lambda')$  which is the contribution of the hydrogenous region to  $J(\lambda')$  is also plotted. For a given reactor core a critical reactor is achieved by adjusting  $\lambda'$  such that

$$J(\lambda') = \frac{1}{\omega_i(H+K)} (k_{\infty} - 1) \tag{6-134}$$

20  
~~SECRET~~

~~SECRET~~

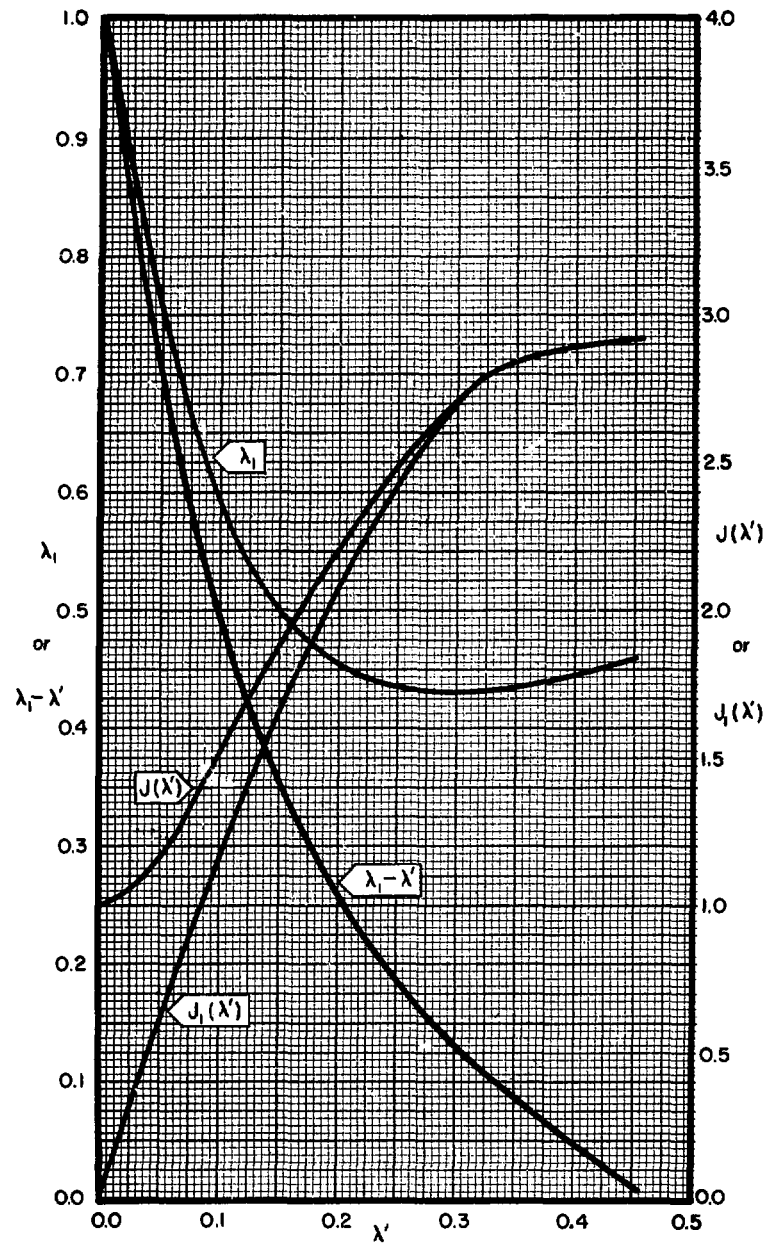


Fig. 6-10: Some Functions of  $\lambda'$

~~SECRET~~

~~SECRET~~

These results are applied to actual motor design problems in Chap. 10. The effect of the use of diffusion theory upon the accuracy of these results is discussed in Sec. 6-9.

6-9: Effects of the Approximations

It is pointed out throughout this chapter that the theory developed here makes a number of approximations. The major approximations are as follows:

- (a) Treatment of the neutron economy by finite groups.
- (b) Method of correcting for lumping effects.
- (c) Accuracy of nuclear data.
- (d) Use of diffusion theory.
- (e) Use of average capture approximation (Eqs. 6-44 and 6-45).
- (f) Achievement of flat flux condition.
- (g) Methods of treatment of the bottom reflector.
- (h) Neglect of higher modes.
- (i) Neglect of thermal neutron diffusion.

Item a: From the study of the numerical examples the use of nine groups seems adequate. Item b: On the basis of numerical results of test problems where lumping was neglected, the lumping correction is negligible in molybdenum reactors and typically results in an 8% increase in  $k$  for tungsten reactors. Refined methods of applying this correction are expected to increase  $k$  by an additional small amount. Item c: The

~~SECRET~~

~~SECRET~~

Effects of the Approximations

Section 6-9

presence of large amounts of moderator, most of the neutron capture takes place in the thermal and epithermal groups where the cross section data are best known.

Approximations d and e are intimately linked, and their accuracy depends largely on the achievement of flat flux within the reactor core. The error in these approximations is mainly in the simplifying assumptions they make about the flow of neutrons. If the core flux is flat, there is no net neutron current and these methods may become quite accurate.\* In the reflector, item e does not apply, but the question of item d on the validity of diffusion theory is pertinent. The diffusion approximation is valid in regions a few diffusion lengths in thickness. The beryllium reflector thicknesses typically range from six to twenty diffusion lengths, so that the use of diffusion theory is justified. On the other hand, the special reflector calculations of Sec. 6-8 must be regarded as somewhat qualitative because of the short-distance limitations of diffusion theory.

Item f: The possibility of obtaining an approximately flat flux is independent of the approximations made previously: for some degree of reflection the flux must be the same at the center as at the surface of the core. The calculations yield a flux which is perfectly flat because of

---

\*In the flat flux situation the diffusion coefficient of the core would disappear from the analysis except for the convenience of using the Fermi age variable which carries a concealed and cancelling dependence on the diffusion coefficient.

~~SECRET~~

~~SECRET~~

Chapter 6 Nuclear Reactor Considerations

the approximation  $e$ , but the actual flux variation can not be very large. This is seen as follows: When, in a typical reactor, the flux-flattening effect of slowing-down capture is neglected, the flux may be calculated by the methods of Sec. 6-2. The radial flux profile in the core, actually a Bessel function, may be well represented by a parabola falling at the edge to 0.6 of the central value, i.e.,

$$\phi(r) = \phi(0) \left\{ 1 - 0.4 \left( \frac{r}{R_0} \right)^2 \right\} \quad (6-135)$$

If it is assumed that the effect of the proper reflector is to add a fourth power term of proper value, a flux distribution of the form

$$\Phi(r) = \Phi(0) \left\{ 1 - 0.4 \left( \frac{r}{R_0} \right)^2 + 0.4 \left( \frac{r}{R_0} \right)^4 \right\} \quad (6-136)$$

is obtained, as shown in Fig. 6-11. Modifying  $\phi$  in this way implies that the smoothing effect of the reflector does not flatten the flux profile at the center of the core. This is a pessimistic assumption. This flux density has an extreme value

$$\Phi_{\min} = 0.900 \Phi(0) \quad (6-137)$$

with the mean value

$$\bar{\Phi} = \frac{1}{A} \int \Phi dA = 0.933 \Phi(0) \quad (6-138)$$

Thus, these considerations indicate a maximum flux intensity 7% above the mean.

~~SECRET~~

~~SECRET~~

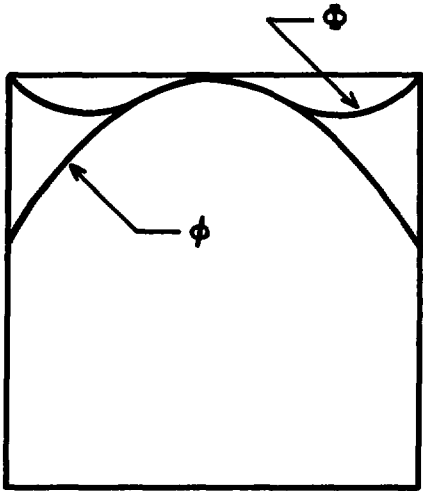


Fig. 6-11

Items g, h, and i all involve diffusion effects: Item g: The use of an albedo boundary condition for treating the bottom reflector yields results insensitive to the albedo. When symmetric end reflectors are assumed, slightly lower values of k are found, due to approximation h. In the fully reflected symmetric geometry a larger fraction of the slowing-down flux is represented by higher buckling modes, so that the complete neglect of these modes is more pessimistic in this case than for the albedo geometry. Item i: In these calculations the diffusion of thermal neutrons is neglected. Since the thermal neutron source, within the core, is flat, any effects due to thermal neutron diffusion are seen at the core surface. Since there is no significant thermal capture in the beryllium reflector, the neutron current flows from the reflector to

~~SECRET~~



~~SECRET~~

Chapter 6

Nuclear Reactor Considerations

---

the core. These neutrons are ignored in the calculations and thus tend to make the reactor more critical. However, they also tend to make the fission density less flat. Readjustment of the reactor parameters may be performed in order to recover flux uniformity. If necessary the return flow of thermal neutrons may be inhibited by introduction of a thermal poison such as boron into the reflector.

REFERENCES

1. S. Glasstone and M. C. Edlund, Elements of Nuclear Reactor Theory, Secs. 6.117 and 6.154, Van Nostrand, New York, 1955.
2. G. I. Bell, Simple Method of Calculating Critical Masses of Proton Moderated Assemblies, Los Alamos Scientific Laboratory Report LA-1548, May 1953.
3. Donald J. Hughes and John A. Harvey, Neutron Cross Sections, Brookhaven National Laboratory Report BNL 325, July 1, 1955.
4. S. Glasstone and M. C. Edlund, Elements of Nuclear Reactor Theory, Secs. 5.106 - 5.108, Van Nostrand, New York, 1955.

~~SECRET~~

Effects of the Approximations

Section 6-9

---

Note added in proof: It has been pointed out by N. H. Baker that the recoil of beryllium nuclei introduces an anisotropy into the neutron scattering by beryllium, and as a result somewhat modifies the neutron transport cross section in the reflector. For neutrons of energies high compared to chemical binding energies ( $\sim 5$  ev), the modification in the cross section amounts to circa 8%. Thus an 8% increase in reflector thicknesses should be applied throughout this report. Actually the 8% correction is an overestimate, since the recoil effect vanishes in the lowest three epithermal neutron groups.

~~SECRET~~

~~SECRET~~

## CHAPTER 7

### HYDRODYNAMIC DESIGN CONSIDERATIONS

Rash and inexperienced traveller, we will now seriously devote ourselves to a little high tension, because if we do not, it is my impression that yonder self-propelling man-of-war with the armour-plated upper deck (and by this, O Best Beloved, he meant the Crocodile), will permanently vitiate your future career.

R. Kipling, The Elephant's Child

#### 7-1: Introduction

This chapter is devoted to the hydrodynamic and heat-exchanger problems associated with Dumbo, exclusive of those already treated in Chap. 2 which involve the primary heat-exchange process occurring in the metal wall.

In Sec. 7-2 the equations governing the turbulent heat exchangers of Dumbo are developed. These exchangers serve to transfer a few percent of the reactor power to the hydrogen as it passes through the reflector, the preheater, and the moderator before entering the metal wall.

In Secs. 7-3 through 7-9 the hydrodynamics governing the gas flow through the main supply and exhaust channels of Dumbo is studied. These problems of flow in a channel whose walls act as a source or sink for fluid are unique to the Dumbo design and their solution plays a most important role in the performance of Dumbo. It is shown that the flows

~~SECRET~~

~~SECRET~~

Chapter 7                      Hydrodynamic Design Considerations

---

through the metal wall at different heights may be made highly uniform without sacrificing uniformity of construction.

7-2: Turbulent Heat Exchangers

In the flow of propellant through the reflector, the preheater, and the moderator there is involved exchange of a few percent of the total power to low temperature hydrogen. These regions are characterized by turbulent flow. The design of such heat exchangers amounts to the prediction for a given geometry, flow rate, and power dissipation, of three quantities:

- (a) The resulting temperature increment  $\delta T$  between the gas and the wall, corresponding to the  $\theta_g$  of Chap. 2.
- (b) The pressure drop  $\Delta p$  experienced by the gas in passing through the exchanger.
- (c) The maximum temperature occurring in the exchanger walls.

The first two of these quantities are determined from empirical correlations of dimensionless parameters. The dimensionless quantities involve the density  $\rho$ , the viscosity  $\eta$ , the thermal conductivity  $\lambda$ , the specific heat  $c_p$ , and the pressure  $P$  of the gas moving with velocity  $v$  in the direction  $z$ . They are:

- (a) The Reynolds number,

$$R = \rho v D / \eta$$

where  $D$  is the hydraulic diameter of the channel(s).

~~SECRET~~

~~SECRET~~

Turbulent Heat Exchangers

Section 7-2

- (b) The Prandtl number of order unity for gases,

$$Pr = c_p \eta / \lambda$$

- (c) The friction factor,

$$\gamma = - \frac{D}{2\rho v^2} \frac{dp}{dz}$$

- (d) The Stanton number,

$$k_H = h / c_p \rho v$$

where  $h$  is the heat transfer coefficient given by

$$h = \frac{U}{A^* \delta T}$$

and  $U$  is the energy transferred per second to the gas,  $A^*$  is the wall surface area, and  $\delta T$  is the temperature increment between gas and wall.

The first problem, that of determining  $\delta T$ , assumes an empirical relation  $k_H(R)$  which is applicable to the system. For a total flow  $Q_0$  the flow density  $\rho v$  is given by  $Q_0/A_0$ , where  $A_0$  is the open cross sectional flow area. The total energy transfer rate  $U$  is related to the flow by

$$U = Q_0 \int_{T_i}^{T_f} c_p(T) dT = Q_0(H_f - H_i) \quad (7-1)$$

where  $H$  is the enthalpy of the gas and the subscripts  $f$  and  $i$  refer to final and initial values, respectively. The power is uniformly distributed along the length  $z$ , whence

~~SECRET~~

~~SECRET~~

Chapter 7 Hydrodynamic Design Considerations

$$\frac{dU}{dz} = \text{const.} = \frac{U}{L} = Q_o c_p \frac{dT}{dz} = \frac{Q_o(H_f - H_i)}{L} \quad (7-2)$$

where L is the total flow distance. Hence, the Stanton number is written as

$$k_H = \frac{A_o}{A^*} \frac{L}{\delta T} \frac{dT}{dz} \quad (7-3)$$

The hydraulic diameter D for noncircular channels is given in terms of the channel perimeter  $A^*/L$  by

$$D = 4 \frac{A_o}{A^*/L}$$

giving a final expression for the Stanton number,

$$k_H = \frac{1}{4} \frac{D}{\delta T} \frac{dT}{dz} \quad (7-4)$$

This problem is concerned with the  $\delta T$  occurring at the hottest point.

The gradient  $dT/dz|_f$  at this point is determined from Eq. 7-2,

$$\left. \frac{dT}{dz} \right|_f = \frac{H_f - H_i}{c_{pf} L} \quad (7-5)$$

which in conjunction with Eq. 7-4 gives  $\delta T|_f$  in terms of  $k_H$ .

The second problem, that of the pressure drop occurring across a heat exchanger, is not obtained in quite so direct a manner. The friction factor  $\gamma$  for flow through a channel gives the pressure gradient  $dp/dz$  for fluid undergoing drag only, and does not include those forces causing changes in the momentum of the stream. For flow which is subsonic

~~SECRET~~

~~SECRET~~

Turbulent Heat Exchangers

Section 7-2

and nearly isobaric, the inclusion of terms for both drag and momentum change yields

$$\frac{dp}{dz} = - \frac{2\rho v^2}{D} \gamma - \rho v \frac{dv}{dz} \quad (7-6)$$

If it is assumed that  $\rho v = J = \text{const.}$  and  $\gamma = \text{const.}$ , Eq. 7-6 becomes

$$\frac{dp}{dz} = - \frac{2J^2\gamma}{D\rho} - J^2 \frac{d}{dz} \frac{1}{\rho} \quad (7-7)$$

If the pressure variation is small,  $\rho$  may be regarded as dependent on the temperature only, which is approximately linear through the exchanger.

Thus  $\frac{1}{\rho}$  is linear in  $z$  and may be written

$$\frac{1}{\rho} = \left( \frac{1}{\rho_L} - \frac{1}{\rho_0} \right) \frac{z}{L} + \frac{1}{\rho_0} \quad (7-8)$$

Substitution of Eq. 7-8 into Eq. 7-7 and integration yields the general heat-exchanger relation for gases, given by

$$p_L - p_0 = -J^2 \left[ \left( \frac{1}{\rho_L} - \frac{1}{\rho_0} \right) + \gamma \frac{L}{D} \left( \frac{1}{\rho_L} + \frac{1}{\rho_0} \right) \right] \quad (7-9)$$

The first term in this expression corresponds to the momentum change and is a stress required to accelerate the gas to its higher velocity, while the second term is a drag contribution.

The third problem, that of conduction within the solid exchanger walls in which power is generated, is solved approximately by the heat conduction relation for one-dimensional heat flow, i.e.,

~~SECRET~~

$$\lambda \frac{d^2 T}{dx^2} = -\sigma \quad (7-10)$$

where  $\sigma$  is the power density (cal/cm<sup>3</sup>-sec) in the walls. Thus

$$T_0 - T(x) = \frac{\sigma}{2\lambda} x^2 \quad (7-11)$$

To use the results of the first two problems, it is necessary to select the function  $\gamma(R)$  and  $k_H(\text{Pr}, R)$ . Of the several functions which have been suggested the simplest is the Blasius formula,

$$\gamma = \frac{0.08}{R^{1/4}} \quad (7-12)$$

For  $k_H$  a corresponding approximate form may be developed from the Reynolds analogy, given by

$$k_H = \frac{\gamma}{2} = \frac{0.04}{R^{1/4}} \quad (7-13)$$

In justification of such an arbitrary choice of forms it should be noted that:

- (1) In these exchangers the momentum term of Eq. 7-9 is dominant.
- (2) The temperature increment  $\delta T$  determines the wall temperature of the exchanger. The gas temperature is determined by the power input and not by the exchanger efficiency. Further, the materials of the exchanger, except in the case of the plastic moderator, are far below any disastrously high temperature limit and the value of  $\delta T$  is not of great consequence.



~~SECRET~~

(3) To compute these temperatures accurately it is necessary to know the power dissipation from these several regions. However, this aspect of reactor performance is only roughly known and awaits either good experimental measurement or refined and detailed computation. The values indicated in Fig. 7-1 are used throughout for purpose of consistency. Some thermodynamic properties<sup>1</sup> of H<sub>2</sub> which are of concern in heat-exchanger design are shown in Fig. 7-2.

7-3: Flow Uniformity Through the Composite Dumbo Wall

A hydrodynamic problem is now considered which is more intimate to the primary heat-exchange process occurring within the Dumbo wall. As shown in Fig. 7-3, hydrogen flows from a comparatively cold central region A at a pressure varying along the length as  $P_A(z)$ . After passage through the wall it enters a region B of hot gas at a lower pressure  $P_B(z)$ . The net flow rate  $J_O(z)$  through the wall is determined by the values of  $P_A$  and  $P_B$  and the impedance of the composite wall. The composite wall consists of moderator channels plus the metal wall structure. Due to the hydrodynamics which occur in regions A and B these pressure distributions may cause severe differences in the flow  $J_O$  at different heights  $z$ . The remainder of this chapter is devoted to the determination of the pressure distributions  $P_A(z)$  and  $P_B(z)$ , and of the resulting degree of uniformity in  $J_O(z)$ .

~~SECRET~~

~~SECRET~~

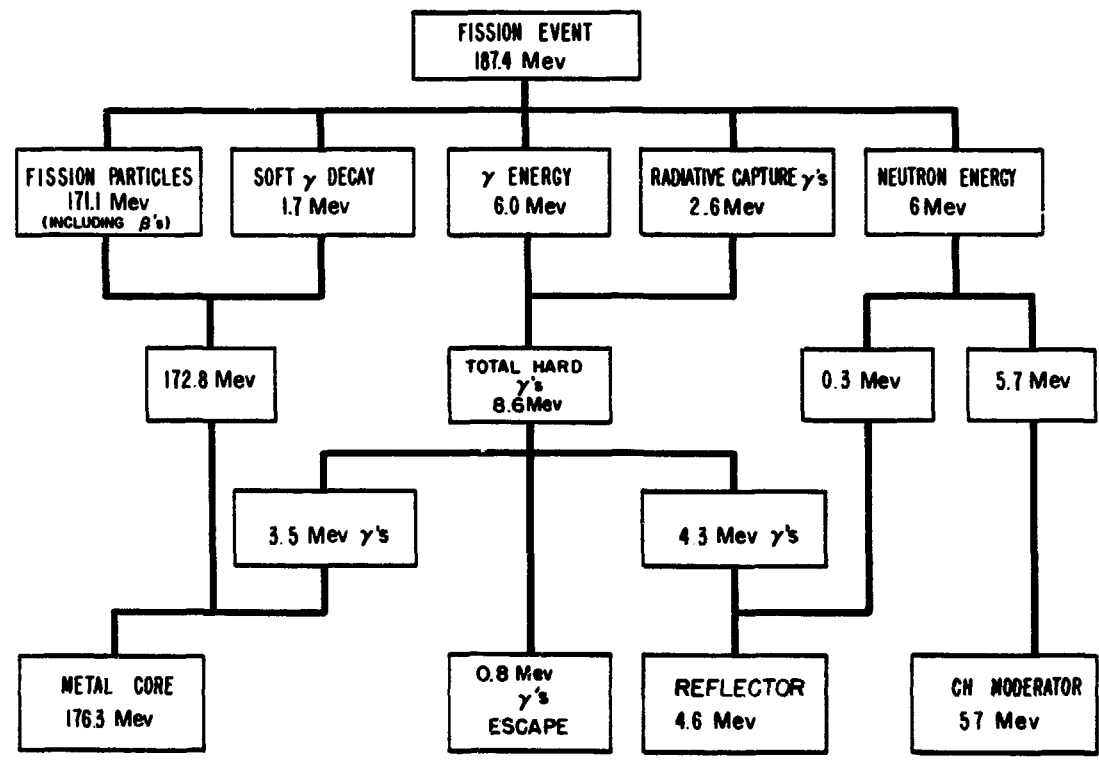


Fig. 7-1: Assumed Distribution of Energy in Dumbo

222

~~SECRET~~

~~SECRET~~

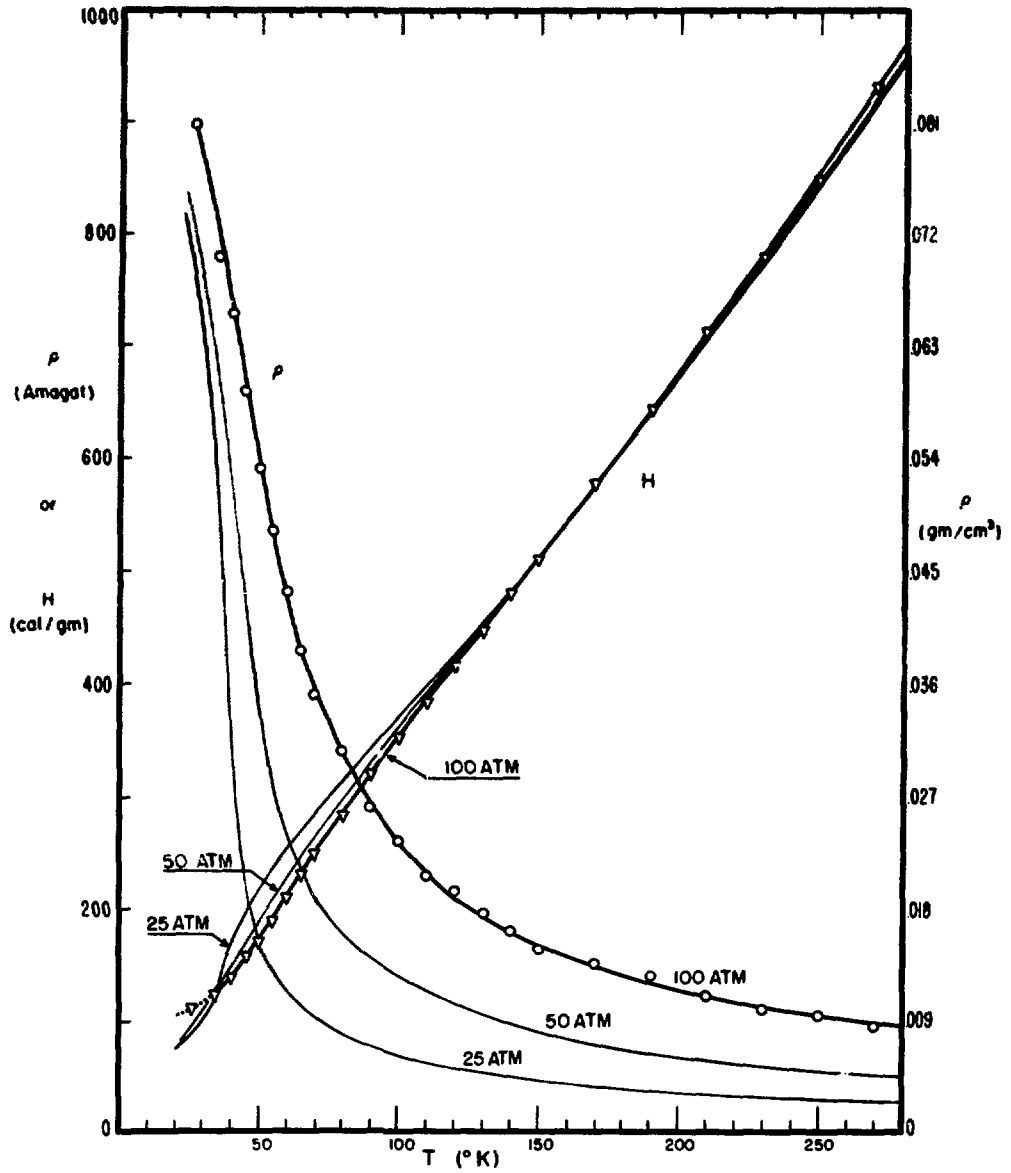


Fig. 7-2: Some Thermodynamic Properties of H<sub>2</sub>

~~SECRET~~

~~SECRET~~

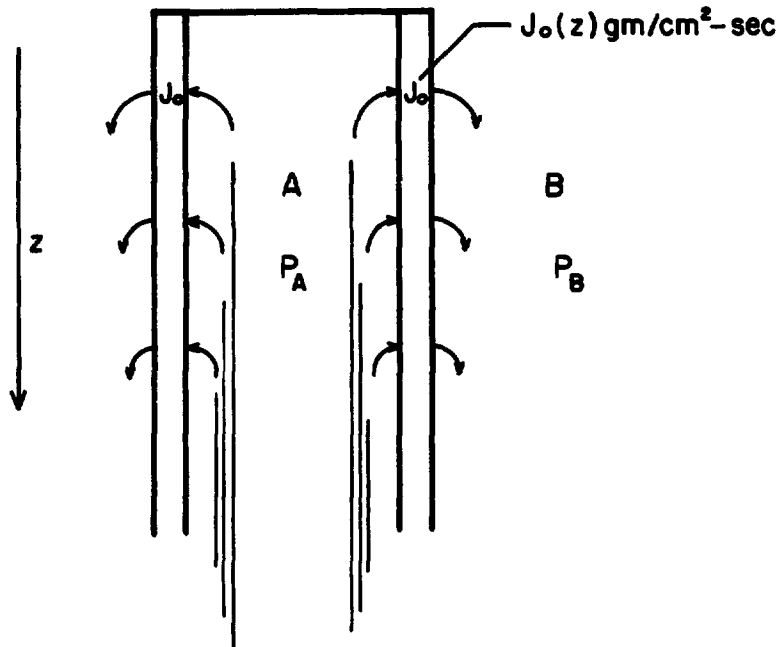


Fig. 7-3

7-4: Turbulent Flow in the Main Ducts

The behavior of the gas in the major passages on either side of the Dumbo heat-exchanger wall is now investigated. The purpose of the present section is to develop expressions for the pressure and the temperature of the cold gas in region A which supplies the moderator, and of the hot-gas region B through which the gas passes from the wall to the nozzle.

The proper equation of motion for the Dumbo flow problem is not obvious. Experience suggests that a plausible equation of motion is the one-dimensional hydrodynamic equation

~~SECRET~~

57

~~SECRET~~

Turbulent Flow in the Main Ducts

Section 7-4

$$\rho v \frac{dv}{dy} = - \frac{dP}{dy} \quad (7-14)$$

This equation is true if shearing forces are negligible. In ordinary duct flow at Reynolds numbers comparable to those of Dumbo designs, the frictional work of the shearing forces is slight compared to the total energy transport rate of the stream. This supports the correctness of Eq. 7-14. However, considerations of momentum conservation indicate a different equation, as follows: If fluid flows through a duct of area  $A$  and circumference  $C$  with velocity  $v$  and if the fluid is supplied from the walls with velocity  $u$ , then a section of fluid of length  $\delta y$ , moving with the stream, is governed by the force equation

$$\frac{D}{Dt} mv = F \quad (7-15)$$

or

$$v \frac{d}{dy} \rho A \delta y v = - A \frac{dP}{dy} \delta y \quad (7-16)$$

Continuity demands

$$\frac{d}{dy} \rho v - \frac{C}{A} \rho u = 0 \quad (7-17)$$

and

$$v \frac{d}{dy} (\rho A \delta y) = \rho u C \delta y \quad (7-18)$$

~~SECRET~~

Combining Eqs. 7-16, 7-17, and 7-18 gives the equation of motion

$$\frac{d}{dy} \rho v^2 = - \frac{dP}{dy} \quad (7-19)$$

Integration of Eq. 7-19 gives

$$\rho v^2 + P = \text{const.} \quad (7-20)$$

If Eq. 7-14 is integrated with constant  $\rho$  Bernoulli's law results, which is given by

$$\frac{1}{2} \rho v^2 + P = \text{const.} \quad (7-21)$$

This equation is in contrast to Eq. 7-20. This suggests that the equation of motion required for this problem is of a general character, including Eqs. 7-14 and 7-19 as particular cases.

The one-dimensional equation of motion is developed from the full three-dimensional theory. As developed in Sec. 2-1, the three-dimensional continuity equation is

$$\partial_\mu \rho v_\mu = 0 \quad (7-22)$$

and the equation of motion is

$$\rho v_\mu \partial_\mu v_\nu = - \partial_\mu P_{\mu\nu} \quad (7-23)$$

where

$$P_{\mu\nu} = P \delta_{\mu\nu} - \eta (\partial_\mu v_\nu + \partial_\nu v_\mu) \quad (7-24)$$

~~SECRET~~

is the stress tensor. The presence of turbulence, as in the momentum transport theory, is regarded as modifying the effective viscosity  $\eta$ . The divergence theorem is used on Eq. 7-22 to give

$$\int_{\sigma} d\sigma_{\mu} \rho v_{\mu} = 0 \quad (7-25)$$

where  $\sigma$  is a closed mathematical surface within the fluid. Combining Eqs. 7-22 and 7-23 yields

$$\partial_{\mu} \{ \rho v_{\mu} v_{\nu} + P_{\mu\nu} \} = 0 \quad (7-26)$$

so that the divergence theorem gives the relation

$$\int_{\sigma} d\sigma_{\mu} \{ \rho v_{\mu} v_{\nu} + P_{\mu\nu} \} = 0 \quad (7-27)$$

This equation states that the net momentum flux across a surface balances the net force from surface stresses.

It is assumed that  $\sigma$  bounds a very short section of the duct, consisting of two flat ends normal to the axis and the intervening duct wall. It is further assumed that the flow velocity is effectively constant over the duct cross section and vanishes suddenly at the wall. Equation 7-25 reduces to Eq. 7-17. If the slight compressional friction term in  $P_{yy}$  is neglected, Eq. 7-27 similarly reduces to

$$\frac{d}{dy} \rho v^2 = - \frac{dP}{dy} + \frac{C}{A} P_{yn} \quad (7-28)$$

~~SECRET~~

~~SECRET~~

Chapter 7                      Hydrodynamic Design Considerations

---

where  $P_{yn}$  is the shearing stress on the fluid in the y direction at the channel wall. This is the equation of motion, with  $P_{yn}$  yet to be evaluated.

To determine  $P_{yn}$ , it is necessary to consider in detail the thin region in which the axial velocity of the stream increases from zero to the full flow velocity.  $x$  is a coordinate measuring from the wall into the stream, ranging to the value  $x_1$ , at which place  $v$  assumes its final value  $v_1$ . Although  $x_1$  and  $v_1$  change along the axis of the duct these variations are slow compared to the variations across the boundary layer. Such slowly changing quantities are regarded as constants for purposes of locally evaluating  $P_{yn}$ . Because the boundary layer does not retain an appreciable portion of the fluid entering it, the condition that

$$\rho u = \text{const.} \tag{7-29}$$

is assumed throughout the boundary layer. Equation 7-22 becomes

$$\frac{\partial \rho u}{\partial x} + \frac{\partial \rho v}{\partial y} = 0 \tag{7-30}$$

-giving

$$v = v(x) \tag{7-31}$$

Because the effective viscosity due to turbulence is determined by the flows, it follows that

$$\eta = \eta(x) \tag{7-32}$$

~~SECRET~~



~~SECRET~~

The x component of Eq. 7-23 is

$$\rho \left( u \frac{\partial u}{\partial x} + v \frac{\partial u}{\partial y} \right) = - \frac{\partial}{\partial x} \left\{ P - \eta \left( 2 \frac{\partial u}{\partial x} \right) \right\} - \frac{\partial}{\partial y} \left\{ -\eta \left( \frac{\partial u}{\partial y} + \frac{\partial v}{\partial x} \right) \right\} \quad (7-33)$$

every term of which now vanishes except  $\partial P / \partial x$ . Hence,

$$\frac{\partial P}{\partial x} = 0$$

or

$$P = P(y) \quad (7-34)$$

Thus there can be no pressure gradient across the boundary layer. The y component of Eq. 7-23 is

$$\rho \left( u \frac{\partial v}{\partial x} + v \frac{\partial v}{\partial y} \right) = - \frac{\partial}{\partial x} \left\{ -\eta \left( \frac{\partial v}{\partial x} + \frac{\partial u}{\partial y} \right) \right\} - \frac{\partial}{\partial y} \left\{ P - \eta \left( 2 \frac{\partial v}{\partial y} \right) \right\} \quad (7-35)$$

which reduces to

$$\rho u \frac{\partial v}{\partial x} = \frac{\partial}{\partial x} \left( \eta \frac{\partial v}{\partial x} \right) - \frac{\partial P}{\partial y} \quad (7-36)$$

The terms not involving P are functions of x only, so the same must be true of  $\partial P / \partial y$ . Together with Eq. 7-34 this gives

$$P(y) = P_0 + P'y \quad (7-37)$$

where  $P_0$  and  $P'$  are constants. Equation 7-36 is integrated once, to give

~~SECRET~~

~~SECRET~~

Chapter 7                      Hydrodynamic Design Considerations

$$\left(\eta \frac{\partial v}{\partial x}\right) - \left(\eta \frac{\partial v}{\partial x}\right)_0 = P'x + \rho uv \quad (7-38)$$

This can be regarded as a special case of Eq. 7-27, and shows that the shearing stress must increase sufficiently to balance the effect of pressure  $P'x$  and the momentum flux  $\rho uv$ . The transformation

$$\xi = \int_0^x \frac{1}{\eta} dx$$
$$x(\xi) = \int_0^\xi \eta d\xi \quad (7-39)$$

is made. Equation 7-38 is integrated, to give

$$v = \frac{1}{\rho u} (e^{\rho u \xi} - 1) \left(\eta \frac{\partial v}{\partial x}\right)_0 + P' \int_0^\xi e^{\rho u(\xi - \xi')} x(\xi') d\xi' \quad (7-40)$$

Equation 7-40 is solved algebraically for the wall stress at  $x = x_1$ .

$$-P_{yn} \equiv \left(\eta \frac{\partial v}{\partial x}\right)_0 = \frac{1}{e^{\rho u \xi_1} - 1} \rho u v_1 - P' \rho u \int_0^{\xi_1} \frac{e^{-\rho u \xi}}{1 - e^{\rho u \xi}} x(\xi) d\xi \quad (7-41)$$

This expression is substituted into Eq. 7-28. In the Dumbo ducts the boundary layer Reynolds number, represented by  $|\rho u \xi_1|$ , is about 10 or 20.

In this case Eq. 7-41 is reduced to two asymptotic forms.

~~SECRET~~

~~SECRET~~

Turbulent Flow in the Main Duct

Section 7-4

Case I: For  $\rho u \xi_1 \gg 1$ ,

$$-P_{yn} = -P' \rho u \int_0^{\xi_1} e^{-\rho u \xi} x(\xi) d\xi = -\eta_0 \frac{P'}{\rho u} \quad (7-42)$$

Case II: For  $\rho u \xi_1 \ll -1$ ,

$$-P_{yn} = -\rho u v_1 + P' \rho u \int_0^{\xi_1} e^{\rho u (\xi_1 - \xi)} x(\xi) d\xi = -\rho u v_1 + P' x_1 \quad (7-43)$$

In the Dumbo ducts, the boundary pressure term  $P'$  is not significant compared to the momentum flux term. This leads to the following expressions:

Case I: For  $u > 0$ ,

$$P_{yn} = 0 \quad (7-44)$$

Case II: For  $u < 0$ ,

$$P_{yn} = \rho u v \quad (7-45)$$

where the subscript 1 has been dropped in conformity with earlier notation.

For channel Reynolds numbers of the order of  $10^5$ , as in typical Dumbo designs, the boundary layer is laminar and  $x_1$  is given approximately by<sup>2</sup>

$$\rho v_1 x_1 / \eta = R_c$$

where the critical Reynolds number  $R_c$  is circa 2100. In this case, the integral of Eq. 7-41 may be performed and compared with the asymptotic equations 7-44 and 7-45. The comparison verifies the asymptotic results.

~~SECRET~~

~~SECRET~~

Chapter 7                      Hydrodynamic Design Considerations

---

For the hot gas duct  $u > 0$ , and Eq. 7-28 together with Eq. 7-44 gives Eq. 7-19 as the equation of motion. For the cold duct  $u < 0$ , and Eqs. 7-28 and 7-45 give

$$\frac{d}{dy} \rho v^2 = - \frac{dP}{dy} + \frac{C}{A} \rho uv \tag{7-46}$$

Multiplying Eq. 7-17 by  $v$  and subtracting from Eq. 7-46 gives Eq. 7-14 as the equation of motion.

To sum up the physical content of these equations, when gas enters the stream it picks up momentum from the stream. The momentum transfer subjects the stream to internal stresses, but the only influence affecting the overall momentum is the pressure gradient. Hence, Eq. 7-19 is the equation of motion. On the other hand, when gas leaves the stream it carries momentum with it to the wall where the momentum is transferred out of the system by shearing stress. Although momentum is not conserved, the shearing stress is confined to the boundary, and the stress-free main stream is governed by Eq. 7-14.

The peculiar two-valued relationship between pressure and flow is more general than the assumptions that have gone into the development above. In App. C the problem of incompressible laminar flow through a channel is solved exactly, and it is shown that in the limit of large Reynolds numbers  $\rho \bar{v}^2 + P$  is a constant for material entering, and  $\frac{1}{2} \rho \bar{v}^2 + P$  is a constant for material leaving the stream.

~~SECRET~~

~~SECRET~~

Expected Hydrodynamics

Section 7-5

7-5: The Expected Hydrodynamics in Dumbo

The results of the preceding section show the one-dimensional equation of motion for the cold gas region to be

$$\rho v \frac{dv}{dz} = - \frac{dp}{dz} \quad (7-14)$$

whereas that for the hot gas region is

$$\frac{d}{dz} \rho v^2 = - \frac{dp}{dz} \quad (7-19)$$

The assumptions are that:

(1) The flow profile of each region is substantially flat with the vertical velocity component  $v$  a function of  $z$  only.

(2) Turbulent drag may be neglected at this stage of analysis and later added as a perturbation of these relations.

Are these assumptions likely to be true of a physical model?

The second of these assumptions is quickly justified insofar as the magnitude of the pressure drop due to drag is much less than that due to dynamic terms in typical problems.

The first assumption is supported in the case of cold gas flow, in which gas leaves the duct and enters the wall, by the following arguments: In turbulent channel flow the nearly flat profile is characteristic. Due to the removal of the boundary layer by the walls of this region the profile flatness is emphasized. Further, the deceleration experienced by the stream produces more than normal instability and turbulence. Finally,

~~SECRET~~

Chapter 7                      Hydrodynamic Design Considerations

---

the stream enters the duct from the preheater plates with uniformly distributed, well-established turbulence.

For the hot gas region these arguments are largely reversed. Gas enters the region from the viscous channels of the Dumbo wall. The acceleration experienced by the stream enhances the stability. The interaction of the stream with the wall is cushioned by the steady out-flow of gas along the walls. With a length of only 10 hydraulic diameters, it is not clear that the stream would exhibit well-established turbulence even though its maximum Reynolds number is  $10^5$ . If laminar flow existed in this hot region, the flat velocity-profile model would be inaccurate. As is shown in App. C, a cosine velocity profile is obtained for two-dimensional laminar flow at very low viscosity.

Without a detailed theoretical understanding of the problem of the onset of turbulence or without experimental testing of this peculiar hydrodynamic problem, one must contemplate for this hot gas one of three conditions:

- (1) Well-established turbulent flow with a flat velocity profile.
- (2) Laminar flow with a cosine-like velocity profile.
- (3) A flow which is laminar in the low velocity regions and which as it accelerates becomes turbulent.

In Secs. 7-6, 7-7, and 7-8 the existence of condition 1 is assumed. In Sec. 7-9 it is shown that a comparatively minor design modification adapts the designs to the existence of condition 2. Deviations resulting

~~SECRET~~

Energy Relations

Section 7-6

from the existence of condition 3 may be estimated and are presented in Sec. 7-9.

7-6: Energy Relations for Compressible Flow in Dumbo

To determine the behavior of a compressible gas, it is necessary to have a relation between mechanical and total energy. The energy equation is developed in this section.

The conservation of energy is stated by the equation

$$\partial_{\mu} \left\{ v_{\mu} \left( \frac{1}{2} \rho v_{\nu} v_{\nu} + \rho c_p T \right) + v_{\nu} P_{\mu\nu} \right\} = 0 \quad (7-47)$$

The divergence theorem gives

$$\int_{\sigma} d\sigma_{\mu} \left\{ v_{\mu} \left( \frac{1}{2} \rho v_{\nu} v_{\nu} + \rho c_p T \right) + v_{\nu} P_{\mu\nu} \right\} = 0 \quad (7-48)$$

Specializing to a slice of the duct yields

$$\frac{d}{dy} v \left( \frac{1}{2} \rho v^2 + \rho c_v T + P \right) + \frac{C}{A} u' (\rho' c_v T' + P) = 0 \quad (7-49)$$

The quantities evaluated at the duct wall are explicitly indicated by a prime. The side-flow kinetic energy  $\frac{1}{2} \rho' u'^2$  is negligible and is omitted for the sake of notational simplicity. The "stagnation enthalpy"  $\phi$  is defined as

$$\phi = \frac{1}{2} v^2 + c_v T + \frac{P}{\rho} = \frac{1}{2} v^2 + c_p T \quad (7-50)$$

Equation 7-49, written in terms of  $\phi$ , is

~~SECRET~~

~~SECRET~~

Chapter 7                      Hydrodynamic Design Considerations

---

$$\frac{d}{dy} \rho v \phi + \frac{C}{A} \rho' u' \phi' = 0 \quad (7-51)$$

The continuity equation 7-17, which is equally valid for  $\rho u$  or  $\rho' u'$ , is applied, giving

$$\frac{d}{dy} \rho v \phi = \phi' \frac{d}{dy} \rho v \quad (7-52)$$

This is the equation of energy balance. The value of  $\phi'$  depends on whether gas is leaving or entering the wall.

For gas leaving,  $\phi'$  is specified in terms of the wall temperature, i.e., for  $u > 0$

$$\phi' = c_p T' \quad (7-53)$$

$T'$  is assumed to be constant, and Eq. 7-52 is integrated to give

$$\rho v (\phi - \phi') = \text{const.} = A \quad (7-54)$$

However, if  $v(y)$  vanishes at any point while  $\rho$  and  $\phi$  remain finite, it is necessary that  $A = 0$ . Therefore, the energy condition governing the hot gas stream is

$$\phi = \phi' = c_p T' = \text{const.} \quad (7-55)$$

For gas entering the wall (cold gas), the value of  $\phi'$  is determined by the state of the stream. It is evaluated by applying Eq. 7-48 to a region bounded by the duct wall and by the inner surface of the boundary

~~SECRET~~



~~SECRET~~

Solution of the Flow Equations

Section 7-7

layer at distance  $x_1$  into the stream. From Eqs. 7-38 and 7-45,  $P_{xy}$  is small at  $x_1$ , and Eq. 7-48 becomes

$$\rho'u'\phi' = \rho u \phi. \quad (7-56)$$

From Eq. 7-29,  $\rho'u' = \rho u$ , so that for  $u < 0$

$$\phi' = \phi \quad (7-57)$$

Thus in both cases flow across the boundary layer is isenthalpic.

7-7: Solution of the Flow Equations

For either type of channel it is necessary to satisfy four simultaneous relations in order to predict the flow characteristics for a compressible fluid, as follows:

- (a) The appropriate one-dimensional equation of motion.
- (b) The appropriate one-dimensional equation of energy balance.
- (c) The equation of state of the gas.
- (d) The one-dimensional equation of continuity.

There are two types of main channels as shown in Fig. 7-4. Region A is the cold gas region in which fluid enters the wall at the boundary. Region B is the hot gas region in which fluid leaves the wall and enters the stream. The equations governing the flow in each of these regions are shown in Table 7-1. The solution of these equations is now developed.

~~SECRET~~

~~SECRET~~

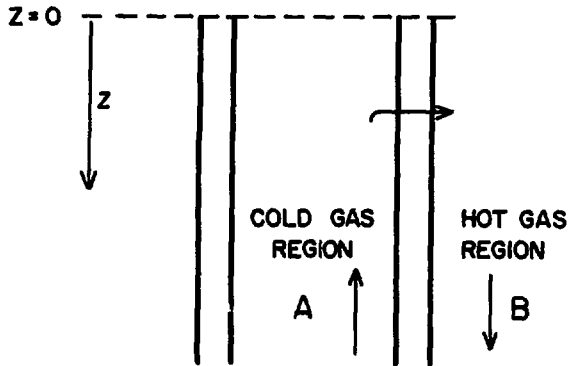


Fig. 7-4

TABLE 7-1 EQUATIONS FOR THE MAIN CHANNELS		
	COLD GAS REGION A	HOT GAS REGION B
(a) EQ. of MOTION	$\rho v \frac{dv}{dz} = - \frac{dp}{dz}$	$\frac{d}{dz} \rho v^2 = - \frac{dp}{dz}$
(b) EQ. of ENERGY BALANCE	$c_p T + \frac{v^2}{2} = c_p T' = \text{const}$	$c_p T + \frac{v^2}{2} = c_p T' = \text{const}$
(c) EQ. of STATE	$p = \rho RT/M$	$p = \rho RT/M$
(d) EQ. of CONTINUITY	$\rho v = - \frac{Q_e}{AL} z$	$\rho v = - \frac{Q_e}{AL} z$

It is convenient to reduce these relations to dimensionless form by the substitutions

~~SECRET~~

~~SECRET~~

Solution of the Flow Equations

Section 7-7

$$R = p/\rho_0$$

$$P = p/p_0$$

$$V = \sqrt{\frac{p_0}{\rho_0}} v$$

$$\theta = T/T'$$

$$\zeta = z/L$$

$$\kappa = \mp \frac{Q_0}{A\sqrt{\rho_0 p_0}}$$

$$\gamma = \frac{c_p}{c_p - R/M}$$

(7-58)

These seven quantities are made dimensionless by use of the initial ( $z = 0$ ) values of  $p$  and  $\rho$ , the constant wall temperature  $T$ , the channel length  $L$ , the total flow handled by the channel  $Q_0$ , the cross sectional area of the channel  $A$ , and the thermodynamic quantities  $c_p$  and  $R$ . Although  $Q_0$  and  $L$  are the same for the two regions, the quantities  $p_0$ ,  $\rho_0$ ,  $T'$ , and  $A$  are not. The resulting dimensionless quantities  $R$  and  $P$  must assume initial values of  $\underline{1}$  at  $\zeta = 0$  where the range of  $\zeta$  is given by  $0 \leq \zeta \leq 1$ . There is a difference in the value of the dimensionless parameter  $\kappa$  for the two regions, and also in its sign. In the cold gas region A,  $\kappa$  assumes negative values, in region B it is positive. The dimensionless formulation of the equations of Table 7-1 is shown in Table 7-2. The difference between the dimensionless formulation of the two problems lies in the equations of motion only. The exact solution of the two problems is easily obtained and is presented in Table 7-3.

~~SECRET~~

~~SECRET~~

**TABLE 7-2  
DIMENSIONLESS FLOW EQUATIONS**

	COLD GAS REGION A	HOT GAS REGION B
(a) EQ. of MOTION	$RV \frac{dV}{d\xi} = - \frac{dP}{d\xi}$	$\frac{d}{d\xi} (RV^2 + P) = 0$
(b) EQ. of ENERGY BALANCE	$\frac{1}{2} V^2 + \frac{\gamma}{\gamma-1} (\theta-1) = 0$	$\frac{1}{2} V^2 + \frac{\gamma}{\gamma-1} (\theta-1) = 0$
(c) EQ. of STATE	$P = R\theta$	$P = R\theta$
(d) EQ. of CONTINUITY	$RV = \kappa \xi$	$RV = \kappa \xi$

It is seen from Table 7-3 that although the equations for region B may be explicitly solved for  $V(\xi)$ ,  $P(\xi)$ , and  $\theta(\xi)$ , this is not possible for region A. Instead, the solutions in region A are presented as  $\xi(V)$ ,  $P(V)$ ,  $R(V)$ , and  $\theta(V)$ , so that the functions  $V(\xi)$ ,  $P(\xi)$ , etc., are only implicitly expressed.

The function  $V(\xi)$  for the cold region is double-valued in  $V$  for  $0 \leq \xi < \xi^*$  and possesses no real solutions for  $V$  when  $\xi > \xi^*$ , where  $\xi^*$  is the maximum value of  $\xi$ . A feature of interest is that at  $\xi^*$  the velocity is Mach 1. One branch of the double-valued curve predicts supersonic flow while the other predicts subsonic flow. However, only the subsonic

~~SECRET~~

~~SECRET~~

Solution of the Flow Equations

Section 7-7

TABLE 7-3  
SOLUTIONS OF THE FLOW EQUATIONS

COLD GAS REGION A

$$\kappa \zeta = V \left( 1 - \frac{\gamma-1}{2\gamma} V^2 \right)^{\frac{1}{\gamma-1}}$$

$$P = \left( 1 - \frac{\gamma-1}{2\gamma} V^2 \right)^{\frac{\gamma}{\gamma-1}}$$

$$R = \left( 1 - \frac{\gamma-1}{2\gamma} V^2 \right)^{\frac{1}{\gamma-1}}$$

$$\theta = 1 - \frac{\gamma-1}{2\gamma} V^2$$

HOT GAS REGION B

$$V = \frac{\gamma}{\gamma+1} \frac{1}{\kappa \zeta} \left\{ 1 - \sqrt{1 - \frac{2(\gamma+1)}{\gamma} \kappa^2 \zeta^2} \right\}$$

$$P = \frac{1}{1+\gamma} \left\{ 1 + \gamma \sqrt{1 - 2 \frac{\gamma+1}{\gamma} \kappa^2 \zeta^2} \right\}$$

$$R = \frac{1}{2} \left\{ 1 + \sqrt{1 - \frac{2(\gamma+1)}{\gamma} \kappa^2 \zeta^2} \right\}$$

$$\theta = 1 + \frac{\gamma-1}{\gamma+1} \left\{ 1 - \frac{\gamma}{\gamma+1} \frac{1}{\kappa^2 \zeta^2} \left( 1 - \sqrt{1 - 2 \frac{\gamma+1}{\gamma} \kappa^2 \zeta^2} \right) \right\}$$

~~SECRET~~

~~SECRET~~

Chapter 7                      Hydrodynamic Design Considerations

branch satisfies the imposed boundary conditions. The function  $V(\zeta)$  for region B possesses real solutions only in the case of subsonic or exactly sonic velocities. At the transition point, Mach 1, the variables assume the values shown in Table 7-4. Specific values are given for  $\gamma = 7/5$  as

TABLE 7-4		
SONIC VALUES OF THE SOLUTIONS		
	COLD GAS REGION A	HOT GAS REGION B
$\kappa \zeta^*$	$-\sqrt{\gamma} \left(\frac{2}{\gamma+1}\right)^{\frac{1}{2}} \frac{\gamma+1}{\gamma-1} \rightarrow -0.685$	$\sqrt{\frac{\gamma}{2(\gamma+1)}} \rightarrow 0.540$
$v^*$	$\sqrt{\frac{2\gamma}{\gamma+1}} \rightarrow 1.080$	$\sqrt{\frac{2\gamma}{\gamma+1}} \rightarrow 1.080$
$P^*$	$\left(\frac{2}{\gamma+1}\right)^{\frac{\gamma}{\gamma-1}} \rightarrow 0.530$	$\frac{1}{\gamma+1} \rightarrow 0.417$
$R^*$	$\left(\frac{2}{\gamma+1}\right)^{\frac{1}{\gamma-1}} \rightarrow 0.634$	$\frac{1}{2} \rightarrow 0.500$
$\theta^*$	$\frac{2}{\gamma+1} \rightarrow 0.833$	$\frac{2}{\gamma+1} \rightarrow 0.833$

in the case of diatomic gases. It is interesting to note that these values become the same for both regions for a hypothetical gas where  $\gamma = 1$ , in which case

~~SECRET~~

~~SECRET~~

Solution of the Flow Equations

Section 7-7

$$\pm \kappa \zeta^* = P^* = R^* = \frac{1}{2}$$

The values of  $V^*$ ,  $P^*$ ,  $R^*$ , and  $\theta^*$  shown in Table 7-4 for the region A are exactly those resulting from conventional one-dimensional nozzle theory. The entire formulation for region A is strongly analogous to the nozzle problem if the variable  $\zeta$  is regarded as the inverse of the nozzle area. The maximum value  $\zeta^*$  corresponds to the nozzle throat area.

Because the flow dynamics of the hot region are different from those generally occurring in compressible flow, it is well to investigate the thermodynamic consistency of the two flow laws. If  $s$  is the entropy of a gram of gas in one of the channels, does the gas move into a region in which it has a greater entropy as is required by thermodynamics? To investigate this question, use is made of the usual expression for the entropy of an ideal gas, which is

$$s = c_p \ln T - \frac{R}{M} \ln P \quad (7-59)$$

A dimensionless entropy  $S$  is defined by

$$S = \frac{\gamma}{\gamma-1} \ln \theta - \ln P \quad (7-60)$$

An immediate check on this question for the cold channel is found from Table 7-3, since for region A

$$P = \theta^{\frac{\gamma}{\gamma-1}} \quad (7-61)$$

~~SECRET~~

~~SECRET~~

Chapter 7                      Hydrodynamic Design Considerations

Substitution into Eq. 7-60 yields the result that  $S = 0$  everywhere, therefore there is no change at all and the cold flow is isentropic.

For the hot region B, it is convenient to introduce a new variable  $\xi$ , defined by

$$\xi = \sqrt{1 - 2 \frac{\gamma+1}{\gamma} \kappa^2 \zeta^2}$$

or

$$\zeta = \frac{1}{\kappa} \sqrt{\frac{\gamma}{2\gamma+1}} \sqrt{1 - \xi^2} \tag{7-62}$$

In terms of  $\xi$  the change of entropy at successive locations of a gram of gas is given by

$$\frac{dS}{d\xi} = \left[ \frac{\gamma}{\gamma-1} \frac{1}{\theta} \frac{d\theta}{d\xi} - \frac{1}{P} \frac{dP}{d\xi} \right] / \frac{d\zeta}{d\xi} \tag{7-63}$$

This quantity,  $dS/d\xi$ , must be positive for thermodynamic consistency.  $P$  and  $\theta$  are given by

$$P(\xi) = \frac{1 + \gamma\xi}{1 + \gamma} \tag{7-64}$$

$$\theta(\xi) = 2 \frac{1 + \gamma\xi}{(1 + \gamma)(1 + \xi)} \tag{7-65}$$

Substitution into Eq. 7-60 yields the result that

$$\frac{dS}{d\xi} = \kappa \sqrt{2\gamma(\gamma+1)} \frac{1}{1 + \gamma\xi} \sqrt{\frac{1 - \xi}{1 + \xi}} \tag{7-66}$$

~~SECRET~~



~~SECRET~~

The Balancing of Pressures

Section 7-8

where  $\kappa > 0$ ,  $\gamma > 1$ , and  $0 < \xi < 1$ . Thus  $\frac{dS}{d\xi} > 0$  and the flow law is thermodynamically consistent.

7-8: The Balancing of Pressures

The interaction of the pressures of regions A and B affect the uniformity of the flow density  $J_0(z)$  through the wall. This effect is considered in this section.

The developments of Sec. 7-7 are based upon three assumptions:

(1) That the flow in either channel A or B is turbulent, obeying the equations of motion developed in Sec. 7-4.

(2) That, as assumed in Eqs. 7-44 and 7-45, the influence of the viscosity of the gas outside the boundary layer is negligible.

(3) That the flow density  $J_0$  is uniform and constant.

The influence of assumptions 1 and 2 is considered in Sec. 7-9.

Assumption 3 is of the nature of a perturbation treatment.  $J_0$  is assumed to be constant and the pressure distributions  $p_A(z)$  and  $p_B(z)$  are developed. The parameters  $\kappa_A$  and  $\kappa_B$  of these distributions are then adjusted to give a high degree of uniformity to  $J_0$  in accordance with the assumed flow law through the wall governing the relation between  $J_0(z)$ ,  $p_A(z)$ , and  $p_B(z)$ . It is shown that this uniformity of  $J_0$  is indeed excellent. If this were not the case, the perturbations in  $J_0(z)$  about its average value could be inserted into the original equations to arrive at the corresponding perturbations in the functions  $p_A(z)$  and  $p_B(z)$  and the process continued.

~~SECRET~~

~~SECRET~~

Chapter 7 Hydrodynamic Design Considerations

It is convenient to write the functions  $P(\zeta)$ , given in Table 7-3, as power series in  $\zeta$ . For the cold gas region A the function is

$$P_A(\zeta) = 1 - \frac{1}{2} \kappa_A^2 \zeta^2 - \frac{3}{8\gamma} \kappa_A^4 \zeta^4 - \frac{5(4+\gamma)}{48\gamma^2} \kappa_A^6 \zeta^6 - \dots \quad (7-67)$$

while for the hot gas region B it is

$$P_B(\zeta) = 1 - \kappa_B^2 \zeta^2 - \frac{1}{2} \frac{\gamma+1}{\gamma} \kappa_B^4 \zeta^4 - \frac{1}{2} \left( \frac{\gamma+1}{\gamma} \right)^2 \kappa_B^6 \zeta^6 - \dots \quad (7-68)$$

The pressure drop from region A to region B at a height  $z$  is the sum of the pressure change through the moderator, where pressure and flow are related by a law of the form

$$\Delta(p^2) \propto J_0^2$$

and the metal wall pressure drop, which proves to be insensitive to small changes in  $J_0$ . The combination yields a flow-pressure relation of the form

$$p_A^2 - p_B^2 = a J_0^2 + b \quad (7-69)$$

As a numerical example the design data for Model A Dumbo are chosen. These data, taken from Chap. 9, are given in Table 7-5. By the use of the data given in Table 7-5, the expression for  $P_B(\zeta)$  from Eq. 7-68\*

---

\*In Secs. 7-7, 7-8, and 7-9 the symbol "p" represents the dimensional pressure and "P" represents the dimensionless pressure defined in Eq. 7-58.

~~SECRET~~

~~SECRET~~

TABLE 7-5 BASIC DATA FOR NUMERICAL EXAMPLE	
$Q_o = 4 \times 10^4 \text{ gm/sec}$	$\rho_B^o = 2.845 \times 10^{-4} \text{ gm/cm}^3$
$\langle J_o \rangle_{\text{avg.}} = 1.22 \text{ gm/cm}^2\text{-sec}$	$\kappa_B^o = 0.1475$
$p_B^o = 29.2 \text{ bar}$	$p_A^o = 31.4 \text{ bar}$

FLOW LAW FOR COMPOSITE WALL

$$J_o = \frac{1}{77.76} (p_A^2 - p_B^2 - 17.61)$$

becomes

$$p_B = 29.20 \left[ 1 - 0.14750 \zeta^2 - 0.01864 \zeta^4 - 0.00472 \zeta^6 \right] \quad (7-70)$$

Two values are used for  $\kappa_A$ , each yielding its own expression for  $p_A(\zeta)$  from Eq. 7-67:

Case I:

$$\begin{aligned} \kappa_A^2 &= 0.25650 \\ p_A(\zeta) &= 31.40 \left[ 1 - 0.12825 \zeta^2 - 0.01762 \zeta^4 - 0.00484 \zeta^6 \right] \end{aligned}$$

Case II:

$$\begin{aligned} \kappa_A^2 &= 0.24936 \\ p_A(\zeta) &= 31.40 \left[ 1 - 0.12468 \zeta^2 - 0.01666 \zeta^4 - 0.00444 \zeta^6 \right] \end{aligned}$$

~~SECRET~~

~~SECRET~~

Chapter 7                      Hydrodynamic Design Considerations

---

The value of  $\kappa_A^2$  selected for approximate design purposes in Chap. 9, given by  $2\kappa_B^2$ , is 0.295. The resulting pressure distributions and variations in  $J_0$  are shown in Fig. 7-5.

The Case II result is an example of the degree of uniformity to be expected in  $J_0$  when the flows are well balanced. The extremes of  $J_0$  differ by 0.66% only with even better balancing attainable by further adjusting  $\kappa_A$ . The comparison of the results of Case I and Case II indicate the degree of sensitivity of flow uniformity to variations of  $\kappa_A$  in the vicinity of the balanced condition.

The phrase "variation of  $\kappa_A$ " is meant to imply two types of adjustments. As defined previously

$$\kappa_A = - \frac{Q_0}{A_A \sqrt{P_{0A} P_{0A}}} \propto \frac{\sqrt{T_{0A}}}{A_A} \quad (7-71)$$

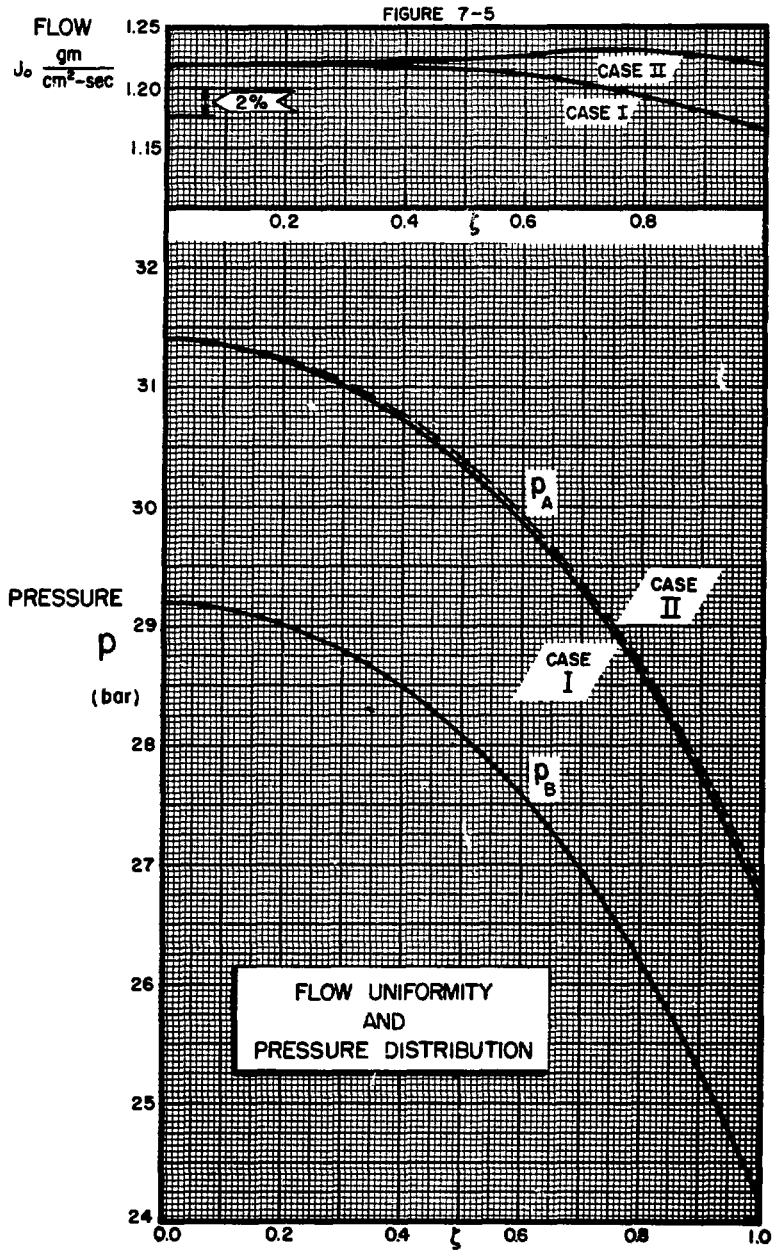
so that its value is affected by both the temperature and the area of the cold region A. The area of the cold region is most easily adjusted by filling up unwanted space with structural material as dictated by detailed calculations, such as those of this chapter or by any available experimental data. Adjustment of  $\kappa_A$  by the temperature  $T_A$  is made by properly varying the degree of the preheating of the gas before it enters the cold region A. The specific motor designs given in Chap. 9 allow for flow nonuniformities appropriate to a device in which there is no preheater adjustment after assembly. However, very precise flow uniformity might be achieved by neutronic controls in the preheaters, actuated by a

~~SECRET~~

~~SECRET~~

The Balancing of Pressures

Section 7-8



~~SECRET~~

~~SECRET~~

Chapter 7                      Hydrodynamic Design Considerations

differential temperature input between two points  $z_1$  and  $z_2$  of region B.

The differences between the  $\kappa_A$  of Cases I and II is 1.4%. This results in shifting the extremes of  $J_0$  from a Case II difference of 0.66% to a Case I difference of 4.6%. The rms deviation is much less, being +1.4% for Case I.

7-9: Effects of Other Flow Laws

The relations used in Sec. 7-8 for  $P(\zeta)$  as a power series in  $\zeta$  may be interpreted physically as follows. The first two terms (including  $\zeta^2$ ) are due to dynamic effects not dependent upon the compressibility of the fluid. It may be shown that these terms above express the hydrodynamics of an incompressible fluid. The remaining terms ( $\zeta^4$  and higher) are corrections for compressibility. By this type of approach the approximate relation  $\kappa_A^2 = 2\kappa_B^2$  is developed, which implies that to order  $\zeta^2$

$$P_A(\zeta) - P_B(\zeta) = \text{const.} \tag{7-72}$$

If the flow laws are modified, it is plausible that the new functions  $P(\zeta)$  may be written as a sum of terms of the form

$$P(\zeta) = \left[ \text{new flow law of incompressible fluid} \right] + \left[ \text{compressibility correction terms from Sec. 7-8} \right]$$

The purpose of this section is to show that although there may be some doubt as to the proper flow law of the regions A and B, nevertheless a

~~SECRET~~

high degree of uniformity can be obtained in  $J_0$  without major readjustments in  $\kappa_A$ .

The first modification of the flow laws of regions A and B results from the distributed eddies of the assumed turbulent flow. Locally (i.e., in the vicinity of some particular  $z$ ) it is tempting to assert that the stream, moving with some average velocity  $v$  with respect to the walls, exercises the same drag as in ordinary channel flow. However, as discussed in Sec. 7-5, the degree of turbulence is expected to be strongly influenced by the flows at the porous walls. For these reasons the following treatment gives only the magnitude of such drag terms.

From Sec. 7-2, the pressure gradients due to drag are

$$\frac{dp}{dz} = -\gamma \frac{2Pv}{D} \tag{7-73}$$

where the friction factor  $\gamma$  is an insensitive function of the Reynolds number and is taken as constant, and  $D$  is the hydraulic diameter of the channel. In the notation of Sec. 7-8, Eq. 7-73 introduces an added term of the form

$$P_{\text{Drag}} = \pm \frac{2}{3} \gamma \kappa^2 \left(\frac{L}{D}\right) \zeta^3 \tag{7-74}$$

For the preceding numerical example this adds to Eq. 7-70 a term

$$-0.0029 \zeta^3$$

contributing at most 0.08 bar to the pressure  $p_B$ . A similar term

~~SECRET~~

Chapter 7                      Hydrodynamic Design Considerations

characterizes the cold region A. Terms of such magnitude are easily balanced out.

A more serious effect than such drag corrections arises from the state of ignorance as to the exact hydrodynamics of the hot region B. As discussed in Sec. 7-5, there are two cases in which the treatment given in Sec. 7-8 are inapplicable. The flow law assumed in Sec. 7-7, when specialized to an incompressible fluid, is given by

$$p_B + \rho \bar{v}^2 = p_B^o \tag{7-75}$$

If the hot region B is laminar and not turbulent, the distributed velocity profile causes this flow law, for the special geometry described in App. C, to be

$$p_B + \frac{\pi^2}{8} \rho \bar{v}^2 = p_B + 1.23 \rho \bar{v}^2 = p_B^o \tag{7-76}$$

So that Eq. 7-68 becomes

$$P_B(\zeta) = 1 - \frac{\pi^2}{8} \kappa_B^2 \zeta^2 - \frac{1}{2} \frac{\gamma+1}{\gamma} \kappa_B^4 \zeta^4 - \frac{1}{2} \left( \frac{\gamma+1}{\gamma} \right)^2 \kappa_B^6 \zeta^6 \tag{7-77}$$

If this relation applies, the approximation

$$(\kappa_A^2 = 2 \kappa_B^2)$$

is modified by matching quadratic terms in Eqs. 7-67 and 7-77, to become

$$\kappa_A^2 \cong \frac{\pi^2}{4} \kappa_B^2 = 2.47 \kappa_B^2 \tag{7-78}$$

~~SECRET~~



~~SECRET~~

This value of  $\kappa_A$  requires an 11% smaller area in the cold region A. The degree of uniformity in  $J_0$ , upon rebalancing, is about as computed previously.

A final possibility regarding the hot region B flow law is that a transition from laminar to turbulent flow occurs as the gas progresses through this region. The effect of such a transition upon the uniformity in  $J_0(z)$ , after balancing, is assumed to give an incompressible flow law of the form

$$P_B + (1.23 - 0.23\zeta) \rho \bar{v}^2 = P_B^0 \quad (7-79)$$

This relation reduces to Eq. 7-76 as  $\zeta \rightarrow 0$  but to Eq. 7-75 as  $\zeta \rightarrow 1$ .

From Eq. 7-79

$$P_B(\zeta) = 1 - \left[ \frac{\pi^2}{8} - \left( \frac{\pi^2}{8} - 1 \right) \zeta \right] \kappa_B^2 \zeta^2 - \frac{1}{2} \frac{\gamma+1}{\gamma} \kappa_B^4 \zeta^4 - \frac{1}{2} \left( \frac{\gamma+1}{\gamma} \right)^2 \kappa_B^6 \zeta^6 \quad (7-80)$$

Substitution of the data of Table 7-5 gives

$$P_B(\zeta) = 29.20 \left[ 1 - 0.18035 \zeta^2 + 0.03447 \zeta^3 - 0.01864 \zeta^4 - 0.00472 \zeta^6 \right] \quad (7-81)$$

whilst  $P_A(\zeta)$  is still given by Eq. 7-68. A good balance is obtained for  $\kappa_A^2 = 0.24734$ , giving values of  $J_0$  whose extreme variation is 4.0% and whose rms variation is +1.5%.

~~SECRET~~

~~SECRET~~

Chapter 7                      Hydrodynamic Design Considerations

---

Thus despite the lack of knowledge of the exact hydrodynamics governing the flow in the hot region B, it appears that an adequate balance is obtained by a value of  $\kappa_A$ , whose uncertainty is within reasonable limits, which yields a good uniformity in  $J_0$ .

REFERENCES

1. Harold W. Woolley, Russell B. Scott, and F. G. Brickwedde, Thermal Properties of Hydrogen, National Bureau of Standards Research Paper RP1932, Vol. 41, November 1948.
2. O. G. Tietjens, Applied Hydro- and Aeromechanics, Based on lectures of L. Prandtl, J. P. Den Hartog (Trans.), 1st ed., McGraw-Hill Book Co., Inc., New York, 1934.

~~SECRET~~

~~SECRET~~

## CHAPTER 8

### FABRICATION METHODS AND MATERIALS\*

...he schlooped up a schloop of mud from the banks of the great grey-green, greasy Limpopo, and slapped it on his head, where it made a cool schloopy-sloshy mud-cap all trickly behind his ears.

R. Kipling, The Elephant's Child

#### 8-1: Introduction

In this chapter some practical problems associated with Dumbo are considered.

Section 8-2 describes pertinent physical properties of the refractory metals. In Sec. 8-3 several methods for incorporating  $UO_2$  into refractory metals are given. Sections 8-4 and 8-5 consider radiation damage to the metal and the moderator. Sections 8-6 and 8-7 are devoted to metallurgical and engineering problems associated with the fabrication of the metal wall structures. Section 8-8 considers the problems associated with the incorporation of magnesium powder into the polystyrene moderator.

#### 8-2: Metallurgical Considerations

Five refractory metals and their alloys are considered for

---

\*This chapter was prepared in collaboration with D. K. Gestson, J. R. Lilienthal, and F. J. Miller of the Los Alamos Scientific Laboratory.

~~SECRET~~

~~SECRET~~

construction of the Dumbo wall. These metals and some of their pertinent physical properties are listed in Table 8-1. More complete data are given in App. B.

TABLE 8-1			
METAL	MELTING POINT	THERMAL CAPTURE CROSS SECTION	SINGLE CRYSTAL TENSILE STRENGTH AT 2800 ° K
TUNGSTEN	3623 °K	19.2 barns	350 kg/cm <sup>2</sup>
TANTALUM	3273	23.3	
MOLYBDENUM	2923	2.4	21
COLUMBIUM	2723	1.1	
RHENIUM	3440	84.0	

The Dumbo models do not require great tensile strength. The calculated hoop stress on the metal wall for a typical Dumbo model is circa 5 kg/cm<sup>2</sup>. This value is much less than the tensile strength of either molybdenum or tungsten at the operating temperature. The main stresses occur where the material is cold and has the highest tensile strength.

Tungsten and molybdenum form a continuous series of solid solutions, so that one may draw a straight line between the two melting points to obtain a melting point versus composition curve. The workability of the solid solutions is better than that of the pure metals.

R. B. Gibney, Lee Richardson, and J. M. Dickinson of LASL have suggested an alloy of circa 20% rhenium and 80% molybdenum. This alloy is

~~SECRET~~

reputed to have excellent workability and a higher melting point than molybdenum, forming an ideal solid solution. The nuclear properties of this alloy approximate those of pure tungsten. No data on tensile strength are available.

Columbium and tantalum also form a continuous series of solid solutions but data are lacking on their tensile strengths.

It is known that tungsten, molybdenum, and rhenium are chemically inert to both hydrogen and ammonia at temperatures typically found in Dumbo.

8-3: Methods for Addition of Uranium to the Refractory Metals

Five methods for adding uranium to the refractory metals are:

- (a) Making cermets of  $UO_2$  and the metal or alloy by various techniques of powder metallurgy.
- (b) Mixing uranium metal with the metal or alloy by powder metallurgy.
- (c) Forming true alloys with uranium.
- (d) Coating the surfaces of the metal with  $UO_2$ .
- (e) Laminating a layer of  $UO_2$  between foils of refractory metal.

Method (a) requires techniques that are similar to those used in the manufacture of tungsten filaments. In the tungsten lamp industry, as much as 5%  $ThO_2$  has been added to tungsten<sup>1</sup> in order to improve its physical properties by inhibition of crystal growth. Since  $UO_2$  is similar to  $ThO_2$  in its chemical and physical properties, no difficulty

~~SECRET~~

Chapter 8                      Fabrication Methods and Materials

---

should be experienced in replacing  $\text{ThO}_2$  by  $\text{UO}_2$ .

Battelle Memorial Institute<sup>2</sup> has recently made mixtures of  $\text{UO}_2$  and molybdenum containing 25 volume percent of  $\text{UO}_2$  and has rolled the resulting cermet to a 0.01 cm foil.

An advantage of this method is that the melting points of the substances remain unchanged since the materials are mutually insoluble. The presence of  $\text{UO}_2$  in the refractory metal retards crystal growth at high temperatures, thereby maintaining a high tensile strength.

Method (b) has the disadvantage that alloys are formed which are liquids trapped in a solid matrix at the temperatures encountered in Dumbo.

Method (c): Solid solutions are formed in the columbium-uranium system. In the interesting region of composition the melting point is about 2570°K only. Further, in any method involving metallic uranium, the formation of  $\text{UH}_3$  with the propellant gas is a possibility.

Method (d): Electrophoretic techniques have been employed by W. J. McCreary of LASL to deposit thin uniform coatings of  $\text{UO}_2$  on refractory metals. No chemical bonding occurs, but the coatings withstand mild abrasion and considerable distortion.

Method (e) consists of folding longitudinally a  $\text{UO}_2$ -coated refractory metal strip to form a sandwich. This strip is fabricated into a linearized wall (see Sec. 8-7).

Methods (d) and (e) possess certain advantages in common. These are:

~~SECRET~~

- (1) Higher loadings of  $UO_2$  are possible than with cermet.
- (2) Commercial refractory metal foil can be used.
- (3) In special wall structures, such as linearized models, portions may be unloaded or of graded loadings.

8-4: Radiation Damage to the Metal Structure

Typically, the metal core structure of a Dumbo reactor receives an integrated flux of  $8.3 \times 10^{18}$  neutrons/cm<sup>2</sup>. Nucleonics, p. 56, December, 1954, states:

Molybdenum in its commercially pure form is embrittled to such an extent after reactor irradiation to  $1.9 - 5.9 \times 10^{20}$  thermal neutrons/cm<sup>2</sup> that it is unsafe for use in load carrying reactor components at low temperatures, according to tests by KAPL.

No other data are given. However, the neutron irradiation levels for Dumbo are only a few percent of that used in the KAPL tests. Thus there is no indication that such embrittlement would occur in Dumbo.

8-5: Radiation Damage to the Moderator

The moderator in Dumbo is typically irradiated to  $3.8 \times 10^{24}$  ev/gm. Sisman and Bopp<sup>3</sup> have made an extensive study of the physical properties of irradiated plastics. Irradiation levels up to  $6.7 \times 10^{23}$  ev/gm were studied. For styrene polymers little change except darkening was noted. The radiation level for Dumbo is about 5.7 times the maximum levels used by Sisman and Bopp. Since darkening was the only observed change, it is reasonable to hope that the moderator material will withstand  $3.8 \times 10^{24}$  ev/gm.

~~SECRET~~

8-6: Fabrication of Dumbo Rings

The engineering work to date has been directed toward the fabrication of the metal elements of Dumbo tubes. This work is largely that of D. K. Gestson and F. J. Miller. The experience gained in fabricating and assembling a linearized section of Dumbo wall was valuable in designing and building the three dies for the circular wall. The dies are: (1) A die, shown in Fig. 8-1, for blanking the parts to be corrugated. (2) A corrugating die, shown in Fig. 8-2, for partially corrugating the spacers. (3) A corrugating die, shown in Fig. 8-3, for forming the channel rings.

In lieu of 0.0025 cm molybdenum or tungsten foil, the dies were tested using 0.0025 cm brass foil. A preliminary investigation indicated that the depth of corrugations at the impedance section could be held to  $\pm 0.00025$  cm for any given ring. The depth of corrugations across the width of the ring surface can be held to  $\pm 0.0005$  cm for any given ring. No attempt was made to control the forming pressure so that some variation in amplitude from ring to ring was noted. However, this amplitude variation appears easy to reduce. Figure 8-4 shows some of the typical washers blanked and corrugated by the dies. Enough rings were corrugated to assemble a stack approximately 1 cm high.



~~SECRET~~

Fabrication of Rings

Section 8-6

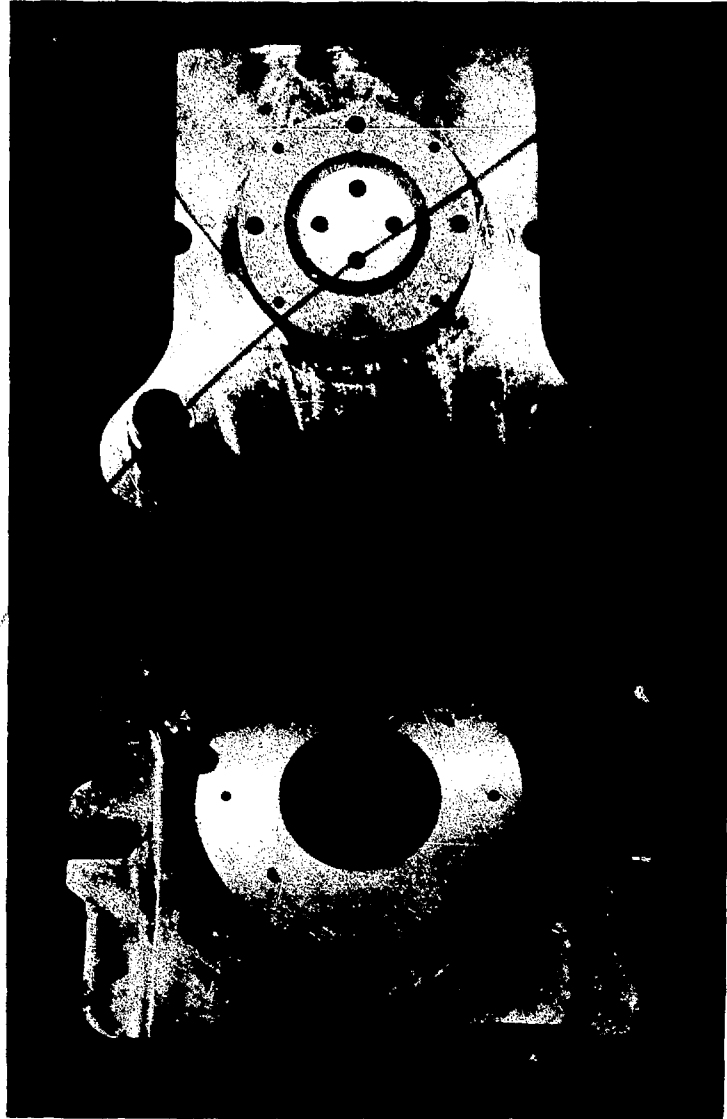


Fig. 8-1: A Blanking Die

~~SECRET~~

~~SECRET~~

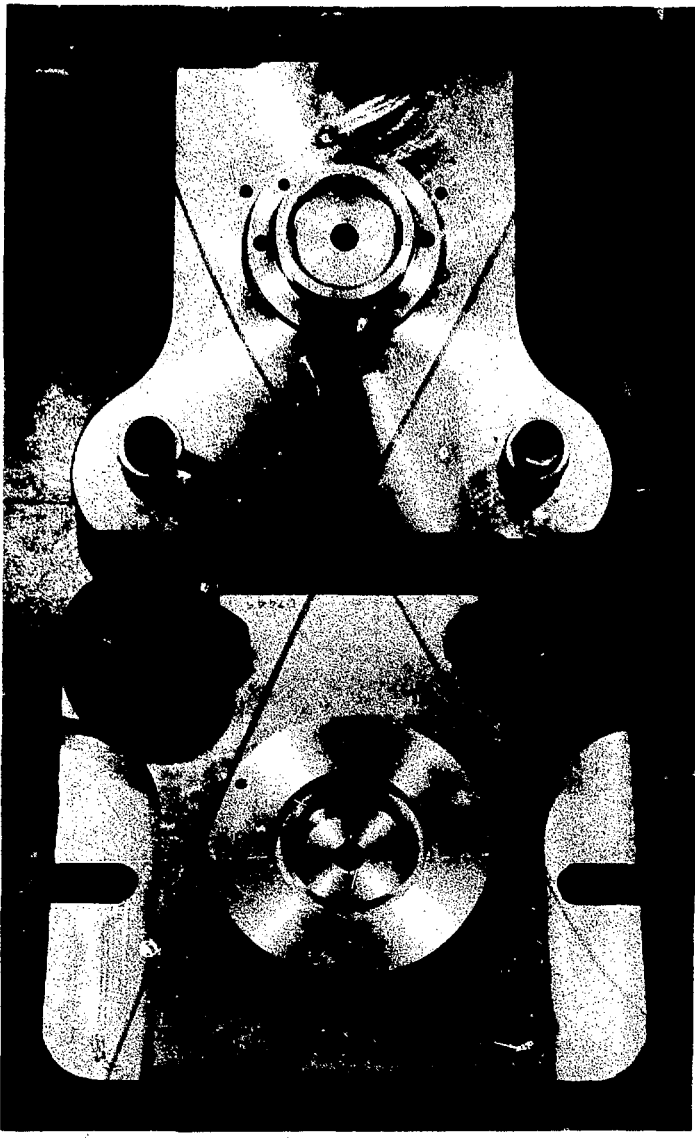


Fig. 8-2: A Corrugating Die for Partially Corrugating the Spacers

~~SECRET~~

~~SECRET~~



Fig. 8-3: A Corrugating Die for Forming the Channel Rings

~~SECRET~~

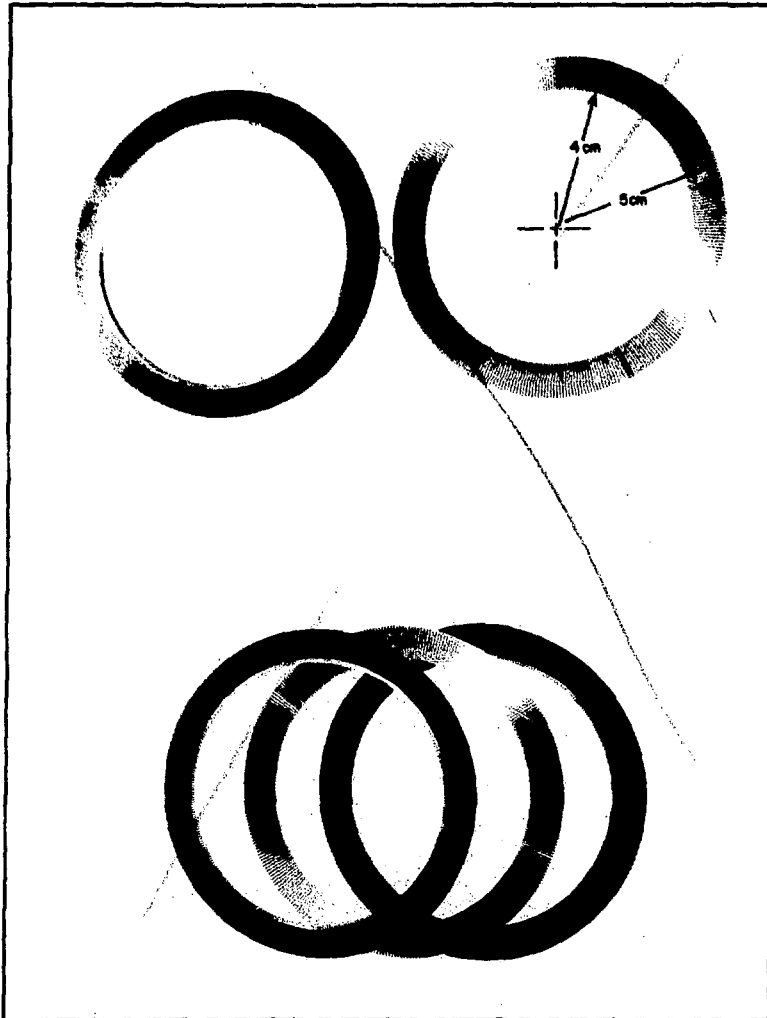


Fig. 8-4: Washers Blanked and Corrugated by the Dies

~~SECRET~~

8-7: Metallurgical Fabrication Problems

The known fabrication problems that present the greatest difficulty are as follows:

(a) Preferred orientation of the rolled out sheets of molybdenum. Rings of the refractory metals have not been made. However, it is known from work on linearized wall sections that corrugating a sheet of molybdenum with the grooves running parallel to the rolling direction tends to produce pieces which crack along the ridges of the corrugations. Corrugating normal to the direction in which the sheet was rolled produces pieces which do not crack.

A. C. Briesmeister and P. J. Pallone of LASL have shown for linearized sections of Dumbo wall that the orientation problem may be avoided. To do this, the corrugations are made by rolling the foil through meshed gears, so that bending of the metal without stretching occurs. Figures 8-5 and 8-6 show successfully corrugated foils of molybdenum and tungsten and the dies used for this technique.

There are metallurgical methods for coping with preferred orientation difficulties, but no particular work has been done in this problem for Dumbo.

(b) Rolling of sheets of refractory metal impregnated with  $UO_2$ . Metallurgical studies are necessary before cermets containing  $UO_2$  can be rolled out to the foil thickness specified in Chap. 9.

~~SECRET~~

~~SECRET~~

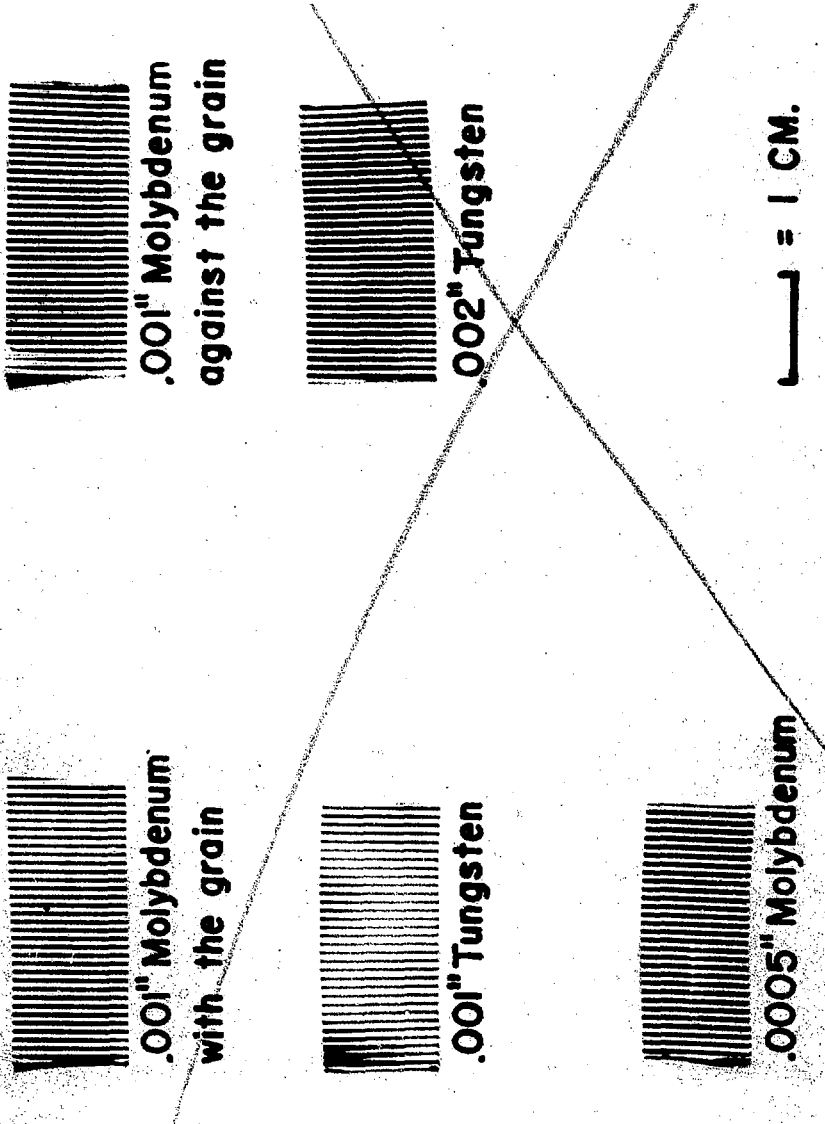


Fig. 8-5: Linear Corrugated Foils

~~SECRET~~

~~SECRET~~

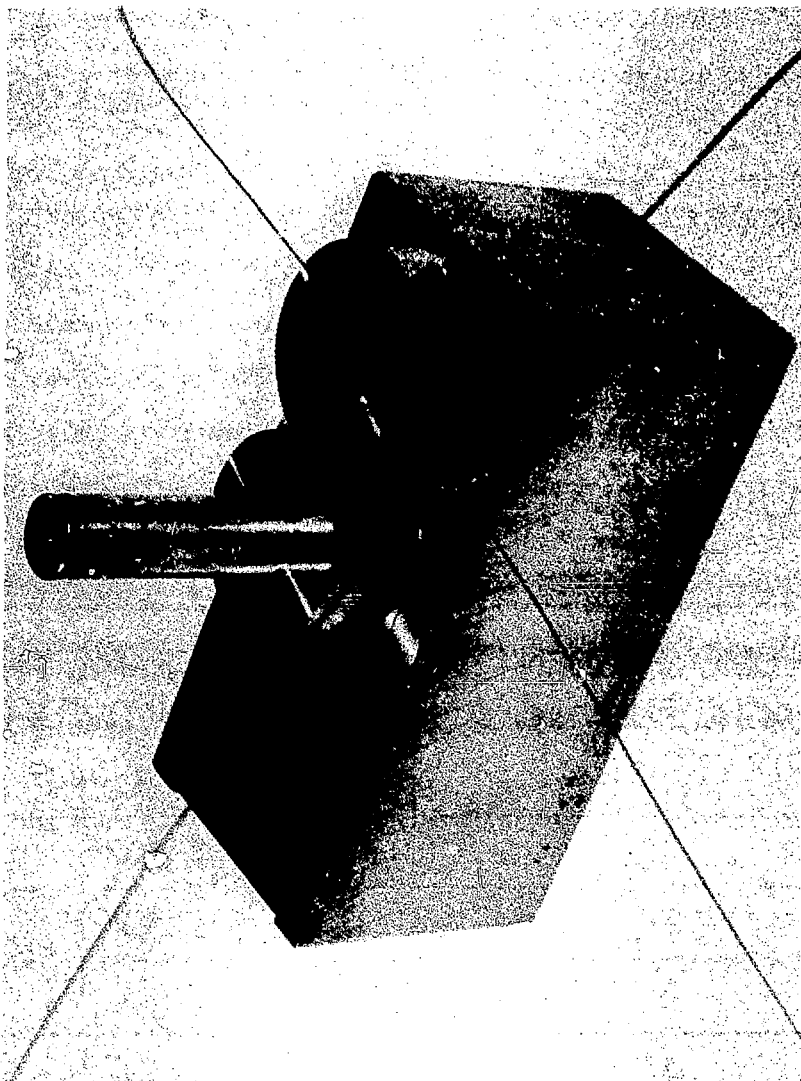


Fig. 8-6: Die for Folds of Fig. 8-5

~~SECRET~~

~~SECRET~~

This problem could be made easier by rolling sheets to smaller width, such as would be used in designs involving linearized wall sections. In these cases it is necessary to roll a ribbon of only about 1 cm width.

8-8: The Moderator Material

The moderator consists of molded polystyrene into which magnesium powder has been incorporated to improve the thermal conductivity. Preliminary samples of this plastic, incorporating 10 to 50% magnesium powder, have been made by J. S. Church of LASL. Thermal conductivity measurements of these samples are given in Table 8-2. These measurements

VOLUME PERCENT MAGNESIUM IN POLYSTYRENE	THERMAL CONDUCTIVITY watt/cm-deg
10	$4 \times 10^{-3}$
20	$5 \times 10^{-3}$
30	$6 \times 10^{-3}$
40	$13 \times 10^{-3}$
50	$45 \times 10^{-3}$

~~SECRET~~



~~SECRET~~

The Moderator Material

Section 8-8

are due to R. L. Powell of the National Bureau of Standards, Boulder, Colorado. The thermal conductivity of the 50% sample is satisfactory. With more experimental work it should be possible to achieve this thermal conductivity with less magnesium.

REFERENCES

1. C. J. Smithells, Tungsten, p. 129, Fig. 101, Chem. Pub. Co., Brooklyn, 1953.
2. Battelle Memorial Institute, EMI-889, November 25, 1953.
3. O. Sisman and C. D. Bopp, Physical Properties of Irradiated Plastics, Oak Ridge National Laboratory, ORNL-928, June 29, 1951.

~~SECRET~~

~~SECRET~~

## CHAPTER 9

### NUMERICAL DESIGN OF SOME SELECTED MOTORS

The rest of the time he picked up the melon rinds that he had dropped on his way to the Limpopo -- for he was a Tidy Pachyderm.

R. Kipling, The Elephant's Child

#### 9-1: Introduction

An extensive and largely complete array of theoretical tools pertaining to the design of rocket motors of the Metal Dumbo type are developed and presented in previous chapters. The utility of these developments in practical motor designs may be obscured not only by the necessary mathematical detail but also by the large number of subjects which it is necessary to treat. Nevertheless, these many lines of attack do converge upon a practical and attractive type of nuclear rocket motor whose features and behavior are shown in this chapter.

A few distinctive models of the Dumbo type are presented in this chapter as typical. Each model is considered as completely as current understanding permits insofar as performance under various conditions is concerned.

#### 9-2: Description of Models A - D

The four models described in this chapter are:

Model A: This Dumbo motor is constructed of nineteen Dumbo tubes

~~SECRET~~

~~SECRET~~

Chapter 9 Numerical Design of Some Selected Motors

with normal flow path for the hydrogen. The Dumbo heat exchanger is constructed of molybdenum foil 0.0025 cm thick, corrugated into washers of 4 cm inner radius and 5 cm outer radius. The molybdenum is impregnated with 25 volume percent  $UO_2$ .<sup>\*</sup> The tubes are 55 cm long within a reflector having a cavity 60 cm high. Moderation is provided by polystyrene (CH) impregnated with 20% magnesium. This mixture is assumed to have a thermal conductivity of 0.01 cal/cm-sec-deg or more. This model is capable of  $1.5 \times 10^9$  watts power, heating  $H_2$  gas to 2500°K with an operating pressure of 25 atmospheres. The power density is flat and temperature uniformity of the hottest parts of the metal wall is maintained to  $\pm 200^\circ$ . This model is perhaps the simplest of the Dumbo type to construct and test and has good performance characteristics. Detailed analysis is treated in Sec. 9-3.

Model B: This motor, described in Sec. 9-4, is designed to be in the 10 megawatt class and is constructed of 169 tubes of the dimensions described in Model A. It is larger, heavier, and more powerful than Model A. It is constructed similarly of molybdenum.

Model C: This motor, described in Sec. 9-5, is distinguished from Model A by use of a tungsten heat-exchanger material containing 25 volume percent  $UO_2$ . The higher temperature properties of the tungsten may be used either to produce a higher gas temperature, or to allow less intimate heat transfer in the Dumbo exchanger, or to allow a larger factor of

---

<sup>\*</sup>Throughout this report "uranium" or "U" refers to pure  $U^{235}$ .

~~SECRET~~

safety when operated as Model A. This motor requires inverted geometry and flow patterns. The nineteen tubes are constructed with similar dimensions to those of Model A, although the small introductory impedances in the metal wall are located at the outer edge of the tubes.

Model D: This motor, described in Sec. 9-6, is a large version of the tungsten Dumbo (Model C) with 169 tubes and appropriately larger power.

A comparison of these four models is given in Sec. 9-7.

9-3: Model A Design Features

This "domestic size" motor is composed of nineteen Dumbo tubes with their moderating cores, the entire reactor core being reflected by beryllium on all sides. The lower reflector contains exit ports for the heated hydrogen as well as supply ducts for very cold supply hydrogen.

Design features are developed in the following order:

- (a) Moderator and reflector requirements.
- (b) Energetics, flow, and pressure design.

Considerable construction detail of the metal Dumbo wall is imposed from the start on the basis of preliminary design. This information is compiled in Table 9-1. A drawing of this wall is shown in Fig. 9-1.

The moderator and reflector design is associated with the hydrodynamic problems discussed in Chap. 7. As shown in Sec. 7-8, it is possible to approximately satisfy the condition for flow uniformity by

~~SECRET~~

TABLE 9-1 MODEL A METAL WALL

DIMENSIONS	
FULLY CORRUGATED PIECES	PARTIALLY CORRUGATED PIECES
FOIL THICKNESS, $\tau$ 0.0025 cm	FOIL THICKNESS, $\tau/2$ 0.00125 cm
INNER RADIUS 4.00 cm	INNER RADIUS 4.00 cm
OUTER RADIUS 5.00 cm	OUTER RADIUS 5.00 cm
NO. of CORRUGATIONS 336	NO. of CORRUGATIONS 336
CORRUGATION PERIOD, $\nu$ AT INNER RADIUS 0.075 cm AT OUTER RADIUS 0.09375 cm	CORRUGATION PERIOD, $\nu$ AT INNER RADIUS 0.075 cm AT OUTER RADIUS 0.09375 cm
CORRUGATION HEIGHT, $a_2$ 0.015 cm	CORRUGATION HEIGHT, ( $a_2 a_1$ ) 0.01193 cm
CORRUGATION LENGTH 1.00 cm	CORRUGATION LENGTH 0.147 cm

CALL ONE "UNIT" A STACK OF 2 PARTIALLY CORRUGATED WITH ONE FULLY CORRUGATED PIECE.

Total No. Units for 19 tubes	52,250
Total Mass $M_o$ for 19 tubes	57.06 kg
Total Volume Metal in Wall	7.388 li
$M_o$	5.541 li
$UO_2$	1.847 li

ASSUME PREHEATER REQUIREMENTS TO CORRESPOND TO 2.22 cm EXTRA WALL PER TUBE.

Total Mass $M_o$ in Motor	59.4 kg
Total Mass $UO_2$ in Motor	21.1 kg
Total Mass U in Motor	18.6 kg

(CONTINUED)

~~SECRET~~

~~SECRET~~

TABLE 9 - 1 CONT.

Number of channels per unit	672
Total number of channels in motor	$35 \times 10^6$
Heat exchange surface per unit	$113 \text{ cm}^2$
Heat exchange surface per channel	$0.169 \text{ cm}^2$
Total heat exchange surface in motor	$5.90 \times 10^6 \text{ cm}^2$
<hr/>	
Total outer tube area	$32.8 \times 10^3 \text{ cm}^2$
Total inner tube area	$26.3 \times 10^3 \text{ cm}^2$

CHANNEL GEOMETRY

AT EXIT (OUTER RADIUS OF TUBE)	AT ENTRANCE (INNER RADIUS OF TUBE)
$v = 0.09375 \text{ cm.}$	$v = 0.075 \text{ cm.}$
$a_2 = 0.015 \text{ cm}$	$a_1 = 0.00307 \text{ cm}$
Cross sectional area = $1/2 a_2 v$ $= 0.70 \times 10^{-3} \text{ cm}^2$ (Total open area, $24.5 \times 10^3 \text{ cm}^2$ )	Cross sectional area = $1/2 a_1 v$ $= 0.115 \times 10^{-3} \text{ cm}^2$ (Total open area, $4.03 \times 10^3 \text{ cm}^2$ )

~~SECRET~~

~~SECRET~~

Chapter 9

Numerical Design of Some Selected Motors

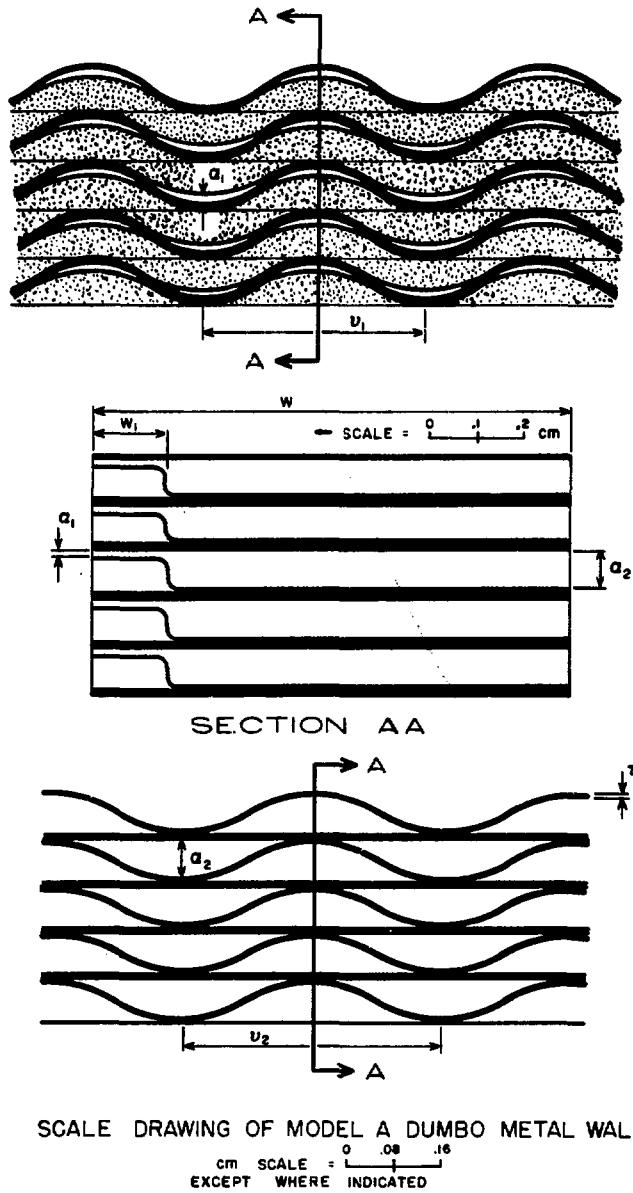


Fig. 9-1

~~SECRET~~

~~SECRET~~

adjusting the areas of hot gas and cold gas flow, given by  $A_B$  and  $A_A$ , respectively, such that

$$\left(\frac{A_B}{A_A}\right)^2 = 2 \frac{T_B}{T_A} \tag{9-1}$$

For  $T_B = 2500^\circ\text{K}$  and  $T_A = 255^\circ\text{K}$  the ratio becomes

$$A_B / A_A = 4.427 \tag{9-2}$$

As shown in Chap. 7, it is possible to readjust  $T_A$  as a vernier control for purposes of balancing the flow nonuniformities along a Dumbo tube. The simple relation of Eq. 9-2 is that chosen for the nuclear phase of the design problem. Table 9-2 presents the reactor design characteristics of the Model A Dumbo motor. Figs. 9-2 and 1-1 are drawings of the reactor design of Dumbo Model A.

Another aspect of this motor is the temperature to which it heats the hydrogen. If heat transfer were perfect and all regions behaved uniformly, then the gas temperature would be chosen as the highest possible working temperature of the metal wall. Because of the extensive investigations of the preceding chapters it is possible to take account of deviations from this ideal condition. Corrections are made for the following effects:

Effect a: Imperfect heat transfer, resulting in a temperature difference  $\theta_g$  between the gas and the metal wall, as developed in Chap. 2.

~~SECRET~~



~~SECRET~~

Chapter 9 Numerical Design of Some Selected Motors

TABLE 9-2 NUCLEAR DESIGN AND MATERIALS OF MODEL A MOTOR			
Materials	kg	moles	N <sub>i</sub> , moles/li
Mo	59.4	619	3.91
CH	28.6	2200	13.90
Mg	18.5	762	4.82
UO <sub>2</sub>	21.1	79	0.50
U	(18.6)	79	0.50
Be (reflector)	577.6		
Total mass	705.2		
REFLECTOR DESCRIPTION			
Inside radius	28.97 cm	Inner height	60.00 cm
Outer radius	42.22 cm	Outer height	84.08 cm
		Volume of Be	312.2 li
MOTOR DESCRIPTION			
Height, L <sub>o</sub>	60.00 cm	Hydraulic Diameter	
Radius, R <sub>o</sub>	28.97 cm	Hot region	7.05 cm
Volume, V <sub>o</sub>	158.2 li	Cold region	4.42 cm
AREAS			
Moderator region	663.3	cm <sup>2</sup>	
Cold gas flow	258.5		
Structural bracing	33.3*		
Metal wall	537.2		
Hot gas flow	1144.4		
Total area	2636.7	cm <sup>2</sup>	
MODERATOR REGION (For metal wall see table 9-1)			
Volume distribution		Effective densities	
CH	68.4 %	CH	0.719 gm/cm <sup>3</sup>
Mg	26.8 %	Mg	0.466 gm/cm <sup>3</sup>
Void	4.8 %		
N <sub>Mg</sub> = 0.347 N <sub>CH</sub>			
Outer radius	4.0	cm	
Inner radius	2.21	cm	
*NOTE: Structural allotment equivalent to one 1.5 cm diameter rod per Dumbo tube.			

~~SECRET~~

~~SECRET~~

Model A Design Features

Section 9-3

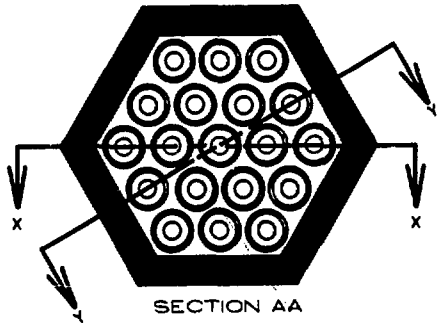
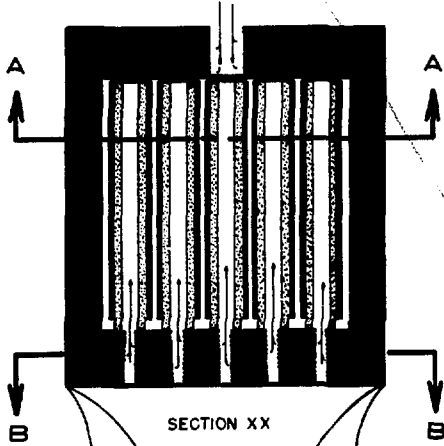



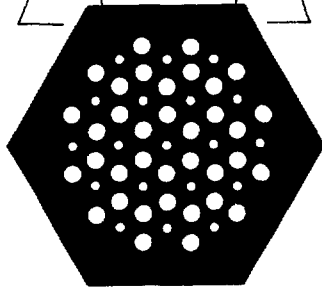




FIGURE 9-2

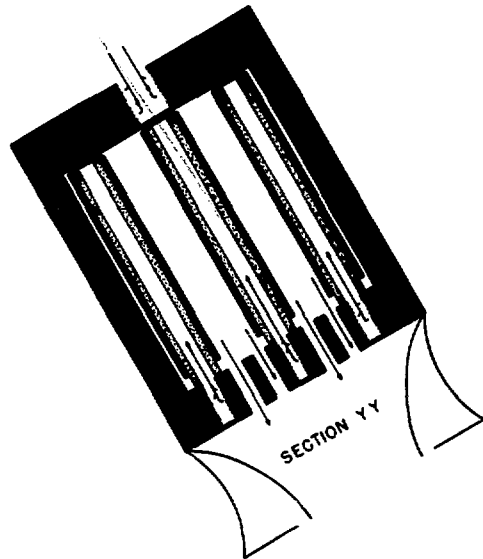
SECTIONAL VIEWS  
MODEL A DUMBO  
SCALE 



- MATERIALS:
-  Be REFLECTOR
  -  METAL WALL
  -  MODERATOR



- SECTION BB
-  HOT GAS OUTLET
  -  COLD GAS INLET



~~SECRET~~

~~SECRET~~

Chapter 9      Numerical Design of Some Selected Motors

Effect b: Deviations from the flat flux condition which is approximately satisfied by the design methods of Chap. 6.

Effect c: Variations of flow through the wall at various heights along a tube, resulting in temperature variations, as described in Chap. 7.

Effect d: Hot and cold spots along the wall due to nonuniformities of wall construction, as described in Chap. 4.

In order to predict these several corrections estimates regarding nonuniformities must be assumed. The authors have attempted to assign two extreme values to each of three quantities, representing the optimistic 😊 and pessimistic 😞 extremes, as follows:

	😊	😞
Maximum working temperature of the wall	2923°K (M.P.)	2700°K
Maximum flux intensity* above the mean	3%	7%
rms deviations in $Q_1$	1%	12%

Effect a: From Eqs. 2-105 and 2-53  $\theta_g$  is expressed in terms of the average flow density  $J_0$  issuing from the outside of the Dumbo tubes as

$$\theta_g = 181 J_0 = 0.552 \times 10^{-2} Q_0 \quad (9-3)$$

---

\*It is expected that flow variations from effect c are dominated by flux nonuniformities. Such variations are regarded as lumped into this figure.

~~SECRET~~

~~SECRET~~

Effects b and c: Effects of local power variations are interpreted in terms of the gas heat capacity  $c_p$  at the high temperature and the enthalpy increase  $\Delta H$  of the gas in passing through the wall, so that each 1% power variation about the mean results in a temperature increase  $\delta_1 T$ , given by

$$\delta_1 T = \frac{\Delta H}{100 c_p} = 20^\circ \quad (9-4)$$

where  $c_p$  is 4.3 cal/gm-deg and  $\Delta H$  is 8400 cal/gm.

Effect d: Relations involving the wall construction are complicated but computations for this model fit the linear empirical relation

$$(\delta T)_{\max} = 12.1 J. \quad (9-5)$$

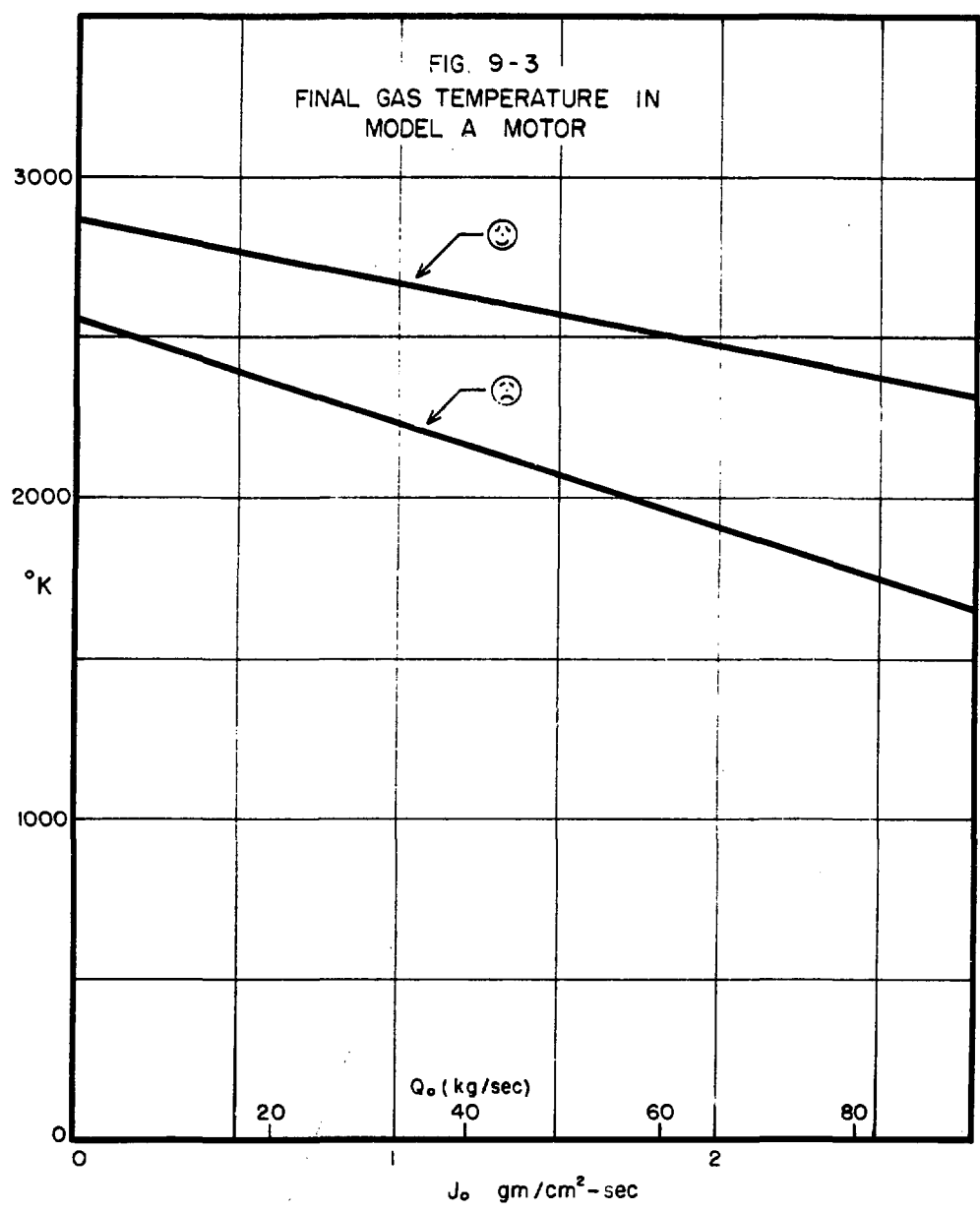
for each 1% rms deviation in  $\alpha_1$ . These relations predict the results shown in Fig. 9-3 for the final gas temperature corresponding to various flow densities  $J_0$  or total flows  $Q_0$ . As a rough practical index of the performance of the motor one may consider the thrust occurring from a nozzle whose exit velocity is twice the velocity of sound at the chamber temperature ( $\sim 0.9$  that for complete expansion). The performance is shown in Fig. 9-4. Conversions to power levels are shown in Fig. 9-5.

All the preceding design results are independent of the choice of operating pressure for the Model A Dumbo motor. Within the motor, it is generally desirable to maintain the pressures sufficiently high so that flows are sub-sonic. For the Model A motor the rule that

~~SECRET~~

~~SECRET~~

Chapter 9 Numerical Design of Some Selected Motors



~~SECRET~~

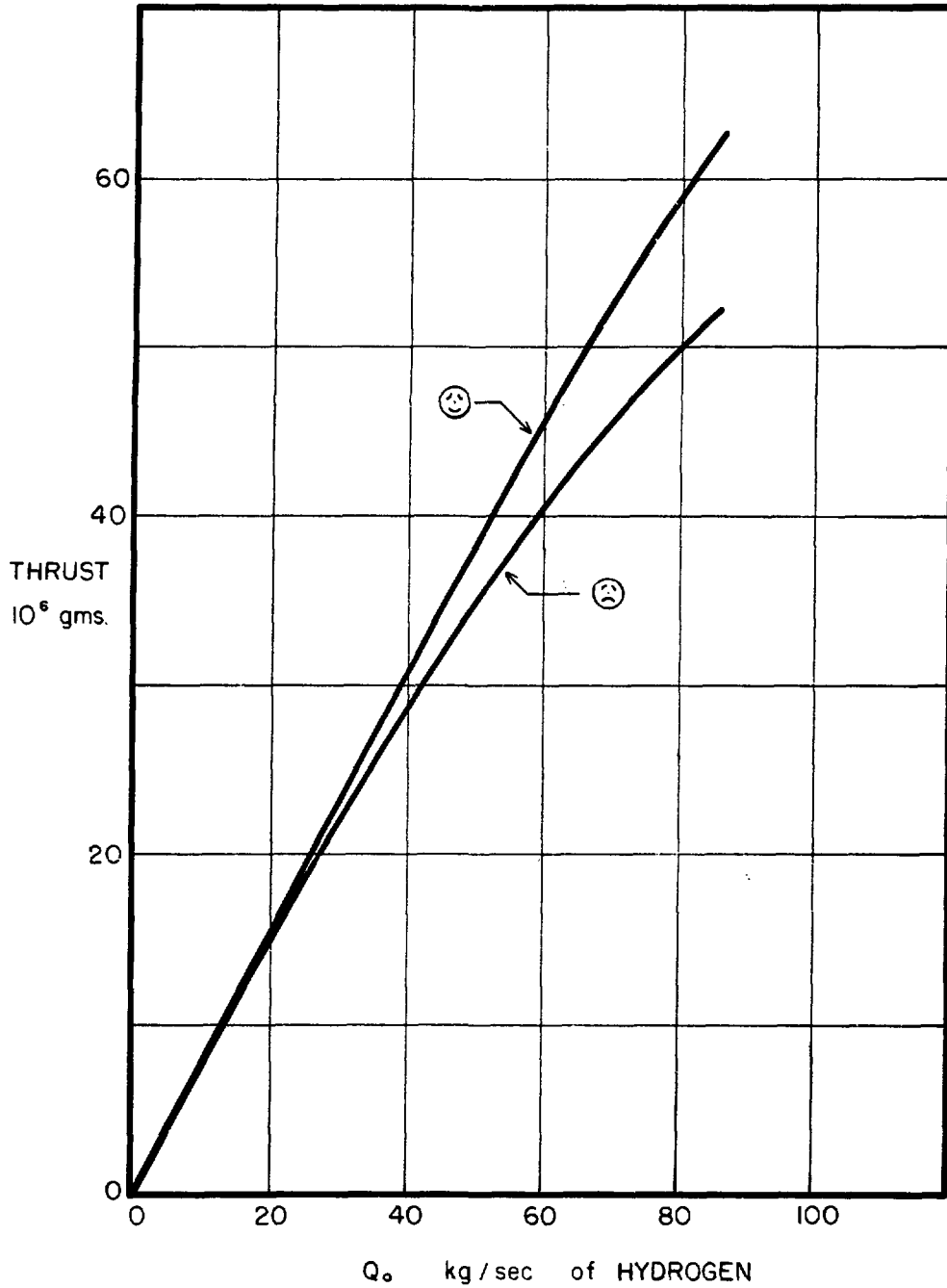


Fig. 9-4: Performance of Model A Motor

~~SECRET~~

Chapter 9 Numerical Design of Some Selected Motors

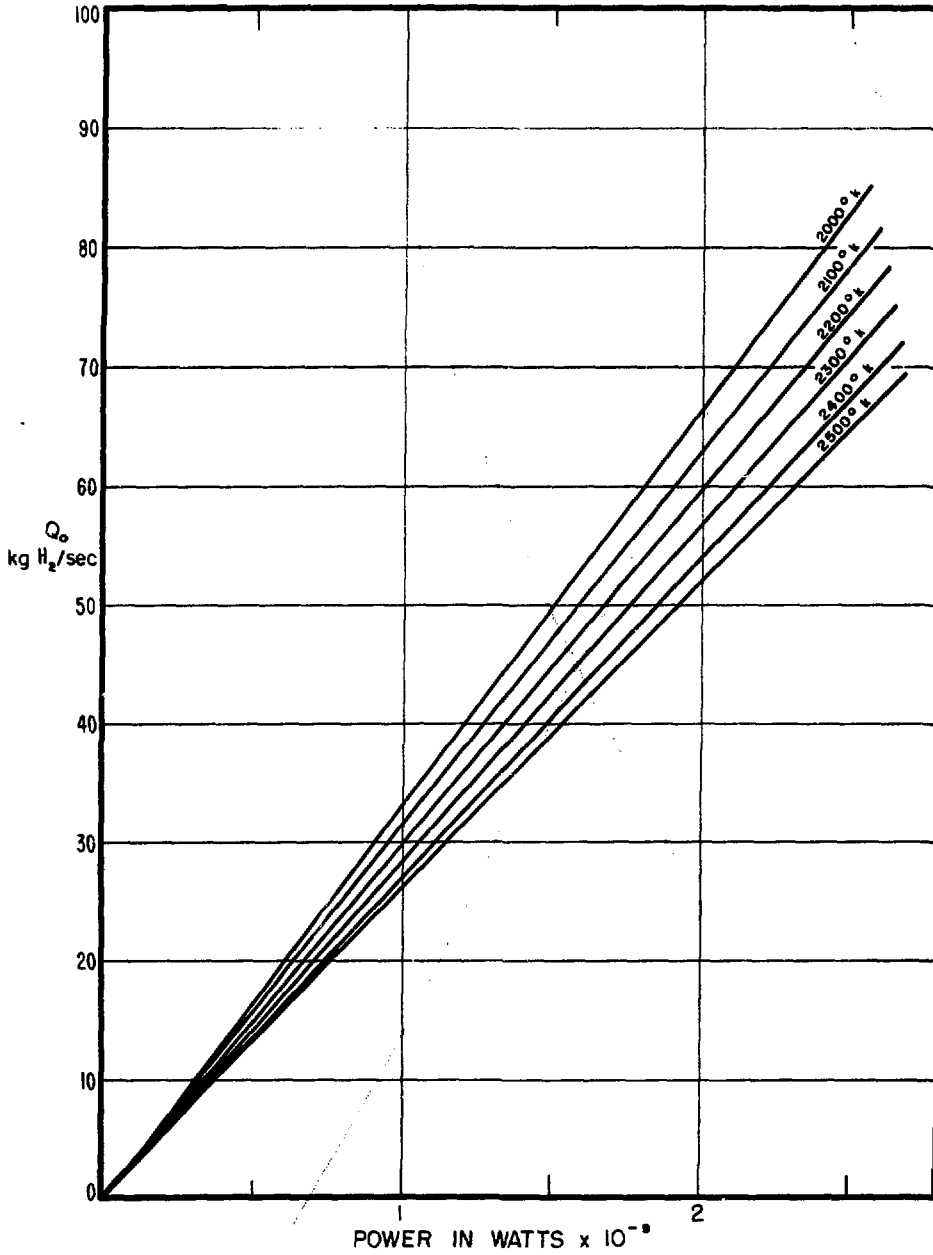


Fig. 9-5: Total Flow of  $H_2$  for Various Power Levels

~~SECRET~~

~~SECRET~~

Model A Design Features

Section 9-3

$$p_B = 6 \times 10^{-4} Q \quad (\text{bar}) \quad (9-6)$$

insures that the hot gas velocity does not exceed Mach 0.4 (referred to 2500°K). As an example, for  $Q_0 = 4 \times 10^4$  gm/sec (power approximately 1500 megawatts) the operating pressure is 24 bar, according to this rule. This value is consistent with the pressure distribution given in Fig. 7-5 and Table 7-5. This distribution is computed for the Model A Dumbo motor.

Relations of Chap. 3 are used to obtain the pressure drop across the metal wall. For the Model A motor the rule that the pressure drop through the moderator is six times that of the metal wall insures reasonable lack of sensitivity of performance to variations in the metal wall construction between different gross regions of a tube. With this factor of six each 1% error in the introductory height  $\alpha_1$ , causes ~5.4 degrees change in the output temperature due to the modified flow through the wall.

If larger operating pressures are selected, all pressure variations within the motor are reduced proportionately. Since pressures in the range of 100 bar are technically feasible, comparatively minor considerations might justify the choice of larger pressures.

Table 9-3 lists dimensions of the plastic moderator wafers and some flow data from the numerical example of Table 7-5 and Fig. 7-5. Each

~~SECRET~~



~~SECRET~~

Chapter 9 Numerical Design of Some Selected Motors

TABLE 9-3			
<u>(a) DETAILS OF PLASTIC WAFERS</u>			
INNER RADIUS	2.21 cm	THICKNESS	0.0975 cm
OUTER RADIUS	4.00 cm	MOSAIC CELL TABS	every 3mm
SEMI-CIRCULAR HOLES (in plastic)		NUMBER CELLS per WAFER	84
DIAM.	0.025 cm		
LENGTH	1.79 cm		
NUMBER HOLES per WAFER	336		
<u>(b) MOSAIC CELLS</u>			
WIDTH	0.30 cm = $4 \nu$		
HEIGHT	0.10 cm = $5(a_2 + 2\tau)$		
NUMBER OF METAL CHANNELS	per CELL	40	
NUMBER OF SUPPLY HOLES IN PLASTIC	per CELL	4	
<u>(c) TYPICAL FLOW DATA THRU WALL</u>			
	ENTERING PLASTIC	ENTERING METAL WALL	LEAVING METAL WALL
TEMPERATURE	220° K	305° K	2500° K
PRESSURE	31.4 atm	29.5 atm	29.2 atm
VELOCITY	$2.19 \times 10^4$ cm/sec	—	$0.57 \times 10^4$ cm/sec
MACH NO.	0.17	—	0.015
REYNOLDS NO.*	8700	133	69
* REYNOLDS NO. AT $W_1$ (FIG. 9-1) IS 163.			

~~SECRET~~

~~SECRET~~

plastic wafer alternates with a 0.0025 cm thick Dural wafer as shown in Fig. 1-12.

Some aspects of the Dumbo motor are not peculiar to pachydermalates but are found in most nuclear rocket motor designs. Solutions of this type of problem are avoided in this study as far as possible although two plausible details, the beryllium reflector and the preheater design, are described at this point.

The beryllium reflector: Although this reflector is computed as a circular cylindrical shell, the Dumbo tube array suggests an equivalent hexagonal geometry, as shown in Figs. 1-1 and 9-2. A hexagonal geometry allows the reflector to be made of many flat slabs yielding a laminated type of structure. Controlled spacing between these plates provides flow paths for the "liquid H<sub>2</sub>" feed as coolant for the reflector. All interior surfaces of the reflector are thermally insulated from the hot gas in order to protect the metal from excessive temperatures and to avoid losses of energy from the surfaces. This is accomplished with thin tungsten or molybdenum foil to which 0.05 cm ZrO<sub>2</sub> is bonded.\* The composite foils are used with the ZrO<sub>2</sub> adjacent to the beryllium surfaces and with the refractory metal backing exposed to the hot gas.

A particular construction problem arises at the lower plate in which thirty-six holes of 6 cm diameter are required for exhausting the hot

---

\*Such a bonding which is highly tenacious and withstands strong thermal shocks has been accomplished by W. J. McCreary at Los Alamos.

~~SECRET~~

~~SECRET~~

Chapter 9      Numerical Design of Some Selected Motors

gas. The area of these holes equals the total hot area  $A_B$  of the chamber, and represents 40% of the total lower plate area. The resulting loss of neutron reflection presumably can be compensated by making a correspondingly thicker reflector plate. However, the open area may be reduced if the operating pressure is increased to insure that the gas velocities remain sub-sonic.

Preheater design: Although some heating of the hydrogen occurs in the Be reflector, the exit temperature of this gas is only approximately 100°K so that some added heating of this gas will be necessary to arrive at the 220°K temperature required for the cold gas duct. For this purpose the lowest 3 cm of each Dumbo tube is devoted to a low power turbulent heat exchanger. Table 9-4 gives the energy requirements of

	TEMPERATURE*	ENTHALPY	
HOTTEST GAS	2500° K	9475cal/gm	} 90.23 % 3.00 4.27 2.50
GAS ENTERS DUMBO WALL	305	1025	
GAS ENTERS MODERATOR	220	744	
GAS ENTERS PREHEATER	97.5	344	
GAS ENTERS REFLECTOR	27	110	
LIQUID (H <sub>2</sub> )	20.3	(63)	100.00 %
* COMPUTED ON BASIS OF 100 BAR PRESSURE.			

~~SECRET~~

the gas\* at each stage of its flow on the basis of Fig. 7-1. No detailed design of the preheater is proposed, but channels of hydraulic diameter 0.03 cm with a pressure drop of 0.3 bars are typical. Power density is similar to that of the major portion of the reactor so that no serious neutronic coupling problem with the lower portion of the Dumbo tubes is expected.

9-4: Model B Design Features

This enlarged version of the Model A motor consists of 169 Dumbo tubes with their moderating core. The metal wall of each tube is identical with that of Model A, as described in Table 9-1. The description of the nuclear design of this motor is given in Table 9-5. Fig. 9-6 presents a drawing of the Model B motor. The temperature performance for a given  $J_0$  is identical to that of Model A. However, the total flow  $Q_0$  and the thrust indicated in Figs. 9-3 and 9-4 must be multiplied by 8.895 due to the larger number of tubes. For example, the temperature performance characteristics obtained when Model A operates at 1.5 megawatts are obtained by Model B at 13.3 megawatts.

Operating pressure may be less in the Model B Dumbo motor than that of Model A because of the 63% larger gas flow area for each tube. For this model the rule

---

\*Since the Dumbo motors always operate above the critical pressure of  $H_2$  (12.8 bar) there is no discontinuous phase transition from liquid to gas. (See Fig. 7-2.)

~~SECRET~~

**TABLE 9-5**  
**NUCLEAR DESIGN AND MATERIALS OF**  
**MODEL B MOTOR**

Materials	kg	moles	$N_i$ , moles/li
Mo	528.3	5,506	3.07
CH	135.8	10,446	5.83
Mg	87.8	3,610	2.01
UO <sub>2</sub>	187.7	703	0.39
U	(165.4)	703	0.39
Be (reflector)	1820.2		
Total mass	2759.8		

**REFLECTOR DESCRIPTION**

Inside radius	97.53 cm	Inner height	60.00 cm
Outer radius	106.66 cm	Outer height	77.68 cm
Volume of Be		983.3 li	

**MOTOR DESCRIPTION**

Height, $L_o$	60.00 cm	Hydraulic Diameter	
Radius, $R_o$	97.53 cm	Hot region	11.22 cm
Volume, $V_o$	1793 li	Cold region	2.88 cm

**AREAS**

Moderator region	3,148	cm <sup>2</sup>
Cold gas flow	3,752	
Structural bracing	1,595*	
Metal wall	4,778	
Hot gas flow	16,610	
Total area	29,883	cm <sup>2</sup>

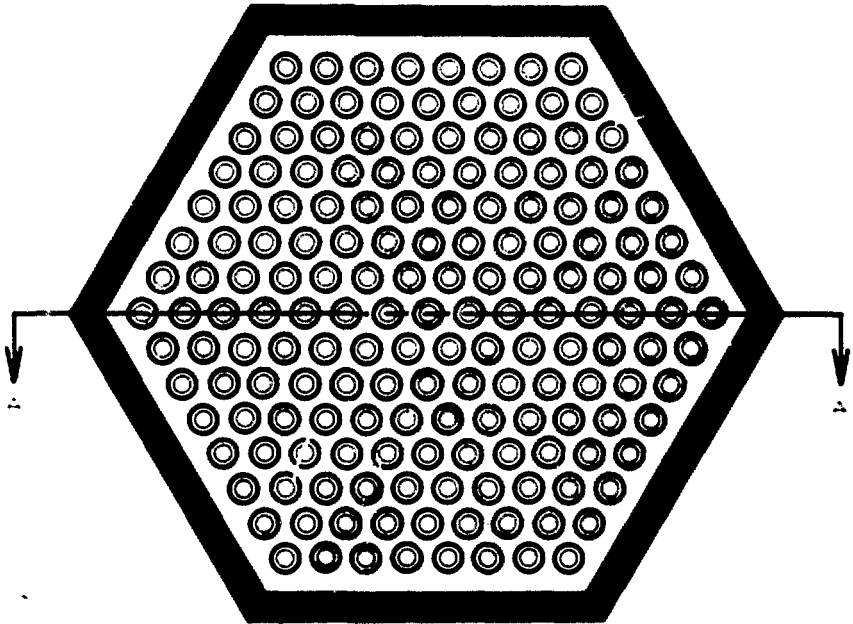
**MODERATOR REGION**

Outer radius	4.0 cm	Inner radius	3.175 cm
--------------	--------	--------------	----------

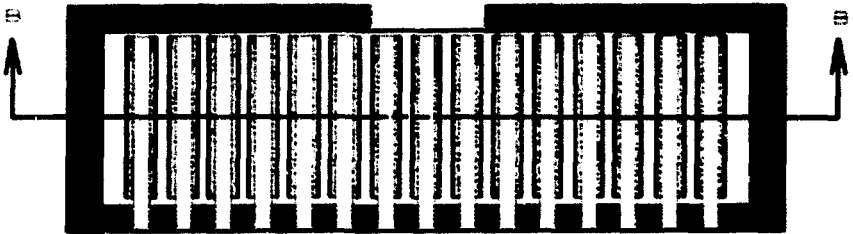
\* NOTE: Structural allotment equivalent to one 1.74 cm radius rod per Dumbo tube.

Model B Design Features

Section 9-4



SECTION BB



SECTION AA

MODEL B DUMBO

SCALE: 1/2" = 1"

FIGURE 9-6

$$p_B = 0.41 \times 10^{-4} Q_0 \text{ bar} \tag{9-7}$$

insures gas velocities to be less than Mach 0.4. For example, if  $Q_0$  is  $35.6 \times 10^6$  gm/sec then  $p_B$  is 14.6 bar by Eq. 9-7.

Model B moderator wafers require only half as many semi-circular holes as those of Model A, and only two such holes supply each mosaic cell of the Model B metal wall. This occurs because the inner radius of the Model B wafers is larger than for Model A. Otherwise the construction and performance of the Model A motor apply. Reflector construction and preheater design is similar to that of Model A.

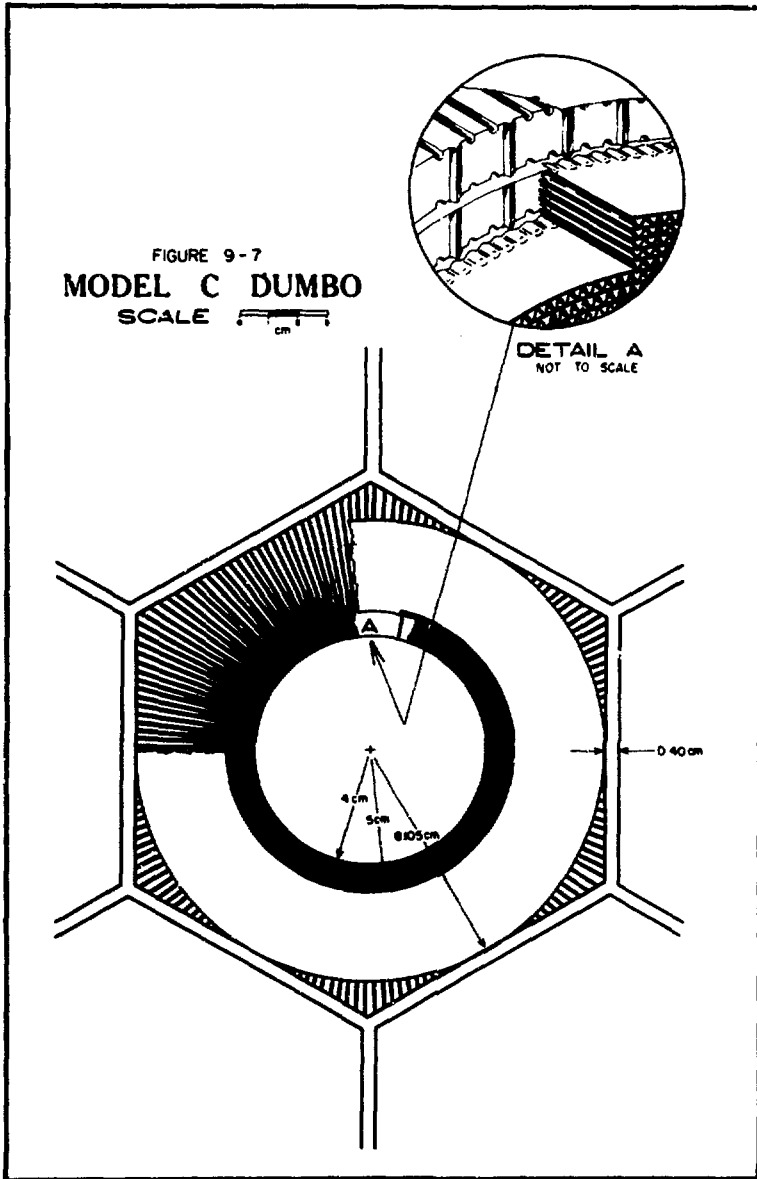
9-5: Model C Design Features

The Model C motor uses nineteen Dumbo tubes made of 0.0025 cm thick foil. The tungsten is impregnated with 25 volume percent  $UO_2$ . Due to the increased moderator requirements of a tungsten reactor, this model uses the inverted Dumbo geometry in which the moderator surrounds the metal wall. The gas flow passes through the plastic and the metal wall in turn, with the hot gas flowing down the inside of each Dumbo tube. The metal wall geometry is that of Table 9-1 and Fig. 9-1 except that the partially corrugated pieces form the stabilizing impedance along the outer radius of the metal wall and produce a different channel geometry. Table 9-6 and Figs. 9-7 and 9-8 present the nuclear design of this motor. Compared to the Model A motor this model possesses a large beryllium

TABLE 9-6 NUCLEAR DESIGN AND MATERIALS OF MODEL C MOTOR			
Materials	kg	moles	$N_i$ , moles/li
W	112.3	610	2.24
CH	123.6	9507	34.89
Mg	79.9	3285	12.06
UO <sub>2</sub>	21.1	79	0.29
U	(18.6)	79	0.29
Be (reflector)	1755.1		
Total mass	2092.0		
REFLECTOR DESCRIPTION			
Inside radius	38.02 cm	Inner height	60.00 cm
Outer radius	61.58 cm	Outer height	102.54 cm
	Volume of Be 948.7 li		
MOTOR DESCRIPTION			
Height, L <sub>o</sub>	60.00 cm	Hydraulic Diameter	
Radius, R <sub>o</sub>	38.02 cm	Hot region	10.0 cm
Volume, V <sub>o</sub>	272.5 li	Cold region	0.633cm
AREAS			
	Moderator region	2803.2 cm <sup>2</sup>	
	Cold gas flow	215.7	
	Structural bracing	30.0	
	Metal wall	537.2	
	Hot gas flow	955.1	
	Total area	4541.2 cm	
MODERATOR REGION (See figure 9-7)			
	Effective density		
	CH 0.735 gm/cm <sup>3</sup>		



~~SECRET~~



~~SECRET~~

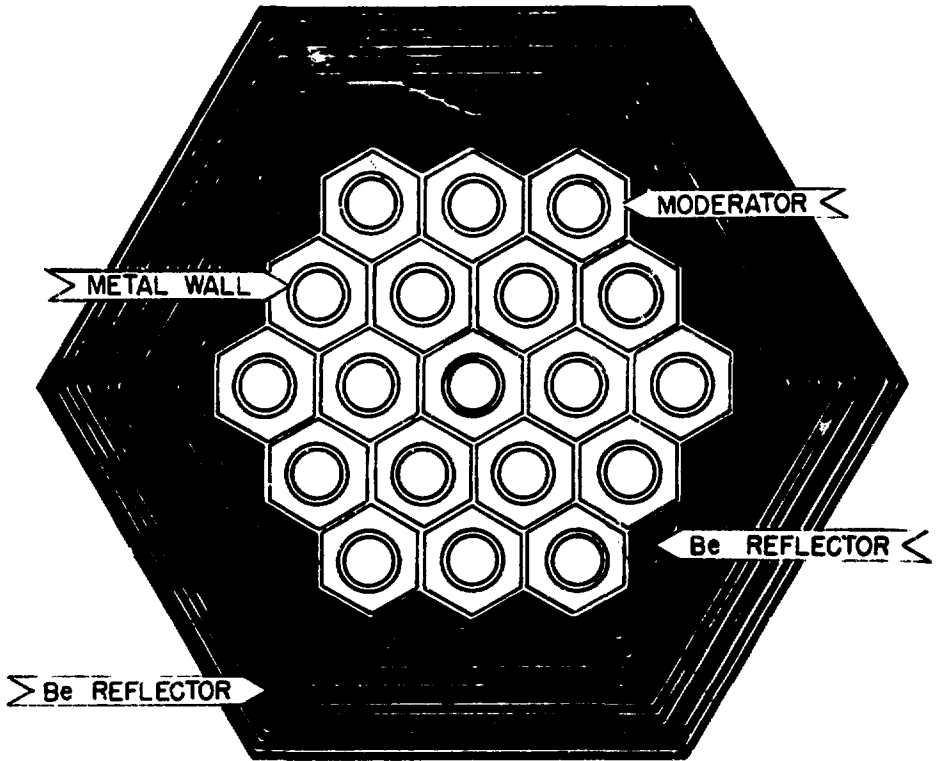
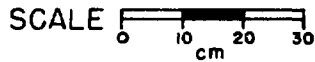


FIGURE 9-8

# MODEL C DUMBO



reflector and is consequently much heavier.

The temperature performance of this motor is analyzed in a manner like that for the Model A. The following quantities are assumed:

	☺	☹
Maximum working temperature of the wall	3640°K (M.P.)	3300°K
Maximum flux intensity above the mean	3%	7%
rms deviation in $Q_1$	1%	12%

Values of  $\theta_g$  for this model are given by

$$\theta_g = -287 J_o = 1.093 \times 10^{-2} Q_o \quad (9-8)$$

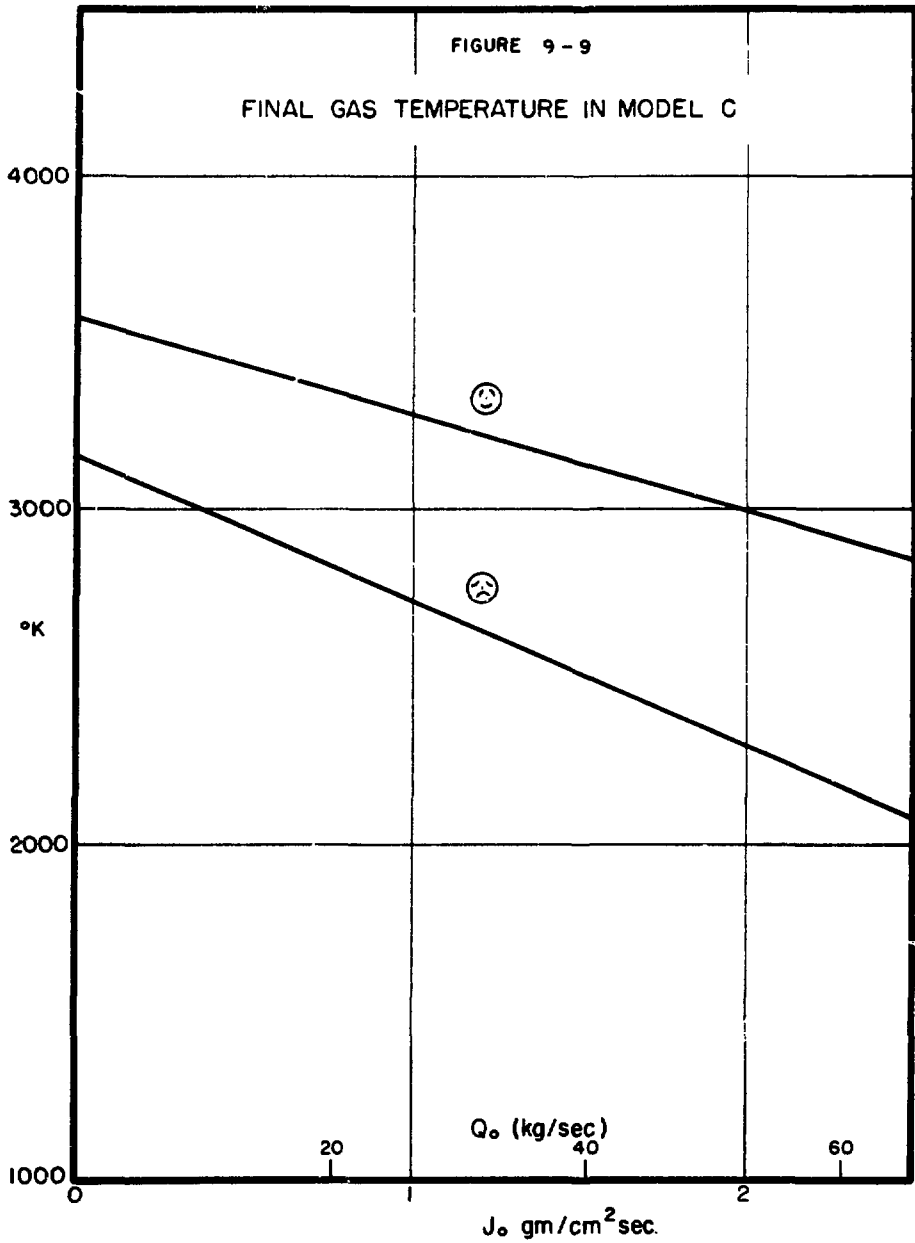
where  $J_o$  is the flow per  $\text{cm}^2$  of interior tube surface. The effects of power variations, flow variations, and wall construction variations are similar to those described for Model A. The performance for this motor is shown in Fig. 9-9.

For the Model C motor, the rule that

$$p_B = 7.7 \times 10^{-4} Q_o \text{ bar} \quad (9-9)$$

insures gas velocities to be less than Mach 0.4. Thus  $p_B$  is 28% larger than in Model A.

The reflector of the Model C rocket might be made as shown in Fig. 9-8. However, the feasibility of such construction with beryllium has not been investigated. Preheaters are similar to those of Model A.



~~SECRET~~

Chapter 9 Numerical Design of Some Selected Motors

9-6: Model D Design Features

This device is a tungsten motor having 169 Dumbo tubes. It is an inverted Dumbo model, like Model C. Its nuclear design is described in Table 9-7. Operating temperatures for a given  $J_0$  are the same as those for Model C, as shown in Fig. 9-8, although the corresponding total flow  $Q_0$  is 8.895 times greater.

For the Model D motor, the rule that

$$p_B = 0.87 \times 10^{-4} Q_0 \text{ bar} \quad (9-10)$$

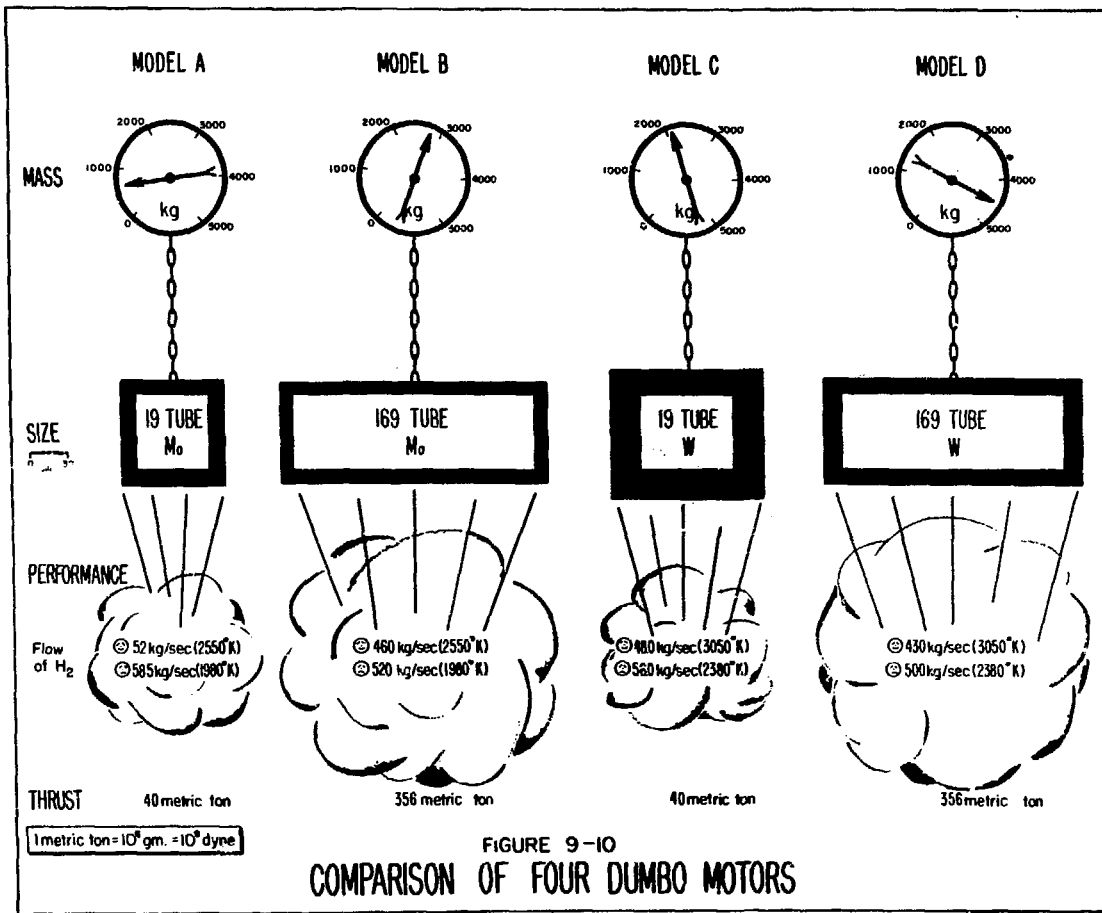
insures gas velocities to be less than Mach 0.4.

9-7: Comparison of the Four Models

A comparison of some features of the previous four models is shown in Fig. 9-10. The comparison of mass, size, and shape is evident from the figure. Performance is evaluated in terms of the hydrogen flow  $Q_0$  required to produce an arbitrary thrust. This thrust is 8.895 times greater for the large motors (Models B and D) than for the small ones (Models A and C). The performance is computed on the basis of molecular hydrogen of constant specific heat, as was described for Fig. 9-4. This assumption underestimates the thrust. According to the chart, Fig. 9-10, the tungsten motors show so small an improvement over the corresponding molybdenum motors that their ranges of uncertainty overlap. However, the presence of hydrogen dissociation, due to the high temperatures

~~SECRET~~

TABLE 9-7			
NUCLEAR DESIGN AND MATERIALS OF MODEL D MOTOR			
Materials	kg	moles	$N_i$ , moles/li
W	998.9	5,429	3.57
CH	421.3	32,408	21.32
Mg	272.4	11,201	7.37
UO <sub>2</sub>	187.7	703	0.46
U	(165.4)	703	0.46
Be (reflector)	2646.0		
Total mass	4526.3		
REFLECTOR DESCRIPTION			
Inside radius	89.80 cm	Inner height	60.00 cm
Outer radius	103.79 cm	Outer height	87.18 cm
	Volume of Be		1430.3 li
MOTOR DESCRIPTION			
Height, $L_o$	60.00 cm	Hydraulic Diameter	
Radius, $R_o$	89.80 cm	Hot region	10.0 cm
Volume, $V_o$	1520.0 li	Cold region	0.6 cm
AREAS			
	Moderator region	9,767	cm <sup>2</sup>
	Cold gas flow	1,920	
	Structural bracing	369	
	Metal wall	4,778	
	Hot gas flow	8,500	
	Total area	25,334	cm <sup>2</sup>



~~SECRET~~

attainable by tungsten, can prove so advantageous in several ways that the comparison given by Fig. 9-10 is grossly affected. The possible improvements from these dissociation effects are discussed in App. D.

9-8: Variants on the Designs

Several variations of these designs possess attractive features. Among these are the following:

- (1) The number, arrangement, and size of tubes may be adjusted as desired.
- (2) The degree of loading the metal wall with  $UO_2$  may be adjusted over a considerable range which is consistent with nuclear demands and metallurgical properties.
- (3) Alloys of molybdenum with tungsten or rhenium, having intermediate thermal properties and better fabrication properties than either pure metal, may be used.
- (4) It is interesting to consider the effect of making the Dumbo wall of heavier gauge foil, which may ease fabrication problems. Table 9-8 shows that this procedure, keeping the moderator construction the same, allows reduction in the reflector thickness and in the total mass of the motor. Changes in the criticality  $k$  are shown for this variant.
- (5) The composite CH-Be reflector described in Sec. 6-8 may be applied with success to the large Model B motor, although it presents no

~~SECRET~~



~~SECRET~~

TABLE 9-8			
THE USE OF THICKER FOILS IN			
19 TUBE DUMBO DESIGNS			
(a) Molybdenum, Regular Flow			
PLY	1*	2	3
CRITICALITY, k	1.000	1.049	1.066
CORE RADIUS, R <sub>o</sub>	27.9cm	27.9	27.9
CORE HEIGHT, L <sub>o</sub>	60.0cm	60.0	60.0
REFLECTOR RADIUS	40.2 cm	36.4	34.6
REFLECTOR HEIGHT	82.7 cm	76.1	72.9
REFLECTOR MASS	507.2 kg	315.0	237.2
UO <sub>2</sub> MASS	21.1 kg	42.2	63.3
TOTAL MASS	632.7 kg	521.0	523.7
*THESE DATA ARE SIMILAR TO, BUT NOT IDENTICAL TO, MODEL A			
(b) Tungsten, Inverted Flow			
PLY	1*	2	3
CRITICALITY, k	1.000	1.012	0.987
CORE RADIUS, R <sub>o</sub>	38.0 cm	38.0	38.0
CORE HEIGHT, L <sub>o</sub>	60.0 cm	60.0	60.0
REFLECTOR RADIUS	61.6 cm	54.6	51.9
REFLECTOR HEIGHT	102.5cm	90.6	85.9
REFLECTOR MASS	1755.2 kg	1065.0	841.5
UO <sub>2</sub> MASS	21.1 kg	42.2	63.3
TOTAL MASS	2092.0 kg	1535.2	1445.2
* MODEL C DATA			

302  
~~SECRET~~

advantage with the large Model D motor. Some indication of the utility of this modification is seen in Table 9-9. However, the details of how to protect plastic or other hydrogenous moderator which is arranged inside the Be reflector are not covered in this report.

TABLE 9-9		
	MODEL B WITH Be REFLECTOR	MODEL B' WITH COMPOSITE REFLECTOR
CORE RADIUS	97.5 cm	82.8
CORE HEIGHT	60 cm	60
REFLECTOR RADIUS	106.7 cm	88.9
REFLECTOR HEIGHT	87.7 cm	69.8
MASS Be	1820 kg	498
MASS CH in REFLECTOR	— kg	173
TOTAL MASS	2760 kg	1787

It should be pointed out that no attempt has been made to obtain optimum designs. Many of the parameters are chosen either arbitrarily or for convenience. With the material of this chapter as a background, optimization of design obviously can be carried out. Similarly, the choice of hydrogen for the propellant is to some extent arbitrary, and some other propellants can be considered in optimization.

~~SECRET~~

CHAPTER 10  
CONCLUDING TOPICS

At last things grew so exciting that his dear families went off one by one in a hurry to the banks of the great grey-green greasy Limpopo River, all set about by fever trees, to borrow new noses from the Crocodile. When they came back nobody spanked anybody any more.

R. Kipling, The Elephant's Child

10-1: Introduction

The preceding chapters of this report are devoted to consideration of the theory and practical information relating to a specific type of rocket reactor. These considerations culminate in the numerical designs of Chap. 9. In Sec. 10-2, variants of Dumbo are considered which depart, more-or-less radically, from the standard Dumbo motors of Chap. 9. In Sec. 10-3, other uses of Dumbo-type reactors are mentioned. In Sec. 10-4, topics are listed which are salient to the Dumbo design, and for which more information is required.

10-2: Variants of Dumbo

Many variants of this type of reactor are possible which still preserve its basic features. Some of these variations are in the fine structure of the heat-exchanger wall, the geometry of the cold regions, and the materials in the wall.

~~SECRET~~

Chapter 10

Concluding Topics

---

Some of the changes that can be made in the wall which still allow laminar flow and dynamic insulation are:

(a) Porous metal walls, of either sintered metal powder or fine wire. These possess extremely efficient heat-transfer characteristics. Design of these heat exchangers must include consideration of three-dimensional temperature-flow stability.\*

(b) Walls which have regular channels and which are stabilized in the same fashion as the regular Dumbo walls. Concentric layers of uniform wire mesh, concentric perforated cylinders, or a combination of these two methods are examples. An advantage of this type of design is that it allows the use of materials of small neutron cross section for the initial portion of the heating channel, and tungsten for the high temperature regions.

(c) Linearized versions of the conventional Dumbo wall. These offer the following advantages: The narrow width of the foil allows the rolling process to be easier and more accurate. Virtually no wastage occurs in the fabrication of the foil. The simple and accurate method of forming the heating channels discussed in Sec. 8-7 is permitted. The linearized version allows the use of the laminated foil described in Sec. 8-3.

---

\*This subject has been treated in part by B. W. Knight, Jr. and is to be issued at a later date. It can be shown that no 3-dimensional flow effects unstabilize an exchanger which is stable according to the 1-dimensional criterion of Eq. 3-5.

A possible modification in the basic geometry of Dumbo is the concentric cylinder model, shown in Fig. 10-1. The hot and cold gas flow passages are the annuli between adjacent Dumbo walls and between adjacent moderator regions, respectively. Several advantages of this model are suggested by its radial symmetry. Linearized walls can be used either in polygonal Dumbo tubes or in polygonal versions of the concentric cylinder model.

Another variant is a metal wall which is constructed of fully corrugated rings made of Mo-UO<sub>2</sub> and flat (partially corrugated) rings made of W-UO<sub>2</sub>. The W-UO<sub>2</sub> rings extend about 15% further than the Mo-UO<sub>2</sub> rings. This heat exchanger heats the gas above the molybdenum temperature, and gives the high-temperature performance of a tungsten motor with half the nuclear poisoning.

10-3: Other Uses of Dumbo-Type Reactors

The properties of Dumbo-type reactors that make other applications feasible are:

- (1) The flow impedance of the heat exchanger is small compared with turbulent types.
- (2) Moderator is distributed throughout the reactor, yet is maintained at a low temperature. This allows the use of high temperature materials that could not be used in unmoderated reactors.
- (3) The flat flux distribution, which is obtained by proper

~~SECRET~~

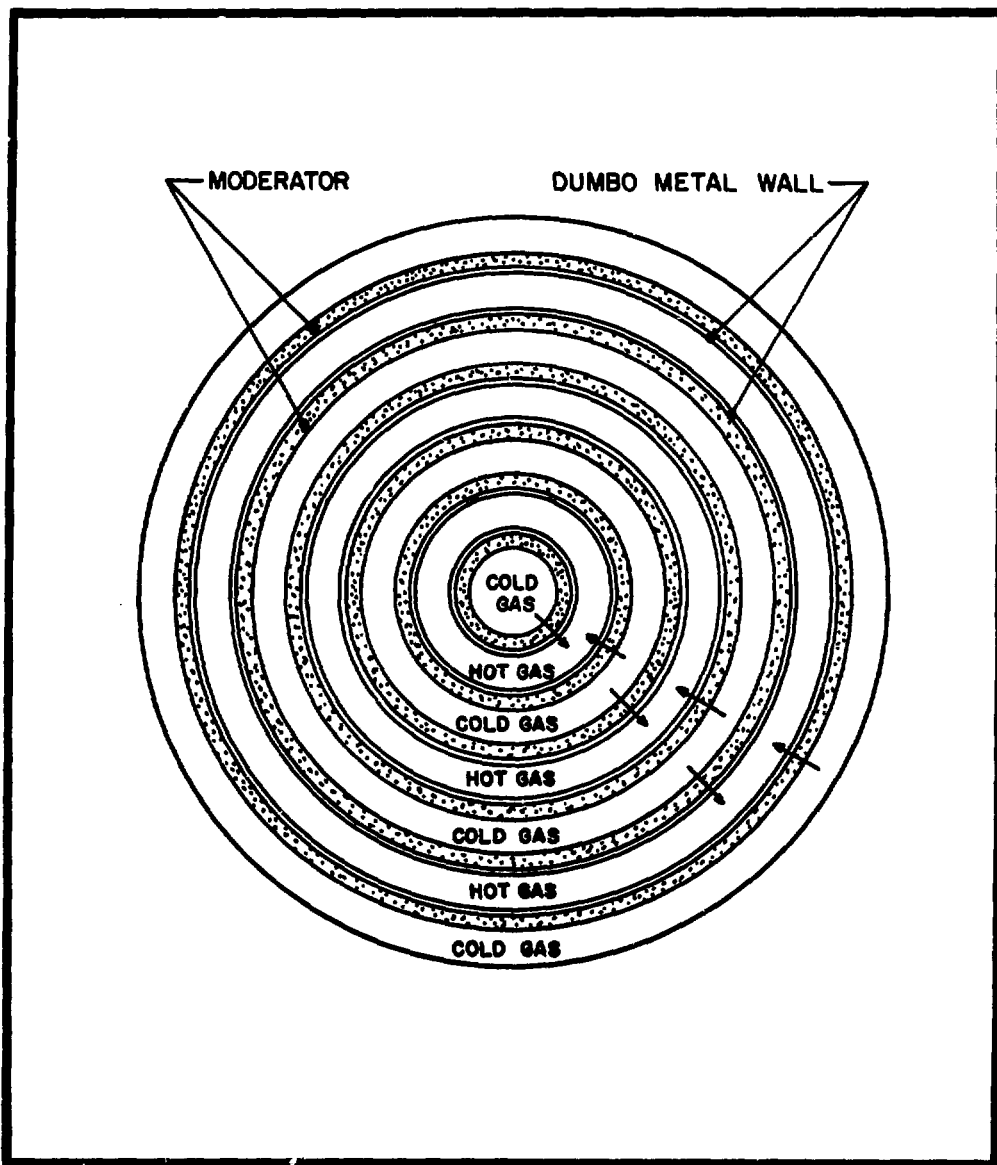


Fig. 10-1: Concentric Cylinder Model

~~SECRET~~

adjustment of moderator and reflector, permits uniform power distribution, even though both the construction and the  $UO_2$ -loading are kept uniform.

(4) These reactors have low mass.

(5) The small size of the reactor permits the use of small gamma ray shields.

There are several types of aircraft that could be driven by a Dumbo reactor. Among these are rocket and ramjet aircraft.

The Dumbo reactor, without major changes, may be applied to rocket aircraft. The small size and mass of the reactor and of the gamma ray shields are important for this application. These reactors may be designed to be smaller than those described in Chap. 9.

Ramjet applications require several changes in the reactor design to avoid oxidation of the heat exchanger by the air. Thus, oxidation resistant metals must be used for the heat exchanger. The low stresses encountered in the Dumbo reactor may permit operation at higher temperatures than normally used for these metals. The uniformity of the power density, low heat-exchanger impedance, lightness, and small size are valuable for this type of application.

Since these reactors are designed to heat gases to high temperatures, they might be adaptable to driving closed-cycle turbine power plants.

~~SECRET~~

10-4: A Research and Development Program for Dumbo

The material of this report suggests several research and development projects. Some of these are necessary to the engineering of a Dumbo reactor. These are as follows:

- (1) Single channel temperature-flow stability investigations. This work is complete and confirms the theory as given in this report. A report will be issued covering this investigation.
- (2) Tests on an electrically heated wall sample. Full scale tests of a sample of heat-exchanger wall are possible. Since such a piece may be very small, a few kilowatts power are enough to do the necessary heating. From these tests information may be obtained on the following:
  - (a) Multi-channel temperature-flow stability.
  - (b) Temperature uniformity of the metal wall within a mosaic cell.
  - (c) Heat transfer data.
  - (d) Demonstration and measurement of the Nerst effect.
  - (e) Measurement of the performance of a small nozzle to obtain information on super-Dumbo operation.
  - (f) Studies of the effectiveness of dynamic insulation.
  - (g) Strength of materials under a range of operating conditions.
  - (h) Effects of system vibration.

*AS*



~~SECRET~~

Research and Development Program

Section 10-4

- 
- (i) Effects of thermal cycling.
  - (j) Chemical and thermal behavior of  $UO_2$  and the refractory metals.
- (3) Hydrodynamic studies. These would reveal the flow law in the hot gas region. While this knowledge is not crucial to the engineering of Dumbo it is of direct scientific interest. The theory of the flow balance over the length of a Dumbo tube could be confirmed.
  - (4) Metallurgical studies. Such studies would consist of the following:
    - (a) Studies of the preparation and rolling of cermet of  $UO_2$  and the refractory metals in the region of interesting concentration.
    - (b) Physical properties of the cermets.
    - (c) Radiation damage to the cermets.
    - (d) Studies of the fabrication of the Dumbo heat exchanger.
  - (5) Plastics studies. These include
    - (a) Impregnation of polystyrene and other plastics with magnesium or other metals.
    - (b) Molding of the impregnated plastic.
    - (c) Studies of radiation damage to moderating plastics.
  - (6) Nuclear studies. These include
    - (a) Experimental critical assemblies for reactor mock-up.

~~SECRET~~

~~SECRET~~


Chapter 10

Concluding Topics

---

- (b) Zero-power operation of these assemblies to yield the flux distribution and the temperature coefficient of the reactor.
- (c) Numerical machine calculation of the preceding quantities as well as the reactor dynamics for start-up and control problems.

~~SECRET~~



Appendix A

NUCLEAR CONSTANTS

This appendix tabulates certain data that are necessary to the nuclear design of the Dumbo reactors. Table A-2 and Figs. A-1 through A-9 present capture cross section data for molybdenum and tungsten. The Doppler broadening widths  $\Delta$  are given for 300°K. These data are new and have been assembled for this report by J. J. Devaney of LASL, to whom the authors are greatly indebted. The job of obtaining capture cross sections from raw nuclear data is a formidable one from the standpoints of both theory and computation.

Table A-1 presents certain general properties of the reactor materials. Table A-3 presents averaged cross section data on the basis of J. J. Devaney's values.

~~SECRET~~

Appendix A

Nuclear Constants

TABLE A - 1					
SUBSTANCE	MOL. WT.	DENSITY	$\sigma_{tr}$ SCATTERING CROSS SECTION	$\eta_i$	$\rho_i^*$
Mo	95.95	10.2	7 barns	0.20	1.7
W	183.9	19.3	11	0.20	1.5
Mg	24.3	1.74	3.4	0.0	1.3
U	235	—	20	4	2.0
UO <sub>2</sub>	267	10.9	27.6	4.08	4.0
C	12	—	4.7	0.065	1.20
H	1	—	6.67	1.00	1.00
CH	13	1.05	11.37	1.065	2.20

TABLE A - 2					
CAPTURE CROSS SECTION DATA					
for					
MOLYBDENUM					
ENERGY RANGE	E <sub>0</sub> (ev)	$\sigma$ (barns)	$\Gamma$ (ev)	$\Delta$ (ev)	ACCURACY
0.0253-400 ev.	SEE FIGURE A - 1				10% - 30%
400 - 710 ev.	406*	55.4 88.0	0.34 0.29	} 0.66	~ 30%
	440	183.7	0.37		
	480	251.8	1.0	0.71	SEE FIGURE A - 1
	510	158.1	0.37	0.74	
	570	78.7	0.38	0.79	
	580	43.4	0.93	0.79	
	700	55.2	1.0	0.87	
400 - 10 ev.	SEE FIGURE A - 2				~ 60%
* TWO PEAKS AT THE SAME E <sub>0</sub> .					

10-4

**TABLE A-3**  
**AVERAGE CROSS SECTIONS OVER ENERGY**

SUBSCRIPT <sub>F</sub> — FISSION CROSS SECTION (barns)

SUBSCRIPT <sub>C</sub> — CAPTURE CROSS SECTION (barns)

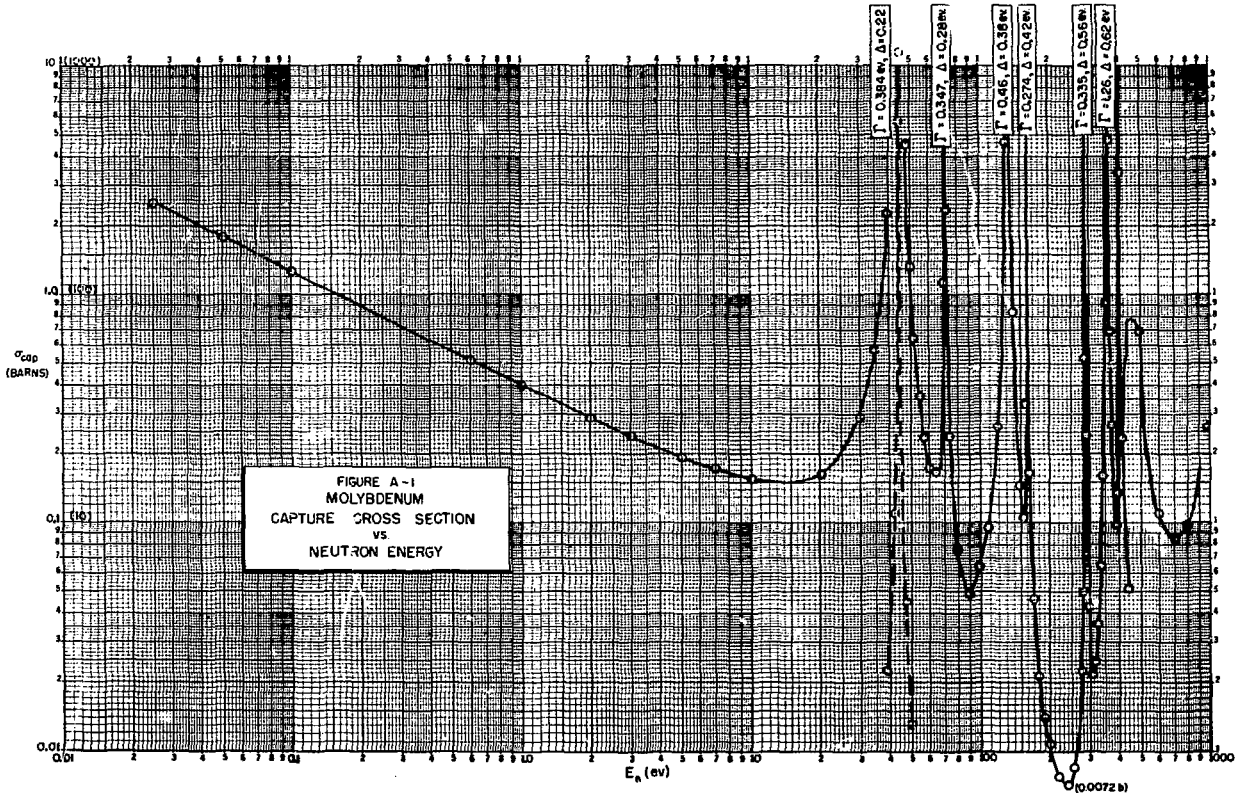
SUBSCRIPT <sub>S</sub> — SCATTERING CROSS SECTION (barns)

ENERGY RANGE	$U_F$	$U_{F+C}$	$H_{S+C}$	$H_C$	$Mo_C$	$W_C$	$C_S$
$10^5 - 10^6$	1.4	1.67	7.8	0	0.085	0.06	3.5
$10^4 - 10^5$	2.5	3.28	16.3	0	0.22	0.32	4.6
$10^3 - 10^4$	5.8	8.35	20	0	0.26	0.91	4.7
$10^2 - 10^3$	15.6	23.4	20	0	1.0**	1.45*	4.7
$10 - 10^2$	49.6	63.0	20	0	3.0**	0.6*	4.7
1 - 10	39.8	51.7	20.5	0.03	0.25	2.5*	4.7
0.1 - 1	145.1	174.1	23.6	0.1	0.75	6.06	4.8
0.025 - 0.1	402	474.4	30.2	0.2	1.72	14.0	4.8
THERMAL	580	687	—	0.33	2.5	19.2	—

\* AVERAGE  $\sigma_c$  OVER INTERVAL WITHOUT RESONANCES.

\*\* AVERAGE  $\sigma_c$  OVER INTERVAL INCLUDING RESONANCES.

*Handwritten signature*

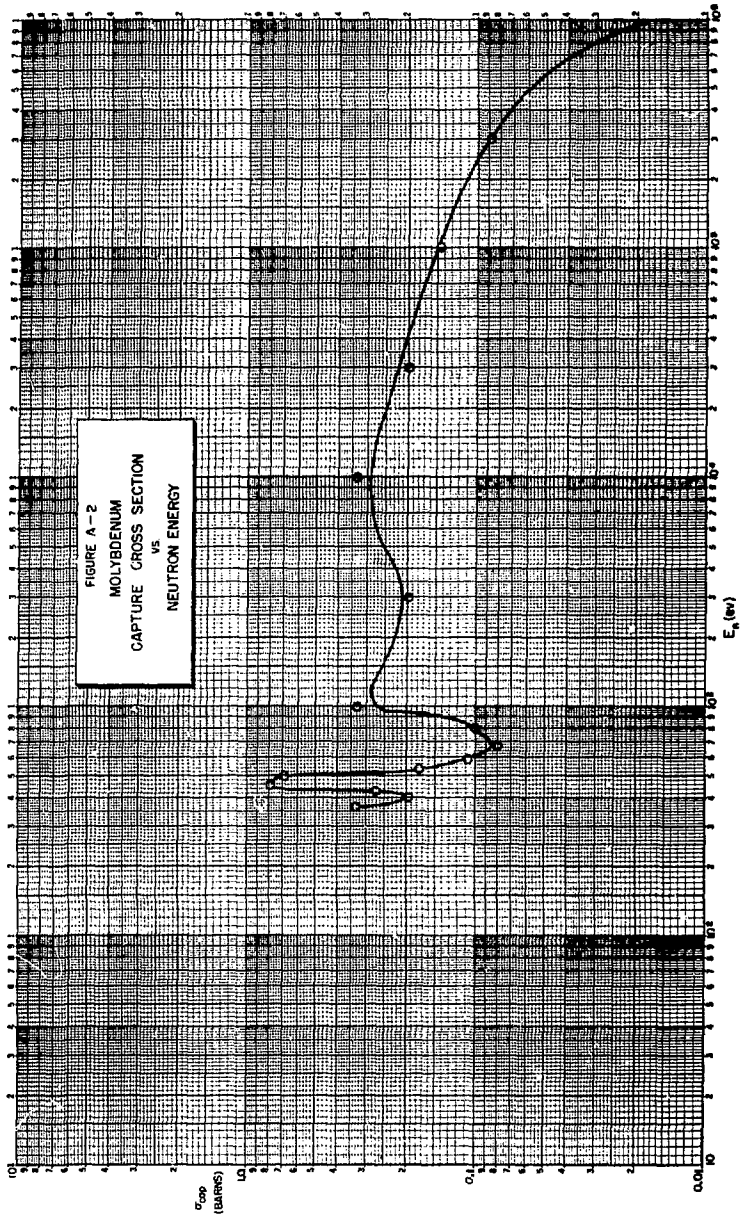


*Handwritten signature*

~~SECRET~~

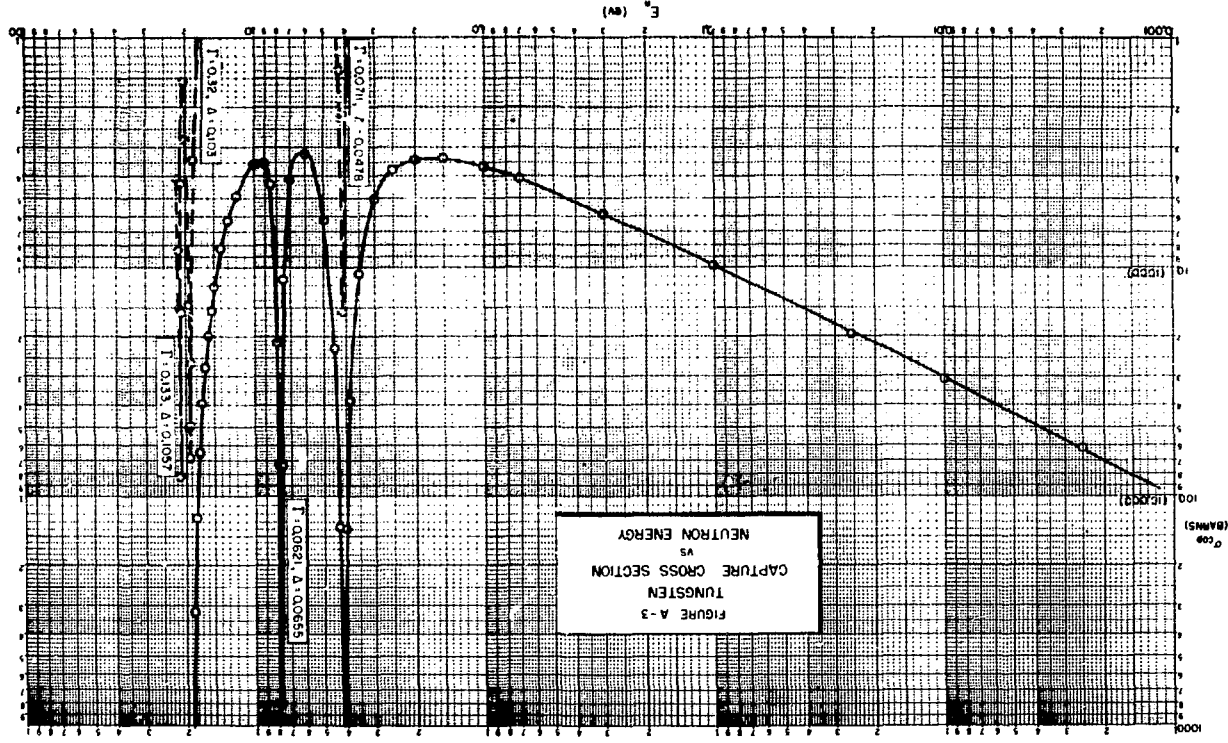
Appendix A

Nuclear Constants



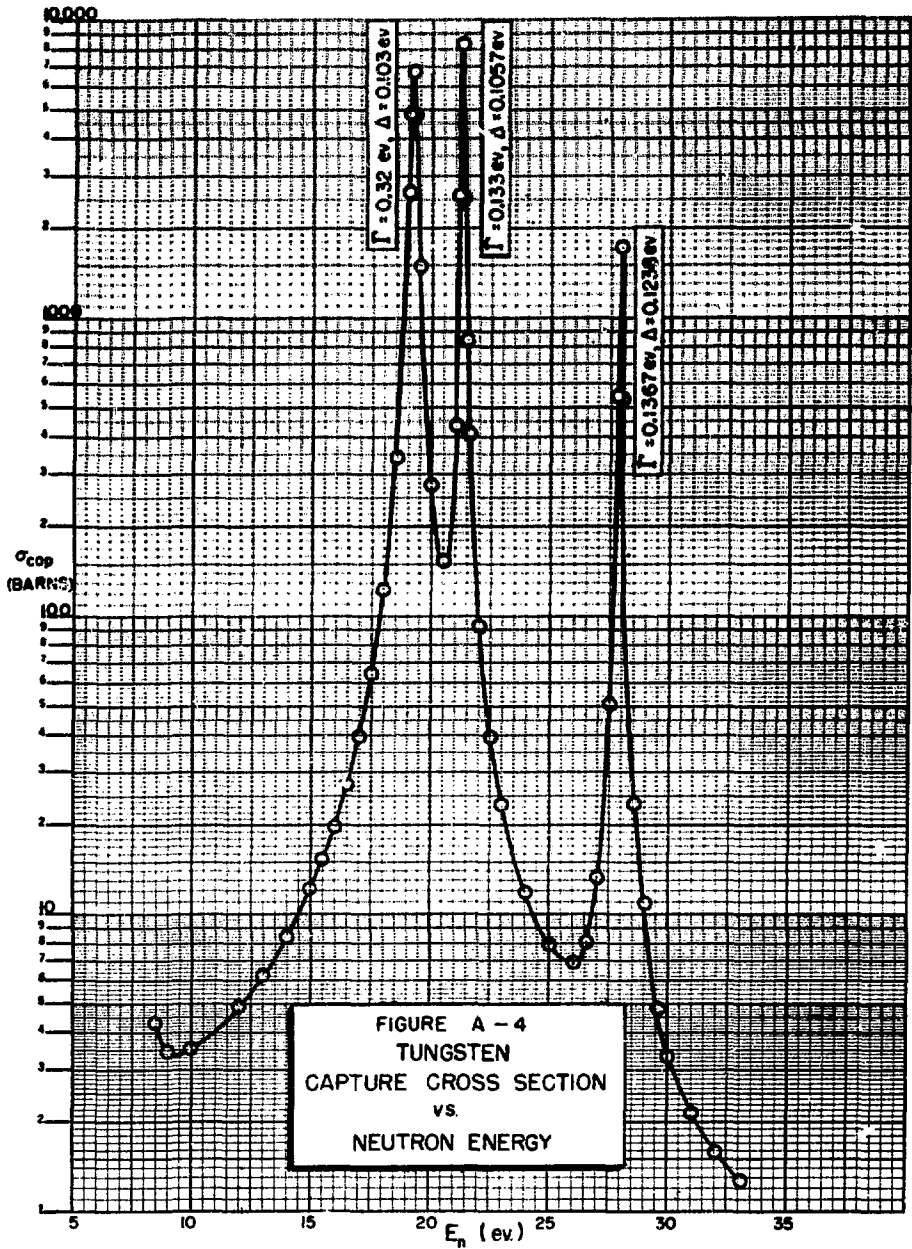
~~SECRET~~

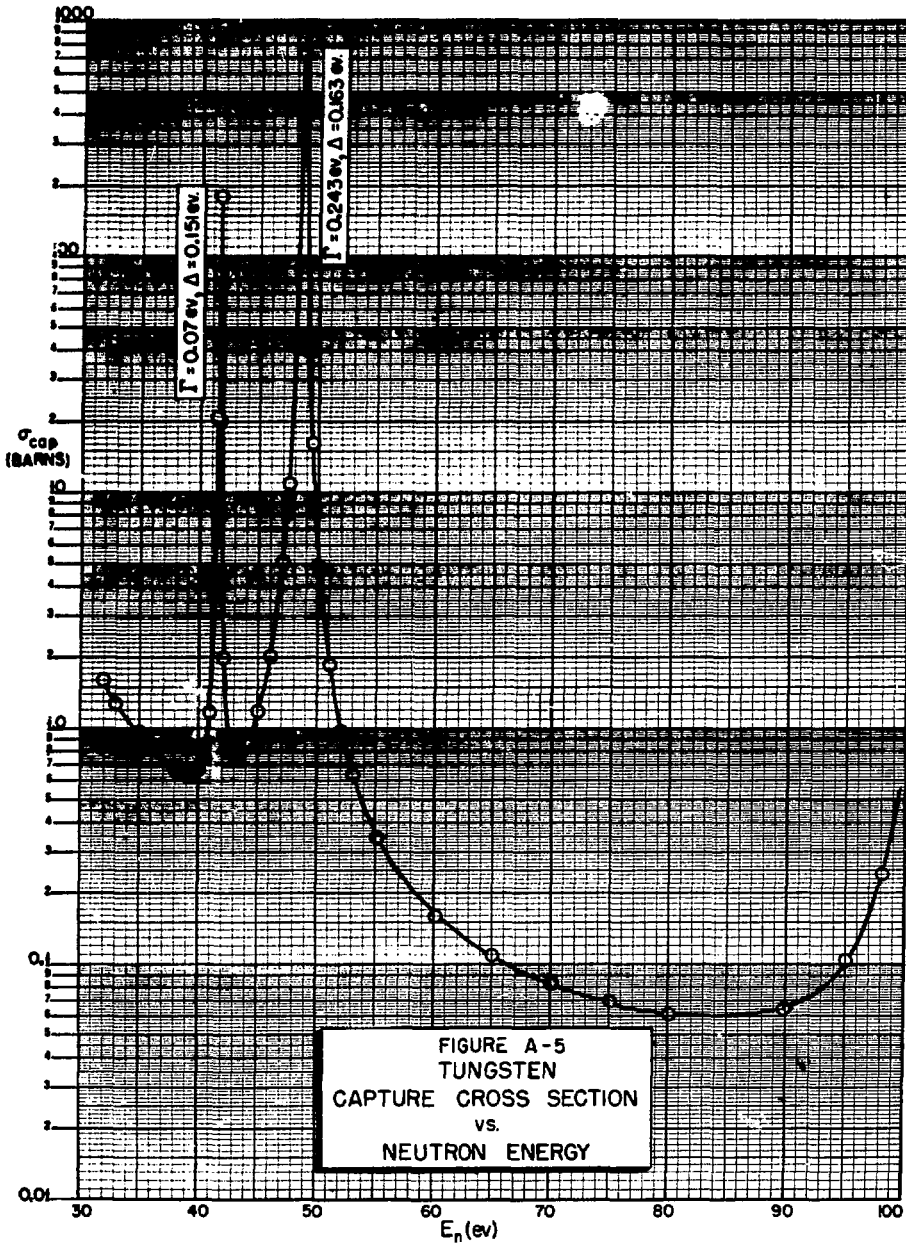
*Handwritten signature*



318  
*Handwritten signature*







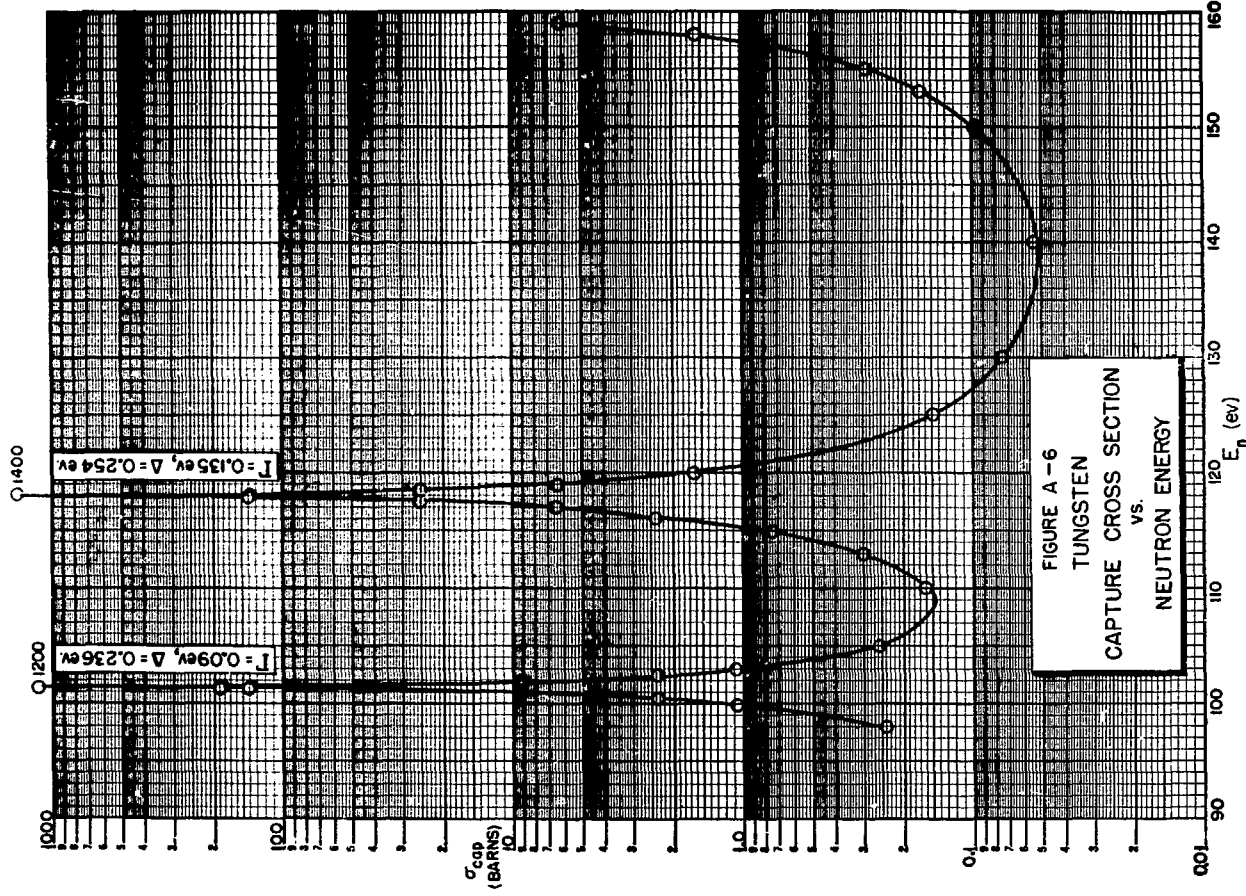
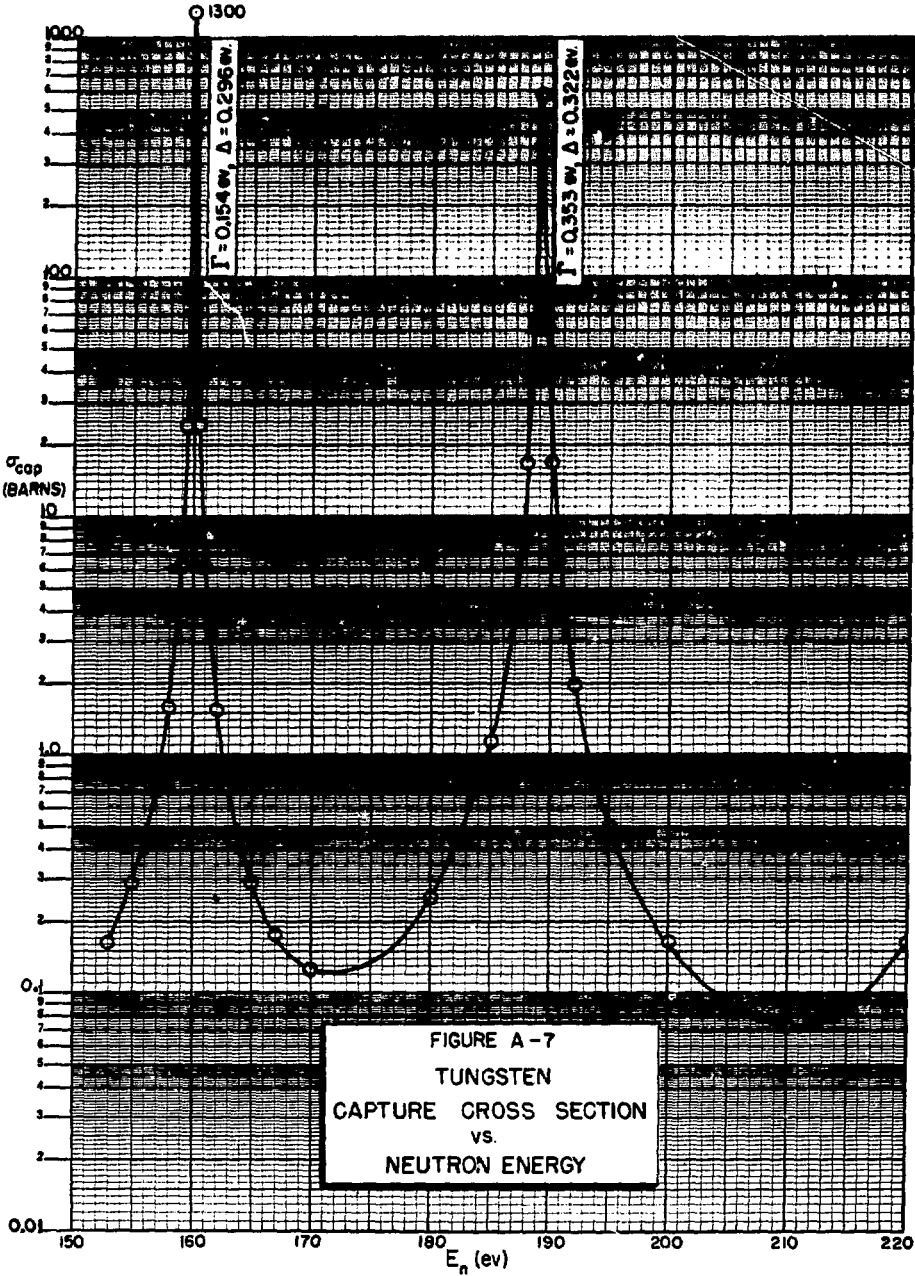


FIGURE A-6  
TUNGSTEN  
CAPTURE CROSS SECTION  
vs.  
NEUTRON ENERGY

*[Handwritten signature]*



*[Handwritten signature]*

~~SECRET~~

Appendix A

Nuclear Constants

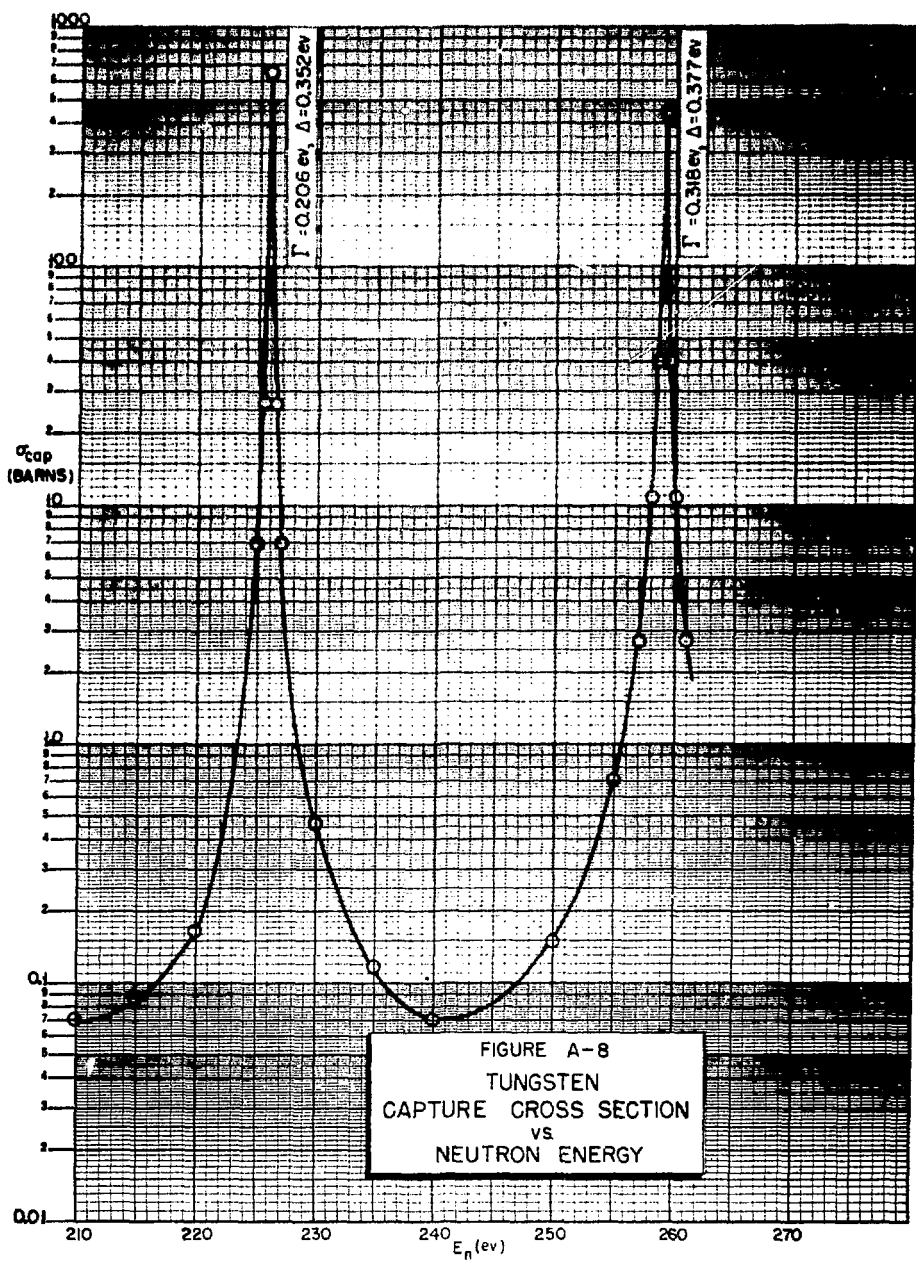
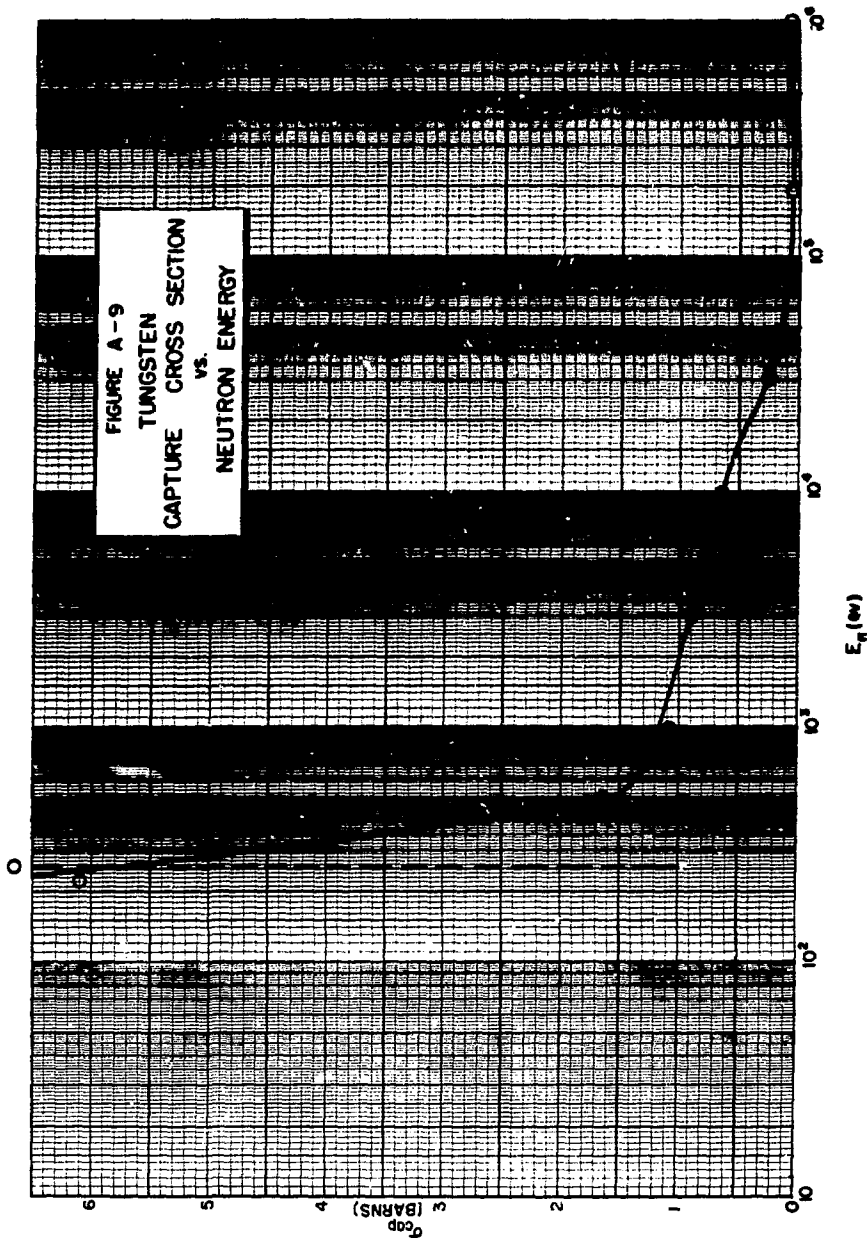


FIGURE A-8  
TUNGSTEN  
CAPTURE CROSS SECTION  
VS  
NEUTRON ENERGY

~~SECRET~~



~~SECRET~~

Appendix B

PHYSICAL PROPERTIES OF REFRACTORY METALS  
by R. B. Gibney

B-1: Introduction

Because of the current interest in refractory metals, a brief survey of the literature on thermal conductivity, coefficient of thermal expansion, and strength properties of the common high melting metals has been made. In general, the data are sketchy, contradictory, and are useful as qualitative information only.

B-2: Thermal Conductivity

The thermal conductivities of molybdenum and tungsten have been measured in the temperature range 1100 - 1900°K. The electrical resistivities have been measured at temperatures up to 2800°K. Shown in Fig. B-1 are the experimental data for the thermal conductivity of molybdenum and the linear extrapolation of these data to higher temperatures. Also shown are points calculated from the experimental electrical resistivity data for molybdenum by judicious use of the "Lorenz constant." These points agree with the extrapolated values, and have been used to compile the data given in Table B-1. Also given in this table are values

Appendix B Physical Properties of Refractory Metals

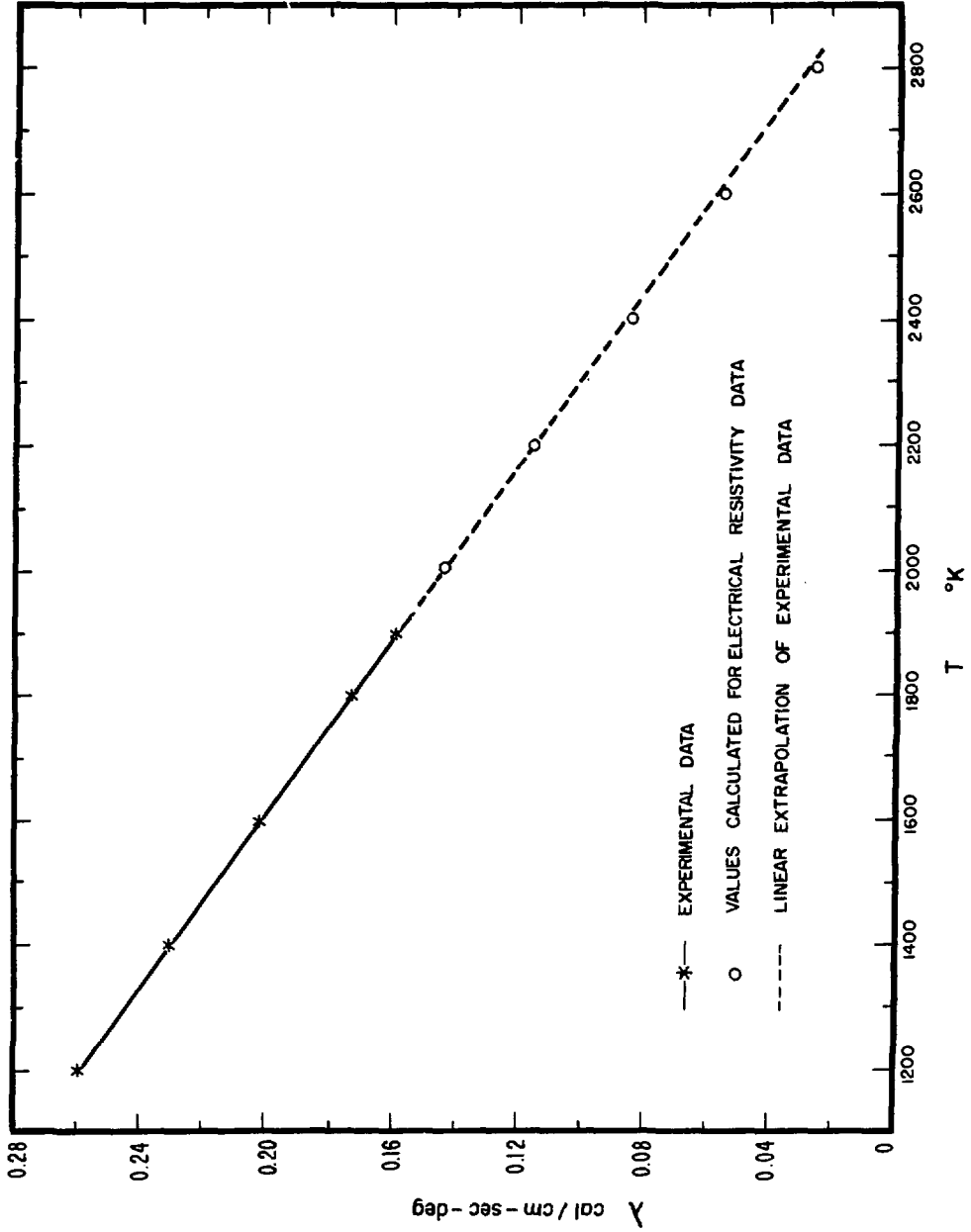


Fig. B-1: Thermal Conductivity of Molybdenum



of the thermal conductivity of tungsten obtained in the same manner.

TABLE B-1 THERMAL CONDUCTIVITY OF TUNGSTEN AND MOLYBDENUM ( watt/cm-deg)		
T (°K)	TUNGSTEN	MOLYBDENUM
1100	1.17	
1200	1.15	1.08
1300	1.14	1.02
1400	1.12	1.96
1500	1.11	0.90
1700	1.07	0.79
1900	1.04	0.67
2100	1.01	0.54
2300	0.98	0.42
2500	0.94	0.30
2700	0.91	0.17

It should be pointed out that the values for thermal conductivity of tungsten found in Smithell's book Tungsten<sup>1</sup> are probably wrong. These are old values by Worthing (1914) who found a positive slope for both molybdenum and tungsten. The work was repeated by Osborn<sup>2</sup> in 1941 with an improved apparatus. The later results are the ones given in Table B-1.

B-3: Coefficient of Thermal Expansion

Equations for the thermal expansion of molybdenum, tungsten, and tantalum, as obtained by Worthing,<sup>3</sup> are given by Eqs. B-1, B-2, and B-3,

~~SECRET~~

Appendix B      Physical Properties of Refractory Metals

respectively. For molybdenum,

$$\frac{L - L_0}{L_0} = 5.00 \times 10^{-6} (T - 300) + 10.5 \times 10^{-10} (T - 300)^2 \quad (B-1)$$

for tantalum,

$$\frac{L - L_0}{L_0} = 6.6 \times 10^{-6} (T - 300) + 5.2 \times 10^{-10} (T - 300)^2 \quad (B-2)$$

for tungsten,

$$\frac{L - L_0}{L} = 4.44 \times 10^{-6} (T - 300) + 4.5 \times 10^{-11} (T - 300)^2 + 2.2 \times 10^{-13} (T - 300)^3 \quad (B-3)$$

where  $L_0$  is the length at 300°K.

B-4: Tensile Strength

The available data on tensile strength at elevated temperature are meager. Since the only work above 2000°K has been on single crystals of molybdenum and tungsten and on some special tungsten wires, the data probably are not applicable to this report. These data are given in Table B-2.

TABLE B-2 TENSILE STRENGTH (psi)				
TEMPERATURE	1500°K	2000°K	2500°K	2800°K
TUNGSTEN	—	10,000	6,000	5,000
TUNGSTEN	12,000	7,500	3,500	—
MOLYBDENUM*	2,200	900	550	300
(*YIELD STRENGTH)				

~~SECRET~~

Tensile Strength

Section B-4

The single crystal of molybdenum had a room temperature yield strength of 8000 psi as compared to 84,000 psi for rolled sheet.

REFERENCES

1. Colin J. Smithells, Tungsten, Chem. Pub. Co., Inc., New York, 1953.
2. R. H. Osborn, J. Opt. Soc. Am. 31, 428 (1941).
3. A. G. Worthing, Phys. Rev. 28, 190 (1926).

329-330

~~SECRET~~

~~SECRET~~

LA-2091 (EXCERPT)

Appendix C

LAMINAR INCOMPRESSIBLE FLOW IN  
CHANNELS WITH POROUS WALLS  
by B. K. Knight, Jr. and B. B. McInteer

C-1: Introduction

In recent years attention has been given to solutions of the Navier-Stokes hydrodynamic equations (or of the boundary-layer equations which approximate them) for problems in which a breathing surface is placed in a stream. Such a surface represents a distributed source or sink of fluid, such a porous wall whose pores are so small and frequent that they may be regarded as continuously distributed. A further characteristic usually applied to these walls is that their flow is specified as a boundary condition of the problem. In other words, for a sufficiently high wall impedance, the flow is determined externally and is not affected by the surface distribution of pressure.\* It is the purpose of this appendix to present solutions to the problem of steady two-dimensional flow through a channel bounded by porous walls which supply or remove an incompressible fluid with a uniform normal velocity.

---

\*This restriction is not necessary to such problems. Recently Taylor has presented a study of an example in which the flow mechanics within a porous wall was intimately linked to the external hydrodynamics. Proc. Roy. Soc. 234A, 456 (1956).

~~SECRET~~

This problem has a number of unusual features of general interest:

(1) The task of solving the problem is reduced to the integration of a single ordinary differential equation; in this sense the problem is solved exactly.

(2) A solution to the problem, satisfying all boundary conditions, is found for the case of vanishing viscosity. This is in contrast to usual boundary-layer analysis, in which wall slippage is avoidable only because of viscosity-dependent terms in the equations.

(3) When the wall is a fluid source the finite-viscosity solutions converge uniformly to that for zero viscosity. However, when the wall is a fluid sink the finite-viscosity solutions do not converge to the zero-viscosity solution but, instead, converge nonuniformly to a flow involving wall slippage in the typical boundary-layer fashion.

(4) The zero-viscosity solution furnishes the basis of a perturbation method which yields results of great precision in the case where the wall is a source. However, when the wall is a sink the same method yields completely erroneous results. For sufficiently small viscosity the perturbation solutions satisfy the exact equations to an arbitrary degree of accuracy, but there is no nearby exact solution. This furnishes a striking counter example to the heuristic justification of perturbation methods in general.

C-2: Formulation of the Problem

Fluid of density  $\rho$  and viscosity  $\eta$  is supplied or removed by two porous walls at a uniform steady rate. The channel width is  $2a$  with the coordinate axes defining planes of symmetry, as shown in Fig. C-1. The

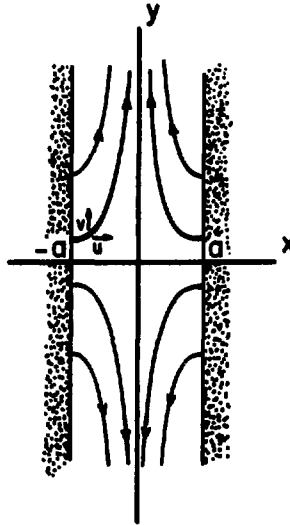


Fig. C-1

velocity components,  $u$  and  $v$ , and pressure  $p$  are related by the Navier-Stokes equations and the equation of continuity, as given by

$$\rho u \frac{\partial u}{\partial x} + \rho v \frac{\partial v}{\partial y} + \frac{\partial p}{\partial x} - \eta \left( \frac{\partial^2 u}{\partial x^2} + \frac{\partial^2 u}{\partial y^2} \right) = 0 \tag{C-1}$$

$$\rho u \frac{\partial v}{\partial x} + \rho v \frac{\partial v}{\partial y} + \frac{\partial p}{\partial y} - \eta \left( \frac{\partial^2 v}{\partial x^2} + \frac{\partial^2 v}{\partial y^2} \right) = 0 \tag{C-2}$$

~~SECRET~~

Appendix C

Laminar Flow Problem

$$\frac{\partial u}{\partial x} + \frac{\partial v}{\partial y} = 0 \quad (C-3)$$

The boundary conditions are

$$u(a,y) = -u(-a,y) = u_0$$

$$v(a,y) = v(-a,y) = 0$$

It is convenient to reduce the problem to dimensionless form by using the dimensionless variables

$$P = \rho/\rho_0^2$$

$$X = x/a$$

$$Y = y/a$$

$$U = -u/u_0$$

$$V = -v/u_0$$

and the dimensionless constant

$$\epsilon = -\eta/\rho_0 a$$

The transformed equations are

$$U \frac{\partial U}{\partial X} + V \frac{\partial U}{\partial Y} + \frac{\partial P}{\partial X} - \epsilon \left( \frac{\partial^2 U}{\partial X^2} + \frac{\partial^2 U}{\partial Y^2} \right) = 0 \quad (C-4)$$

~~SECRET~~

~~SECRET~~

Formulation of the Problem

Section C-2

$$U \frac{\partial V}{\partial X} + V \frac{\partial V}{\partial Y} + \frac{\partial P}{\partial Y} - \epsilon \left( \frac{\partial^2 V}{\partial X^2} + \frac{\partial^2 V}{\partial Y^2} \right) = 0 \quad (C-5)$$

$$\frac{\partial U}{\partial X} + \frac{\partial V}{\partial Y} = 0 \quad (C-6)$$

These equations are of the same form as Eqs. C-1, C-2, and C-3 with unit density and a viscosity  $\epsilon$ . Boundary conditions for X are

$$-U(1) = U(-1) = 1$$

$$V(1) = V(-1) = 0$$

It is plausible that when Y becomes large the flow profile is of the form

$$V = Y f'(X) \quad (C-7)$$

where  $f'$  is the derivative of a function  $f(X)$ . The continuity equation C-6 then requires that

$$U = -f(X) \quad (C-8)$$

The form of Eqs. C-7 and C-8 leads to exact solutions for all values of Y. This is demonstrated as follows: Substitution of these forms into Eq. C-4 indicates each term to be a function of X only, indicating  $\partial P / \partial X$  is a function of X only. Therefore, P must be of the form

$$P = P_0(X) + P_1(Y)$$

Similarly, substitution in Eq. C-5 reveals each term to be of the form

~~SECRET~~



$Y \cdot F(X)$ , so that  $dP_1/dY$  must be of this form, or

$$dP_1/dY = \gamma Y$$

where  $\gamma$  is a constant. Therefore, assigning to  $P(X, Y)$  the form

$$P = \frac{1}{2} \gamma Y^2 + P_0(X) \quad (C-9)$$

allows Eqs. C-4 and C-5 to be reduced to two ordinary differential equations:

$$ff' + P_0'(X) - \epsilon f'' = 0 \quad (C-10)$$

$$\epsilon f''' - f'^2 + ff'' = \gamma \quad (C-11)$$

Solutions of these two equations which satisfy the proper boundary conditions yield an exact solution of the problem. These solutions, hinging upon the arbitrary assumption of Eq. C-8, are not necessarily exhaustive but represent an interesting and informative type of solution.

Equation C-10 is integrated to give

$$P_0 = -\frac{1}{2} f^2 + \epsilon f' + \text{const.} \quad (C-12)$$

The solution of the problem has now been reduced to the solution of Eq. C-11.

The function  $f(X)$  satisfying the differential equation C-11 must satisfy the four boundary conditions

$$f(1) = -f(-1) = 1$$

$$f'(1) = f'(-1) = 0$$

(C-11a)

The four boundary conditions thus stated are to be satisfied by choice of the three constants of integration and the proper value of  $\gamma$ . Equation C-11 is therefore a third order non-linear ordinary differential eigenvalue equation for  $\gamma$  as a function of  $\epsilon$ .

Among the solutions to Eq. C-11 are those which have the symmetry property

$$f(X) = -f(-X)$$

since each term of Eq. C-11 is unchanged under this transformation. This odd symmetry in  $U$  and the resulting even symmetry in  $V$  and  $P$  about  $X = 0$  allow the four boundary conditions to be restated as

$$f(1) = 1$$

$$f'(1) = 0$$

$$f(0) = f''(0) = 0$$

(C-11b)

All solutions presented here satisfy this more restrictive although more convenient combination of boundary conditions. Only the range  $0 \leq X \leq 1$  needs to be considered.

Equation C-11 with the boundary conditions (Eq. C-11b) may be transformed into an initial value problem. This is advantageous, particularly

for purposes of numerical integration. The initial value equation is

$$\frac{d^3g}{dz^3} - \left(\frac{dg}{dz}\right)^2 + g \frac{d^2g}{dz^2} = C \quad (\text{C-13})$$

with the initial conditions  $g(0) = g''(0) = 0$ . Assigning an initial slope  $g'(0)$  and a value to the parameter  $C$  determines a function  $g(z)$ . If  $g'(z)$  vanishes at some point where  $z = z_0$  and  $g$  assumes the value  $g_0$ , then the variables  $X$  and  $f$  are defined as

$$X = z/z_0$$

$$f = g/g_0$$

Equation C-13 then becomes

$$\frac{1}{g_0 z_0} f''' - f'^2 + ff'' = C \frac{z_0^2}{g_0^2} \quad (\text{C-14})$$

which is of the form of Eq. C-11 and satisfies the boundary conditions (Eq. C-11b), when

$$\epsilon = \frac{1}{g_0 z_0}$$

$$\gamma = C \frac{z_0^2}{g_0^2} \quad (\text{C-15})$$

The parameter  $C$  is eliminated by a further scaling property of Eq. C-13. Multiplying  $z$  by any constant  $a$ , and  $g$  by  $1/a$ , yields the same differential equation but with  $Ca^4$  replacing  $C$ . The choice  $|C| = 1/a^4$  reduces

Eq. C-13 to either

$$g''' - g'^2 + gg'' = 1 \tag{C-16}$$

or

$$g''' - g'^2 + gg'' = -1 \tag{C-17}$$

These equations give  $g_0$  and  $z_0$  as functions of  $g'(0)$  only, and together with Eq. C-15 specify  $\gamma(\epsilon)$  by giving  $\gamma$  and  $\epsilon$  parametrically in terms of  $g'(0)$ . Positive values of  $\gamma$  are obtained by Eq. C-16, negative values by Eq. C-17.

C-3: Some Qualitative Features

A few remarks of a physical nature should be made before proceeding with the solution of the formal mathematical problem. On physical grounds, the qualitative behavior of the functions  $f(X)$  and  $\gamma(\epsilon)$  is examined.

In the limit of high-viscosity creeping flow ( $|\epsilon| \gg 1$ ) the flow profile  $f'(X)$  should resemble the familiar Poiseuilleian parabolic flow. The low-viscosity limit is less easily pictured. If fluid is flowing from stream to wall, a flat profile as in potential flow might be maintained throughout the duct, perhaps reverting to shearing flow only in a thin boundary layer, where the fluid approaches very near to the wall and the slight viscosity becomes important. On the other hand, for flow from wall to stream no boundary-layer type of profile is expected, since the

~~SECRET~~

Appendix C

Laminar Flow Problem

boundary layer is continually being carried into the stream.

The function  $\gamma(\epsilon)$  is proportional to the pressure gradient and is determined by the joint effects of viscosity and inertia. When the viscous drag dominates ( $|\epsilon| \gg 1$ ) the pressure gradient is proportional to the viscosity, and in a direction opposite to the flow, giving

$$\gamma \propto (-\epsilon) \tag{C-18}$$

However, the inertial effect is to establish a pressure gradient in a direction opposite to that of fluid acceleration. Since, regardless of the flow direction the fluid acceleration is toward larger values of  $Y$ , for  $|\epsilon| \ll 1$  a negative value of  $\gamma$  is expected. At some negative value of  $\epsilon$  the inertial and viscous effects just balance and there is an intercept where  $\gamma = 0$ .

These general features are verified in the next section.

C-4: Methods of Solution

Four types of solution of Eqs. C-11 and C-11b are used:

- A. Exact solutions for special cases.
- B. Perturbations upon these solutions.
- C. Solutions from a variational method.
- D. Machine integration by a Runge-Kutta method.

These types are considered separately.

A. Solutions in Closed Form

Exact analytical solutions of Eq. C-11 are obtained for two special

~~SECRET~~ 693 030

cases only. Further analysis of these cases is made in Sec. C-5.

Case I: In this case  $1/\epsilon = 0$ . If all terms not involving  $\epsilon$  are omitted from the l.h.s. of Eq. C-11 it simplifies to

$$\epsilon f''' = \gamma \quad (\text{C-19})$$

The solution of this equation satisfying the boundary conditions is

$$f = \frac{3}{2} X - \frac{1}{2} X^3 \quad (\text{C-20})$$

$$\gamma = -3\epsilon \quad (\text{C-21})$$

This result corresponds to viscous creeping flow without momentum terms. Differentiation of Eq. C-20 yields the familiar parabolic flow distribution for  $V$ .

Case II: For this case  $\epsilon = 0$ . As is well known, caution must be exercised in omitting all terms involving viscosity  $\epsilon$  in the hydrodynamic equations to obtain solutions describing slightly viscous fluids. Formally, this omission reduces the order of the differential equations and might not allow all boundary conditions to be satisfied. Physically, the fluid must not slip on the walls even though its viscosity is vanishingly small.

In this problem, however, the dropping of the term involving  $\epsilon$  in Eq. C-11 leaves an equation which may be solved satisfying all boundary conditions. The modified differential equation is

*[Handwritten signature]*

$$-f'^2 + ff'' = \gamma \tag{C-22}$$

A set of eigenfunctions and eigenvalues that form solutions to this problem are given in Table C-1. The second and higher functional forms

TABLE C-1 SOLUTIONS OF EQ. C-22			
f	$\sin \frac{\pi}{2} X$	$-\sin \frac{3\pi}{2} X$	$\sin \frac{5\pi}{2} X \dots$
$\gamma$	$-\frac{\pi^2}{4}$	$-\frac{9\pi^2}{4}$	$-\frac{25\pi^2}{4} \dots$

for f, shown in this table, are startling since the corresponding velocity profile V is positive for some values of X and negative for others. The first function is physically plausible and is not greatly different from the parabolic profile considered in Case I.

In summary, exact analytic solutions of Eq. C-11 are obtained only for cases in which certain terms vanish.

It is interesting that the  $\epsilon = 0$  situation gives rise to an infinite set of solutions, while for  $\frac{1}{\epsilon} = 0$  the solution is unique. This suggests that for finite  $\epsilon$  there are several solutions, corresponding to counter-flow situations, until  $\epsilon$  exceeds some critical value.

B. Perturbation Methods

Perturbation solutions are obtained about the Case I solution and the first of the Case II solutions.

Case I Perturbation Solutions: If  $R = 1/\epsilon$ , the previous exact

342  
*[Handwritten signature]* 653 012

solution, given by Eqs. C-20 and C-21, is that for  $R = 0$ . This solution is denoted by  $f_0$ . It is assumed that  $f$  may be expanded as

$$f = f_0 + f_1 R + f_2 R^2 + f_3 R^3 + \dots \tag{C-23}$$

Since  $\gamma = -3\epsilon$  is the eigenvalue of the exact solution, a quantity  $\lambda = \gamma/\epsilon$  is defined. It is assumed that  $\lambda$  may also be expanded as

$$\lambda = \lambda_0 + \lambda_1 R + \lambda_2 R^2 + \lambda_3 R^3 + \dots \tag{C-24}$$

where  $\lambda_0 = -3$ . Inserting these expressions into Eq. C-11 and equating the coefficient of each power of  $R$  to zero yields the perturbation equations given by

$$\begin{aligned} f_0''' &= \lambda_0 \\ f_1''' &= \lambda_1 + f_0'^2 - f_0 f_0'' \\ f_2''' &= \lambda_2 + 2f_0' f_1'' - f_1 f_0''' - f_0 f_1'' \\ f_3''' &= \lambda_3 + f_1'^2 + 2f_0' f_2' - f_0'' f_2 - f_1 f_1'' - f_0 f_2'' \\ &\vdots \end{aligned} \tag{C-25}$$

with the boundary conditions, for  $n > 0$ ,

$$f_n(0) = f_n''(0) = f_n(1) = f_n'(1) = 0 \tag{C-26}$$

Each equation equates the third derivative of the unknown solution to a known function of  $X$  involving previously obtained solutions. All solutions are polynomials. Carrying out this procedure through the second



~~SECRET~~

Appendix C

Laminar Flow Problem

---

order perturbation yields for  $f$

$$\begin{aligned} f = & X(1.500 + 0.0071428R - 0.0005434 R^2) \\ & - X^3(0.5000 + 0.0107142R - 0.0006772 R^2) \\ & + X^7(0.0035714 R + 0.0001530 R^2) \\ & - 0.0002976 R^2 X^9 + 0.0000108 R^2 X^{11} + \dots \end{aligned} \quad (C-27)$$

with additional terms being of the order  $R^3$  and higher. The corresponding expression for  $\gamma$  is

$$\gamma = -3\epsilon - 2.3142857 - 0.0173655/\epsilon + \dots \quad (C-28)$$

Case II Perturbation Solutions: A similar procedure is followed for obtaining perturbation solutions about the Case II exact solution. It is convenient to make the substitutions

$$\xi = \frac{\pi}{2} x$$

$$\eta = \frac{\pi}{2} \epsilon$$

$$\lambda = \left(\frac{2}{\pi}\right)^2 \gamma$$

and Eq. C-11 becomes

$$\eta f''' - f'^2 + ff'' = \lambda \quad (C-29)$$

with the boundary conditions

~~SECRET~~

$$f(0) = f''(0) = f'(\frac{\pi}{2}) = 0; \quad f(\frac{\pi}{2}) = 1$$

where primes denote differentiation with respect to  $\xi$ . Assuming that

$$f = f_0 + \eta f_1 + \eta^2 f_2 + \dots$$

$$\lambda = \lambda_0 + \eta \lambda_1 + \eta^2 \lambda_2 + \dots$$

yields the perturbation equations, given by

$$-f_0'^2 + f_0 f_0'' = \lambda_0$$

$$f_0 f_1'' - 2 f_0' f_1' + f_0'' f_1 = \lambda_1 - f_0'''$$

$$f_0 f_2'' - 2 f_0' f_2' + f_0'' f_2 = \lambda_2 - f_1''' + f_1'^2 - f_1 f_1''$$

⋮

(C-30)

with the boundary conditions, for  $n > 0$ ,

$$f_n(0) = f_n''(0) = f_n(\frac{\pi}{2}) = f_n'(\frac{\pi}{2}) = 0$$

The previous solution of the zeroth order equation is

$$f_0 = \sin \xi$$

$$\lambda_0 = -1$$

(C-31)

The remaining equations are linear with variable coefficients, having the form

350119

$$\sin \xi f_n'' - 2 \cos \xi f_n' - \sin \xi f_n = \lambda_n + F(\xi)$$

The solution of the first order perturbation equation is given by

$$f_1 = -\frac{1}{2} \lambda_1 \xi \cos \xi - \frac{1}{2} \sin \xi \ln \tan \xi/2 + \frac{1}{2} \cos \xi \int_0^\xi \ln \tan \xi'/2 d\xi' \quad (C-32a)$$

or, alternatively,

$$f_1 = -\frac{1}{2} \lambda_1 \xi \cos \xi - 2 \sum_{\substack{k=2 \\ k \text{ even}}}^{\infty} \frac{1}{(k-1)^2 (k+1)^2} \sin k \xi \quad (C-32b)$$

where

$$\begin{aligned} \lambda_1 &= \frac{2}{\pi} \left[ 1 + \int_0^{\pi/2} \ln \tan \xi/2 d\xi \right] \\ &= \frac{2}{\pi} \left[ 1 + 2 \sum_{k=0}^{\infty} \frac{(-)^{k+1}}{(2k+1)^2} \right] = \frac{8}{\pi} \sum_{\substack{k=2 \\ k \text{ even}}}^{\infty} \frac{(-)^{\frac{k}{2}} k}{(k+1)^2 (k-1)^2} = -0.5290 \end{aligned} \quad (C-33)$$

This gives

$$\gamma = -2.46741 - 2.053 \epsilon + O(\epsilon^2) \quad (C-34)$$

Figure C-2 shows a plot of  $\gamma$  versus  $\epsilon$ . For large  $\epsilon$ ,  $\gamma(\epsilon)$  is asymptotic to the straight line  $\gamma = -3\epsilon - 2.314$ . For small  $\epsilon$  the perturbation solution is given by  $\gamma = -2.05\epsilon - 2.467$ . The similarity of these functions suggests that they might merge smoothly to form the primary

*[Handwritten signature]*

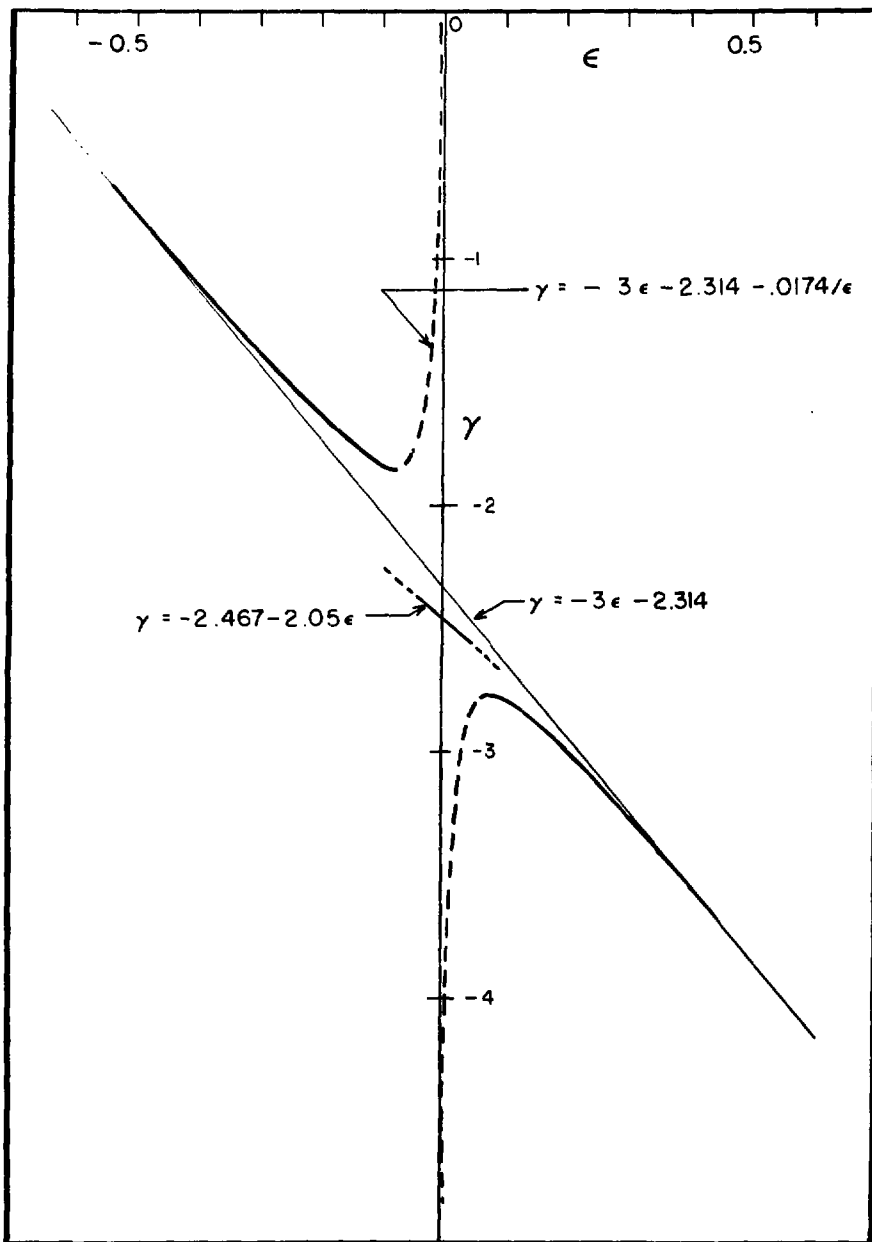


Fig. C-2: Perturbation Results

structure of the complete curve. The modified parabolic (large  $\epsilon$ ) and the modified cosine (small  $\epsilon$ ) flow profiles also might blend smoothly, lending weight to this possibility. However, this suggested behavior does not occur, as is shown by the variational and numerical solutions which follow.

### C. The Variational Method

As a numerical method of determining  $\gamma(\epsilon)$  with only moderate computational effort, a variational method is applied to this problem as follows: A trial function  $f$ , which satisfies the boundary conditions, is assumed to contain a variational parameter  $\alpha$ . Then Eq. C-11 is not satisfied unless  $f$  is an exact solution. Functions  $F$  and  $I$  are defined by

$$F = \epsilon f''' - f'^2 + ff'' - \gamma \quad (C-35)$$

and

$$I(\alpha, \gamma, \epsilon) = \int_0^1 F^2 dX \quad (C-36)$$

A least squares fit is obtained when  $I$  is minimized, requiring that

$$\frac{\partial I}{\partial \alpha} = 0.$$

$$\frac{\partial I}{\partial \gamma} = 0 \quad (C-37)$$

The pair of relations, given in Eq. C-37, between  $\alpha$ ,  $\gamma$ , and  $\epsilon$  are solved for  $\gamma(\epsilon)$ .

The trial functions used for this computation are

$$f' = \alpha(1-X^2) + \beta(1-X^n) \tag{C-38}$$

where  $n = 2, 4, 8,$  and  $16$ , and  $\beta$  is expressed in terms of  $\alpha$  by using Eq. C-11b. The case where  $n = 2$  is degenerate, with no real variational parameter included in  $f$ . The resulting functions  $\gamma(\epsilon)$  are shown in Fig. C-3. Table C-2 lists the values of  $\gamma(0)$  and the limiting asymptotes

TABLE C-2		
RESULTS OF THE VARIATIONAL METHOD		
	$\gamma(0)$	LIMITING ASYMPTOTE ( $\epsilon \rightarrow \infty$ )
EXACT	-2.46741	$\gamma = -3\epsilon - 2.314286$
$n = 2$	-2.4000	$\gamma = -3\epsilon - 2.40000$
$n = 4$	-2.46712	$\gamma = -3\epsilon - 2.314284$
$n = 8$	-2.4559	$\gamma = -3\epsilon - 2.310200$
$n = 16$	-2.34	$\gamma = -3\epsilon - 2.43158$

of  $\gamma(\epsilon)$  for large  $\epsilon$ . For very large and very small  $|\epsilon|$ , the values for  $n = 4$  and  $8$  are in close agreement with the exact solutions already obtained. Only a few spot checks of the actual values of  $I$  have been made on these two cases. The poorest fit is found along the sharp drop exhibited by both these functions as they change from above the asymptotic

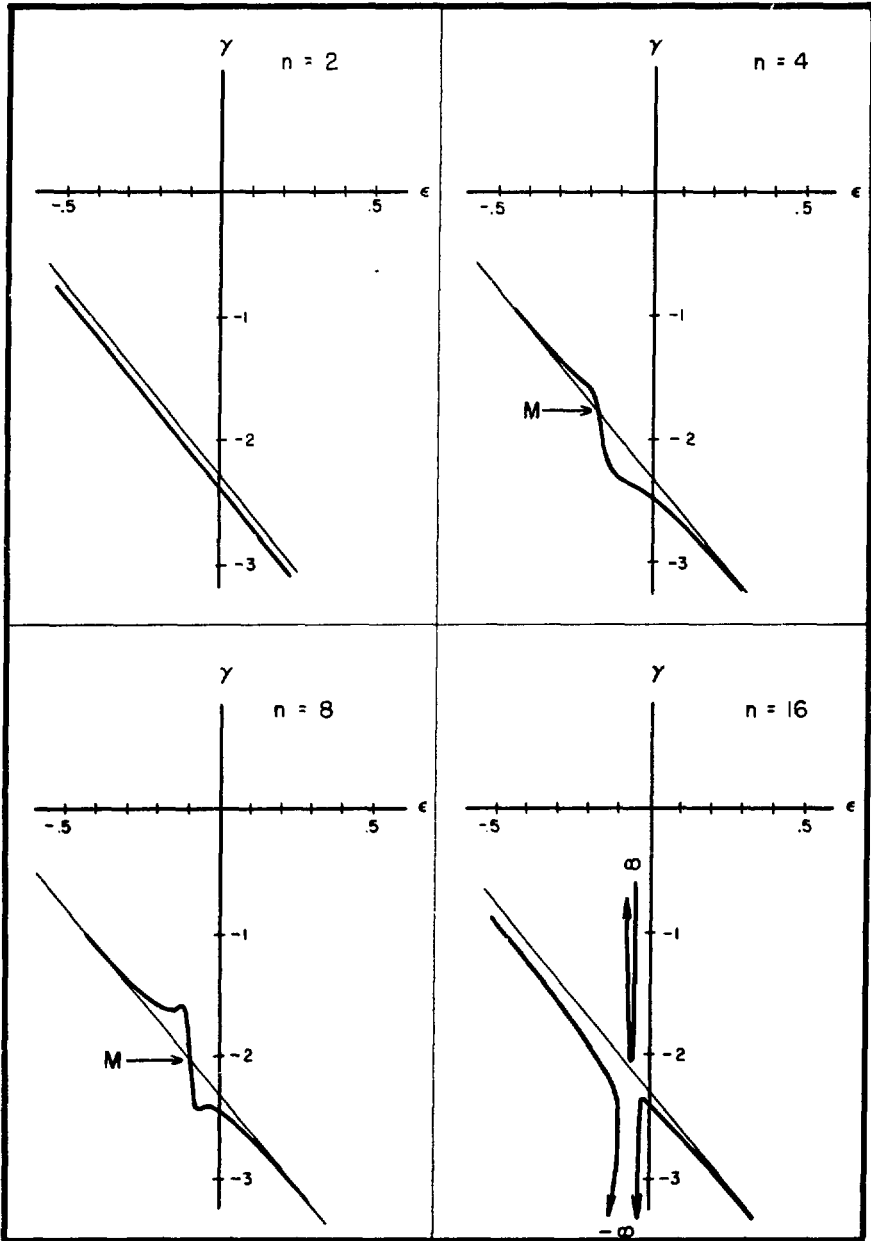


Fig. C-3: Variational Results

straight line to below it, at the point M, as shown in Fig. C-3. Near the point M the trial function for  $n = 8$  is a better fit than for  $n = 4$ .

For  $n = 4$  and  $n = 8$  the corresponding flow profiles for values of  $\epsilon$  immediately to the left of the point M are of the flattened boundary-layer type, mentioned in Sec. C-3. Crossing the point M causes an abrupt transition to a cosine-like profile.

#### D. Exact Numerical Solutions

Equation C-11 is integrated numerically, for various values of  $\epsilon$ , in the forms given by Eqs. C-16 and C-17. An  $h^4$  Runge-Kutta method has been used on the Los Alamos 704 digital computer. The resulting  $\gamma(\epsilon)$  curve is shown in Fig. C-4 and some of the corresponding flow profiles are given in Fig. C-5. Table C-3 presents numerical results for  $\gamma(\epsilon)$  obtained by all methods.

The  $\gamma(\epsilon)$  curve which is obtained by numerical integration consists of several branches, denoted by A, B, and C in Fig. C-4. The curve A is obtained from Eq. C-17 with  $-\infty < g'(0) < -1$ . The curve C is obtained from Eq. C-17 with  $0 < g'(0) < 1$ .

Two unexpected branches of the  $\gamma(\epsilon)$  curve were uncovered by these computations. One is curve B of Fig. C-4, which is obtained from Eq. C-17 when  $-1 < g'(0) < 0$ . A second unexpected branch is generated by Eq. C-16 when  $0 < g'(0) < 1$ . It consists of small positive values of  $\gamma$  for positive  $\epsilon$ , and is not shown in the figure. Solutions yielding this remarkable behavior are hard to imagine, since a vanishing  $\gamma$  implies



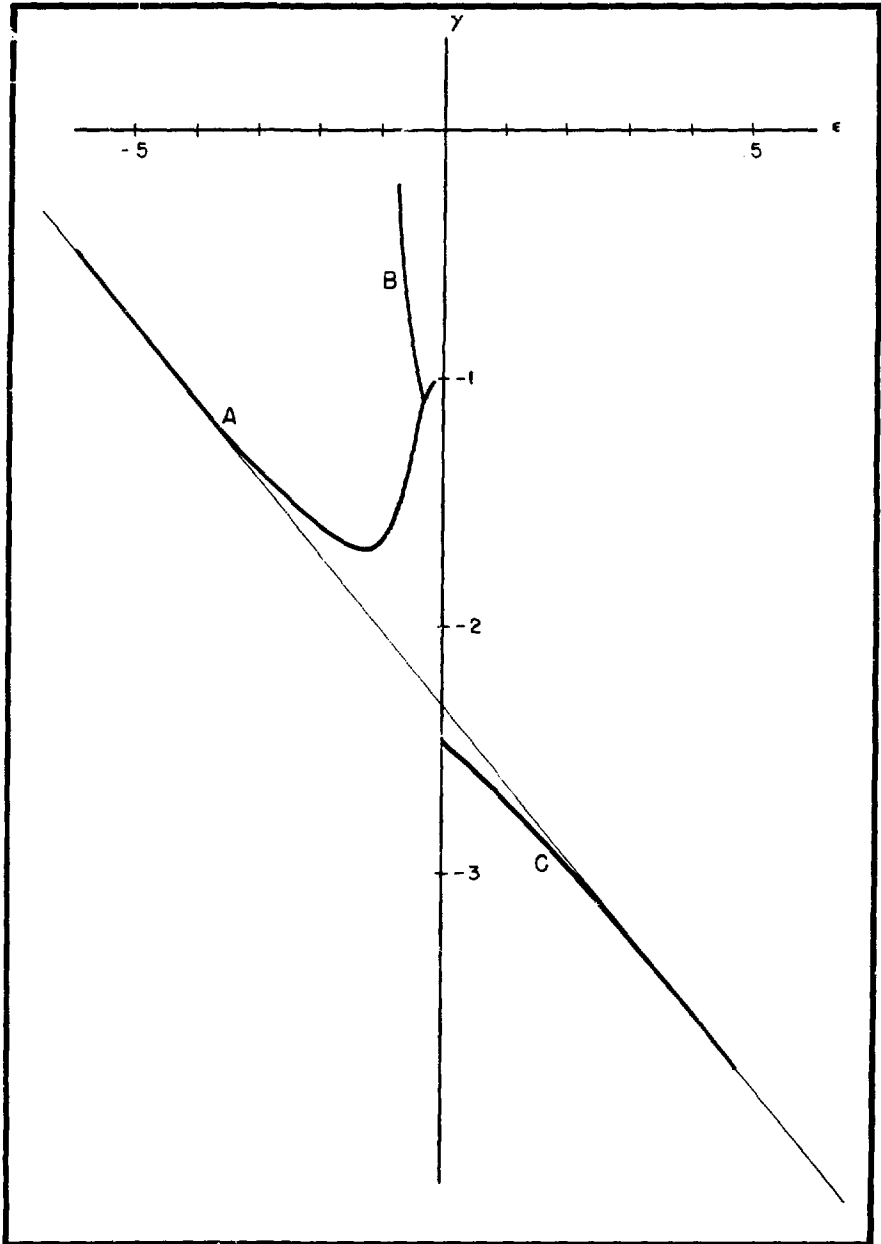


Fig. C-4: Machine Integration Results

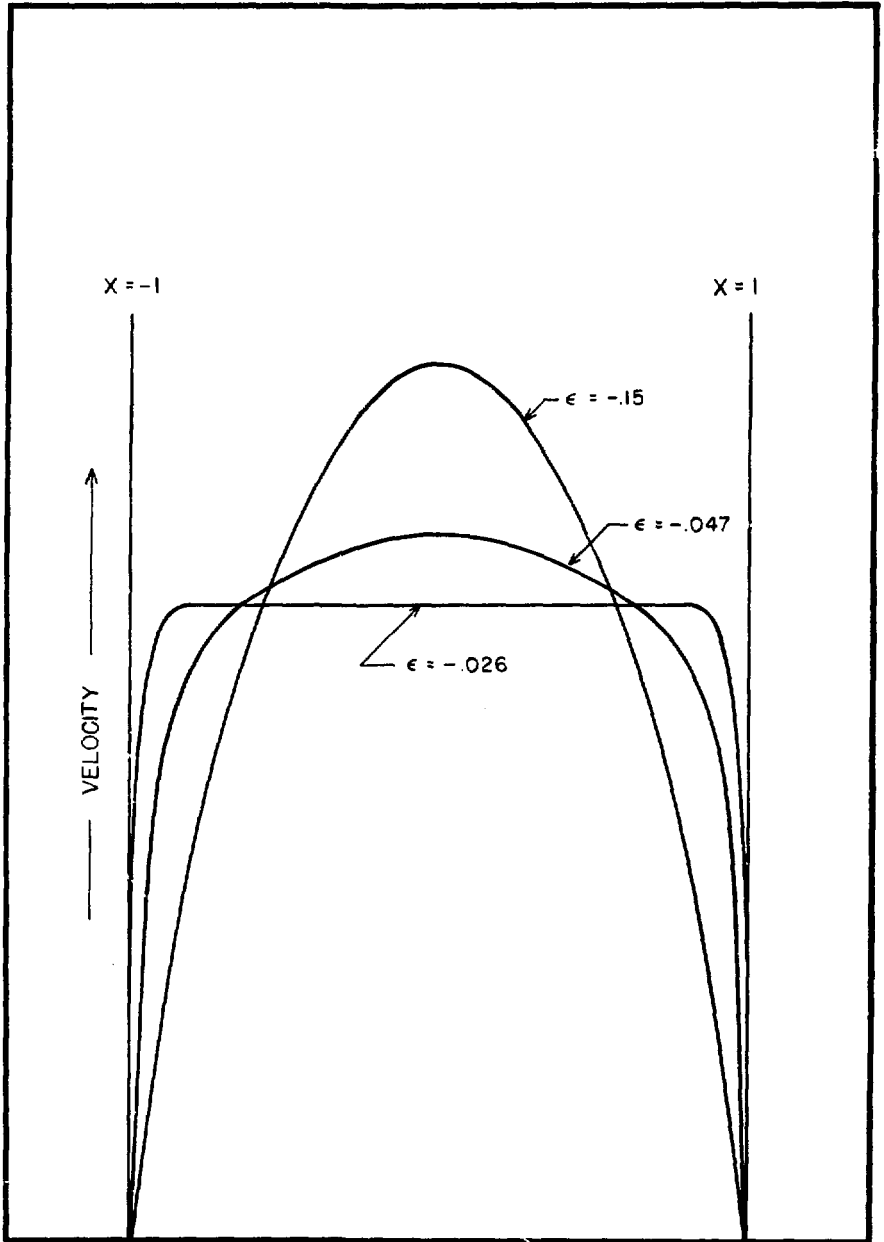


Fig. C-5: Flow Profiles for Negative  $\epsilon$

~~SECRET~~

Appendix C

Laminar Flow Problem

Table C-3

Values of  $\gamma$  Obtained by Different Methods

$\epsilon$	Large $\epsilon$ Perturbation	Small $\epsilon$ Perturbation	Variational Method		Runge- Kutta
			n = 4	n = 8	
-.50	-0.780		-	-.787	-.774
-.45	-0.926		-	-.935	-.917
-.40	-1.071		-	-1.079	-1.063
-.35	-1.215		-1.180	-1.218	-1.207
-.30	-1.356		-1.307	-1.352	-1.342
-.25	-1.495		-1.438	-1.481	-1.465
-.20	-1.628		-1.608	-1.589	-1.574
-.18	-1.678		-1.754	-1.622	-1.612
-.16	-1.726		-1.997	-1.639	-1.647
-.14	-1.770		-2.213	-1.628	-1.676
-.12	-1.810		-2.303	-1.592	-1.678
-.11	-1.826		-2.316	-1.648	-1.668
-.10	-1.841		-2.322	-1.845	-1.647
-.09	-1.851		-2.331	-2.295	-1.615
-.08	-1.957		-2.342	-2.417	-1.567
-.07	-1.856		-2.353	-2.431	-1.502
-.06	-1.845		-2.366	-2.422	-1.410
-.05		-2.365	-2.381	-2.414	-1.300
-.04		-2.385	-2.396	-2.412	-1.197
-.03		-2.406	-2.412	-2.417	-1.083
-.02		-2.426	-2.430	-2.425	-1.030
-.01		-2.447	-2.449	-2.438	-1.007
.0		-2.467	-2.468	-2.454	-1.000
.02		-2.509	-2.510	-2.494	-2.510
.04		-2.550	-2.556	-2.538	-2.553
.06	-2.784		-2.603	-2.585	-2.603
.08	-2.771		-2.653	-2.636	-2.653
.1	-2.788		-2.704	-2.688	-2.692
.15	-2.880		-2.836	-2.827	-2.823
.20	-3.001		-2.973	-2.970	-2.973
.25	-3.134			-3.118	-3.118
.30	-3.272			-3.265	-3.265
.35	-3.414			-3.411	-3.411
.40	-3.558			-3.556	-3.556
.45	-3.703			-3.703	-3.703
.50	-3.849			-3.848	-3.848

~~SECRET~~

zero pressure drop. Unfortunately no provision for exhibiting the corresponding flow profiles was made in the computer program.

Other solutions could be found by integrating to further zeros of  $g'$ . These would lead to other branches of the  $\gamma(\epsilon)$  curve shown in Fig. C-4. However, these physically questionable solutions have not been investigated.

Except in the region  $-0.3 < \epsilon < 0$ , the numerical results are in excellent agreement with the approximate results already given. When  $\epsilon \rightarrow 0+$  the flow profile is a cosine function and  $\gamma$  equals  $\pi^2/4$ , as predicted previously. However, when  $\epsilon \rightarrow 0-$  the flow assumes the boundary-layer type of profile, shown in Fig. C-5, and  $\gamma$  equals -1. The perturbation and variational results in this range are misleading.

C-5: Three Limiting Results

Among the solutions which have been presented here, three merit special attention as limiting forms of practical physical solutions.

Special Result 1: Strongly viscous flow ( $\epsilon \rightarrow +\infty$ )

This case of highly viscous flow is presented as Case I of the exact solutions. Its existence and that of its perturbation is verified by the numerical integrations. It is convenient to average  $V = Y f'(X)$  over  $X$ , so that  $\bar{V} = Y$  and  $\bar{v} = u_{0Y}$  since  $\bar{f}' = \int_0^1 f' dx = 1$ .

Appendix C

Laminar Flow Problem

Solutions

$$f = \frac{3}{2} X - \frac{1}{2} X^3$$

$$\gamma = -3 \epsilon$$

$$U = \frac{1}{2} X^3 - \frac{3}{2} X$$

$$V = \frac{3}{2} Y (1 - X^2)$$

$$P = -\frac{3}{2} \epsilon Y^2 + \frac{3}{2} \epsilon X^2$$

$$p = \frac{3}{2} \frac{\eta u_0}{\sigma^3} (y^2 - x^2)$$

$$p = \frac{3}{2} \frac{\eta}{\sigma} \frac{\bar{v}^2}{u_0} - \frac{3}{2} \frac{\eta u_0}{\sigma^3} x^2$$

$$v = \frac{3}{2} \bar{v} (1 - \frac{x^2}{a^2})$$

$$u = -u_0 x (\frac{1}{2} x^2 - \frac{3}{2})$$

**Special Result 2: Fluid entering channel from walls ( $\epsilon \rightarrow 0+$ )**

The solution obtained as Case II of the exact solutions is shown by machine integration to be the limiting form for  $\epsilon \rightarrow 0$  from the positive side. It is an unusual flow pattern for a fluid of vanishingly small viscosity, and has none of the characteristics predicted by boundary-layer assumptions.

Solutions

$$f = \sin \frac{\pi}{2} X$$

$$\gamma = -(\pi/2)^2$$

$$U = -\sin \frac{\pi}{2} X$$

$$V = Y \frac{\pi}{2} \cos \frac{\pi}{2} X$$

$$P = -\frac{1}{2} \left(\frac{\pi}{2}\right)^2 Y^2 - \frac{1}{2} \sin^2 \frac{\pi}{2} X$$

$$p = -\frac{1}{2} \left(\frac{\pi}{2}\right)^2 \rho u_0^2 \left(\frac{Y}{a}\right)^2 - \frac{1}{2} \rho u_0^2 \sin^2 \frac{\pi}{2} \frac{X}{a}$$

$$p = -\frac{1}{2} \left(\frac{\pi}{2}\right)^2 \rho \bar{v}^2 - \frac{1}{2} \rho u_0^2 \sin^2 \frac{\pi}{2} \frac{X}{a}$$

$$v = \bar{v} \frac{\pi}{2} \cos \frac{\pi}{2} \frac{X}{a}$$

$$u = u_0 \sin \frac{\pi}{2} \frac{X}{a}$$

The coefficient of  $\rho \bar{v}^2$  in  $p$  is 1.234 and is exactly  $\rho \bar{v}^2$ . If a naive one-dimensional Bernoulli law approach is used on this problem without analysis, only half this pressure variation is predicted. Along a streamline, however, the Bernoulli relation  $p + \frac{1}{2} \rho v^2 = \text{const.}$  applies.

Special Result 3: Fluid leaving channel through walls ( $\epsilon \rightarrow 0^-$ )

When  $\epsilon \rightarrow 0$  from the negative side a squared-off profile is attained as indicated by machine results. Except near the boundaries the solution is given by

$$f = X$$

$$\gamma = -1$$

$$U = -X$$

$$V = Y$$

$$P = -\frac{1}{2} Y^2 - \frac{1}{2} X^2$$

$$p = -\frac{1}{2} \rho \bar{v}^2 - \frac{1}{2} \rho u_0^2 \frac{X^2}{a^2}$$

$$v = \bar{v}$$

$$u = u_0 \frac{X}{a}$$

The velocity components  $U$  and  $V$  in Special Result 3 may be obtained from the potential function  $\Phi = \frac{1}{2} (Y^2 - X^2)$ , and thus the flow is irrotational. Irrotational flow at large values of  $Y$  insures that the flow is irrotational everywhere, because in a non-viscous fluid the vorticity is constant along a streamline. On the other hand, in Special Result 2 the fluid enters the channel from the wall with a finite vorticity, and potential flow can never be established.

#### C-6: Some Unanswered Problems

Certain gaps are evident in the foregoing analysis and results.

1. It is not clear whether skewed solutions of Eq. C-11 may exist which satisfy the boundary conditions given by Eq. C-11a but not the symmetry requirements of Eq. C-11b. No evidence for such skewed solutions has been found.

2. No analytical development of the limiting functional form for  $f$  as  $\epsilon \rightarrow 0^-$  has been performed.

3. There has been found no rigorous analytic prediction of the non-uniform convergence of  $f$  for  $\epsilon \rightarrow 0^-$ . The discontinuities in  $f$  and  $\gamma$  occurring about this point should be evident from analysis of the differential equation. A perturbation treatment of Eq. C-13 with  $C = -1$  and  $g'(0) = +1 - \delta$  is suggestive of the machine results. It is shown that if the positive sign is chosen all orders of perturbation are well behaved, but choosing the negative sign yields a second order perturbation behaving asymptotically like  $e^{\frac{1}{2}z^2}$ . Although this gives the observed sharp break in the flow profile, it also invalidates the perturbation assumptions. No mathematical proof of this profile shape has yet been achieved.

A problem related to the solutions for the steady state flow is a stability analysis of the various types of flow predicted here. However, this problem is not considered in this report.

#### C-7: Other Channel Shapes

The general procedure of Sec. C-2 is applied to arbitrary uniform channel cross sections, resulting in a non-linear partial differential eigenvalue equation of the fourth order with one dependent and two independent variables.



~~SECRET~~

Appendix C

Laminar Flow Problem

The three-dimensional Navier-Stokes equations for time-independent incompressible flow are

$$\rho(\vec{\nabla} \cdot \vec{\nabla}) \vec{v} - \eta \nabla^2 \vec{v} = -\nabla p$$

$$\nabla \cdot \vec{v} = 0$$

(C-39)

The normal flow-velocity at the walls is  $u_0$ . If the channel area is  $A$  and its perimeter  $S$ , then the length

$$L = A/S$$

(C-40)

may be defined. The dimensionless quantities

$$\vec{v} = \vec{v}/u_0$$

$$P = p/\rho u_0^2$$

$$\vec{r} = \vec{r}/L$$

$$\epsilon = \eta/L\rho u_0$$

(C-41)

reduce Eq. C-39 to

$$(\vec{\nabla} \cdot \vec{\nabla}) \vec{v} - \epsilon \nabla^2 \vec{v} = -\nabla P$$

$$\nabla \cdot \vec{v} = 0$$

(C-42)

Henceforth, vector notation is used to signify vector components in the X-Y plane only, where Z measures along the axis of the duct. The assumptions

~~SECRET~~

~~SECRET~~

Other Channel Shapes

Section C-7

$$V_z = Z g(X, Y)$$

and

$$\vec{V} = \vec{V}(X, Y) \tag{C-43}$$

bring Eq. C-42 to the form

$$(\vec{V} \cdot \nabla) \vec{V} - \epsilon \nabla^2 \vec{V} = -\nabla P \tag{C-44a}$$

$$(\vec{V} \cdot \nabla) g + g^2 - \epsilon \nabla^2 g = -\frac{1}{Z} \frac{\partial P}{\partial Z} \tag{C-44b}$$

$$\nabla \cdot \vec{V} + g = 0 \tag{C-44c}$$

Since Eqs. C-44a and C-44b are independent of Z, they demand that P be of the form

$$P = \frac{1}{2} \gamma Z^2 + H(X, Y) \tag{C-45}$$

The identity

$$(\vec{V} \cdot \nabla) \vec{V} = \nabla \frac{1}{2} V^2 - \vec{V} \times (\nabla \times \vec{V})$$

brings Eqs. C-44a and C-44b to the form

$$\nabla \frac{1}{2} V^2 - \vec{V} \times (\nabla \times \vec{V}) - \epsilon \nabla^2 \vec{V} = -\nabla H \tag{C-46a}$$

$$(\vec{V} \cdot \nabla) g + g^2 - \epsilon \nabla^2 g = -\gamma \tag{C-46b}$$

~~SECRET~~

Appendix C

Laminar Flow Problem

The r.h.s. of Eq. C-46a is the gradient of a scalar. Thus  $\vec{V}$  must be a vector such that the curl of the l.h.s. of Eq. C-46a vanishes. This is satisfied if  $\vec{V}$  is derivable from a potential

$$\vec{V} = -\nabla \phi \tag{C-47}$$

When  $\vec{V}$  is of this form, Eq. C-46a may be solved for H. Substitution of Eqs. C-44b and C-47 into Eq. C-46b gives the eigenvalue equation

$$\epsilon \nabla^4 \phi - (\nabla^2 \phi)^2 + (\nabla \phi) \cdot \nabla (\nabla^2 \phi) = \gamma \tag{C-48}$$

with boundary conditions analogous to those in the two-dimensional problem.

In the case where  $\epsilon = 0$ , Eq. C-46b may be written

$$\nabla \cdot g \vec{V} + 2g^2 = -\gamma \tag{C-49}$$

The requirement of no wall slippage gives  $g = 0$  at the boundary, and the divergence theorem may be applied to Eq. C-49 to give

$$2 \int g^2 dA = -\gamma A$$

or

$$\gamma = -2 \bar{g}^2$$

whence

$$P = H(X,Y) - \bar{V}_z^2 \tag{C-50}$$

or, using dimensional quantities

$$p = \rho u_0^2 H(X, Y) - \rho \overline{v_z^2} \quad (C-51)$$

The second term of Eq. C-51 differs by a factor of 2 from that obtained by a naive application of Bernoulli's law. This result is a generalization of the conclusions of Sec. C-4. When  $\bar{V}$  satisfies Eq. C-47, Eq. C-46a is integrated for H and Eq. C-50 becomes

$$P = - \left[ \frac{1}{2} (V_x^2 + V_y^2) + V_z^2 \right] \quad (C-52)$$

In the case of a circular channel Eq. C-48 becomes an ordinary differential equation. For  $\epsilon = 0$  the integration is easily performed. The equation is

$$-\left(\frac{d\phi}{dR}\right) \frac{d}{dR} \left(\frac{1}{R} \frac{d}{dR} R \frac{d\phi}{dR}\right) + \left(\frac{1}{R} \frac{d}{dR} R \frac{d\phi}{dR}\right)^2 + \gamma = 0 \quad (C-53)$$

If the substitutions

$$\zeta = \frac{1}{4} R^2$$
$$f = \frac{1}{2} R \frac{d\phi}{dR} \quad (C-54)$$

are made, then Eq. C-53 becomes

$$-ff'' + f'^2 + \gamma = 0$$

~~SECRET~~

Appendix C

Laminar Flow Problem

where primes indicate differentiation with respect to  $\zeta$ . This is Eq. C-22 which is solved in Sec. C-4. In terms of the dimensionless transformation equations C-40 and C-41, the boundary of the channel is at  $R = 2$ , or  $\zeta = 1$ . The boundary conditions again become those of Eq. C-11b, and the solution proceeds as before, giving the eigenvalue  $\gamma = -(\pi/2)^2$ , and  $\sqrt{2}/\sqrt{v^2} = \pi^2/8$ . However, the flow profile in terms of  $R$  is given by

$$V_z = \frac{\pi}{2} Y \cos \frac{\pi}{8} R^2$$

which is a flatter profile than that given in Table C-1. For the general case of finite viscosity, the transformation given by Eq. C-54 does not reduce the circular duct problem to the two-dimensional flow problem treated in Sec. C-4.

C-8: Summary

Some solutions of the non-turbulent flow problem are developed. Among these is the family in which, for negative  $\epsilon$  approaching zero,  $v$  changes continuously from the parabolic profile to the squared-off boundary-layer profile; and in which, for positive  $\epsilon$  approaching zero,  $v$  changes from the parabolic shape to a  $\cos \zeta$  functional form. The family of solutions so described appear to present a physically consistent and plausible answer to the problem.

~~SECRET~~

C-9: Note on Previous Work

Since the completion of this work several earlier papers have been brought to the attention of the authors.

An equation of the form of Eq. C-11 was investigated by Hiemenz<sup>1</sup> in 1911 and the reduction to the form of Eq. C-17 was performed. However, the boundary conditions were different and the problem considered was not an eigenvalue problem.

The formulation of the two-dimensional porous wall flow problem appearing in Sec. C-2 is given by Berman<sup>2</sup> through the derivation of Eq. C-11. Berman's subsequent analysis of the equation is confined to perturbations about the high viscosity limit, and is similar to the treatment given by Eqs. C-23 through C-28, inclusive. Berman mentions the inherent difficulty of treating the low viscosity limit of Eq. C-11.

A similar analysis for a cylindrical duct is presented by Yuan and Finkelstein.<sup>3</sup> The analysis is confined to perturbation results, but the investigation includes perturbations about zero viscosity. However, no distinction is made between small positive and negative values of the parameter corresponding to  $\epsilon$ . Although the Yuan-Finkelstein geometry is different from that of this report, the non-uniform convergence encountered here for small negative  $\epsilon$  would seem to cast doubts on the validity of the low viscosity perturbation solutions for stream-to-wall flow.

~~SECRET~~

Appendix C

Laminar Flow Problem

---

C-10: Acknowledgments

The authors would like to express thanks to numerous members of Los Alamos Scientific Laboratory for their interest and help in this problem. Particular thanks are due C. L. Longmire, G. Birkhoff, and J. Lehner for enjoyable and fruitful discussions. M. Goldstein and Clarice Wruck performed the numerical integrations on the 704 digital computer. R. M. Potter and E. S. Robinson have been of major assistance in this study.

REFERENCES

1. K. Hiemenz, (Thesis, Göttingen 1911.) Dingl. Polytech. J., 326, 321 (1911).
2. A. S. Berman, J. App. Phys., 24, 1232 (1953).
3. S. W. Yuan and A. B. Finkelstein, Paper XVII in 1955 Heat Transfer and Fluid Mechanics Institute, University of California, Los Angeles, Calif., June 23, 24, 25, 1955.

~~SECRET~~

~~SECRET~~

## Appendix D

### THE SUPER-DUMBO\*

#### D-1: Introduction

The thermal energy which is added to the propellant in the heat exchanger of a nuclear rocket motor is transformed, during expansion through the nozzle, to kinetic energy in the exhaust stream, thereby lowering the temperature of the gas. The dissociation of hot gas in the heat exchanger and subsequent recombination in the nozzle offers possibilities for improved performance. Although the step-by-step analysis of this process may be complicated, the simple relation

$$H + v^2/2 = \text{const.} \quad (\text{D-1})$$

contains the basis of the transformation process, where H is the enthalpy per gram of the stream and v is the hydrodynamic velocity. This relation is developed in Sec. 7-6 for flow in either the hot region or cold region of the reactor, and applies to flow through the nozzle under very

---

\*That great gains are to be made by utilizing dissociation-recombination reactions of the type discussed in this appendix was pointed out to the authors by R. W. Spence of LASL.

~~SECRET~~



ACRM

Appendix D

The Super-Dumbo

general conditions, including the case of a stream which is chemically reacting. If  $H_c$  is the enthalpy of the heated stream in the chamber of the rocket,  $H_e$  the enthalpy of the exhaust stream, and  $v_e$  the exhaust velocity, then Eq. D-1 for negligible chamber velocity, states that

$$\frac{v_e^2}{2} = H_c - H_e \quad (D-2)$$

This equation relates the exhaust velocity to the change in the enthalpy of the stream between conditions in the chamber and the exhaust.

The chamber enthalpy  $H_c$  is increased for a given chamber temperature by the presence of a dissociation reaction in the propellant, whereas the exhaust enthalpy  $H_e$  is decreased by a corresponding recombination reaction. Thus, when both reactions are present the exhaust velocity is increased. If the stream, between the chamber and the end of the nozzle, is caused to react chemically with a second stream, a further lowering of  $H_e$  may occur, although the enthalpy of the second stream must be included as an effective contribution tending to lower  $H_c$ , concomitantly.

These ideas are applied in this appendix to evaluate the possible improvement in the performance of Dumbo by utilizing the dissociation and subsequent recombination reactions. Section D-2 considers the effects of dissociation-recombination reactions of  $H_2$  in hydrogen or decomposed ammonia ( $H_2$  and  $N_2$ ). Section D-3 treats the two stream systems, where one stream is assumed to be thermally dissociated  $H_2$  in hydrogen or decomposed ammonia. These variants are classed as "super-Dumbo" because of their

ACRM

~~SECRET~~

potentially superior performance. Both sections are based on the assumption of local thermodynamic equilibrium in the reactions involved. It should be emphasized that the effects considered here may be limited not by thermodynamics but by slow recombination rates which may reduce or vitiate the performance improvements.

For appreciable hydrogen decomposition to occur, it is necessary that chamber temperatures be higher and pressures lower than in the designs described in Chap. 9. The necessary modifications to the Dumbo design are considered in Sec. D-4.

D-2: H<sub>2</sub> Dissociation-Recombination Applications

The Dumbo models given in Chap. 9 heat the propellant to a temperature in the range 2500-3050°K at operating pressures in the range 15-100 bar. Since the heated gases are either hydrogen or decomposed ammonia (H<sub>2</sub> and N<sub>2</sub>), the large amounts of energy that may be added to hydrogen via the dissociation reaction



should be considered. Figure D-1 shows the equilibrium enthalpy of hydrogen as a function of temperature with the pressure P as a parameter. The curve P = ∞ shows the enthalpy of hydrogen with no dissociation. As an example, at 3000°K the enthalpy increase of the gas as indicated by the P = ∞ curve is 10.8 Kcal/gm. This may be compared with the enthalpy increase for complete dissociation at 3000°K, given by 66 Kcal/gm. Thus,

~~SECRET~~

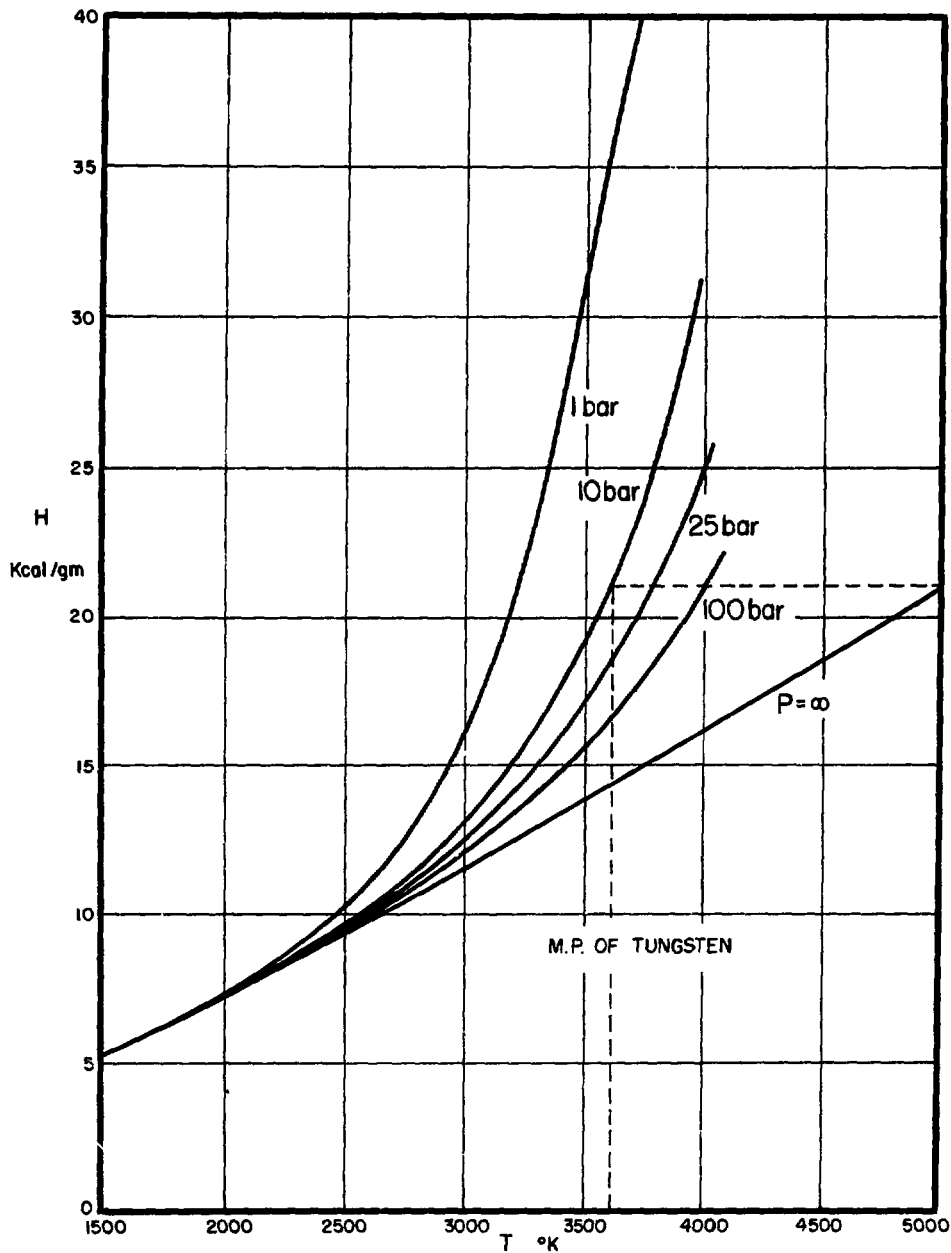


Fig. D-1: Enthalpy of Hydrogen

~~SECRET~~

the enthalpy of the gas at a given temperature in the chamber is greatly increased by the dissociation reaction.

The reaction given by Eq. D-3 is governed by the familiar law of mass action, from which it follows that

$$P_H^2 / P_{H_2} = K(T) \quad (D-4)$$

where  $P_H$  and  $P_{H_2}$  are the partial pressures of H and H<sub>2</sub>, respectively, and  $K(T)$  is the equilibrium constant. The fraction  $x$  of the originally totally nondissociated hydrogen which has dissociated is given by

$$x = \sqrt{\frac{K}{K+4P}} \quad (D-5)$$

where  $P$  is the total pressure. Values of  $K$  are presented by Woolley, et al.,<sup>1</sup> and are used in Fig. D-2 to show the degree of dissociation occurring at various temperatures and pressures. This figure shows that increased dissociation results from increased temperature or decreased pressure.

The dissociation which is indicated in Fig. D-2 results in an increased enthalpy of the gas, which is computed by methods given in Ref. 1. The resulting data are given in Fig. D-1. For example, this figure shows the enthalpy for dissociated hydrogen at 10 bar to be 21 Kcal/gm at 3623°K, which is equal to the enthalpy of nondissociated hydrogen at 5000°K! At lower pressures this effective temperature is still higher.

~~SECRET~~

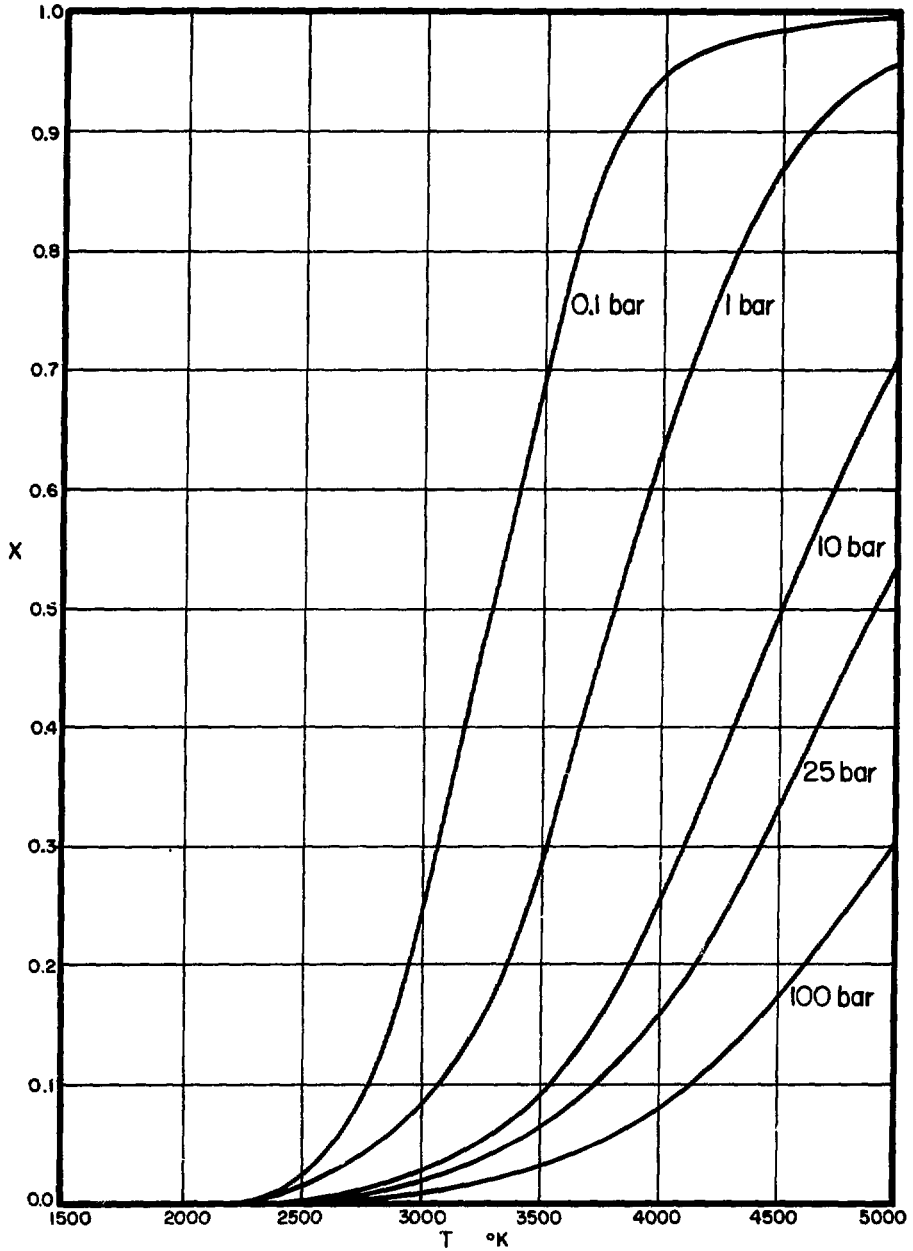


Fig. D-2: Fraction of Hydrogen Dissociated under Various Conditions

These data are used in Fig. D-3 to predict the exhaust velocity  $v_e$  from Eq. D-1, with the exhaust enthalpy  $H_e$  equal to 1.0 Kcal/gm which corresponds to an exhaust temperature of 300°K. The potential gains available by use of the tungsten melting temperature at low pressures are evident when compared with 2500°K performance.

D-3: Ammonia Systems

In this section, a system is considered in which ammonia is heated nuclearly and burned with nuclearly heated oxygen, and the products expanded by means of an ideal nozzle. Also considered is the case where ammonia alone is heated and expanded. Local thermodynamic equilibrium is assumed throughout.

A previous treatment of this problem is given by Anderson and Cotter<sup>2</sup> of LASL. Because they chose the maximum preheating temperature to be 3000°K and the minimum pressure to be 33 1/3 atm, they observed no major increases in exhaust velocity due to H<sub>2</sub> dissociation. The following is an extension of this type of system into the regions of temperature and pressure where dissociation plays a more important role.

Oxygen nuclearly preheated to 2000°K is stoichiometrically burned with ammonia nuclearly preheated to various pressures and temperatures. The products of this combustion are isentropically expanded to zero pressure. The ideal exhaust velocity is calculated by means of Eq. D-2 where  $H_e = 0$ .  $H_c$  is obtained from a simplified analysis of the thermochemistry.

~~SECRET~~

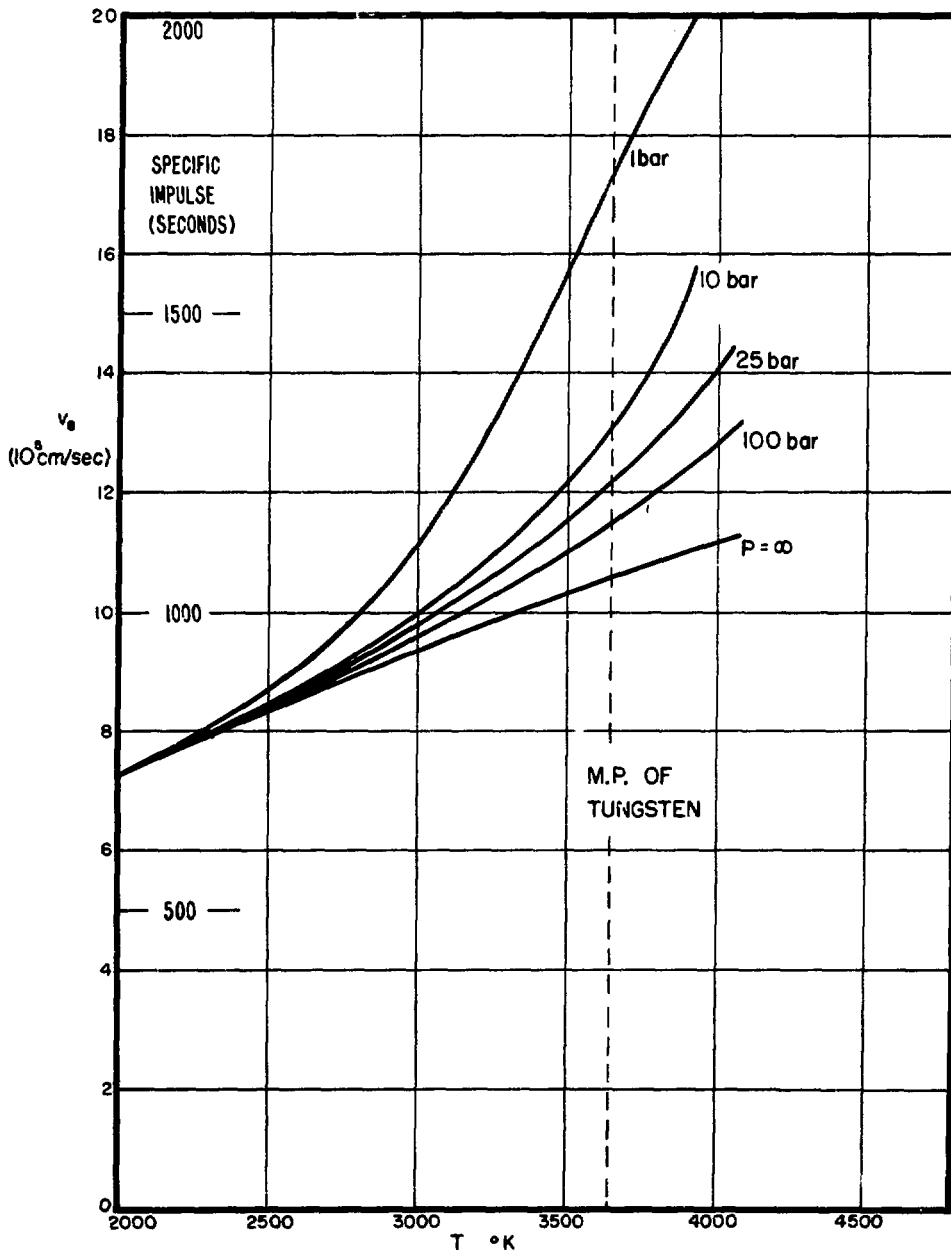


Fig. D-3: Potential Performance of Super-Dumbo with Hydrogen

~~SECRET~~

Comparison in the case of a specific problem shows good agreement with the work of Anderson and Cotter. A similar treatment is presented in which ammonia alone is nuclearly heated, so that the effects of the addition of oxygen may be shown. The results are presented in Fig. D-4.

D-4: Dumbo Design Modifications

The utilization of these reaction effects requires a Dumbo design of very high gas temperature and low operating pressure. The requirement of high temperature clearly suggests a tungsten wall operated near its maximum working temperature. This temperature probably exceeds the melting point of  $UO_2$  (3113°K). Since there is a question as to whether a cermet retains its tensile strength when the  $UO_2$  inclusions are liquid, the lamination technique, described in Sec. 8-3, may be preferable for the super-Dumbo motor.

Although numerical designs suitable for super-Dumbo operation have not been developed, several features of this type of motor may be predicted. Attainment of the highest possible gas temperature imposes the following demands on the designs:

- (a) The tensile strength of the metal wall in the hottest regions is low.
- (b) The difference between gas and wall temperature  $\theta_g$  must be very small.
- (c) The temperature variation within a mosaic cell  $\delta_1 T$ , caused by constructional errors, must be made small.



~~SECRET~~

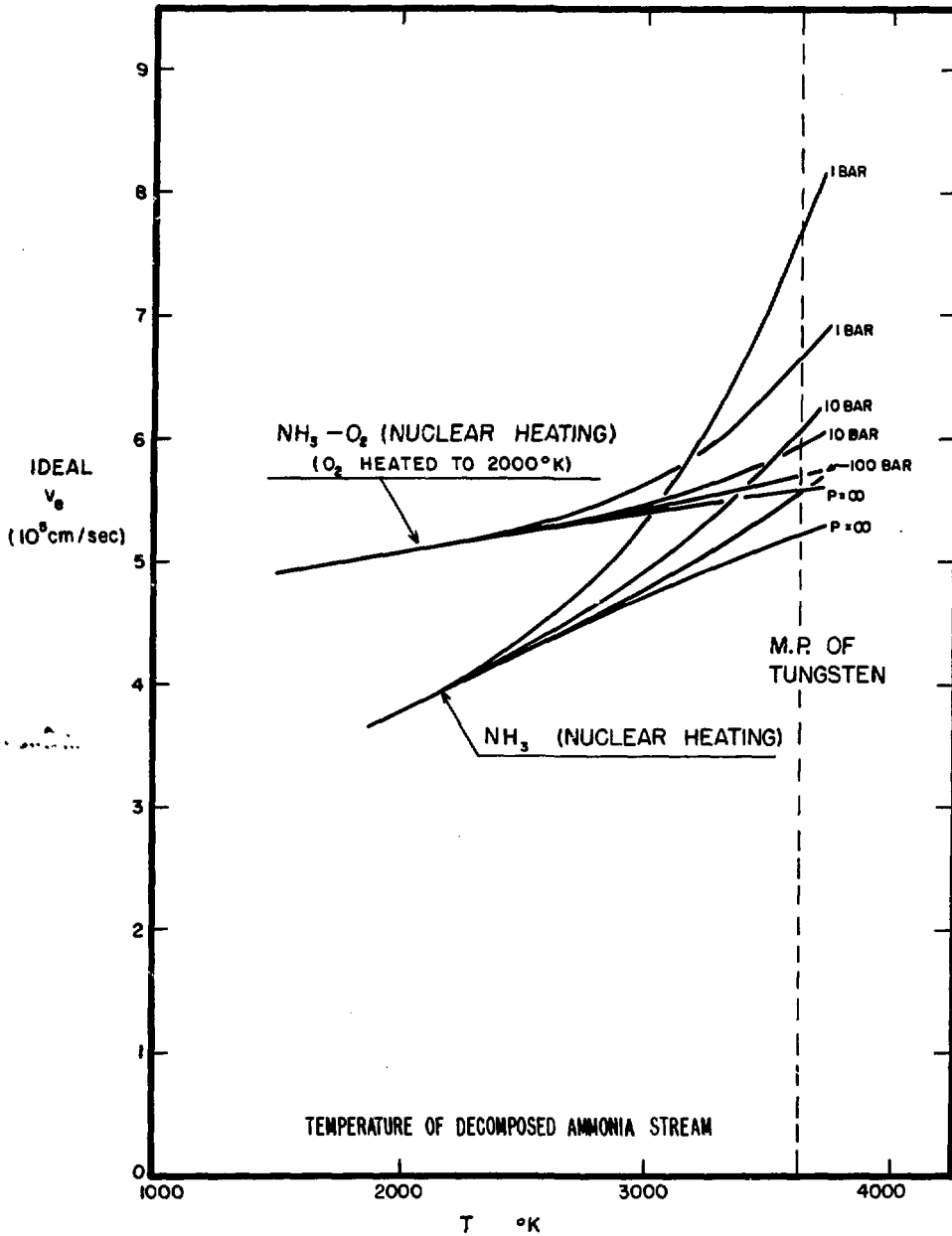


Fig. D-4: Ideal Exhaust Velocity for Two Ammonia Systems

~~SECRET~~

(d) The flow  $J_0(z)$  through the wall must be maintained very uniform.

(e) The power density must be made very uniform.

These requirements, along with that of low operating pressure, might appear to be ominously stringent. However, the high performance of the motor and the presence of dissociation processes introduce several compensating effects. The lowered flow rate increases temperature uniformity within a mosaic cell and tends to reduce the pressure drop across the wall, thereby permitting reduced tensile strength. The dissociation process gives rise to the Nernst effect in the heat exchanger (see Sec. 4-7) which effectively increases the thermal conductivity of the gas by a large factor, and reduces  $\theta_g$  and  $\delta_1 T$  correspondingly.

The requirement of low operating pressure applies throughout the hot gas region, so that the  $\rho v^2$  effects in this region must be made small, which tends to insure a uniform  $J_0(z)$ . The implied low velocity requires short tubes which are widely spaced.

The neutronics of the super-Dumbo reactor suggest higher loadings with  $UO_2$  (a) because of the flattened shape, and (b) because of the larger flow areas. Since the power density through the super-Dumbo reactor must be made highly uniform, it may be advantageous to make local small adjustments of either  $UO_2$ -loading, or moderator, or both.

~~SECRET~~

Appendix D

The Super-Dumbo

---

REFERENCES

1. Harold W. Woolley, Russell B. Scott, and F. G. Brickwedde, Thermal Properties of Hydrogen, National Bureau of Standards Research Paper RP1932, Vol. 41, November 1948.
2. R. C. Anderson and T. P. Cotter, Combustion and Nozzle Expansion of Preheated Ammonia and Oxygen, Los Alamos Scientific Laboratory Report LAMS-1941, August 1955.

Note added in proof: F. J. Krieger\* has considered the reaction kinetics in a dissociating-recombining stream of hydrogen and their influence on rocket nozzle design. Assuming chamber conditions of 3500°K and 20 atm with a 1 atm exit pressure and a total flow of  $10^3$  gm/sec, he finds performance closer to instantaneous equilibrium than the constant composition condition. The methods of this article when applied to Dumbo indicate a still greater recombination effect.

---

\*F. J. Krieger, Chemical Kinetics and Rocket Nozzle Design, J. Am. Rocket Soc., 21, 179 (1951). Other references also given.

~~SECRET~~

Appendix E

HEAT EXCHANGE INSTABILITY\*  
by B. W. Knight, Jr.

E-1: Introduction

In dimensionless form, the equation relating heat and mass flow is

$$\frac{\partial \theta}{\partial \tau} + q(\tau) \frac{\partial \theta}{\partial \zeta} = \sigma(\zeta) \quad (\text{E-1})$$

where  $\theta$  is temperature,  $\tau$  time,  $q$  mass flow,  $\zeta$  length, and  $\sigma$  power density per unit length. The inlet temperature boundary condition is  $\theta = 1$  at  $\zeta = 0$ , and the heat exchanger extends from  $\zeta = 0$  to  $\zeta = 1$ . The three terms of Eq. E-1 represent energy accumulation, energy flow, and energy production. The dimensionless pressure  $\pi$  is given by

$$\frac{\partial \pi}{\partial \zeta} = -g(q, \theta, \zeta) \quad (\text{E-2})$$

which states that the dimensionless pressure gradient  $\partial\pi/\partial\zeta$  depends in

---

\*This investigation resulted from a conjecture by J. L. Tuck and was carried on with C. L. Longmire and B. B. McInteer. This presentation generalizes the results given by Longmire in a LASL memo on the Poiseullian flow problem. (Stability of Viscous Flow Heat Exchange, July 11, 1955.) Appendix E has been taken from the notes of a seminar talk given by B. W. Knight, Jr. at LASL on December 28, 1955.

~~SECRET~~

some fashion on the mass flow, local temperature, and the local specifications of the heat exchanger. It is necessary that

$$\frac{\partial g}{\partial q} \equiv g_q > 0$$

$$\frac{\partial g}{\partial \theta} \equiv g_\theta > 0 \tag{E-3}$$

The first of these conditions is evident; the second is generally correct for gases, and is what makes the theory lead to interesting results.

Equations E-1 and E-2 involve several assumptions: (a) the specific heat of the gas is constant, (b) inertial forces are small compared to frictional forces, that is, acoustical effects may be ignored, (c) in any region  $\Delta \zeta$ , the heat capacity of the exchanger is large compared to that of the gas it contains, (d) the temperature of the gas is always the same as that of the exchanger at a given  $\zeta$ , and (e) there is no thermal conduction along the  $\zeta$  axis.

E-2: Equilibrium Conditions

The integrated power is defined as

$$\epsilon(\zeta) = \int_0^\zeta \sigma(\zeta') d\zeta' \tag{E-4}$$

The time independent solution of Eq. E-1 is then

$$\theta_0(\zeta) = \frac{1}{q_0} \epsilon(\zeta) + 1 \tag{E-5}$$

Equilibrium quantities are denoted hereafter by the subscript zero. The total pressure drop is obtained from Eq. E-2, whence

$$\Delta \pi_0(q_0) = - \int_0^1 g[q_0 \theta_0(\zeta)] d\zeta \quad (\text{E-6})$$

From here on the explicit  $\zeta$  dependence of  $g$  is not mentioned. The general character of  $\Delta \pi_0(q_0)$  is seen by differentiating Eq. E-6, giving

$$\frac{d\Delta \pi_0}{dq_0} = - \int_0^1 g_q d\zeta + \frac{1}{q_0^2} \int_0^1 g_{\theta} \epsilon d\zeta \quad (\text{E-7})$$

For large flows, the negative term dominates. For low flows, the positive second term dominates. Thus  $\Delta \pi_0(q_0)$  is of the form given in Fig. E-1. The slope of this curve, given by Eq. E-7, is interpreted

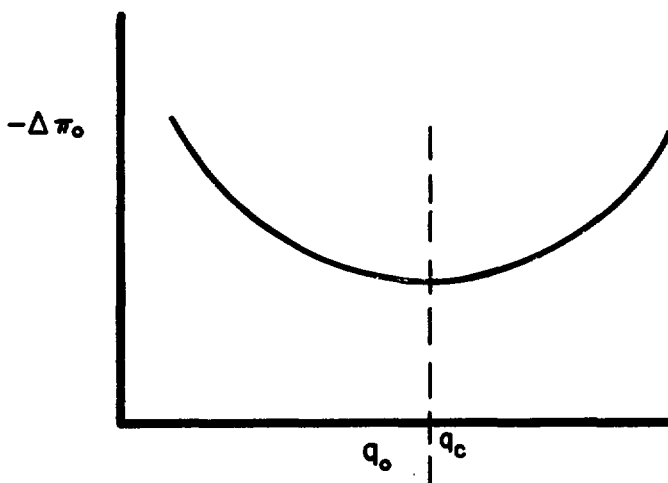


Fig. E-1

physically as a hydrodynamic impedance. There exists a critical flow  $q_c$  below which this impedance becomes negative. It is a plausible conjecture that if the pressure drop across the heat exchanger is fixed then the flow in the negative-impedance region is unstable. This is similar to the case for negative-impedance electric circuits. This implies that there is a critical temperature  $\theta_c$  above which the exchanger cannot deliver gas in a steady manner. In the next sections this conjecture is proven.

E-3: Effect of Perturbations

If the equilibrium situation, given by Eq. E-5, is perturbed, solutions to Eq. E-1 may be expected to be of the form

$$q = q_0 + q_1(\tau)$$

$$\theta = \theta_0(\zeta) + \theta_1(\zeta, \tau)$$

(E-8)

where  $\theta_1$  and  $q_1$  are small. The boundary pressures are assumed to be constant, and given by

$$\Delta \pi = \Delta \pi_0$$

(E-9)

Substituting Eq. E-8 into Eq. E-1 yields the first order perturbation equation

$$\frac{\partial \theta_1}{\partial \tau} + q_0 \frac{\partial \theta_1}{\partial \zeta} = - \frac{q_1}{q_0} \sigma(\zeta)$$

(E-10)

The pressure condition, given by Eq. E-9, yields

$$\int_0^1 g(q_0 + q_1, \theta_0 + \theta_1) d\zeta = -\Delta\pi_0 \quad (\text{E-11})$$

which is reduced to a first order perturbation relation

$$q_1 \int_0^1 g_q d\zeta + \int_0^1 g_\theta \theta_1 d\zeta = 0 \quad (\text{E-12})$$

This relation must be satisfied by  $q_1$  and  $\theta_1$ .

The solution of Eqs. E-10 and E-12 may be reduced to the solution of an eigenvalue problem by assuming that

$$\begin{aligned} \theta_1(\zeta, \tau) &= \sum_{\alpha} A_{\alpha} \theta_{\alpha}(\zeta) e^{a\tau} \\ q_1(\tau) &= \sum_{\alpha} A_{\alpha} e^{a\tau} \end{aligned} \quad (\text{E-13})$$

Direct substitution into Eqs. E-10 and E-12 yields

$$\frac{d\theta_{\alpha}}{d\zeta} + \frac{a}{q_0} \theta_{\alpha} = -\frac{1}{q_0^2} \sigma(\zeta) \quad (\text{E-14})$$

and

$$\int_0^1 g_q d\zeta = -\int_0^1 g_\theta \theta_{\alpha} d\zeta \quad (\text{E-15})$$

Equation E-13 may be used only if the  $\theta_{\alpha}$  form a set complete enough to expand the arbitrary initial perturbation  $\theta_1(\zeta, 0)$ . Completeness of the



eigenfunctions in Eq. E-13 has been demonstrated by J. Lehner\* for the case of Poiseullian flow through a uniform channel with uniform power generation. The same method may be applied to more general situations.

The condition of stability demands that all the  $\alpha$ 's of Eq. E-13 have real parts which are negative. Instability implies that there is at least one  $\alpha$  with a positive real part. It will be demonstrated that the question of stability depends on the sign of  $d\Delta T_0/dq_0$ .

#### E-4: The Stability Criterion

Equation E-14 integrates to

$$\theta_\alpha = -\frac{1}{q_0^2} \int_0^{\xi} \sigma(\xi') e^{-\frac{\alpha}{q_0} (\xi - \xi')} d\xi' \quad (\text{E-16})$$

This is substituted into Eq. E-15 to obtain an explicit eigenvalue equation for  $\alpha$ .

There is always exactly one real  $\alpha$  which solves Eq. E-15. This is demonstrated as follows: By Eq. E-16,  $\theta_\alpha$  is continuous and monotonic in  $\alpha$ , with the limits  $\theta_\infty = 0$  and  $\theta_{-\infty} = -\infty$ . Thus the right hand side of Eq. E-15 must be monotonically continuous in  $\alpha$ , ranging from 0 to  $+\infty$ , and for the entire range of  $\alpha$  the value of the left hand side of Eq. E-15 must occur only once.

---

\*"Completeness of the System of Eigenfunctions in a Problem of Viscous Flow Heat Exchange." LASL memo by J. Lehner, March 9, 1956.

~~SECRET~~~~CONFIDENTIAL~~

## The Stability Criterion

Section E-4

A relationship between  $\alpha$  and  $d\Delta\pi_0/dq_0$  is now demonstrated. A new eigenvalue relation is obtained by combining Eqs. E-15 and E-7, given by

$$\begin{aligned} \frac{d\Delta\pi_0}{dq_0} &= \int_0^1 g_\theta \theta_\alpha d\zeta + \frac{1}{q_0^2} \int_0^1 g_\theta \epsilon d\zeta \\ &= \frac{1}{q_0^2} \int_0^1 d\zeta g_\theta \int_0^\zeta d\zeta' \sigma(\zeta') \left[ 1 - e^{-\frac{\alpha}{q_0}(\zeta-\zeta')} \right] \end{aligned} \quad (\text{E-17.})$$

where the last step follows from Eqs. E-16 and E-4.

It is shown that if  $d\Delta\pi_0/dq_0$  is positive, the flow is unstable. For, by Eq. E-17, if  $\alpha$  is real then  $\left[ 1 - e^{-(\alpha/q_0)(\zeta-\zeta')} \right]$  must be positive as must  $d\Delta\pi_0/dq_0$ . Since  $\zeta - \zeta' > 0$ , this implies  $\alpha > 0$ , which is the condition for instability.

Similarly it may be shown that if  $d\Delta\pi_0/dq_0$  is negative then the flow is stable. For, in general,

$$\frac{\alpha}{q_0} = \beta + i\gamma \quad (\text{E-18})$$

which gives for the real part of the bracketed term in Eq. E-17

$$1 - e^{-\beta(\zeta-\zeta')} \cos \gamma(\zeta-\zeta') \quad (\text{E-19})$$

which must be negative. However, if  $\beta > 0$  this expression is intrinsically positive. Thus  $\beta$ , and the real part of any  $\alpha$ , must be negative, and the flow is stable.

385

~~SECRET~~~~CONFIDENTIAL~~